Optimal Design and Operation of Community Energy Systems

Optimal Design and Operation of Community Energy Systems

By Sayyed Faridoddin Afzali, B.Eng., M.A.Sc

A Thesis Submitted to the School of Graduate Studies in Partial Fulfillment of the Requirements for the Degree

Doctor of Philosophy

Ph.D. Candidate (2020) McMaster University

Chemical Engineering Hamilton, Ontario

TITLE: Optimal Design and Operation of Community Energy Systems

AUTHOR: Sayyed Faridoddin Afzali
B.Eng. (Petroleum University of Technology)
M.A.Sc (Sharif University of Technology)

SUPERVISOR: Professor Vladimir Mahalec

NUMBER OF PAGES: xii, 118

Abstract

Energy demand for buildings has been rising during recent years. Increasing building energy consumption has caused many energy-related problems and environmental issues. The on-site community energy system application is a promising way of providing energy for buildings. Community energy system usage reduces the primary energy consumption and environmental effects of greenhouse gas (GHG) emissions compared to the implementation of the stand-alone energy systems. Furthermore, due to the increase in electricity price and shortage of fossil fuel resources, renewable energies and energy storage technologies could be great alternative solutions to solve energy-related problems. Generally, the energy system might include various technologies such as internal combustion engine, heat recovery system, boiler, thermal storage tank, battery, absorption chiller, ground source heat pump, heating coil, electric chiller, solar photovoltaics (PV) and solar thermal collectors, and seasonal thermal energy storage.

The economic, technical and environmental impacts of energy systems depend on the system design and operational strategy. The focus of this thesis is to propose unified frameworks, including the mathematical formulation of all of the components to determine the optimal energy system configuration, the optimal size of each component, and optimal operating strategy. The proposed methodologies address the problems related to the optimal design of the energy system for both deterministic and stochastic cases. By the use of the proposed frameworks, the design of the energy system is investigated for different specified levels of GHG emissions ratio, and the purpose is to minimize the annual total cost.

To account for uncertainties and to reduce the computational times and maintain accuracy, a novel strategy is developed to produce scenarios for the stochastic problem. System design is carried out to minimize the annual total cost and conditional value at risk (CVaR) of emissions for the confidence level of 95%. The results demonstrate how the system size changes due to uncertainty and as a function of the operational GHG emissions ratio. It is shown that with the present-day technology (without solar technologies and seasonal storage), the lowest amount of GHG emissions ratio is 37%. This indicates the need for significant technological development to overcome that ratio to be 10% of stand-alone systems.

This thesis introduces novel performance curves (NPC) for determining the optimal operation of the energy system. By the use of this approach, it is possible to identify the optimal operation of the energy system without solving complex optimization procedures. The application of the proposed NPC strategy is investigated for various case studies in different locations. The usage of the proposed strategy leads to the best-operating cost-saving and operational GHG savings when compared to other published approaches. It has shown that other strategies are special (not always optimal) cases of the NPC strategy.

Based on the extensive literature review, it is found that it is exceptionally complicated to apply the previously proposed models of seasonal thermal energy storage in optimization software. Besides, the high computational time is required to obtain an optimum size and operation of storage from an optimization software. This thesis also proposes a new flexible semi-analytical, semi-numerical methodology to model the heat transfer process of the borehole thermal energy storage to solve the above challenges. The model increases the flexibility of the storage operation since the model can control the process of the storage by also deciding the appropriate storage zone for charging and discharging.

Research Contributions and Highlights

- Optimal design and operation of energy systems (ES), including gas turbine, fired heat recovery steam generator (HRSG), boiler, electric chiller and absorption chiller, is investigated.
- Analytical criteria for determining the optimal structure of an ES and its optimal operation modes are presented.
- An optimization framework for optimal ES design under uncertainty is presented to minimize the ATC and limiting the risk of CDE.
- A new method, known as a random vector sampling (RVS) method, is developed to generate scenarios for uncertain parameters in stochastic problems. RVS significantly speeds up convergence and its performance is substantially better than the Monte Carlo Sampling method.
- A novel operating strategy, known as Novel Performance Curve (NPC) strategy, is developed to optimize ES operation. The proposed strategy considers changes in energy prices, primary energy consumption (PEC) and CO_2 emission factors.
- Following the electrical load strategy, following the thermal load strategy, following the hybrid load strategy and match performance strategy are special cases of NPC strategy. Economic, environmental and technical performances of ES improve significantly by using NPC strategy compared to the application of the mentioned strategies.
- A new linear flexible semi-analytical, semi-numerical methodology is proposed to model the heat transfer process of the borehole thermal energy storage. Compared to the other models, this model can be utilized by any optimization software to identify the optimal storage size and operation.
- The proposed model increases the operational flexibility of seasonal storages. The model can control the storage operation by selecting a storage zone for charging and discharging.

Acknowledgements

First and foremost, my deepest gratitude is extended to my supervisor Prof. Vladimir Mahalec. I am grateful for the opportunity he gave me to work under his supervision, as well as the trust and freedom he gave me to explore my research interests. I am thankful for his support, constant encouragement and his positive attitude. I cannot imagine ever having a better supervisor and teacher for my Ph.D. studies.

I'm also thankful to Dr. Jim Cotton for his help, support and his valuable ideas and advice. He is one of the most inspiring people whom I have had the fortune to work with him in the ICE-Harvest project. I want to thank my committee member, Dr. Thomas A. Adams II, for his insightful questions, suggestions and research feedbacks to improving the quality of this thesis. It was my honor to get advice from him during my Ph.D.

I would like to thank my fellow MACC friends and friends of ICE-Harvest project for their support, their friendship, their ideas and advice during meetings. It was an absolute pleasure to join those bright people and learn from them each day. Over the years, I have formed strong friendships with my fellow MACC students and with my friends in the ICE-Harvest project, which I believe will last a lifetime, and will miss all the fantastic discussions in the JHE 324 and penthouse.

Last but not least, I would like to thank my family and express my love and gratitude to my wife Hasti, and my parents toward their endless love and for supporting me spiritually throughout my life. Finally, I give all glory to God for good health and guidance throughout this academic journey. Without His mercies, I would have been unable to achieve this educational milestone.

Table of Contents

List of Acronyms

ATC	Annual Total Cost
CCHP	Combined Cooling, Heating and Power
CDE	CO_2 Emission
CHP	Combined Heating and Power
COP	Coefficient of Performance
CVaR	Conditional Value at Risk
DES	Distributed Energy System
ES	Energy System
FEL	Following the Electrical Load
FHL	Following the Hybrid Load
FLB	Following the Load Of Buildings
FSS	Following Seasonal Strategy
FTL	Following the Thermal Load
GHG	Greenhouse Gas
GSHP	Ground Source Heat Pump
GT	Gas Turbine
HRSG	Heat Recovery Steam Generator
MCS	Monte Carlo Sampling
MILP	Mixed Integer Linear Programming
MINLP	Mixed Integer Non-Linear Programming
MP	Match Performance

NG	Natural Gas
NLP	Nonlinear Programming
NPC	Novel Performance Curves
ORC	Organic Rankine Cycle
PEC	Primary Energy Consumption
PECR	Primary Energy Consumption Ratio
PGU	Power Generation Unit
PV	Photovoltaic
SF	Supplementary Firing
SP	Separate Production System
VOC	Variable Operational Cost
RVS	Random Vector Sampling
SP	Separate Production System
SAA	Sample Average Approximation

Chapter 1

Introduction

1.1.Introduction and literature review

Buildings require a large part of worldwide energy sources [1]. This causes a significant increase in the greenhouse gas emission intensity in the atmosphere that leads to severe environmental challenges. To solve this concern, some of the countries have developed some strategies [2] for constructing buildings in a way to be more energy-efficient. In residential areas, the heat required for domestic hot water (DHW) and space heating is engaged for almost 80% in the north of Europe [3] and Canada [4]. Due to the rise in electricity price and curtailment of fossil fuel resources, renewable energies and energy storage technologies could be applied to the energy system as generator and storage technologies, respectively, and that leads to a significant reduction in the greenhouse gas (GHG) emissions.

It is highlighted that the consumption of natural gas and oil would increase drastically by 92% and 48%, respectively, from 2003 to 2030 [5]. The reason is that it is predicted that the consumption of the world's total energy will rise by 71% from 2003 to 2030 [5] [6]. As the energy demand of the buildings rises, it is becoming more crucial to discover effective ways to employ the energy and to reduce the use of fossil fuels.

The utilization of on-site community energy systems and distributed energy systems (DES) has been increasing recently [7] as they can decrease the total cost and CO2 emissions [8] relative to the standalone system's usage. The performance of energy systems has been studied for several kinds of buildings, such as office buildings [9], hotels [10], residential buildings [11] [12] and commercial buildings. By the use of a power generation unit (PGU) for producing electricity in household sectors, there is a substantial quantity of generated waste heat. Using this waste heat through the utilization of the heat recovery systems can significantly enhance the system efficiency compared to a separate production energy system. By the use of separate production systems, the electricity is provided by the grid, and heat and cooling are supplied by the boiler and electric chiller, respectively. The efficiency of an energy system would increase from 35-55% to more than 90% by harvesting the waste heat for heating and cooling demands usage.

The energy system might incorporate different technologies. The simple structure of the energy system contains a power generation unit (PGU), a heat recovery system, a heating coil or a heat exchanger, an absorption chiller, and a backup boiler [13]. Some energy systems include hybrid chillers to heighten cooling efficiency [7,8,12,14–16]. Liu et al. [14] suggested an operating strategy for an energy system, including hybrid chillers such that the ratio of cooling energy provided by the electric chiller to the cooling load varies hourly. Zheng et al. [15] applied hybrid chillers to the energy system. They examined the economic performance of the combined cooling, heat and power (CCHP) system following a feed-in tariff policy. Zheng at al. [7] studied the operation of an energy system, including hybrid chillers, by proposing a new operating strategy based on the minimum distance between loads and the CCHP operating curve.

One of the practical methods to mitigate the discrepancy between the supply and demand and to increase the capability of the energy system is the employment of thermal energy storage (TES). Short-term thermal energy storage might be used to achieve a broad range of electric output to thermal output ratio , [17]. Mago et al. [18] analyzed the operation of a combined heat and power (CHP) system involving dual power generation units and short-term thermal energy storage. Wang et al. [19] proposed a model for a community energy system, including short-term thermal energy storage. In this study, a day-ahead scheduling strategy was proposed to control the operation of the system during a day. The battery additionally can be added to the energy system to manage the electric output of the system [20]. Amongst diverse storage technologies, thermal energy storage and battery have been frequently utilized to improve the energy system efficiency. Short-term thermal energy storage has almost 100% efficiency, and battery efficiency is about 80% [21].

Geothermal energy is employed either directly by the exploitation of groundwater of the sub stream or with the application of ground source heat pumps (GSHP). GSHP has been integrated with an energy system [22–24] to attain flexibleness in providing heating and cooling energies. Liu et al. [25] investigated the performance of a CCHP system, which included a GSHP and thermal energy storage. Besides the mentioned technologies, some other technologies might also be added to energy systems. The use of a CCHP system driven by a gas-steam combined cycle at an educational center in China was studied in [26]. Distributed energy resources (e.g., solar energy and wind energy) have been integrated with the energy system to improve the economic and environmental performances of the system [27]. Fu et al. [28,29] examined the performance of a CCHP system composed of an internal combustion engine, a flue gas heat exchanger, a jacket water heat exchanger, and an absorption heat pump.

Some researchers have studied the employment of solar photovoltaic (PV) panels and solar thermal collectors in the energy systems. Rodriguez et al. [30] assessed the performance of the several energy system configurations consisting of solar thermal collectors, photovoltaic panels and internal combustion engines by using TRNSYS software. The authors utilized different performance criteria; GHG emissions, primary energy consumption and life cycle cost analysis. The dimension of the multi-source energy system for varying climate scenarios is investigated by Barbieri [31].

The thermal load limits electricity production, and peak periods in demand for energy often do not align with supply [32]. These limitations lead to increased energy rates and short supplies in the periods of highest demand. One of the effective methods to alleviate the discrepancy between the supply and demand for energy and to increase the electrical generation capacity of the energy system is the application of thermal energy storage (TES).

The variations in outside temperatures throughout summer and winter cause large heat load and cooling load fluctuations over the year. This causes an imbalance of the cooling and heating demands. However, the heat load and cooling load are not commonly well-matched with energy provided by energy systems or stand-alone systems [33]. As an example, the recovered heat from industrial plants depends on the working load of an industrial process or the industrial electricity demand, and it is consistent during a year. In this case, there would be extra heat during the summer, while the heating demand and cooling demand are small. Accordingly, the seasonal demand mismatch signifies an occasion for the employment of the seasonal thermal energy storage (STES) systems. Seasonal storage systems can be integrated with either large-scale solar thermal collectors or community energy systems or industrial waste heat to compensate for the seasonal demand mismatch.

In summary, electrical, cooling and heating demands of a building alter during a day and also during a year. The energy output of an energy system cannot balance with the building energy demands. As a result, selecting a proper system configuration, an appropriate sizing of each component and using an efficient operating strategy are essential to delivering high energy efficiency, economic benefits, and further reducing GHG emissions. It means the economic, environmental and energy performances of the energy system depend on the configuration of the system, the size of each component and the system operating strategy [16].

Considering the extensive literature review, there is still a gap in simultaneous environmental assessment and economic assessment of the energy system, including all potential technologies.

This is valuable to understand what size the energy system would be to entail both environmental and economic benefits. Moreover, the optimal design and operation of an energy system regarding both economic and environmental criteria is a complicated task. Equipment models introduce nonlinear terms, which makes the model tougher to solve.

1.2.Research Outline

The main object of this thesis is to propose different design and operation frameworks for community energy systems. The frameworks include the mathematical formulation of all of the components, optimization criteria, and suitable methodologies to solve the optimal design problem of an energy system. The outputs of the applied framework are the optimal energy system configuration, the optimal size of each component and optimal operating strategy. In each design framework, a detailed model is presented for energy systems, including non-linear terms associated with the partial load operation of each component, and on/off coefficient of each component. The system model is turned to the mixed-integer linear programming (MILP) model to lower the computational time of the optimization problem. Moreover, the change in the energy system size is investigated for different levels of GHG emission ratios (the ratio of the GHG emission from the energy system application to those due to the stand-alone system usage).

This thesis comprises six chapters, including introduction and conclusion chapters. A summary for each of the chapters and publications therein is given here:

Chapter 2: In this chapter, optimal design and operation of combined cooling, heat and power (CCHP) system comprising the gas turbine, a fired heat recovery steam generator (HRSG), absorption chiller, electric chiller and a boiler are examined comprehensively. Besides, appropriate operation strategies concerning different seasons are proposed to optimize the performance of the CCHP system based on annual total cost (ATC), primary energy consumption (PEC) and carbon dioxide emissions (CDE). The application of the proposed methodology is investigated for a case study assuming different climate zones. In this chapter, analytical expressions are derived that enable determination of regions where specific operating strategies and modes (specific parts of the system are on while others are off) are optimal. These analytical expressions depend on the price ratio (the ratio of the electricity price to the natural gas price) and energy demands. The contents of this chapter have been published in the Energy Journal [34] after peer review.

Chapter 3: In this chapter, a novel operating strategy that uses overall optimal partial loads of power generation unit (PGU) and novel performance curves (NPC) is proposed to optimize the energy system operation. Analytical formulations are developed to determine the overall optimum partial load of PGU for demands above and below the CCHP operating curve. The designed methodology accounts for energy prices, carbon dioxide emissions, primary energy consumption factors and load varieties due to the diverse climate zones. Other strategies, such as following match performance, hybrid load, electric load, and thermal load strategies, are shown to be the particular cases of the NPC methodology. The performance of a CCHP following the NPC methodology is compared to the CCHP performances following other mostly used operating strategies such as following match performance, hybrid load, electric load, and thermal load strategies. The comparison is made for two small hotel buildings in San Francisco and Miami and residential buildings in Dalian, holding different energy demand profiles. The contents of this chapter have been published in the Applied Energy Journal [12] after peer review.

Chapter 4: In this chapter, a design methodology is proposed to addresses the problems associated with the optimal design and optimal operation of the energy system under uncertainties in energy demand and energy prices. A detailed MILP model is proposed, which captures nonlinear performance characteristics of the equipment. The energy system includes all practically available technologies such as power generation unit, boiler, heat recovery system, electric chiller, GSHP, absorption chiller, heating coil, battery, and thermal storage. The model contains the risk of occasionally high CDE.

A new strategy is developed to generate scenarios for the stochastic problem, which we call RVS (random vector sampling) method. First, discrete distributions of the uncertain parameters are obtained by the moment matching technique by three points. Then, candidate vectors for different sets of three scenarios are built, and their probabilities are normalized. Finally, one vector is randomly selected for each uncertain parameter. The proposed methodology is applied to the case study in Dalian, China. The size of the system is investigated for both deterministic and stochastic cases. The contents of this chapter have been published in the Applied Energy Journal [35] after peer review.

Chapter 5: In this chapter, an extensive literature review regarding various models of borehole heat exchangers is presented. It is a somewhat complicated task to use the available models in optimization software for optimal sizing and optimal operation of the seasonal storage due to the high computational time. To solve this challenge, in the second part of this chapter, a new flexible semi-analytical, semi-numerical methodology to model is expressed for describing the heat transfer process of the borehole thermal energy storage. Based on the previous models, the heat extracted/ injected from/into the storage can be regulated by either changing the water flow rate inside each borehole or adjusting the inlet water temperature. However, by offering the new model, the flexibility of the storage operation increases because one can control the heat input or heat output by choosing an appropriate storage section as well (has a different number of boreholes).

1.3.References

[1] Beerepoot M, Ada M. Policies for renewable heat. International Energy Agency; 2012.

[2] Helm D. The European framework for energy and climate policies. Energy Policy 2014;64:29–35. doi:10.1016/j.enpol.2013.05.063.

[3] Economidou M, Atanasiu B, Despret C, Maio J, Nolte I, Rapf O. Europe's buildings under the microscope. A country-by-country review of the energy performance of buildings. 2011.

[4] Energy use data handbook tables (Canada)—Residential Sector. Http://DataGc.ca/Data/En/Dataset/ 27155507-0644-4077-9a97-7b268dfd8e58 n.d.

[5] Som SK, Datta A. Thermodynamic irreversibilities and exergy balancein combustion processes. Prog Energy Combust Sci 2008;34:351–76.

[6] McDaniel B, Kosanovic D. Modeling of combined heat and power plant performance with seasonal thermal energy storage. J Energy Storage 2016;7:13–23. doi:10.1016/j.est.2016.04.006.

[7] Zheng CY, Wu JY, Zhai XQ. A novel operation strategy for CCHP systems based on minimum distance. Appl Energy 2014;128:325–35. doi:10.1016/j.apenergy.2014.04.084.

[8] Wang J, Chun-fa Z, You-yin J. Multi-criteria analysis of combined cooling , heating and power systems in different climate zones in China. Appl Energy 2010;87:1247–59. doi:10.1016/j.apenergy.2009.06.027.

[9] Mago PJ, Hueffed AK. Evaluation of a turbine driven CCHP system for large office buildings under different operating strategies. Energy Build 2010;42:1628–36. doi:10.1016/j.enbuild.2010.04.005.

[10] Smith AD, Mago PJ. Effects of load-following operational methods on combined heat and power system efficiency. Appl Energy 2014;115:337–51. doi:10.1016/j.apenergy.2013.10.063.

[11] Li L, Mu H, Gao W, Li M. Optimization and analysis of CCHP system based on energy loads coupling of residential and office buildings. Appl Energy 2014;136:206–16. doi:10.1016/j.apenergy.2014.09.020.

[12] Afzali SF, Mahalec V. Novel performance curves to determine optimal operation of CCHP systems. Appl Energy 2018;226:1009–36. doi:10.1016/j.apenergy.2018.06.024.

[13] Jing Y, Bai H, Wang J, Liu L. Life cycle assessment of a solar combined cooling heating and power system in different operation strategies. Appl Energy 2012;92:843–53. doi:10.1016/j.apenergy.2011.08.046.

[14] Liu M, Shi Y, Fang F. A new operation strategy for CCHP systems with hybrid chillers. Appl Energy 2012;95:164–73. doi:10.1016/j.apenergy.2012.02.035.

[15] Zheng CY, Wu JY, Zhai XQ, Wang RZ. Impacts of feed-in tariff policies on design and

performance of CCHP system in different climate zones. Appl Energy 2016;175:168–79.

[16] Wang J, Jing Y, Zhang C. Optimization of capacity and operation for CCHP system by genetic algorithm. Appl Energy 2010;87:1325–35. doi:10.1016/j.apenergy.2009.08.005.

[17] Zheng CY, Wu JY, Zhai XQ, Wang RZ. A novel thermal storage strategy for CCHP system based on energy demands and state of storage tank. Electr Power Energy Syst 2017;85:117–29.

[18] Mago PJ, Luck R, Knizley A. Combined heat and power systems with dual power generation units and thermal storage. Int J Energy Res 2014;38:896–907. doi:10.1002/er.

[19] Wang C, Lv C, Li P, Song G, Li S, Xu X. Modeling and optimal operation of community integrated energy systems : A case study from China. Appl Energy 2018;230:1242–54.

[20] Wang J, Sui J, Jin H. An improved operation strategy of combined cooling heating and power system following electrical load. Energy 2015;85:654–66. doi:10.1016/j.energy.2015.04.003.

[21] Evans A, Strezov V, Evans TJ. Assessment of utility energy storage options for increased renewable energy penetration. Renew Sustain Energy Rev 2012;16:4141–7. doi:10.1016/j.rser.2012.03.048.

[22] Holjevac N, Capuder T, Zhang N, Kuzle I, Kang C. Corrective receding horizon scheduling of flexible distributed multi- energy microgrids. Aplied Energy 2017. doi:10.1016/j.apenergy.2017.06.045.

[23] Kang L, Yang J, An Q, Deng S, Zhao J, Li Z, et al. Complementary configuration and performance comparison of CCHP-ORC system with a ground source heat pump under three energy management modes. Energy Convers Manag 2017;135:244–55. doi:10.1016/j.enconman.2016.12.055.

[24] Kang L, Yang J, An Q, Deng S, Zhao J, Wang H, et al. Effects of load following operational strategy on CCHP system with an auxiliary ground source heat pump considering carbon tax and electricity feed in tariff. Appl Energy 2017;194:454–66. doi:10.1016/j.apenergy.2016.07.017.

[25] Liu W, Chen G, Yan B, Zhou Z, Du H, Zuo J. Hourly operation strategy of a CCHP system with GSHP and thermal energy storage (TES) under variable loads : A case study. Energy Build 2015;93:143–53. doi:10.1016/j.enbuild.2015.02.030.

[26] Tan ZF, Zhang HJ, Shi QS, Song YH, Ju LW. Multi-objective operation optimization and evaluation of large-scale NG distributed energy system driven by gas-steam combined cycle in China. Energy Build 2014;76:572–87. doi:10.1016/j.enbuild.2014.03.029.

[27] Ju L, Tan Z, Li H, Tan Q, Yu X, Song X. Multi-objective operation optimization and evaluation model for CCHP and renewable energy based hybrid energy system driven by distributed energy resources in China. Energy 2016;111:322–40. doi:10.1016/j.energy.2016.05.085.

[28] Fu L, Zhao X, Zhang S, Li Y, Jiang Y, Li H, et al. Performance study of an innovative natural gas CHP system. Energy Convers Manag 2011;52:321–8.

doi:10.1016/j.enconman.2010.07.003.

[29] Zhao XL, Fu L, Zhang SG, Jiang Y, Li H. Performance improvement of a 70 kWe natural gas combined heat and power (CHP) system. Energy 2010;35:1848–53. doi:10.1016/j.energy.2010.01.005.

[30] Rodríguez LR, Lissén JMS, Ramos JS, Jara EÁR, Domínguez SÁ. Analysis of the economic feasibility and reduction of a building's energy consumption and emissions when integrating hybrid solar thermal/PV/micro-CHP systems. Appl Energy 2016;165:828–38. doi:http://dx.doi.org/10.1016/j.apenergy.2015.12.080.

[31] E.S. Barbieri , Y.J. Dai , M. Morini , M. Pinelli, P.R. Spina , P. Sun RZW. Optimal sizing of a multi-source energy plant for power heat and cooling generation. Appl Therm Eng 2014;71:736–50. doi:10.1016/j.applthermaleng.2013.11.022.

[32] McDaniel B. Thermodynamic Analysis of the Application of Thermal Energy Storage to a Combined Heat and Power Plant, Master's Thesis. University of Massachusetts Amherst, 2015.

[33] Xu L, Torrens JI, Guo F, Yang X, Hensen JLM. Application of large underground seasonal thermal energy storage in district heating system: A model-based energy performance assessment of a pilot system in Chifeng, China. Appl Therm Eng 2018;137:319–28. doi:10.1016/j.applthermaleng.2018.03.047.

[34] Afzali SF, Mahalec V. Optimal design, operation and analytical criteria for determining optimal operating modes of a CCHP with fired HRSG, boiler, electric chiller and absorption chiller. Energy 2017;139:1052–65. doi:10.1016/j.energy.2017.08.029.

[35] Afzali SF, Cotton JS, Mahalec V. Urban community energy systems design under uncertainty for specified levels of carbon dioxide emissions. Appl Energy 2019. doi:10.1016/j.apenergy.2019.114084.

Chapter 2

Optimal design, operation and analytical criteria for determining optimal operating modes of a CCHP with fired HRSG, boiler, electric chiller and absorption chiller

The contents of this chapter have been published in the following peer reviewed journal:

Afzali SF, Mahalec V. Optimal design, operation and analytical criteria for determining optimal operating modes of a CCHP with fired HRSG, boiler, electric chiller and absorption chiller. *Energy* 2017;139:1052–65. doi:10.1016/j.energy.2017.08.029.

Energy 139 (2017) 1052–1065

Contents lists available at ScienceDirect

Energy

journal homepage: www.elsevier.com/locate/energy

Optimal design, operation and analytical criteria for determining optimal operating modes of a CCHP with fired HRSG, boiler, electric chiller and absorption chiller

Sayyed Faridoddin Afzali, Vladimir Mahalec*

Department of Chemical Engineering, McMaster University, 1280 Main St. West, Hamilton, ON L8S 4L8, Canada

ARTICLE INFO

Article history:
Received 13 April 2017
Received in revised form
24 July 2017
Accepted 8 August 2017
Available online 11 August 2017

Keywords:
Combined cooling, heating and power (CCHP)
Supplementary firing
Optimal CCHP operating strategy
Optimal CCHP design

ABSTRACT

The configuration, design and operation strategy are the main factors that can affect the technical, economic and environmental performances of combined cooling, heating and power (CCHP) system. In this paper, the operation of a CCHP system with fired heat recovery steam generator (HRSG), electric chiller, absorption chiller and a boiler is classified into one of three scenarios which are determined by gas turbine size and magnitude of thermal and electric loads. The optimal operating strategies are presented for these scenarios. For scenario with high cooling loads, we derive analytical expressions for calculation of ratio (electricity price/natural gas price) values which delimit three optimal modes for providing cooling demand in summer, thereby enabling selection of optimal operating strategy without numerical optimization. We examine the optimal design of CCHP system in three climate zones based on the proposed strategy. Supplementary firing as well as a higher coefficient of performance (COP) of the absorption chiller increase system efficiency and enable reduction of gas turbine size. Our case studies show that supplementary firing, (for some values of price ratio, absorption chiller COP and climate zone) the electric chiller and/or the boiler are necessary components to achieve optimal system performance.

1. Introduction

Combined cooling, heating and power systems (CCHP) are energy efficient alternatives for supplying electricity, heat and cooling to large and small-scale buildings. Since there is a fluctuation in demands for the electricity, cooling and heating during a day and through different months of a year, a CCHP system needs to be able to satisfy such varying demands while maintaining high efficiency and producing minimal greenhouse gas (GHG) emissions.

A schematic diagram of a simple CCHP plant with a fired HRSG is shown in Fig. 1. Large scale systems use the gas turbine (GT) [1,2] as a power generation unit (PGU). HRSG is used to recover a portion of heat from the exhaust gas to generate saturated steam. An auxiliary boiler and an electric chiller are used to provide additional heat and cooling when needed. If the energy recovered from the exhaust gas is not sufficient to produce the required amount of steam or hot water, a supplementary firing fuel is used to compensate for it. Such structure enables the steam flow rates to be controlled by the supplementary firing.

There have been many studies on the CCHP systems, dealing with optimal operational strategies and design methods. In the interest of brevity, we will present a summary of those previous studies that are relevant to our work. Operating strategy of a CCHP system typically either is following the thermal load (FTL) or it follows the electric load (FEL) [3] or it is a hybrid strategy (FHL) [4] which switches between electric load and thermal load following. In addition, optimal configuration and operation of a CCHP system depends on various factors, such as the use of a suitable Organic Rankine Cycle (ORC) [5,6], optimal capacity of the prime mover [7], application of the thermal energy storage [8,9] and the use of renewable energy [10] or distributed energy resources.

Efficiency and economic performance of a CHP system in a sewage treatment plant were analyzed [11,12] by considering different configurations of the prime mover, such as multiple units of the micro gas turbine of the same size and a combination of different sizes of the micro gas turbine. It was found that a higher power generation efficiency is achievable by application of an optimum combination of the micro gas turbines which required a higher capital investment. Fumo et al. [13] presented a

* Corresponding author. Tel.: +1 905 525 9140x26386.
E-mail address: mahalec@mcmaster.ca (V. Mahalec).

http://dx.doi.org/10.1016/j.energy.2017.08.029

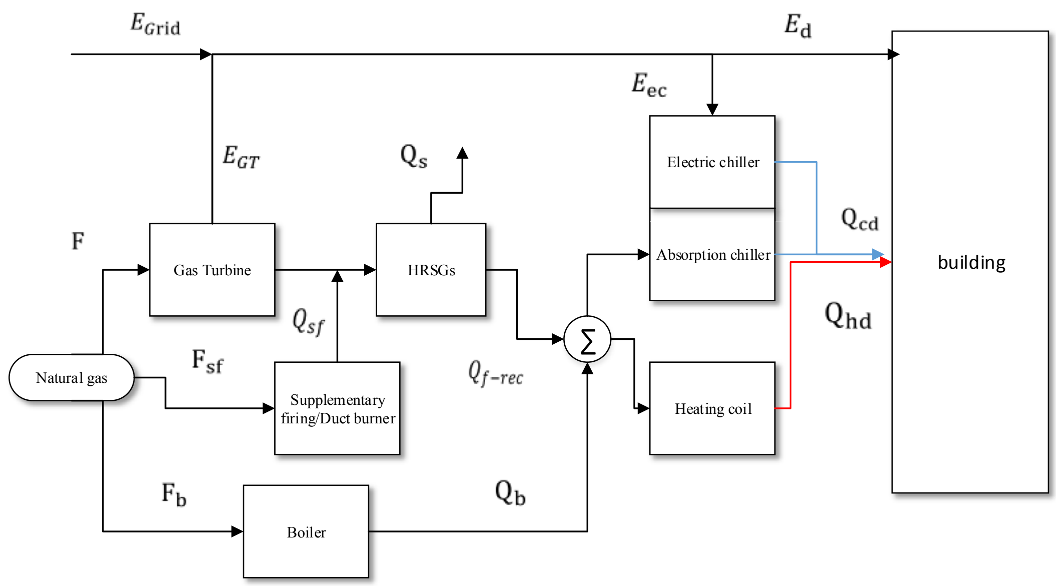

Fig. 1. Energy flow diagram of CCHP system.

methodology based on the ratio of the electrical demand to the PGU capacity and the ratio of electrical demand to thermal demand to select the right operational strategy between FTL and FEL for CHP and CCHP systems with no export of the electricity. An operational strategy proposed by Mingxi et al. [14] for CCHP system with the hybrid chiller that the ratio of the electric cooling (the cooling provided by the electric chiller) to the total cooling demand changes hourly.

Tan et al. [15] followed electric load to optimize the operation of a large-scale combined cycle CCHP system driven by natural gas. In their subsequent work [16], they presented a model for operational optimization of a CCHP system powered by renewable energy resources based on four criteria: energy rate, operational cost, CO_2 emission and a combination of them. Kyungtae et al. [17] presented analytical solutions to determine the optimum operation of a power generation unit of a CHP system. Zheng et al. [18] proposed a novel flexible operational strategy for CCHP systems based on the minimum distance of the load to the performance curve. They also analyzed the impact of feed-in tariff [19] on design and operation of a CCHP system.

Comparison of different operational strategies has been carried out in some of the studies. Basrawi et al. [20] analyzed the effect of four different strategies on the economic and the environmental performances of a CCHP system driven by micro gas turbines. FEL, FTL, mix-match and base load strategies were examined based on net present value and emission reduction index. Under the base load strategy, PGU operates at its full load capacity, while in the mix-match strategy it follows higher of electrical or thermal demand. Li et al. [21] compared CCHP performance under five different strategies: FEL, FTL, FHL, seasonal load following strategy (FSS) and following the electrical-thermal load of buildings (FLB). FLB strategy is based on an optimized value of load ratio. If the ratio of hourly electric load to hourly thermal load is less than this value, the PGU follows the thermal load. Otherwise, the electric load is followed. FSS strategy is similar to FLB strategy; ratio of the monthly electric load to the monthly thermal load is compared to one. If this ratio is more than one, the optimum strategy is following the electric load. Otherwise, the system follows the thermal load. Calise et al. [22] evaluated three different strategies, FEL, FTL and base load strategies, to minimize the plant cost and maximize the CCHP performance. The results showed that FEL strategy could achieve higher profitability. Moreover, FEL, FTL and base load operation strategies [23] were examined for a hybrid photovoltaic and micro gas turbine CCHP system. It was deduced that FEL strategy yields the highest net profit for this scheme.

Besides mentioned strategies, finite time thermodynamics [24–27] has been applied as a powerful tool to optimize the design and operation of CCHP and CHP systems. The endoreversible CHP [28,29], irreversible CHP systems [30–34], endoreversible CCHP system [35] and irreversible CCHP systems [36,37] have been modeled by using finite time thermodynamics and then optimized based on profit rate and exergy efficiency. Furthermore, analytical formulas of dimensionless profit rate and exergy efficiency were developed to utilize as some guidelines for the designs and operations of practical systems.

An additional degree of freedom enabling better decisions on how to best operate a CCHP system is offered by the supplementary firing. Supplementary firing (via a duct burner) can be used in a simple cycle or in a combined cycle based cogeneration and trigeneration systems in order to adjust the power to heat ratio as required to meet power, heat and cooling demands. It is more efficient than deploying an additional boiler which leads to the fuel savings of 10–20% when compared to the boiler [38,39]. Besides natural gas, supplementary firing can use other fuels (e.g. coal [40]). In addition, a duct burner can operate with the exhaust gas containing 12% mole fraction of O_2 [41], while the common combustors are designed to work with the exhaust gas containing 20–21% of the oxygen.

Several studies have published dealing with supplementary firing application in CHP, CCHP and power plant. They include:

i Thermodynamic and exergy analyses in a combined cycle [42,43] at different flow rates of supplementary firing
ii Exergy and environmental analyses [44] in a real combined cycle power plant
iii Cost analysis of the design of a sequential supplementary fired HRSG [45] in combined cycle power plants
iv Life cycle cost analysis of integrated desalination and cogeneration system [46] including GT and fired HRSG

v Analysis of the net electrical efficiency of a steam turbine [47] driven by HRSG and supplementary firing at different loads

Some studies analyzed the effect of supplementary firing on the operation of CHP and CCHP systems, and most of them were focused on economic analysis. Yang et al. [48], Kehlhofer et al. [49] and Shabbir et al. [50] proposed that HRSG supplementary firing can be applied to CCHP and CHP systems to improve flexibility to meet the demand loads. Bindlish [51] studied real-time optimization of a cogeneration plant for scheduling of power production on a daily basis. He investigated the effect of the supplementary firing on exporting the electricity to the grid at different ambient temperatures. Mitra et al. [52] proposed a generalized model for scheduling of CHP systems under sensitivity of the electricity price and at various modes including two modes for HRSG, unfired and fired.

Several other studies addressed supplementary firing as a variable for designing CHP and CCHP systems. Mokheimer et al. [53] investigated the technical and economic feasibilities of solar integrated gas turbine CHP system. They showed that duct burner performance during winter and summer mostly depends on the GT size, solar energy and ambient temperature. Rossiter [54] investigated the economic tradeoff of using a simple cycle and a combined cycle power plants in a cogeneration system. He deduced that for high fuel cost relative to the cost of electricity; the optimum design is a simple cycle with no supplementary firing. At moderate cost ratio, the combined cycle with a little supplementary firing is the optimum design. Finally, when the natural gas cost is low, the combined cycle with high supplementary firing is valuable. Jabbari et al. [55] designed and optimized CCHP system included into a Kraft process for making wood pulp. Supplementary firing flow rate was an important design variable enabling the system to supply the required electricity and steam by using the steam turbine and the extracted steam from the steam turbine, respectively. Application of CCHP system in an industrial facility was examined and reported in Ref. [56] by Environmental Protection Agency of United States. CCHP system comprised a gas turbine, fired HRSG, a boiler, and an absorption chiller. Four different cases were studied by considering different sizes of the gas turbine. The HRSG was analyzed in two modes, fired and unfired. It was deduced that the application of CCHP system with fired HRSG is more economical than the CCHP with unfired HRSG.

Therefore, by using supplementary firing, an electric chiller, an absorption chiller and a boiler, the CCHP system becomes more valuable but also more complicated. Usage of electricity generated via the gas turbine, electricity from the grid, recovered exhaust heat, supplementary firing and the energy of the boiler should be managed appropriately to provide cooling in an optimal manner. Also, recovered exhaust heat, supplementary firing and the energy from the boiler should be utilized efficiently for heating. As a result, proposing a suitable operation strategy is crucial.

In this work, optimal design and operation of a CCHP system comprising GT, a fired HRSG, an absorption chiller, an electric chiller and a boiler are examined in a comprehensive manner. A previous study [57] of a system with a similar configuration with thermal storage focused on optimizing the operational costs via an MILP model. In this work, we first derive analytical expressions which enable determination of regions where specific operating strategies and modes (specific parts of the system are on while others are off) are optimal. These criteria depend on the ratio of the price of electricity to the price of natural gas and energy demands. They can be used either for deciding how to operate an existing system or to decide what is the optimal structure of a system which is being designed. Operation strategy is proposed to optimize the performance of CCHP system based on annual total cost (ATC), primary energy consumption (PEC) and carbon dioxide emissions (CDE). Following that, we present a case study of optimizing CCHP system for a large consumer in different climate zones. Our case studies show that under a specific set of conditions, the supplementary firing, the boiler and the electric chiller are essential components to achieve the optimal system performance.

2. CCHP model

2.1. GT and HRSG without supplementary firing (unfired mode)

Mass and energy balances for individual pieces of equipment relate the fuel consumption and the useful energy production by a CCHP system. We assume that the power generation unit, PGU, is a gas turbine, GT.

Electricity generated by the GT is:

$$E_{GT}(t) = F(t)\eta_{GT}(t) \tag{1}$$

where η_{GT} is the GT efficiency and F [kW] is the energy produced by combustion of fuel.

The GT efficiency varies throughout the operating range and can be modeled [3] by Eqs. (2)–(4):

$$\eta_{GT} = \eta_{nom,GT}\left(0.1797 + 2.329f - 2.334f^2 + 0.8264f^3\right) \tag{2}$$

where f [−] is the partial load of GT and is defined as follows:

$$f = \frac{E_{GT}}{E_{nom}}, \quad f_{min} = 0.25 \quad and \ f_{max} = 1 \tag{3}$$

where E_{nom} [kW] is the nominal capacity of GT cycle, f_{min} and f_{max} [−] are the minimum and the maximum partial load operations of GT, respectively, and $\eta_{nom,GT}$ is the efficiency of GT running at full load and is defined [3] by Eq. (4):

$$\eta_{nom,GT} = 0.0409\ln(E_{nom}) - 0.0687 \tag{4}$$

The electrical power generation efficiency of GT depends on its partial load operation and its capacity. As stated by Eq. (2), the GT efficiency increases by increasing the partial load operation. Also, according to Eq. (4), increasing the capacity of the GT yields an increase in the electrical generation efficiency.

Recovered heat from GT cycle via HRSG in unfired mode is given by Eq. (5):

$$Q_{rec-unf}(t) = F(t)[1 - \eta_{GT}(\mathrm{t})]\eta_{HRSG-unf} \tag{5}$$

where $\eta_{HRSG-unf}$ is the efficiency of HRSG in unfired mode and $Q_{rec-unf}$ [kW] is the recovered heat.

The electrical output of a CCHP system without supplementary firing is related to the thermal output of the CCHP system by the following equations (Mago et al. [57]):

$$E_{GT} = KQ_{rec-unf} \tag{6}$$

where K [−] is defined by Eq. (7):

$$K = \frac{\eta_{GT}}{\eta_{rec}(1 - \eta_{GT})} \tag{7}$$

where η_{rec} (the same as $\eta_{HRSG-unf}$) is the efficiency of the heat recovery system in the unfired mode.

2.2. Maximum amount of supplementary firing

The maximum amount of supplementary fuel is constrained [58] either because of the mechanical limitations of devices such as the evaporator or due to the oxygen limit in the exhaust gas or in some cases because of the limiting pinch point consideration. After the fuel is added to the exhaust gas coming from the GT cycle, the exhaust gas temperature at the entry to HRSG increases from 450 to 500 °C to 980–1000°C. The actual increase depends on the steam saturation pressure, the load of the prime mover, etc. Hence, at the design stage, the maximum temperature of the gas entering HRSG should be set at a particular value. Previous work [59] suggested that the heat recovery capacity should be such that the stack temperature stays above the minimum value of 100–150°C to avoid acid precipitation and prevent corrosion.

Bischi et al. [60] stated that there is a linear relation between fuel burnt in the GT cycle and the supplementary firing fuel, but they didn't provide an analytical relationship. This relationship can be derived from energy balance (see the supplementary material) as shown by Eq. (8):

$$F_{sf}(t) = F(t)\left[\frac{(1-\eta_{GT})}{\eta_{DB}}\left(\frac{\theta_{ex-f}(t)}{\theta_{ex-unf}} - 1\right)\right] \tag{8}$$

where θ_{ex-f} and θ_{ex-unf} [K] are the exhaust gas temperature entering to the HRSG at fired and unfired modes, respectively and η_{DB} is the duct burner efficiency. Eq. (8) relates the energy generated by burning the supplementary fuel with the exhaust gas temperature in fired and unfired modes.

If $\theta_{ex-f-max}$ is the maximum allowable temperature of the exhaust gas, then the constraint on the supplementary firing fuel is as follows:

$$F_{sf}(t) \le F(t)\left[\frac{(1-\eta_{GT})}{\eta_{DB}}\left(\frac{\theta_{ex-f-max}}{\theta_{ex-unf}} - 1\right)\right] \tag{9}$$

Depending on the variations of power and thermal demands over some periods, supplementary firing may be used up to the amount constrained by Eq. (9).

2.3. HRSG efficiency and amount of heat recovered in fired mode

One of the technical parameters used for CCHP performance assessment is the total efficiency η_{CCHP}, (based on cogeneration efficiency definition) which for a simple CCHP cycle can be expressed as follows:

$$\eta_{CCHP} = 1 - q_s \tag{10}$$

where q_s [−] is the fraction of incoming energy lost in the stack (amount of energy wasted in the stack per unit amount of the energy supplied to the GT cycle).

The difference in CCHP efficiency between the fired and unfired modes can be expressed as follows (refer to the supplementary material):

$$\eta_{CCHP-f} - \eta_{CCHP-unf} = (1-\eta_{GT})\left(c - \eta_{HRSG-unf}\right)\frac{c'M}{c(M+1)} \tag{11}$$

where η_{CCHP-f} and $\eta_{CCHP-unf}$ are the fired and unfired CCHP efficiencies, respectively, and

$$M = \frac{(1-\eta_{GT})}{\eta_{DB}}\left(\frac{\theta_{ex-f}}{\theta_{ex-unf}} - 1\right) \tag{12}$$

Parameters c' and c [−] are correction factors which are used in the definition of CCHP and HRSG efficiencies, respectively (refer to the supplementary material).

By assuming that the mass flow rate and final exhaust gas temperature remain almost constant during supplementary firing [2], HRSG efficiency in the fired mode is as follows (refer to the supplementary material):

$$\eta_{HRSG-f} = \frac{\left(\frac{\theta_{ex-f}}{\theta_{ex-unf}} - 1\right)\left(c - \eta_{HRSG-unf}\right)}{\left(\frac{\theta_{ex-f}}{\theta_{ex-unf}}\right)} + \eta_{HRSG-unf} \tag{13}$$

where η_{HRSG-f} and $\eta_{HRSG-unf}$ are fired and unfired HRSG efficiencies, respectively.

The efficiency of the HRSG increases by increasing the partial load or increasing the supplementary firing fuel [61] as stated by Eq. (13).

Total heat recovered by HRSG in a fired mode is as follows:

$$Q_{rec-f}(t) = \left\{F(t)[1-\eta_{GT}(t)] + F_{sf}(t)\eta_{DB}\right\}\eta_{HRSG-f}(t) \tag{14}$$

Substituting Eq. (13) and Eq. (8) into Eq. (14) leads to (refer to the supplementary material):

$$Q_{rec-f}(t) = F(t)[1-\eta_{GT}(t)]\eta_{HRSG-unf} + c\,\eta_{DB}F_{sf}(t) \tag{15}$$

Using $c\,\eta_{DB} = 1$ leads to small errors and it makes optimization simpler while still achieving acceptable accuracy. Theoretical duct burner efficiency is 100% [44,58,62,63] which means that the HRSG absorbs all of the fuel consumed by the duct burner.

2.4. CCHP demand energy balance

If the heat loss in HRSG is designated as $\eta_{HRSG-loss}$ (it is usually 1%–2% as shown in Ref. [38]) then the remaining heat recovered by the system is:

$$Q_{eff}(t) = Q_{rec-f}(t)(1-\eta_{HRSG-loss}) \tag{16}$$

The total electricity consumed by the users is the sum of the electricity produced by GT and the electricity imported from the grid minus the electricity used to power the electric chiller. Hence, the electrical energy balance is shown by Eq. (17):

$$E_d(t) = E_{GT}(t) + E_{grid}(t) - \frac{\alpha(t)Q_{cd}(t)}{COP_{ec}} \tag{17}$$

where α is the portion of cooling demand supplied by the electric chiller and COP_{ec} is the coefficient of performance of the electric chiller.

Some fraction β of the recovered heat from HRSG and fraction δ of the heat supplied by the boiler are used to meet the demand for heating, which is shown by Eq. (18).

$$\beta(t)Q_{eff}(t) + \delta(t)Q_b(t) = \frac{Q_{hd}(t)}{\eta_{hc}} \tag{18}$$

where Q_{hd} [kW] is the rate of the heating demand at time t [hr], η_{hc} is the heating coil efficiency and Q_b [kW] is the boiler duty.

Since HRSG, boiler and the electric chiller (which is supplied by the excess electricity from the grid) provide energy for the fraction $(1-\alpha)$ of the cooling demand, the energy balance for the cooling demand is as follows:

$$[1-\beta(t)]Q_{eff}(t)+[1-\delta(t)]Q_b(t)-\frac{E_{excess}(t)COP_{ec}}{COP_{ac}} = \frac{[1-\alpha(t)]Q_{cd}(t)}{COP_{ac}} \tag{19}$$

where COP_{ac} is the coefficient of performance of absorption chiller and E_{excess} [kW] is the electricity imported from the grid and sent to the electric chiller. COP of the absorption chiller depends on different manufacturers and varies slightly with changes in the partial load [18,64–66]. This parameter mostly depends on the temperature of the generator and then the temperatures of the evaporator and the condenser [23,67]. Changing evaporator and generator temperatures at fixed condenser temperature [67] changes COP. As a result, we will assume different ranges of COP from 0.7 to 1.2 [68]. We assume the absorption chillers used in Refs. [3,69] for this study.

For all of Eqs. (17)–(19):

$$0 \le \alpha, \beta, \delta \le 1 \tag{20}$$

We should note that α, β and δ cannot take any value. For example when $0<\beta<1$ then $\delta=0$ or when $\alpha=1$ the value of $\beta=1$. It is assumed the recovered exhaust heat is utilized first to satisfy the heating.

3. CCHP operation modes in different seasons

Let us assume that the electric demand and the thermal demand are greater than the minimum output of the CCHP system. We will consider three demand/supply scenarios:

i. Scenario A: Demand for electricity E_d is less than or equal to the amount of the electricity which is generated when burning the amount of fuel required to meet the thermal demand Q_d, i.e. $E_d \le KQ_d$. In addition, demands for electricity plus electricity needed for cooling are less than or equal to the capacity of the gas turbine, Eq. (21). This constraint is valid during some hours of the transition season and the winter.

$$E_d+\frac{Q_{cd}}{COP_{ec}} \le E_{nom} \tag{21}$$

ii. Scenario B: Demand for electricity, E_d, is less than or equal to the amount of electricity which is generated when burning the amount of fuel required to meet the thermal demand Q_d, i.e. $E_d \le KQ_d$. In addition, demands for electricity plus electricity needed for cooling are greater than the capacity of the gas turbine, Eq. (22). This constraint is true during some hours of the winter season when the electrical demand is high and in the summer when the cooling demand is high.

$$E_d+\frac{Q_{cd}}{COP_{ec}} > E_{nom} \tag{22}$$

iii. Scenario C: Demand for electricity is greater than the amount of electricity which is generated when burning the amount of fuel required to meet the thermal demand Q_d, i.e. $E_d > KQ_d$. Thermal demand, Q_d [see Eq. (23)], comprises of the energy required for heating and the energy used to power the absorption chiller for cooling. This scenario exists mostly in the transition season. Thermal demand is calculated as bellow:

$$Q_d=\frac{Q_{hd}}{\eta_{hc}}+\frac{Q_{cd}}{COP_{ac}} \tag{23}$$

Our goal is to derive the optimal operating strategy and configuration (i.e. pattern describing which parts of the CCHP system are “on” or “off”) which produces the minimum excess thermal and electric energies.

3.1. Scenario A

To express the proposed operation strategy clearly, we will use results of comparing operation of CCHP with and without supplementary firing (fired or unfired), which are shown in Fig. 2. These results correspond to a CCHP system operating in winter. Detailed description of the system is given in the supplementary material.

Fig. 2 shows the optimal operation of the CCHP system for different amounts of the heat demand and the fixed values of the electric demand and cooling demand subject to the constraint in Eq. (21). There are two distinct operating regions.

Region I: In this region, the entire heating demand can be supplied by the heat recovered from the exhaust gas of GT cycle. At smaller loads, heating and cooling demands are supplied by the recovered exhaust gas heat and the electric chiller does not operate ($E_d = K\, Q_d$) and all generated electricity is used to meet the electrical demand. Further increases in the heat demand ($E_d \le KQ_d$ constraint remains valid) lead to some portion of the cooling demand being supplied by the electric chiller powered by the electricity generated by the GT cycle, which in turn supplies heat to meet the heating demand via the recovered exhaust heat. This operation continues up to 6300 kW heat demand when GT load reaches to maximum load (which is at $E_d+\frac{Q_{cd}}{COP_{ec}}$) and all heat recovered from the exhaust gas is used in the heating coil to satisfy the heat demand. In this case, the cooling demand is provided totally by the electric chiller.

Region II: In this region, the maximum recovered exhaust gas heat is lower than heating demand, so the supplementary firing supplies extra heat as required to meet the heating demand. Additional heat is generated by the auxiliary boiler when the supplementary firing is at its maximum value as given by Eq. (29).

Let us describe *region I* and *region II* in the form of energy balance equations. In *region I* demands are supplied without using supplementary firing fuel, the boiler and the electricity from the grid. The electric energy balance equation is given by Eq. (24) (HRSG efficiency in unfired mode is represented as η_{rec} for simplicity):

$$E_d=F\eta_{GT}-\frac{\alpha Q_{cd}}{COP_{ec}} \tag{24}$$

Heating and cooling energy balance equations are:

$$\frac{Q_{hd}}{\eta_{hc}}=\beta F[\eta_{rec}(1-\eta_{GT})] \tag{25}$$

$$\frac{(1-\alpha)Q_{cd}}{COP_{ac}}=(1-\beta)F[\eta_{rec}(1-\eta_{GT})] \tag{26}$$

In this case $0<\beta<1$. If $\beta>1$, then $\alpha=1$ and $\beta=1$ since all of the cooling demand should be met by the electricity generated in GT and all recovered heat goes to the heating coil. This situation exists mostly for winter, i.e. low cooling demand and high heating demand. In this situation, scenario A *region II* is applicable. Therefore, the heating balance is described by either by Eq. (27) or Eq. (28).

S.F. Afzali, V. Mahalec / Energy 139 (2017) 1052–1065 1057

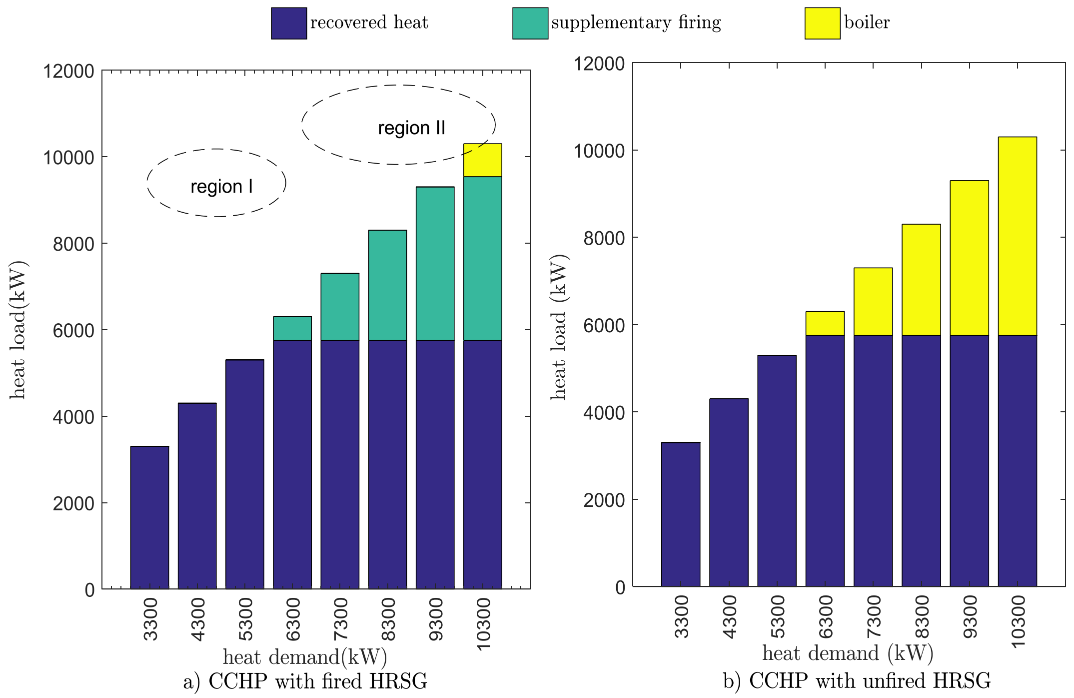

Fig. 2. Supplying heating demands for scenario A for CCHP systems with fired HRSG and CCHP with unfired HRSG with different sources.

$$\frac{Q_{hd}}{\eta_{hc}} = F[\eta_{rec}(1-\eta_{GT}) + M] \tag{27}$$

and in the extreme case if $M > M_{max}$ then:

$$\frac{Q_{hd}}{\eta_{hc}} = F[\eta_{rec}(1-\eta_{GT}) + M_{max}] + Q_b \tag{28}$$

where M_{max} is defined as bellow:

$$M_{max} = \frac{1}{F}\min\left[\frac{\left(1-\eta_{nom,GT}\right)}{\eta_{DB}}\left(\frac{\theta_{ex-f-max}}{\theta_{ex-unf}} - 1\right)F_{nom}, Ca_{DB}\right] \tag{29}$$

where Ca_{DB} [kW] is the supplementary fuel (duct burner) capacity.

3.2. Scenario B

If $E_d \le E_{nom}$, then two different situations may be existed based on the heating demand amount.

(i) $\frac{Q_{hd}}{\eta_{hc}} \le Q_{nom-\mathrm{unf}}$, where $Q_{nom-\mathrm{unf}}$ [kW] is the maximum unfired recovered heat.

In this case, the value of β is calculated from Eq. (24), Eq. (25) and Eq. (26). Otherwise, some of the heating demand should be supplied by supplementary firing and then by the boiler as described by Eq. (27) and Eq. (28), respectively, and by setting $F = F_{nom}$. For cooling demand inequality given by Eq. (30) holds:

$$\frac{(1-\alpha)Q_{cd}}{COP_{ac}} > (1-\beta)F_{nom}\left[\eta_{rec}\left(1-\eta_{nom,GT}\right)\right] \tag{30}$$

Eq. (30) states the remaining amount of the cooling demand $[(1-\alpha)Q_{cd}]$, is more than the remaining amount of the recovered exhaust gas energy. Therefore, Eq. (31) and Eq. (32) describe the supply of the rest of cooling demand. This situation mostly exists in summers.

$$\frac{\gamma Q_{cd}}{COP_{ac}} = (1-\beta)F_{nom}\left[\eta_{rec}\left(1-\eta_{nom,GT}\right)\right] \tag{31}$$

Eq. (31) states exhaust heat recovered can supply γ fraction of cooling demand.

$$(1-\gamma-\alpha)Q_{cd} = Q_{rem} \tag{32}$$

The rest of the cooling demand which is Q_{rem} should be provided by optimum application of supplementary firing, the grid electricity and the boiler.

(ii) $\frac{Q_{hd}}{\eta_{hc}} > Q_{nom-\mathrm{unf}}$

Based on the heating demand value, heating demand energy balance can be established by either Eq. (27) or Eq. (28) when $F = F_{nom}$. This situation exists in winter and when the electric demand is high and not much of cooling is needed.

If the cooling demand is not satisfied by the electricity from the GT, its remaining amount can be provided by optimum usage of supplementary firing, the boiler and the electricity from the grid.

$$(1-\alpha)Q_{cd} = Q_{rem} \tag{33}$$

when $E_d > E_{nom}$, the electric energy balance equation is as Eq. (34) and all of Eq. (26)–(32) should be solved with considering $\alpha = 0$.

$$E_d = F_{nom}\eta_{nom,GT} + E_{grid} \tag{34}$$

3.2.1. Determining Q_{rem}

In general, to supply the cooling demand, there are three modes

1058 S.F. Afzali, V. Mahalec / Energy 139 (2017) 1052–1065

of the system based on different values of the price ratio (cost of electricity/cost of natural gas):

- *Mode 1:* Cooling demand is met first by the use of heat recovered from the exhaust, next by surplus electricity from GT cycle, then by the supplementary firing, and finally by the boiler.
- *Mode 2:* Cooling demand is fulfilled first by the use of heat recovered from the exhaust (if available), next by surplus electricity from GT cycle, then by the supplementary firing, and finally by using the electricity from grid to power the electric chiller.
- *Mode 3*: Initially heat recovered from the exhaust gas powers the absorption chiller, followed by the electric chiller with electricity from the GT cycle and finally the grid.

Eqs. (35) and (36) are used to determine the price ratio limits (σ_L) and (σ_U), which bracket the region where the supplementary firing and the electricity from the grid are utilized while the boiler is shut down.

$$\frac{1}{ATC_{SP}}\left(C_N - \frac{C_E COP_{ac}}{COP_{ec}}\right) = \frac{1}{CDE_{SP}}\left(\frac{\mu_{CO2,E} COP_{ac}}{COP_{ec}} - \mu_{CO2,N}\right) + \frac{1}{PEC_{SP}}\left(\frac{COP_{ac}}{\eta_{grid}\eta_{pgu,sp}COP_{ec}} - 1\right) \tag{35}$$

where $\mu_{CO2,E}$ and $\mu_{CO2,N}$ [g/kWh] are CDE factors of the electricity from the grid and natural gas, respectively, C_E and C_N [\$/kWh] are costs of the electricity and natural gas, respectively, and $\eta_{pgu,sp}$ is the PGU efficiency of SP system. Solution of Eq. (35) for a specific value of the natural gas price, C_N, is the electric price, C_E. Their ratio is the lower bound of the price ratio σ_L.

The analogous procedure is applied to Eq. (36) yields the upper bound of the price ratio, σ_U .

$$\frac{1}{ATC_{SP}}\left(C_N - \eta_b\frac{C_E COP_{ac}}{COP_{ec}}\right) = \frac{1}{CDE_{SP}}\left(\frac{\mu_{CO2,E} COP_{ac}}{COP_{ec}}\eta_b - \mu_{CO2,N}\right) + \frac{1}{PEC_{SP}}\left(\frac{COP_{ac}}{\eta_{grid}\eta_{pgu,sp}COP_{ec}}\eta_b - 1\right) \tag{36}$$

If we minimize objective function ψ comprised of equally weighted total annual cost, carbon dioxide emissions plus primary energy consumption and plot its optimal (lowest possible) values against various values of the price ratio σ for each of these three operating modes and four different absorption chiller COPs, results are as shown in Fig. 3. For example as shown in Fig. 3 (b), by using the absorption chiller with COP = 0.8, the lower limit of price ratio is $\sigma_L = 3.6$, and the upper limit is $\sigma_U = 8$. It means that when the price ratio is less than 3.6, the operating mode 1 is optimal since this mode has the lowest possible objective function (ψ) in this region. If the price ratio is between 3.6 and 8, mode 2 is chosen as the optimal operational strategy. Otherwise, mode 3 is the best one.

Criteria for choosing the optimal operational strategies for different modes are summarized in Table 1.

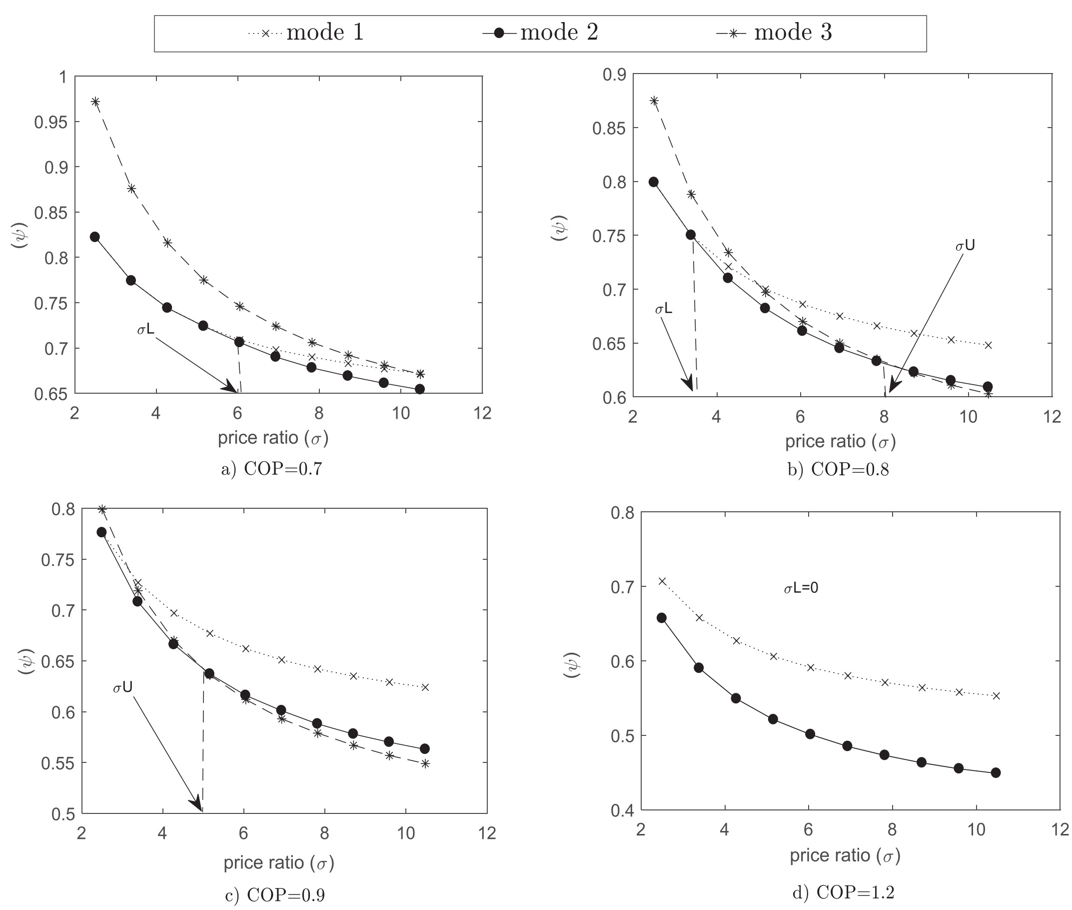

Fig. 3. Determining the lower and the upper price ratios which delimit three optimum operation modes of CCHP system for determining Q_{rem}.

Table 1
Optimal use of energy sources to meet the cooling demand.

	Price Ratio	Exhaust Recovery	Electricity form GT	Supplementary Firing	Boiler	Grid
Mode 1	$\sigma_U < \sigma$	Yes	Yes	Yes	Yes	No
Mode 2	$\sigma_L < \sigma < \sigma_U$	Yes	Yes	Yes	No	Yes
Mode 3	$\sigma < \sigma_L$	Yes	Yes	No	No	Yes

Table 2
Operating strategies for scenario C.

Cases	$E_d \geq E_{nom}$	$E_d < E_{nom}$
$Q_d \geq Q_{nom\text{-}unf}$	If $\frac{Q_{hd}}{\eta_{hc}} \geq Q_{nom}$ The procedure is the same as Scenario A region II If $\frac{Q_{hd}}{\eta_{hc}} < Q_{nom}$ The operation strategy is the same as scenario B	N/A
$Q_d < Q_{nom\text{-}unf}$	supplementary firing is off Electric chiller is off Boiler is off	supplementary firing is off Electric chiller is off Boiler is off

3.3. Scenario C

In this scenario, the supplementary firing is employed when the thermal demand is more than the maximum recovered exhaust gas heat and the GT works at full load. When the thermal demand is lower than the maximum recovered heat, there is no need for a supplementary firing or the boiler, since the thermal demand is satisfied by the thermal output of the CCHP system. If thermal demand is more than Q_{nom}, optimum operating strategy for application of supplementary firing is a combination of scenario A *region II* and scenario B. All possible cases are summarized in Table 2.

When $E_d < E_{min}$ *or* $Q_d < Q_{min}$ the system can operate at its minimum capacity which is:

$$E_{min} = 0.25, \; E_{max} = 0.25 F_{nom} \eta_{nom,GT} \tag{37}$$

In this case, the system operates at its minimum capacity if $\psi_i \leq 1$. Otherwise, the system doesn't operate and the energy demand is met by the SP system.

The decision-making process based on the proposed strategy is summarized in Tables 3 and 4. Following Tables 1, 3 and 4, we can calculate the load of GT, supplementary firing fuel and the optimum application of different equipment to provide the energy for the loads in different seasons.

At the design stage, there are three degrees of freedom: E_{nom}, M_{max} and the electric chiller capacity. They should be determined based on the optimal operating mode (strategy) presented in this section. After determining these three values, sizes of the remaining equipment, such as the absorption chiller and the boiler can be determined.

4. Case study: optimization of a CCHP with supplementary firing

In order to evaluate operation and design of CCHP system with supplementary firing in different climate zones, the hotel located in Dalian, China [3] is selected as a base case study (zone1). There are four single 24 floors buildings in the hotel. The chosen city has warm summers and cold winters. Energy demands of the buildings are shown in Fig. 4. Table 5 provides regional demand coefficients [19] which can be used to determine the demands for other climate zones as shown by Eqs. (38)–(40).

$$E_d^j = f_e^j E_d \tag{38}$$

$$Q_{hd}^j = f_h^j Q_{hd} \tag{39}$$

$$Q_{cd}^j = f_c^j Q_{cd} \tag{40}$$

where superscript j represents different climate zones.

4.1. Solution methodology

Eqs. (1)–(8) and Eqs. (15)–(20) represent the CCHP model which has been optimized based on the performance criteria defined in section 4.2. The model has been written in GAMS version 24.7.4 based on the proposed strategy and solved by finding a starting point (move away from zero value of the variables) by IPOPT version 3.12, finding a local optimum by CONOPT version 3.17A and then solved to optimality by BARON version 16.8.24 (see

Table 3
Decision table for all demands of scenarios A and B.

$E_d < KQ_d$			
	$\frac{Q_{hd}}{\eta_{hc}} > Q_{nom-unf}$		$\frac{Q_{hd}}{\eta_{hc}} \leq Q_{nom-unf}$
	$E_d > E_{nom}$		$E_d \leq E_{nom}$
Scenario B	1-Let $F = F_{nom}$, $\alpha = 0$ 2- Solve Eqs. (24), (27) and (33)	Scenario B	1-Let $F = F_{nom}$, $\alpha = 0$ 2- Solve Eqs. (26), (31), (33) and (34)
	$E_d \leq E_{nom}$		$E_d > E_{nom}$
Scenario A	1-Let $\alpha,\beta = 1$ 2- Solve Eqs. (24) and (27)	Scenario A	Solve (24), (25) and (26)
Scenario B	1-Let $F = F_{nom}$ 2- Solve Eqs. (24), (27) and (33)	Scenario B	1-Solve Eqs. (24)–(26) 2-If α or $\beta \neq 1$, let $F = F_{nom}$ 3- Solve Eqs. (24), (25), (31) and (32)

1060 S.F. Afzali, V. Mahalec / Energy 139 (2017) 1052–1065

Table 4
Decision table for all demands of scenario C.

$E_d \geq KQ_d$	
$Q_d \geq Q_{nom-unf}$	
$\frac{Q_{hd}}{\eta_{hc}} > Q_{nom-unf}$	$\frac{Q_{hd}}{\eta_{hc}} \leq Q_{nom-unf}$
1-Let $F = F_{nom}$, α=0	1-Let $F = F_{nom}$
2-solve Eqs. (27), (33) and (34)	2- Solve Eqs. (25), (31), (32) and (34)
$Q_d \leq Q_{nom-unf}$	
1-Solve Eq. (34) let $F = \frac{Q_d}{(1-\eta_{GT})\eta_{rec}}$	
2- Solve Eqs. (25) and (26)	

separate cooling system.

Primary Energy Consumption Ratio (PECR) is defined as the total amount of fuel used by GT, supplementary firing, the boiler and the electricity imported from the grid in the CCHP system relative to the fuel consumption by the SP system.

$$PECR = \frac{\sum_t \left[F(t) + F_{sf}(t) + \frac{Q_b(t)}{\eta_b} + \frac{E_{grid}(t)+E_{excess}(t)}{\eta_{grid}\eta_{pgu,sp}}\right]}{\sum_t \left\{\left[E_d(t) + \frac{Q_{cd}(t)}{COP_{ec}}\right] \Big/ \left(\eta_{grid}\eta_{pgu,sp}\right) + Q_{hd}(t)/(\eta_b\eta_{hc})\right\}} \tag{41}$$

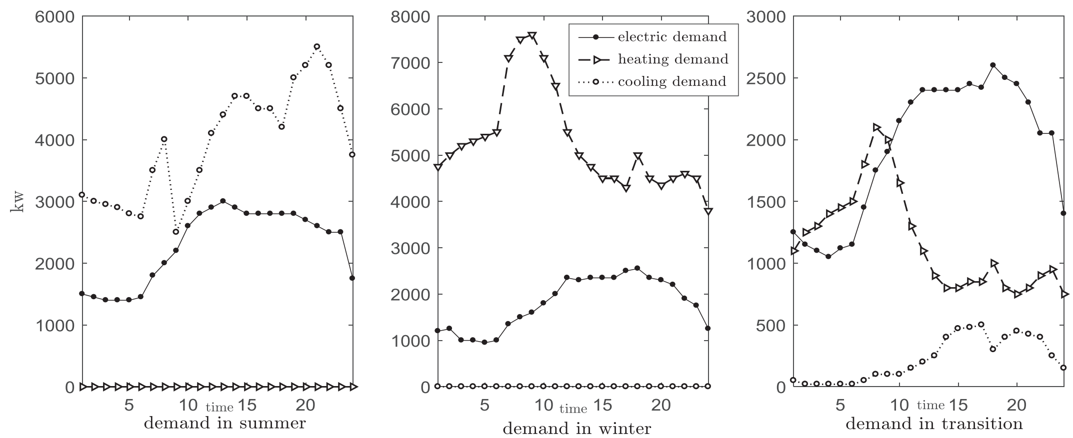

Fig. 4. The energy load of the hotel in zone 1 in respective day.

Table 5
Regional coefficients for calculating annual energy consumption.

Climate zone	climate	Regional coefficient		
		f_e	f_c	f_h
Zone 1	Warm summer, cold winter	1.00	1.00	1.00
Zone 2	Very warm summer, cold winter	1.00	1.5	1.00
Zone 3	Hot summer, cool winter	1.00	2	0.5

Fig. 5).

The maximum execution times for IPOPT, CONOPT and BARON have been set at the 60s, 80s and 3000s, respectively.

4.2. Performance criteria

To optimize the operation of CCHP system with fired HRSG, the sum of equally weighted three indicators is used: primary energy consumption (PEC), CO_2 emissions (CDE), and annual total cost (ATC) which can be expressed as dimensionless ratios in order to be able to consider them simultaneously. The performance with respect to each of these criteria is compared to a separate production system (SP) comprised of a grid, a separate heating, and a

where η_{grid} is the power transmission efficiency.

Annual Total Cost (ATC) includes annualized equipment capital costs and operating costs which include fuel and electricity prices, maintenance cost and other cost related to workers.

$$ATC_{CCHP} = R\sum_i C_i Ca_i + \sum_t \left\{\left[F(t) + F_{sf}(t) + \frac{Q_b(t)}{\eta_b}\right]C_N + \frac{E_{grid}(t) + E_{excess}(t)}{\eta_{grid}}C_E(t)\right\} \tag{42}$$

where Ca_i [kW] is the capacity of each equipment in CCHP, C_i [\$/kW] is the unit price of each equipment per kW, and R [−] is the capital recovery factor defined as follows:

$$R = \frac{i(1+i)^n}{(1+i)^n - 1} \tag{43}$$

Herein i is an interest rate and n is the service life of the equipment. It is assumed that all equipment items have the same service life.

Annual total cost ratio (ATCR) is defined in Eq. (44).

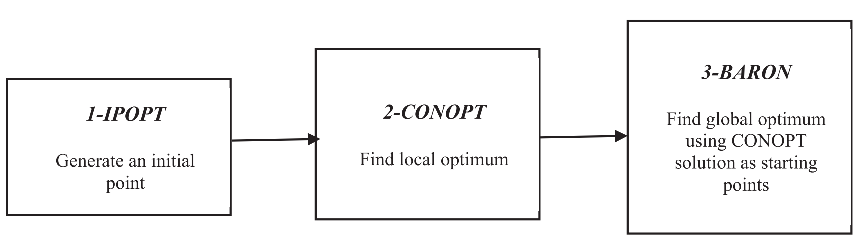

Fig. 5. Application of three different solvers in GAMS for solving NLP.

$$ATCR = \frac{ATC_{CCHP}}{ATC_{SP}} \tag{44}$$

Carbon Dioxide Emissions (CDE) [70] are calculated as follows:

$$CDE = \mu_{CO2,E}E + \mu_{CO2,N}F \tag{45}$$

where E and F represent the electricity from the grid and fuel consumption. *Carbon dioxide emission ratio* (CDER) is defined as shown in Eq. (46).

$$CDER = \frac{\sum_t \left\{ \mu_{CO2,E}\left[E_{grid}(t) + E_{excess}(t)\right] + \mu_{CO2,N}\left[F(t) + F_{sf}(t) + \frac{Q_b(t)}{\eta_b}\right] \right\}}{\sum_t \left\{ \mu_{CO2,E}\left[E_d(t) + \frac{Q_{cd}(t)}{COP_{ec}}\right] + \mu_{CO2,N}\frac{Q_{hd}(t)}{\eta_b \eta_{hc}} \right\}} \tag{46}$$

The objective function is a weighted of sum of the above three criteria, i.e.:

$$\min \psi = \omega_1 PECR + \omega_2 ATCR + \omega_3 CDER \tag{47}$$

where ω_k is a weighting factor for each criteria k. In this work equal weighting factors are assumed, i.e. $\omega_k = \frac{1}{3}, k = 1, 2, 3$.

5. Results and discussions

5.1. Comparison of optimal design of CCHP with fired HRSG and CCHP with unfired HRSG

In order to assess the effectiveness of supplementary firing, design of two configurations is evaluated. The first configuration is a CCHP system with fired HRSG (Y-SF) and the second is a CCHP system with unfired HRSG (N-SF). The CCHP system consists of a GT, fired HRSG, a boiler, an absorption chiller and an electric chiller. Table 6 shows the optimal capacity (output energy) for all three climate zones based on the proposed strategy in section 3. Table 7 shows the improvement [%] in PECR, CDER and ATCR relative to SP system.

For all values of the absorption chiller COPs, the optimal GT size for zone 3 is more than for the other two zones, because the cooling demand in zone 3 is more than the other two zones. This causes some of the cooling demand to be provided by the surplus electricity and the recovered heat produced in the GT Cycle. Because of the larger GT size in this zone, supplementary firing (duct burner) and boiler capacities decrease since more of the recovered exhaust gas heat is available.

In all climate zones and for all absorption chiller COPs (except zone 1 and absorption chiller COP = 0.7), the comparison of CCHP Y-SF and N-SF shows that the use of supplementary firing fuel in the duct burner leads to the reduced sizes of the GT, the electric chiller and the boiler in CCHP Y-SF. This is due to the fact that it is more efficient to meet some of the cooling demand by the surplus fuel burnt in the duct burner instead of using GT with a higher capacity. For zone 1 and with absorption chiller COP = 0.7, use of supplementary firing doesn't change the GT capacity, which is due to the lower COP of absorption chiller, lower efficiency of GT at lower partial load and the lower amount of the cooling demand relative to the other cases.

Improvement in the absorption chiller COP (by e.g. switching from one stage to two stages chiller) causes the capacity of the GT and the electric chiller to decrease. The boiler size will increase because it is more efficient to supplement cooling demand via the absorption chiller. Although the supplementary firing is more effective than the boiler, the supplementary firing size (duct burner size) will decrease, because it has a straight relation with GT size based on Eq. (8).

From Table 6, the boiler is needed in zone 3 of the CCHP Y-SF when the COP of absorption chiller is 1.2 and this is because of the reduction of the GT size. However, the boiler is not needed for other absorption chiller COPs in this zone. Moreover, the electric chiller is a necessary device for all zones of CCHP Y-SF when the single stage absorption chiller is applied. By switching from one stage to two stages chiller, the electric chiller is not required in CCHP Y-SF configuration for zone 1. Also, when the COP = 1.2, the electric chiller is not needed in climate zone 2.

Based on Tables 6 and 7, by using double effect absorption chillers (COP = 0.9 and COP = 1.2), the application of supplementary firing is more valuable. GT size of CCHP Y-SF is less than CCHP N-SF, the boiler and the electric chiller capacity decrease, and the performance of CCHP system based on all criteria will be improved.

In all climate zones, the performance of CCHP system with fired HRSG is more efficient than the CCHP with unfired HRSG. Clearly,

Table 6
Optimal capacity of equipment by using absorption chiller with different COPs.

		GT		SF fuel		Boiler		Absorption chiller		Electric chiller	
		Y-SF	N-SF	Y-SF	N-SF	Y-SF	N-SF	Y-SF	N-SF	Y-SF	N-SF
absorption chiller COP = 0.7	Zone1	2697	2697	3064	0	2514	5236	4700	4400	600	1000
	Zone 2	3295	3326	3040	0	2145	5014	5301	5302	2946	2950
	Zone 3	3683	3700	178	0	0	168	5748	5777	5220	5220
absorption chiller COP = 0.8	Zone1	2350	2406	3050	0	2656	5311	5200	4697	300	798
	Zone 2	3124	3165	3040	0	2543	5079	6520	6270	1840	2010
	Zone 3	3520	3633	1250	0	0	3124	7338	6498	3660	4500
absorption chiller COP = 0.9	Zone1	2273	2350	3048	0	2676	5322	5499	5229	0	468
	Zone 2	2970	3003	3025	0	2368	5136	6986	6740	1260	1509
	Zone 3	3097	3454	2622	0	0	270	8806	7274	2193	3723
absorption chiller COP = 1.2	Zone1	2000	2147	3039	0	2718	5350	5500	5499	0	0
	Zone 2	2354	2406	3010	0	2656	5311	8250	8146	0	102
	Zone 3	2764	2884	1945	0	670	1443	10197	9853	803	1146

Table 7
Improvement [%] of performance criteria due to supplementary firing.

	COP = 0.7			COP = 0.8			COP = 0.9			COP = 1.2		
	Zone1	Zone2	Zone3	Zone1	Zone2	Zone3	Zone1	Zone2	Zone3	Zone1	Zone2	Zone3
Y-SF												
PECR	19.1%	19.4%	11.4%	20.1%	19.9%	12.3%	19.7%	21.2%	14.5%	20.2%	24.1%	19.9%
ATCR	23.1%	24.1%	16.2%	24%	25.4%	18.4%	25.1%	26.6%	20.6%	23.6%	28.7%	24.5%
CDER	32.1%	33.9%	28%	32%	33.9%	28.5%	32.7%	34.7%	29.7%	29.1%	35.6%	33.2%
Ψ	24.8%	25.8%	18.5%	24.7%	26.4%	19.8%	25.8%	27.5%	21.6%	24.3%	29.5%	25.9%
N-SF												
PECR	16.9%	17.5%	10.4%	18.1%	19%	12.7%	17.1%	20.3%	14.4%	19%	23%	19.5%
ATCR	21.4%	22.9%	15.5%	23%	24.1%	17.2%	22.5%	25.2%	19.5%	22.3%	27.5%	23.8%
CDER	30%	32.1%	27%	30%	33.1%	28.7%	26.7%	34%	29.9%	28.4%	34.8%	33.1%
ψ	22.8%	24.1%	17.6%	23.7%	25.4%	19.5%	22.1%	26.5%	21.3%	23.3%	28.4%	25.4%

CCHP system will be improved for all criteria PECR, CDER and ATCR by adding supplementary firing. For zone 1, the best optimal design can be obtained by using an absorption chiller with COP = 0.9 and for CCHP Y-SF configuration. The percentage of reduction of the objective function with respect to SP system is 25.8%. For other two zones, zone 2 and zone 3, the best optimal designs are when COP = 1.2 because of the higher thermal demands with respect to zone1.

Section D of supplementary material explains differences between the optimum design of the CCHP based on a single-objective function and based on a weighted sum of multi-objectives function.

5.2. Sensitivity analysis

The costs of the natural gas and the electricity are very important when designing a CCHP system. To evaluate the effect of the natural gas price on the design of CCHP system for both configurations, the electric price is kept constant and the natural gas price changes from 0.02 to 0.08 $/kWh [71].

Fig. 6 shows the gas turbine sizes for both CCHP configurations for a hotel located in the climate zone 2 and for four different absorption chiller COPs. For when COP = 0.7, the GT size of CCHP Y-SF is smaller than GT size in CCHP N-SF when the natural gas price is less than 0.0371 $/kWh. For a higher natural gas price, both

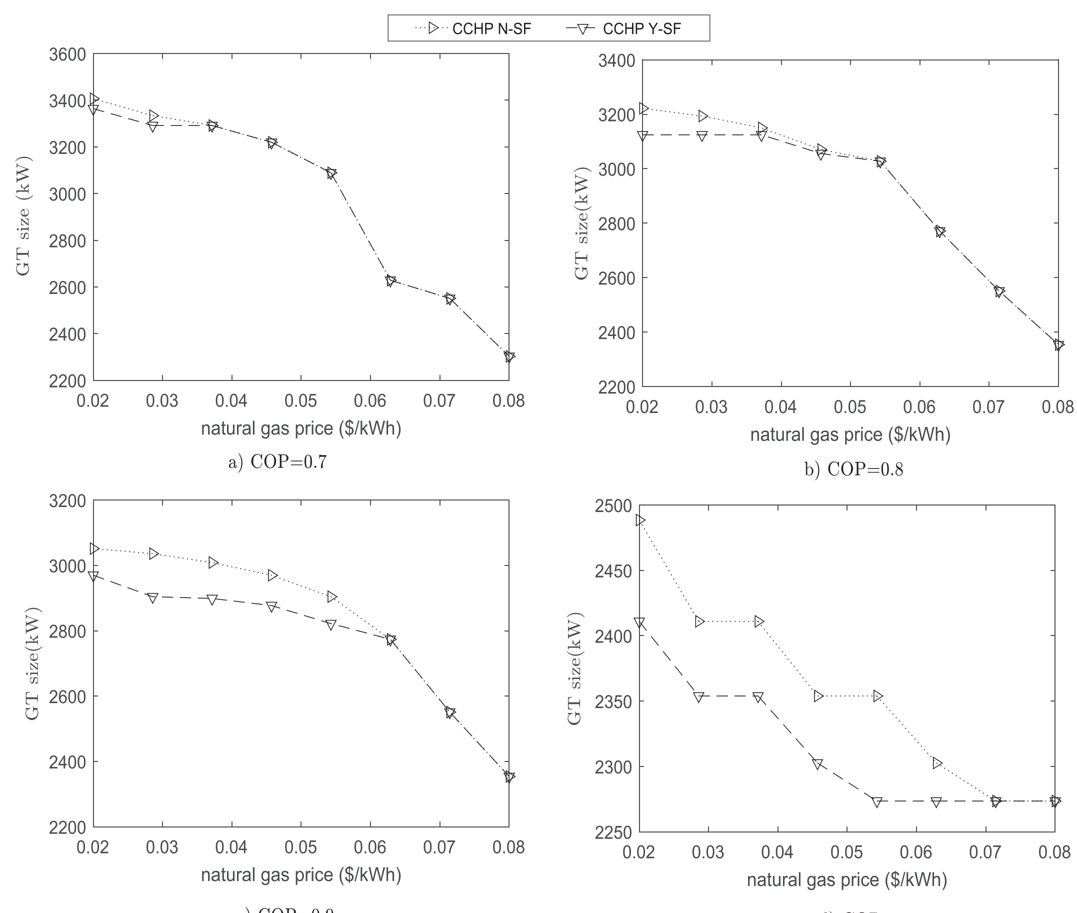

Fig. 6. Comparison of GT sizes for CCHP configurations Y-SF and N-SF for different absorption chiller COPs vs. The natural gas price.

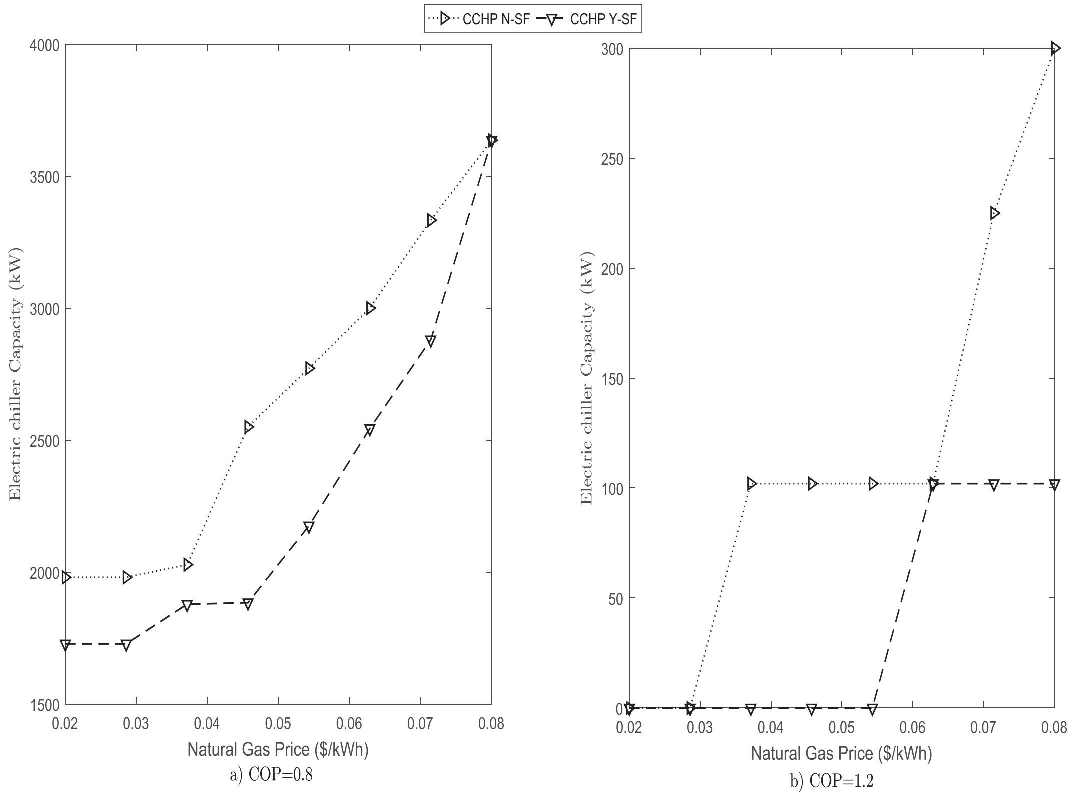

Fig. 7. Comparison of electric chiller sizes for both CCHP configurations for climate zone 2 vs. The natural gas price.

configurations have the same size GTs. This means that introduction of supplementary firing doesn't affect the GT size when the gas price is higher than 0.0371 \$/kWh. Use of absorption chiller with higher COP enables the application of supplementary firing to reduce the GT size in a wider range of natural gas price such as it can be seen in Fig. 6.

The more interesting is the effect of supplementary firing on the electric chiller capacity. As shown in Fig. 7, when an absorption chiller with COP = 0.8 is used, the size of the electric chiller for CCHP Y-SF is smaller than the electric chiller capacity for CCHP N-SF for all natural gas prices except the highest price (0.08\$/kWh). If the absorption chiller has COP = 1.2, there is no need to the electric chiller in CCHP Y-SF when the natural gas price is less than 0.0629 \$/kWh; configuration CCHP N-SF, on the other hand, uses the electric chiller if the natural gas price is higher than 0.0371 \$/kWh.

6. Conclusions

In this paper, optimal design and operation of CCHP system comprising of a gas turbine, a fired HRSG, an electric chiller, an absorption chiller and a natural gas-fired boiler have been investigated. The operation of a CCHP system has been classified in three scenarios based on the GT capacity, thermal loads and the electrical loads. Analytical expressions for computation of the values of the price ratio (price of electricity/price of natural gas) which delimit the three modes of scenario with high cooling loads have been presented. These expressions enable straightforward selection of the optimal operating strategy based on the value of the price ratio, without having to resort to numerical optimizations. Our main conclusions for a CCHP system are as follows:

- CCHP system with fired HRSG has lower primary energy consumption ratio, lower annualized total cost ratio, and lower carbon dioxide emission ratio than the system of the same structure but without having supplementary firing.
- Based on the proposed strategy, application of both CCHP with fired HRSG and CCHP with unfired HRSG is more efficient than the SP system.
- Use of supplementary firing reduces the optimal size of the gas turbine, especially for the climate zones with hot summers (zone 2 and zone 3).
- An improvement in the absorption chiller COP will lead to a smaller capacity of the gas turbine. As a result, the electric chiller capacity decreases and the boiler size increases.
- The increase of COP of the absorption chiller makes possible to decrease the size of the gas turbine over a wider range of price ratio when using supplementary firing.
- Application of supplementary firing enables reduction of the size of the boiler and the electric chiller for all the price ratios and absorption chillers with various values of the coefficient of performance.
- When the cooling demand is low, i.e. there is a ‘warm summer’ (zone 1), application of supplementary firing decreases GT size when the absorption chiller with high COP is used or when the price ratio is high.
- For zone 3 with high cooling demand, optimal design requires an electric chiller in both configurations of CCHP system. In this zone, the boiler is not needed for all absorption chiller COPs except COP = 1.2 in CCHP Y-SF.

Presented here, analytical expressions for determining optimal operating strategy (which parts of the system are “on” or “off”) of the three scenarios and the analytical criteria for determining optimal modes for providing cooling under different (electricity/natural gas) ratios can be readily applied in operation or in design of CCHP systems with supplementary firing.

Appendix A. Supplementary data

Supplementary data related to this article can be found at http://dx.doi.org/10.1016/j.energy.2017.08.029.

References

[1] Keshavarz Ali, Ebrahimi M. Combined cooling, heating and power decision-making, design and optimization. Elsevier; 2015.
[2] Petchers N. Combined heating, cooling & power handbook technologies and applications: an integrated approach to energy resource optimization. Lilburn: Farirmont Press; 2003.
[3] Li M, Mu H, Li N, Ma B. Optimal design and operation strategy for integrated evaluation of CCHP (combined cooling heating and power) system. Energy 2016;99:202–20.
[4] Mago PJ, Chamra LM, Ramsay J. Micro-combined cooling, heating and power systems hybrid electric-thermal load following operation. Appl Therm Eng 2010;30:800–6.
[5] Fang F, Wei L, Liu J, Zhang J, Hou G. Complementary configuration and operation of a CCHP-ORC system. Energy 2012;46:211–20.
[6] Knizley A, Mago PJ, Tobermann J, Warren HR. Performance characterization of a power generation unit – organic Rankine cycle system based on the efficiencies of the system components. Energy Convers Manag 2015;105:480–7.
[7] Wang JJ, Jing YY, Zhang CF. Optimization of capacity and operation for CCHP system by genetic algorithm. Appl Energy 2010;87:1325–35.
[8] Smith AD, Mago PJ, Fumo N. Benefits of thermal energy storage option combined with CHP system for different commercial building types. Sustain Energy Technol Assessments 2013;1:3–12.
[9] Zheng CY, Wu JY, Zhai XQ, Wang RZ. A novel thermal storage strategy for CCHP system based on energy demands and state of storage tank. Electr Power Energy Syst 2017;85:117–29.
[10] Wang JJ, Jing YY, Bai H, Zhang JL. Economic analysis and optimization design of a solar combined cooling heating and power system in different operation strategies, vol. 92. ICIEA; 2012. p. 108–12.
[11] Basrawi F, Ibrahim H, Yamada T. Optimal unit sizing of biogas-fuelled micro gas turbine cogeneration systems in a sewage treatment plant. Energy Procedia 2015;75:1052–8.
[12] Basrawi F, Ibrahim TK, Habib K, Yamada T. Techno-economic performance of biogas-fueled micro gas turbine cogeneration systems in sewage treatment plants: effect of prime mover generation capacity. Energy 2017;124:238–48.
[13] Fumo N, Mago PJ, Smith AD. Analysis of combined cooling, heating, and power systems operating following the electric load and following the thermal load strategies with no electricity export. J Power Energy 2011:1–10.
[14] Liu M, Shi Y, Fang F. A new operation strategy for CCHP systems with hybrid chillers. Appl Energy 2012;95:164–73.
[15] Tan ZF, Zhang HJ, Shi QS, Song YH, Ju LW. Multi-objective operation optimization and evaluation of large-scale NG distributed energy system driven by gas-steam combined cycle in China. Energy Build 2014;76:572–87.
[16] Ju L, Tan Z, Li H, Tan Q, Yu X, Song X. Multi-objective operation optimization and evaluation model for CCHP and renewable energy based hybrid energy system driven by distributed energy resources in China. Energy 2016;111:322–40.
[17] Yun K, Luck R, Mago PJ, Smith A. Analytic solutions for optimal power generation unit operation in combined heating and power systems. J Energy Resour Technol 2012;134:1–8.
[18] Zheng CY, Wu JY, Zhai XQ. A novel operation strategy for CCHP systems based on minimum distance. Appl Energy 2014;128:325–35.
[19] Zheng CY, Wu JY, Zhai XQ, Wang RZ. Impacts of feed-in tariff policies on design and performance of CCHP system in different climate zones. Appl Energy 2016;175:168–79.
[20] Basrawi F, Ibrahim TK, Habib K, Yamada T. Effect of operation strategies on the economic and environmental performance of a micro gas turbine trigeneration system in a tropical region. Energy 2016;97:262–72.
[21] Li L, Mu H, Li N, Li M. Analysis of the integrated performance and redundant energy of CCHP systems under different operation strategies. Energy Build 2015;99:231–42.
[22] Calise F, Dentice M, Libertini L, Quiriti E, Vicidomini M. A novel tool for thermoeconomic analysis and optimization of trigeneration systems: a case study for a hospital building in Italy. Energy 2017;126:64–87.
[23] Basrawi F, Yamada T. Economic and environmental based operation strategies of a hybrid photovoltaic – microgas turbine trigeneration system. Appl Energy 2014;121:174–83.
[24] Chen L, Wu C, Sun F. Finite time thermodynamic optimization or entropy generation minimization of energy systems. J Non-Equilibrium Thermodyn 1999;24:327–59.
[25] Ge Y, Chen L, Sun F. Progress in finite time thermodynamic studies for internal combustion engine cycles. Entropy 2016;18:139.
[26] Chen L, Wu C, Chen J. Recent advances in finite time thermodynamics. New York: Nova Science Publishers; 1999.
[27] Chen L, Feng H, Xie Z. Generalized thermodynamic optimization for Iron and Steel production processes: a theoretical exploration and application cases. Entropy 2016;18:353.
[28] Yang B, Chen L, Sun FR. Exergetic performance optimization of an endoreversible variable-temperature heat reservoirs intercooled regenerated Brayton cogeneration plant. J Energy Inst 2015;89:1–11.
[29] Tao G, Chen L, Sun F. Exergoeconomic performance optimization for an endoreversible regenerative gas turbine closed-cycle cogeneration plant. Riv Mex Fis 2009;55:192–200.
[30] Yang B, Chen LG, Sun FR. Finite time exergoeconomic performance of an irreversible intercooled regenerative Brayton cogeneration plant. J Energy Inst 2011;9671:5–12.
[31] Bo Y, Chen L, Ge Y, Sun F. Exergy performance analyses of an irreversible two-stage intercooled regenerative reheated closed Brayton CHP plant. Int J Exergy 2014;14:459–83.
[32] Chen L, Yang B, Ge Y, Sun FR. The finite-time exergoeconomic performance of a real, intercooled, regenerated gas-turbine cogeneration plant. Part 1: model description and parametric analyses. Int J Low-Carbon Technol 2014;2014(9):29–37.
[33] Yang B, Chen L, Ge Y, Sun F. Finite-time exergoeconomic performance of a real intercooled regenerated gas turbine cogeneration plant. Part 2: heat conductance distribution and pressure ratio optimization. Int J Low-Carbon Technol 2014;9:262–7.
[34] Yang B, Chen L, Ge Y, Sun FR. Exergy performance optimization of an irreversible closed intercooled regenerative brayton cogeneration plant. Arab J Sci Eng 2014;39:6385–97.
[35] Chen L, Feng H, Sun F. Exergoeconomic performance optimization for a combined cooling, heating and power generation plant with an endoreversible closed Brayton cycle. Math Comput Model 2011;54:2785–801.
[36] Feng H, Chen L, Sun FR. Exergoeconomic optimal performance of an irreversible closed Brayton cycle combined cooling, heating and power plant. Appl Math Model 2011;35:4661–73.
[37] Chen LG, Feng HJ, Sun FR. Exergy optimisation of irreversible closed Brayton cycle combined cooling, heating and power plant. J Energy Inst 2013;86:97–106.
[38] Schneider M, Jacobs III J. Cogeneration application considerations. GE Energy Rep 2009:1–48. http://site.geenergy.com/prod_serv/products/tech_docs/en/downloads/GER3430G.pdf.
[39] Al-Abri BA. Surface-subsurface model for the techno-economic and risk evaluation of thermal EOR projects. PhD Thesis. Bedfordshire, UK: Cranfield University; 2011.
[40] Gnanapragasam NV, Reddy BV, Rosen MA. Effect of supplementary firing options on cycle performance and CO_2 emissions of an IGCC power generation system. Int J Energy Res 2009;33:645–61.
[41] Li H, Ditaranto M, Berstad D. Technologies for increasing CO_2 concentration in exhaust gas from natural gas-fired power production with post-combustion, amine-based CO_2 capture. Energy 2011;36:1124–33.
[42] Ahmadi P, Dincer I, Rosen MA. Exergy, exergoeconomic and environmental analyses and evolutionary algorithm based multi-objective optimization of combined cycle power plants. Energy 2011;36:5886–98.
[43] Ahmadi P, Dincer I. Thermodynamic analysis and thermoeconomic optimization of a dual pressure combined cycle power plant with a supplementary firing unit. Energy Convers Manag 2011;52:2296–308.
[44] Boyaghchi FA, Molaie H. Advanced exergy and environmental analyses and multi objective optimization of a real combined cycle power plant with supplementary firing using evolutionary algorithm. Energy 2015;93:2267–79.
[45] Díaz AG, Fernández ES, Gibbins J, Lucquiaud M. Sequential supplementary firing in natural gas combined cycle with carbon capture: a technology option for Mexico for low-carbon electricity generation and CO_2 enhanced oil recovery. Int J Greenh Gas Control 2016;51:330–45.
[46] El-Nashar A. Cogeneration for power and desalination—state of the art review. Desalination 2001;134:7–28.
[47] Martelli E, Amaldi E, Consonni S. Numerical optimization of heat recovery steam cycles: mathematical model, two-stage algorithm and applications. Comput Chem Eng 2011;35:2799–823.
[48] Yang C, Huang Z, Yang Z, Ma X. Analytical off-design characteristics of gas turbine-based CCHP system. Energy Procedia 2015;75:1126–31. Elsevier B.V.
[49] Kehlhofer R, Hannemann F, Stirnimann F, Rukes B. Combined-cycle gas & steam turbine power plants. Tulsa, Okla: USA: PennWell Corporation; 2009.
[50] Shabbir I, Mirzaeian M. Feasibility analysis of different cogeneration systems for a paper mill to improve its energy efficiency. Int J Hydrogen Energy 2016;1:16535–48.
[51] Bindlish R. Power scheduling and real-time optimization of industrial cogeneration plants. Comput Chem Eng 2016;87:257–66.
[52] Mitra S, Sun L, Grossmann IE. Optimal scheduling of industrial combined heat and power plants under time-sensitive electricity prices. Energy 2013;54:194–211.
[53] Mokheimer EMA, Dabwan YN, Habib MA, Said SAM, Al-sulaiman FA. Development and assessment of integrating parabolic trough collectors with steam generation side of gas turbine cogeneration systems in Saudi Arabia. Appl Energy 2015;141:131–42.
[54] Rossiter AP. Criteria for Integration of Combined cycle cogeneration systems in the process industries. Heat Recover Syst CHP 1990;10:37–48.
[55] Jabbari B, Tahouni N, Ataei A, Panjeshahi MH. Design and optimization of CCHP system incorporated into kraft process, using Pinch Analysis with pressure drop consideration. Appl Therm Eng 2013;61:88–97.
[56] Combined heat and power (CHP) level 1 feasibility analysis. Environ prot agency. 2015. http://www.epadatadump.com/pdf-files/combined_heat_and_

power_chp_level_1_feasibility_analysis_ethanol_facility.pdf.
[57] Mago PJ, Chamra LM. Analysis and optimization of CCHP systems based on energy, economical, and environmental considerations. Energy Build 2009;41:1099–106.
[58] Ganapathy V. Efficiently generate steam from cogeneration plants. Chem Eng 1997:104.
[59] Tymofii T, Nord N. Uncertainty of the allocation factors of heat and electricity production of combined cycle power plant. Appl Therm Eng J 2015;76:410–22.
[60] Bischi A, Taccari L, Martelli E, Amaldi E, Manzolini G, Silva P, et al. A detailed optimization model for combined cooling, heat and power system operation planning. ECOS 2013;2013(74):1–10.
[61] Ganapathy V. Industrial boilers and heat recovery steam generators. 2003. Texas, U.S.A.
[62] Boyaghchi FA, Molaie H. Investigating the effect of duct burner fuel mass flow rate on exergy destruction of a real combined cycle power plant components based on advanced exergy analysis. Energy Convers Manag 2015;103:827–35.
[63] Charles E. Baukal j. Industrial burners handbook. New York: CRC Press; 2003.
[64] Schöpfer MD. Absorption chillers: their feasibility in district heating networks and comparison to alternative technologies. Instituto Superior Técnico Lisboa; 2015.
[65] Conte B, Bruno JC, Coronas A. Optimal cooling load sharing strategies for different types of absorption chillers in trigeneration plants. Energies 2016;9:1–16.
[66] Kang L, Yang J, An Q, Deng S, Zhao J, Wang H, et al. Effects of load following operational strategy on CCHP system with an auxiliary ground source heat pump considering carbon tax and electricity feed in tariff. Appl Energy 2017;194:454–66.
[67] Gomri R. Second law comparison of single effect and double effect vapour absorption refrigeration systems. Energy Convers Manag 2009;50:1279–87.
[68] Jiang R, Qin FGF, Yin H, Yang M, Xu Y, Yin H, et al. Thermo-economic assessment and application of CCHP system with dehumidification and hybrid refrigeration. Appl Therm Eng 2017. http://dx.doi.org/10.1016/j.applthermaleng.2017.07.048.
[69] Jiang-jiang W, Chun-fa Z, You-yin J. Multi-criteria analysis of combined cooling, heating and power systems in different climate zones in China. Appl Energy 2010;87:1247–59.
[70] Mago PJ, Smith AD. Evaluation of the potential emissions reductions from the use of CHP systems in different commercial buildings. Build Environ 2012;53:74–82.
[71] Kang L, Yang J, An Q, Deng S, Zhao J, Li Z, et al. Complementary configuration and performance comparison of CCHP-ORC system with a ground source heat pump under three energy management modes. Energy Convers Manag 2017;135:244–55.

Nomenclature

Acronyms

ATC: annual total cost [$]
ATCR: annual total cost ratio
CCHP: combined cooling, heat and power system
CDE: CO_2 emission
CDER: CO_2 emission ratio
CHP: combined heating and power system
COP: coefficient of performance
FEL: following the electrical load
FLB: following the load of buildings
FSS: following seasonal strategy
GHG: greenhouse gas
FTL: following the thermal load
GT: gas turbine
HRSG: heat recovery steam generator
kW: kilowatt
MILP: mixed integer linear programming
N-SF: CCHP without supplementary firing
NLP: nonlinear programming
ORC: Organic Rankine Cycle
PEC: primary energy consumption
PECR: primary energy consumption ratio
PGU: power generation unit
SF: supplementary firing
SP: separate production system
VOC: variable operational cost
Y-SF: CCHP with supplementary firing

Variables

C: cost ($)
c,c': correction factors
Ca: capacity of equipment [kW]
Cp: heat capacity [kJ/kg K]
E: electric energy [kW]
F: fuel energy [kW]
i: interest rate
K: electrical to thermal outputs of CCHP
M : ratio of supplementary firing fuel energy to the gas turbine fuel energy
n: service life [year]
Q: thermal energy [kW]
R: capital recovery factor
W: exhaust gas flow rate [kg/s]

Superscripts

j: climate zone

Greek

η: efficiency
δ: portion of the boiler energy absorbed by heating coil
θ: temperature [K]
μ: emission conversion factor
β: portion of recovered heat absorbed by heating coil
α: electric cooling to cool ratio
δ: portion of the boiler energy absorbed by the heating coil
σ: the electricity price to the fuel price
ω: weighting factor
ψ: objective function
γ: portion of recovered heat used in the absorption chiller

Subscripts

ac: absorption chiller
b: boiler
cd: cooling demand
d: demand
DB: duct burner
ec: electric chiller
eff: effective
ex: exhaust gas
Excess: excess
f: fired mode
grid: grid
hc: heating coil
hd: heating demand
k: the kth criteria
loss: loss
N: natural gas
nom: nominal
rec: recovery
rem: remaining
s: stack
SP: separate production system
unf: unfired mode

Chapter 3

Novel performance curves to determine optimal operation of CCHP systems

The contents of this chapter have been published in the following peer reviewed journal:

Afzali SF, Mahalec V. Novel performance curves to determine optimal operation of CCHP systems. *Appl Energy* 2018;226:1009–36. doi:10.1016/j.apenergy.2018.06.024.

Applied Energy 226 (2018) 1009–1036

Contents lists available at ScienceDirect

Applied Energy

journal homepage: www.elsevier.com/locate/apenergy

Novel performance curves to determine optimal operation of CCHP systems

Sayyed Faridoddin Afzali, Vladimir Mahalec*

Department of Chemical Engineering, McMaster University, 1280 Main St. West, Hamilton, ON L8S 4L8, Canada

HIGHLIGHTS

- Novel performance curve (NPC) to optimize CCHP operation.
- NPC considers changes in energy prices, fuel consumption and CO_2 emissions factors.
- NPC methodology leads to the better CCHP operation than other strategies.
- Thermal, electric, hybrid load following strategies are subset of NPC strategy.
- Match performance strategy is a subset of NPC strategy.

ARTICLE INFO

Keywords:
CCHP system
Operation strategies
CCHP novel performance curves
PGU optimal load
CCHP operating curve

ABSTRACT

Economic and environmental impact of a combined cooling, heating and power (CCHP) system depends not only on its structure but also on the way it is operated. In this paper, a novel methodology which utilizes overall optimal partial loads of power generation unit (PGU) and novel performance curves (NPC) is proposed to optimize CCHP operation. The PGU overall optimum partial loads for demands below and above the CCHP operating curve are determined based on the optimization criteria and system characteristics. Proposed methodology is flexible and adaptable; it accounts for energy prices, carbon dioxide emissions, primary energy consumption factors and load variations with the weather conditions. Other strategies, such as following match performance, hybrid load, electric load, and thermal load strategies are shown to be the special cases of the NPC methodology. The performance of a CCHP system which operates based on the NPC methodology is compared to the CCHP performances when following match performance, hybrid load, electric load, and thermal load strategies. The comparison is carried out for two small hotel buildings in San Francisco and Miami and residential buildings in Dalian having different energy demand profiles. These locations have different energy prices, carbon dioxide emissions and primary energy consumption factors. The proposed methodology leads to the best operation when compared to other operating strategies based on operating cost, carbon dioxide emissions, primary energy consumption and a combination of them which is not always the case for other operating strategies. Proposed methodology provides a unifying framework which includes all previously operating strategies.

1. Introduction

Combined cooling, heating and power systems (CCHP) are widely utilized as effective energy production systems to provide electricity, cooling and heating. Applications of CCHP systems have been increasing in large and small-scale buildings to solve the energy-related problems, such as increasing energy cost, increasing energy demand and environmental issues [1].

The use of CCHP systems has been investigated for various kinds of buildings, such as office buildings [2], hotels [3], residential buildings [4] and other types of commercial buildings. Electrical, cooling and heating demands of a building vary during a day and also vary throughout a year. The energy output of a CCHP system typically cannot match either the electrical demand or the heating load or the cooling load. As a result, scheduling of the CCHP operation, selecting an appropriate system configuration and a proper size of power generation unit are vital in order to achieve a high energy efficiency, economic benefits and also reduce the greenhouse gas (GHG) emissions.

There have been many papers dealing with different configurations of a CCHP system. The common and simple CCHP system comprises a power generation unit (PGU), a heat recovery system, a heating coil or a heat exchanger, an absorption chiller and a boiler [5]. To improve the cooling efficiency, an electric chiller has been added to the CCHP system to provide additional cooling from the electricity [6]. In order to

* Corresponding author.
E-mail address: mahalec@mcmaster.ca (V. Mahalec).

https://doi.org/10.1016/j.apenergy.2018.06.024
Received 20 February 2018; Received in revised form 1 June 2018; Accepted 2 June 2018
Available online 20 June 2018
0306-2619/

Nomenclature

Acronyms

ATC	annual total cost
CCHP	combined cooling, heating and power
CDE	CO_2 emission
CHP	combined heat and power
COP	coefficient of performance
FEL	following the electrical load
FTL	following the thermal load
FHL	following hybrid load
FLB	following the load of the building
FSS	following seasonal strategy
GSHP	ground source heat pump
LB	lower bound
MP	match performance
NPC	novel CCHP performance curve
kW	kilowatt
ORC	Organic Rankine cycle
PEC	primary energy consumption
PGU	power generation unit

Variables

C	cost [$/kW]
E	electric energy [kW]
F	fuel energy [kW]
f	partial load of PGU
G	PEC ratio
k	CCHP operating curve equation
Q	heating energy [kW]
R	price ratio
S	CDE ratio
Cr	criteria

Greek

η	efficiency
μ	emission conversion factor
δ	objective function
Δ	increasing the objective function
φ	objective function
ω	weighting factor
ψ	performance curve

Subscripts

ab	heating to absorption chiller
ac	absorption chiller
b	base
boiler	boiler
cd	cooling demand
CDE	carbon dioxide emission
combination	a combination of criteria
cost	cost
d	demand
f	partial load
th	thermal
SP	separate production
UB	upper bound
diff	difference of LB and UB
E	electricity
ec	electric chiller
f	fuel
fb	partial load at base
fl	partial load at f
g	natural gas
grid	grid
hc	heating coil
hd	heating demand
i	number of criteria
LB	lower bound
min	minimum
max	maximum
nom	nominal
rec	recovery
SP	separate production
UB	upper bound

Superscripts

above	above the operating curve
below	below the operating curve
LHS	left-hand side
mid	mid-peak period
off	off-peak period
on	on-peak period
RHS	right-hand side

obtain a wide range of electric output to thermal output ratio, application of the thermal energy storage has been analyzed extensively [7]. Thermal energy storage can help manage CCHP thermal output to meet cooling and heating demands at peak loads. Mago et al. [8] investigated the operation of a combined heat and power system with dual power generation units and thermal energy storage. Song et al. [9] studied the performance of CCHP system utilized in a data center; the cooling storage was employed to store the excess cooling energy and then provide cooling energy when it was needed. Furthermore, a battery has been employed to manage the electric output of the system [10]. Fang et al. [11] investigated performance of a CCHP integrated with an organic ranking cycle (ORC) and an electric chiller by proposing a strategy which is applicable for a wide range of loads. Knizley et al. [12] compared performance of an ORC-CHP system to the conventional system in terms of operating cost, primary energy consumption (PEC) and carbon dioxide emissions (CDE). To attain flexibility in heating and cooling outputs, ground source heat pump (GSHP) was added to a CCHP system and analyzed in [13]. Liu et al. [14] analyzed performance of a CCHP system which included a GSHP and thermal energy storage. The CCHP performance was studied by assuming two types of PGU; gas turbine and an internal combustion engine. A CCHP system driven by gas–steam combined cycle was suggested for application in an educational center in China [15]. Distributed energy resources, such as solar energy and wind energy have been integrated with a CCHP system to enhance the efficiency of the system and reduce the pollution [16]. Fu et al. [17] studied the performance of a CCHP system consisting of an internal combustion engine, a flue gas heat exchanger, a jacket water heat exchanger and an absorption heat pump. They compared the operation of this system to the performance of conventional CHP system [18].

Operating strategies for CCHP systems have been studied in many papers. In the review below, we will summarize the extent of reduction as% of the specific objective; positive% means that the objective was reduced, negative% means that the objective was increased as a result of applying specific strategy. Following the electrical load (FEL) and following the thermal load (FTL) are two frequently used operating strategies. Jing et al. [5] carried out exergy analysis and energy analysis and also assessed the annual total cost (ATC) and CDE of a CCHP system by examining FEL and FTL strategies. Following hybrid load (FHL) is an improved strategy which has been applied to CCHP systems by [19]; this strategy switches the operation of the CCHP system between FTL and FEL with the aim of reducing the excess electric and thermal outputs of a CCHP system. The comparison of the performances of CCHP employed in the residential building in Columbus was carried out for FHL, FEL and FTL strategies. The percentages of PEC, operating cost and CDE reductions due to FHL were 7.47%, 4.36%, and 14.62%. Results were not as good when applying either FEL strategy (−0.5%%, −12%, and 13.7%, respectively) or FTL strategy (5%, −2%, and 12.5%, respectively). Zheng et al. [6] investigated the effect of the feed-in tariff on the design and performance of CCHP system. They assumed four different operating strategies which are FEL, FTL FHL, and maximum load strategy. In the maximum load strategy, the larger demand of the thermal demand and the electrical demand is satisfied by CCHP system. Liu et al. [20] presented a new operating strategy for a CCHP system which has hybrid chillers (both: thermally powered and also electricity-powered chillers). Electric cooling (cooling energy which is provided by the electric chiller) ratio to the total cooling demand changes hourly in this strategy. This strategy is designated as MP strategy because the intent is to match the CCHP energy outputs with demands. The proposed strategy was implemented for managing the operation of a CCHP system deployed at a hotel in Victoria, Canada. It was shown that the percentage of PEC reduction was 8% via MP strategy, while FEL and FTL had reductions (increase) of −8% and 2%, respectively. ATC reductions were 37%, 6%, and 32% by applying the MP, FEL and FTL strategies, respectively. Similarly, the highest CDE reduction (25%) was obtained by implementing MP strategy, while other strategies had worse performance FEL (21%) and FTL (7%). The strategy was developed when a fired heat recovery steam generator was added to a CCHP system [21]. The proposed strategy was applied to determine the size of a CCHP system for a hotel in Dalian, China. The reductions of PEC, ATC, and CDE were 19.1%, 23.1%, and 32.1%, respectively, when the CCHP system included the fired heat recovery steam generator. By using the unfired heat recovery steam generator, the values of the criteria reduction were 16.9%, 21.4%, and 30%, respectively. Wang et al. [22] optimized the capacity of PGU with hybrid chillers by using FTL strategy. Wang et al. [23] assumed the cooling ratio to be fixed during CCHP operation. Wang et al. [10] proposed an improved FEL strategy to optimize the performance of a CCHP system based on PEC. In this strategy, PGU operated to meet daily average electrical demand. The proposed strategy was applied to four types of buildings; hotel, hospital, office and a mall. The improvements of PEC due to the application of improved FEL strategy over base FEL strategies were 0.89%, 0.4%, −0.08%, and 0.01% for hotel, hospital, office and mall, respectively. Li et al. [24] proposed two additional strategies, following the thermal-electrical load of buildings (FLB) and following the seasonal strategy (FSS). In FLB, an optimum load ratio is computed. If the ratio of hourly electric load to hourly thermal load is less than this value, then the system should follow FTL strategy. Otherwise, FEL strategy is applied. FSS strategy follows the same procedure. The ratio of monthly electric load to monthly thermal load is compared to one. If the ratio is more than one, then the optimum strategy is FEL. Otherwise, CCHP system operates based on FTL. In this study, the applications of FEL, FTL, FHL, FSS, and FLB strategies were examined for CCHP system deployed in residential buildings and office buildings in Dalian, China. For example, for office buildings, the percentages of ATC reduction via FEL, FTL, FHL, FSS, and FLB were 20%, 8%, 9%, 18%, and 22%, respectively in comparison to the standalone systems. The PEC reduction via implementing these strategies were 11%, 9%, 10%, 8%, and 13%, respectively, while CDE reductions were 37%, 22%, 22%, 36%, and 39%, respectively. Ligai et al. [25] compared four different strategies, FTL, FEL, FHL and maximum efficiency of PGU. Based on the maximum efficiency of PGU, the PGU operates at a constant load level which corresponds to the maximum PGU efficiency whatever thermal demand or electric demand is. They have demonstrated that following the maximum electric efficiency of PGU is more beneficial when carbon tax and electricity feed-in tariff are included in the economic analysis. In this case, it was demonstrated that the highest reductions due to the application of the Maximum efficiency strategy were 4.2%, 42.5%, 78.5% and 169.5% for ATC, operating cost, CDE, and PEC, respectively. The operating cost, CDE and PEC reduction of the FEL were 34.8% and 42.3% and 46%, respectively, while the reduction of these criteria by employing FTL strategy were 25%, 40%, and 68.7%, respectively. The smallest reductions in operating cost, CDE and PEC were obtained by applying FHL strategy which were 25.9%, 32.0% and 44.1%, respectively. Another operating strategy based on the minimum distance of the load to the operating curve of a PGU was introduced by Zheng et al. [26]. They concluded that the proposed strategy was more beneficial than FTL, FEL and FHL strategies for CDE and ATC criteria. For instance, the percentages of the ATC reduction were 40%, 37%, 34%, and 36% when employing the minimum distance, FEL, FTL, and FHL, respectively. FHL was the best for reducing the PEC (44%) compared to the minimum distance (42%), FEL (34%), and FTL (37%). FEL was improved in [27] when two PGU units were deployed in parallel, since operational flexibility increased due to availability of the parallel PGUs. Fang et al. [28] proposed an optimal switching strategy based on an integrated performance criterion. The integrated performance criterion included primary energy consumption, carbon dioxide emissions and operating cost. Based on the value of the integrated performance criterion either FEL or FTL were selected to manage the PGU operation. The performance of CCHP system stemming from this strategy was compared to the CCHP performance operates based on FHL strategy. When this strategy was implemented, the reductions of the PEC, CDE and operating cost were 8%, 22.5%, and 24%, respectively, for a typical winter day. By employing FHL strategy, the reductions were 15.2%, 20%, and 19%, respectively. Urbanucci and Testi [29] employed two-stage stochastic programming to optimize the design and operation of CHP system under demand uncertainties by using minimum cost strategy that lead to the minimum annual operating cost. Fumo et al. [30] proposed an emission reduction operating strategy for managing the way CCHP system operates. As a part of this strategy, the ratio of the carbon dioxide emissions via the separate production system application to the carbon dioxide emissions from CCHP system usage is calculated. If the ratio is more than or equal to one, the CCHP system should operate to supply the demand. Otherwise, PGU is off and the separate production system is utilized to provide the demand.

Optimal operating strategy for a CCHP system needs to consider various performance criteria, such as operating cost, CDE and PEC while meeting demands for heating, cooling and electricity throughout a year. In this work we introduce a novel framework for such optimization and demonstrate that improvements are possible when compared to the previously published operating strategies; in addition, we show that the previously published operating strategies are special cases of the methodology introduced by this work.

Novelties in this work are summarized as follows:

- We introduce a new way of characterizing CCHP system performance via novel CCHP performance curves (NPC curves).
- Optimal operation of the PGU is determined by using overall optimal partial loads of the PGU with respect to the performance curves (NPC) and the limits of the PGU operating range.
- Formulas to determine the overall optimal partial loads and NPC curves are derived and can be utilized for optimizing the CCHP performance based on different criteria.
- Most of the previously published operating strategies, such as FTL FEL, FHL, MP, Base Load and Maximum Efficiency strategies do not change the CCHP operation if energy price, PEC factor and CDE factor change. Our work demonstrates that CCHP optimal operation is sensitive to these changes and it needs to be adjusted accordingly

in order to stay at the optimum.

- Proposed strategy depends on the characteristics of the CCHP system (i.e. efficiency of the PGU, COP of the absorption chiller and the electric chiller and the efficiency of the boiler).
- NPC curve enables one to calculate the optimum operation of the system without having to carry out numerical optimization of the entire system model.

Operating strategy based on the NPC curves (NPC strategy) is examined for three different buildings; two hotel buildings in San Francisco and Miami and residential buildings in Dalian. These buildings have different energy demand profiles, CDE factors, PEC factors and energy prices. The results of NPC strategy are compared to the results of MP, FHL, FEL and FTL strategies for five different optimization cases; operating cost optimization, CDE optimization case, PEC optimization case and two optimization cases combining all criteria with different weighting factors.

Comparing to the operation of standalone systems, reductions in operating costs due to the deployment of CCHP are: (i) for the hotel in Miami: 11.2%, 6.5%, −2.4%, 0.2% and 4.9%, (ii) for the hotel in San Francisco: 26.8%, 13.24%, 9.6%, 24.09, and 8.1%, (iii) for residential buildings in Dalian: 30.7%, 19.4%, 19.4%, 27.9%, 17.5% when NPC, MP, FHL, FEL, and FTL strategies are applied, respectively. For CDE optimization case of the CCHP system with PGU1, the CDE reductions for hotel in Miami are 11.5%, 5.4%, 1.3%, 8.2% and 4.1% when NPC, MP, FHL, FEL and FTL strategies are applied, respectively. The text contains further data quantifying the amount of improvement over the previously published operating strategies at different sites and different optimization criteria when NPC strategy is used.

The remainder of this paper is organized as follows:

Section 2 presents energy balance equations of a CCHP system. The ratio of the electric cooling to cooling demand is assumed to change along the operating horizon (at one-hour intervals). Section 3 introduces novel performance curves (NPC curves) for loads above and below the CCHP operating curve. NPC curve formulas for combined several criteria are presented in Section 4. Section 5 explains how to utilize the NPC curves and overall optimal partial loads to determine the optimum PGU operation. In Section 6, the NPC curve based methodology is examined in a case study involving different types of CCHP systems and different performance criteria including operating cost, CDE, PEC and two combinations of these criteria. In addition, the results of NPC-based operation are compared to FTL, FEL, FHL and the MP strategy. The conclusions in Section 7 summarize the results attainable by the proposed strategy.

2. CCHP system – energy balance model

A typical CCHP system with hybrid chillers shown in Fig. 1 consists of a power generation unit (PGU), a heat recovery system, an absorption chiller, an electric chiller, a heating coil and a boiler. PGU generates electricity, while the heat recovery systems recover heat from PGU. Thermal energy is fed into the heating coil to produce heat and into the absorption chiller to provide cooling. The priority in using the recovered heat is to satisfy the heating demand. An electric chiller provides cooling load by using electricity from either the PGU or the grid or both of them.

The electrical energy balance is as follows [26]:

$$\begin{cases} E_{grid} = E_d + E_{ec} + E_s - E_{pgu} E_{pgu} < E_d + E_{ec} + E_s & \text{(a)} \\ E_{excess} = E_{pgu} - E_d - E_{ec} - E_s E_{pgu} \geqslant E_d + E_{ec} + E_s & \text{(b)} \end{cases} \tag{1}$$

where E_{grid} is the electricity from the grid, E_{excess} is the excess electricity produced by the PGU that can be sold back to the grid, E_{pgu} is the electricity generated by the PGU, E_d is the electric demand, E_{ec} is the electricity supplied to the electric chiller and E_s is the electric consumption of the CCHP system. Electricity generated by the PGU is expressed by Eq. (2):

$$E_{pgu} = F\eta_{pgu} \tag{2}$$

where η_{pgu} is the efficiency of the PGU, and F is the energy supplied by the fuel.

The efficiency of the PGU is a function of its partial load which is defined as follows:

$$f = \frac{E_{pgu}}{E_{nom}} \tag{3}$$

where E_{nom} is the nominal capacity of the PGU running at full load.

It is assumed that f_{min} equals to 0.25. If $f < f_{min}$ then $E_{pgu} = 0$, else if $f_{min} \leqslant f \leqslant 1$ then $E_{pgu} = fE_{nom}$ and if $f > 1$ then $E_{pgu} = E_{nom}$.

The recovered heat is calculated via Eq. (4):

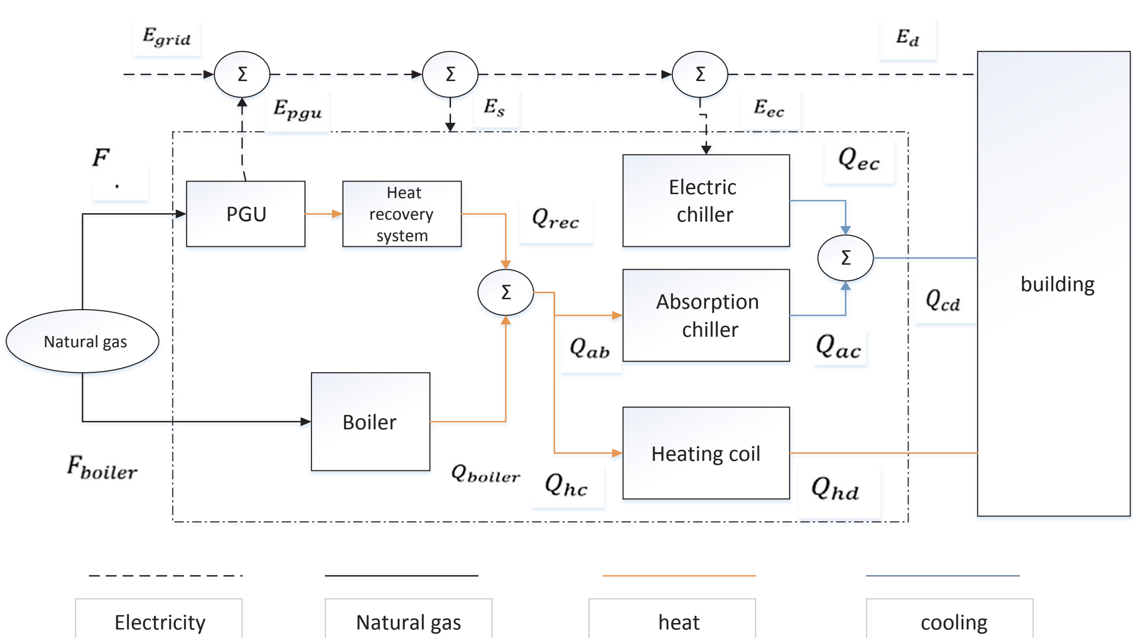

Fig. 1. Energy flows of CCHP system.

$$Q_{rec} = \frac{(1-\eta_{pgu})\eta_{rec}}{\eta_{pgu}} E_{pgu} = k(E_{pgu}) \quad (4)$$

where η_{rec} is the efficiency of the heat recovery system.

The boiler duty is calculated as follows:

$$\begin{cases} Q_{boiler} = Q_{hc} + Q_{ab} - Q_{rec} \quad Q_{hc} + Q_{ab} > Q_{rec} & \text{(a)} \\ Q_{boiler} = 0 \quad Q_{hc} + Q_{ab} \leqslant Q_{rec} & \text{(b)} \end{cases} \quad (5)$$

where Q_{boiler} is the boiler duty, Q_{hc} and Q_{ab} are heat duties for the heating coil and absorption chiller, respectively.

All the heating demand and a part of cooling demand are provided by the heating coil and the absorption chiller, respectively, i.e.

$$Q_{hc}\eta_{hc} = Q_{hd} \quad (6)$$

and

$$Q_{ab} COP_{ac} = Q_{ac} \quad (7)$$

where η_{hc} is the heating coil efficiency, COP_{ac} is the absorption chiller's coefficient of performance (COP), Q_{hd} and Q_{ac} are the heating demand and absorption chiller output.

The cooling demand balance is described by Eq. (8):

$$Q_{ac} + Q_{ec} = Q_{cd} \quad (8)$$

where Q_{cd} is the cooling demand and Q_{ec} is the amount of cooling supplied by the electric chiller. Electric energy E_{ec} consumed by the electric chiller can be determined from Eq. (9):

$$Q_{ec} = E_{ec} COP_{ec} \quad (9)$$

where COP_{ec} is the electric chiller's COP.

The relationship between the generated electricity by PGU and recovered heat is expressed by Eq. (4). The demand load, (E_d, Q_d), is either above the CCHP system operating curve when $Q_d > k(E_d)$ or below the operating curve when $Q_d < k(E_d)$ or on the operating curve when $Q_d = k(E_d)$. Q_{min} and Q_{nom} are the minimum and the maximum amounts of recovered heat from the CCHP system.

Thermal demand is calculated as follows:

$$Q_d = \frac{Q_{cd}}{COP_{ac}} + \frac{Q_{hd}}{\eta_{hc}} \quad (10)$$

In this paper, we derive formulas to determine overall optimum partial loads of the PGU and their performance (NPC) curves for demands below and above the CCHP operating curve and demonstrate how to use them to arrive at the optimal operation of the system. To implement this idea, the PGU should operate in a particular operating range for each demand. For instance, as shown in Fig. 2, the proper operating range of the PGU for demand (a) is $[E^a_{FEL}, E^a_{FTL}]$, where E^a_{FEL} and E^a_{FTL} are the electric outputs of CCHP system when the PGU operates based on FEL and FTL strategies, respectively. In the next section, we present details of the operating strategies for demand loads below and above the system CCHP operating curve.

3. Novel CCHP performance curve (NPC curves)

Fig. 2 shows how the areas above and below the CCHP operating curve are divided into ten different regions based on the magnitude of electric and thermal loads. The x axis in Fig. 2 represents the output power of PGU, while the y axis represents the thermal load on the system. Five of these regions are below the operating curve and five of them are above it. Table 1 shows different regions as well as the lower bound (LB) and the upper bound (UB) values of the PGU operating ranges for demands in different regions.

3.1. Novel performance curve for demands above the CCHP operating curve

Cooling and heating demands vary significantly during a year. Summer and winter are the cooling and heating periods, respectively, while both heating and cooling demands may exist in the transition season.

Let's define point (E_1), corresponding to the PGU operating at the partial load (f_1), represents the electricity generated by the PGU to supply all of the electric demand and the cooling demand via the electric chiller. f_1 is defined by Eq. (11).

$$f_1 = \frac{E_1}{E_{nom}} = \frac{E_d + \frac{Q_{cd}}{COP_{ec}}}{E_{nom}} \quad (11)$$

In addition, let point (E_2) (with the PGU operating at the partial load (f_2)) be the electric output of the PGU when the recovered waste heat equals to the heating demand; f_2 is defined by Eq. (12).

$$f_2\left(\frac{1}{\eta_{pgu}}-1\right) = \frac{E_2}{E_{nom}}\left(\frac{1}{\eta_{pgu}}-1\right) = \frac{\frac{Q_{hd}}{\eta_{hc}\eta_{rec}}}{E_{nom}} \quad (12)$$

The aim is to find the optimum partial load of the PGU in the operating range. Three different scenarios may be created by moving from LB toward load UB of the operating range, (for instance moving from E^a_{FEL} to E^a_{FTL} for demand (a) in Fig. 2). f_1 and f_2 are utilized to describe these scenarios as presented in Table 2:

Moving from LB to UB of the operating range may be based on more than one scenario. This happens when one starts from Scenario #1 and ends either at Scenario #2 or at Scenario #3. The value of the objective function, e.g. operating cost, changes by moving from LB to UB of the PGU. The optimum PGU load is the load in the PGU operating range, [LB, UB], that leads to the minimum of the objective value.

Let's define a new performance curve (novel performance curve, NPC) which has a minimum at the optimal load of PGU. NPC formulas are derived in Appendix A for each of the scenarios presented in Table 2.

3.1.1. Scenario #1

This scenario occurs mostly during some time periods of the transition season. Also, for a load in summer or winter, by moving from LB toward UB, this scenario might take place first and then it is followed by either scenario #3 or scenario #2. If the aim is to optimize the operation of the CCHP system based on the operating cost, then performance (NPC) curve formula for a load above the CCHP system CCHP operating curve and scenario #1 is as follows:

$$\psi^{above}_{scenario\#1}(f) = f\left[\frac{1}{\eta_{pgu}}\left(1-\frac{\eta_{rec}}{\eta_{boiler}}\right) + \left(\frac{\eta_{rec}}{\eta_{boiler}} - R\right)\right] \quad (13)$$

where R is the price ratio (electricity price / natural gas price). For each PGU operating range, [LB, UB], by moving from LB toward UB, the PGU

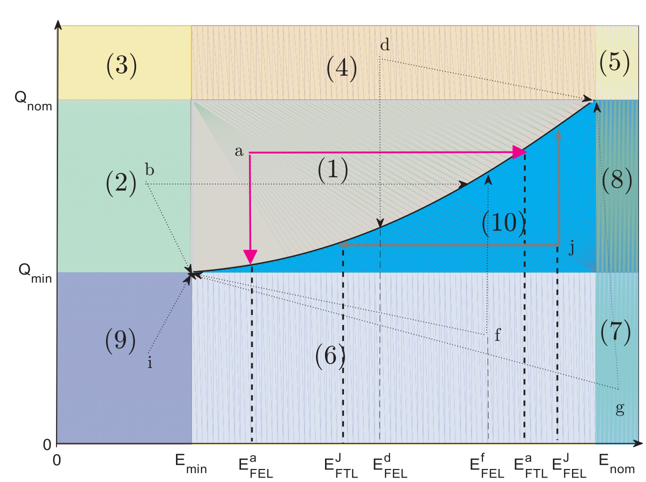

Fig. 2. Different regions above and below the CCHP operating curve.

Table 1
Operating regions and PGU operating ranges for demand loads above and below the CCHP operating curve.

Region	Electric demand	Thermal demand	LB of operating range	UB of operating range
(1)	$E_{min} \leqslant E_d \leqslant E_{nom}$	$Q_{min} \leqslant Q_d \leqslant Q_{nom}$	$E_d = E_{FEL}^a$	E_{FTL}^a
(2)	$E_d < E_{min}$	$Q_{min} \leqslant Q_d \leqslant Q_{nom}$	E_{min}	E_{FTL}^b
(3)	$E_d \leqslant E_{min}$	$Q_d > Q_{nom}$	E_{min}	E_{nom}
(4)	$E_{min} < E_d \leqslant E_{nom}$	$Q_d > Q_{nom}$	$E_d = E_{FEL}^d$	E_{nom}
(5)	$E_d > E_{nom}$	$Q_d > Q_{nom}$	E_{nom}	E_{nom}
(6)	$E_{min} \leqslant E_d \leqslant E_{nom}$	$Q_d \leqslant Q_{min}$	E_{min}	$E_d = E_{FEL}^f$
(7)	$E_d > E_{nom}$	$Q_d < Q_{min}$	E_{min}	E_{nom}
(8)	$E_d \geqslant E_{nom}$	$Q_{min} \leqslant Q_d \leqslant Q_{nom}$	E_{FTL}^h	E_{nom}
(9)	$E_d < E_{nom}$	$Q_d < Q_{min}$	E_{min}	E_{min}
(10)	$E_{min} < E_d < E_{nom}$	$Q_{min} < Q_d < Q_{nom}$	E_{FTL}^j	$E_d = E_{FEL}^j$

Table 2
Scenarios above the CCHP operating curve.

Scenario #	Partial load of PGU ($f_1 \leqslant f_2$)	Partial load of PGU ($f_1 > f_2$)
1	$f < f_1$	$f < f_2$
2	$f \leqslant f_2$ and $f \geqslant f_1$	–
3	–	$f \geqslant f_2$ and $f \leqslant f_1$

partial load, f, changes from load L (corresponding to the LB of the operating range) to PGU partial load U. Therefore ψ varies across the PGU operating range. A partial load which yields the minimum of ψ is the optimum partial load of PGU across the operating range [LB, UB]. For a fixed value of R, ψ is a function of one variable, f, and it doesn't depend on the magnitude of the demand. Hence, Eq. (13) can be used for all of demands which meet the conditions defining Scenario #1. Since Eq. (13) is a decreasing function of f, the upper bound of the operating range of this scenario is the optimum PGU operation.

Let us define S as the ratio of the carbon dioxide emissions conversion factors of the electricity from the grid to natural gas $\left(\frac{CDE_e}{CDE_f}\right)$ and G as the ratio of primary energy conversion factors of the electricity to natural gas $\left(\frac{PEC_e}{PEC_f}\right)$. To minimize Carbon Dioxide Emissions (CDE) and Primary Energy Consumption (PEC), S and G are substituted instead of R in Eq. (13), respectively.

3.1.2. Scenario #2

This scenario occurs most often during a winter. In this case, the NPC curve formula is as follows:

$$\psi^{above}_{Scenario\#2}(f) = f\left[\frac{1}{\eta_{pgu}}\left(1-\frac{\eta_{rec}}{\eta_{boiler}}\right) + \frac{\eta_{rec}}{\eta_{boiler}}\right] \tag{14}$$

Eq. (14) depends on only the boiler efficiency and the partial load of the PGU; it does not depend on the price ratio or on PEC factors or on CDE factors. In most systems, the efficiency of heat recovery system is lower than or equal to the boiler efficiency [31]. Under such conditions, Eq. (14) is an increasing function of f. Therefore, the lower bound of the operating range of any demand corresponds to the lowest ψ and it is the optimum partial load operation of PGU. This means that it is not beneficial to operate the PGU above LB to satisfy incrementally more of the heating demand by recovered waste heat and also have an excess production of the electricity.

3.1.3. Scenario #3

This scenario takes place during some time periods in a summer when there is a considerable cooling demand. By applying the same procedure as in Scenario #1 and Scenario #2, the NPC curve formula shown in Eq. (15) is derived:

$$\psi^{above}_{Scenario\#3}(f) = f\left\{\frac{1}{\eta_{pgu}} - [1 + \frac{COP_{ac}}{COP_{ec}}\eta_{rec}\left(\frac{1}{\eta_{pgu}}-1\right)]R\right\} \tag{15}$$

For all demands in regions **(2)** and **(3)**, it needs to be decided whether the application of a CCHP system is more efficient than the separate production (SP) system or not. Eqs. (16) and (17) are utilized for a demand which has a heating load higher than the minimum thermal output of CCHP system. If the electricity needed to supply the electric and cooling demands is more than the minimum electric output of CCHP system, i.e. $(E_d + \frac{Q_{cd}}{COP_{ec}} > E_{min})$, then Eq. (16) is employed; otherwise, Eq. (17) is applied.

$$\eta_{pgu_{min}} R \geqslant 1 - \frac{(1-\eta_{pgu_{min}})\eta_{rec}}{\eta_{boiler}} \tag{16}$$

$$E_d R + \frac{Q_{cd}}{COP_{ec}} R \geqslant F_{min} - \frac{Q_{min}}{\eta_{boiler}} \tag{17}$$

If the heat demand is less than the minimum thermal output of CCHP system, and the cooling demand is more than the remaining of the waste heat and excess electricity produced, $Q_{cd} \geqslant COP_{ac}[Q_{min} - \frac{Q_{hd}}{\eta_{hc}}] + COP_{ec}(E_{min} - E_d)$, then Eq. (18) is used:

$$E_{min} R \geqslant F_{min} - \frac{COP_{ac}}{COP_{ec}} Q_{min} R + \frac{Q_{hd}}{\eta_{hc}}\left(\frac{COP_{ac}}{COP_{ec}} R - \frac{1}{\eta_{boiler}}\right) \tag{18}$$

Derivation of these equations is presented in Appendix B. The procedure is the same if the objective is to minimize either CDE or PEC.

3.2. Novel performance curve for demand below the CCHP operating curve

Following the same procedure as in Scenario #1, the NPC is derived to be:

$$\psi^{below}(f) = \frac{f}{\eta_{pgu}} - fR \tag{19}$$

For a demand in region **(6)** or **(7)**, Eq. (20) is employed to decide whether or not here is a benefit of using a CCHP system instead of a standalone production system SP.

$$\exists\ f \leqslant f_{FEL}\ \text{such that}\ \psi^{below}(f) \leqslant \frac{1}{E_{nom}}\left[\frac{Q_{hd}}{\eta_{hc}\eta_{boiler}} + \frac{Q_c}{COP_{ec}} R\right] \tag{20}$$

If the demand satisfies the inequality in Eq. (20), then the optimum partial load of PGU is located in the interval $[f_{min}, f_{FEL}]$.

4. Novel performance curve formula for a combination of the performance criteria

Eq. (21) is the NPC curve formula to optimize the CCHP operation based on a combination of the operating cost, CDE and PEC.

$$\psi_{combination}(f) = \sum_i \omega_i \frac{\psi^i}{Cr_i + \frac{f_h}{f_e}\left(\frac{1}{\eta_h}-1\right)\eta_{rec}} \tag{21}$$

where i is either operating cost, or CDE or PEC , ω_i is the weighting factor of the ith criteria and is determined by the government policy; Cr_i is the ratio of ith criteria and it can use R, S and G for price ratio, CDE ratio and PEC ratio, respectively; f_e is the partial load of PGU to generate the required electricity and cooling demand via an electric chiller; f_h is the partial load of PGU to provide required heat of a demand.Because the demands can have different values of f_e and f_h (i.e. demands vary with time) there is no single NPC curve formula for all demands. But $\psi_{combination}$ is a weak function of both f_e and f_h. This implies that the overall optimum partial values and the slope (decreasing or increasing features) of $\psi_{combination}$ may change slightly by varying the demand or both f_e and f_h. To determine accurately the optimum operation, it is recommended to plot $\psi_{combination}$ using different values of f_e and f_h near the optimum point and then take an average of the corresponding values of f.

5. Application of the novel performance curve and overall optimum partial loads

To explain the application of the NPC strategy, NPC curves (ψ) for loads below and above the CCHP operating curves are shown in Figs. 3 and 4; these curves have been calculated by using Eqs. (15) and (19). The partial load that yields the minimum of the NPC curve for when $0.25 \leqslant f \leqslant 1$ is called the overall optimal partial load of PGU (f_{opt-o}). As shown in Fig. 3, $f = 0.25$ and $f = 1$ also yield the maximum values of the ψ on the left-hand side, (ψ_{max}^{LHS}), and on right-hand side, (ψ_{max}^{RHS}), of f_{opt-o}, respectively. In this case, by using f_{opt-o} and by determining the location of the PGU operating range in the NPC curve, optimum partial load of PGU is found. Otherwise, for when $[\psi_{max}^{LHS} \neq \psi(0.25)]$ or $[\psi_{max}^{RHS} \neq \psi(1)]$, the optimum PGU load is found by considering the location of the PGU operating range relative to the f_{opt-o} and f_{max}^{LHS} or f_{opt-o} and f_{max}^{RHS}. f_{max}^{LHS} and f_{max}^{RHS} are PGU partial loads that lead ψ_{max}^{LHS} and ψ_{max}^{RHS}, respectively. Two NPC curves for loads below and above the CCHP system operating curve are shown in Fig. 4 that in each curve $[\psi_{max}^{LHS} \neq \psi(0.25)]$ and $[\psi_{max}^{RHS} = \psi(1)]$.

As displayed in Figs. 3 and 4, because of the variation of the magnitude of loads over a year and through a day, the locations of the PGU operating ranges might be different with respect to the PGU overall optimum partial load. A PGU operating range can be on the left-hand side (LHS) of f_{opt-o} such as load #1 and load #9 below the CCHP operating curve and load # 4 and load #14 above the CCHP operating curve. On the contrary, it can be on the right-hand side (RHS) of f_{opt-o} such as load #3 and load # 6 which are located below and above the CCHP operating curve, respectively. Otherwise, the PGU operating range includes the f_{opt-o} (load #2 and load #5).

As demonstrated in Figs. 3 and 4, by applying NPC strategy, if the PGU operating range includes an overall optimum partial load (f_{opt-o}) then the optimum load of the PGU is set at $f = f_{opt-o}$. Since running PGU at this load yields the minimum of ψ across the PGU operating range.

In Figs. 3(a) and 4(a), for a load below the CCHP operating curve, if its PGU operating range is on the left-hand side of the f_{opt-o}^{below} and right-hand side of the f_{max}^{LHS}, then the optimal PGU load is $f = f_{FEL}$. For example, f_{FEL}^{1} and f_{FEL}^{9} are the optimum partial loads of PGU for load #1 and load #9, respectively. This means that FEL strategy is the optimum operating strategy for PGU. For a load which is on the left side of both f_{opt-o}^{below} and f_{max}^{LHS}, optimal PGU load is f_{FTL} (e.g. load #7 in Fig. 4). On the other hand, if the operating range is on the right side of f_{opt-o}^{below} and on the left side of f_{max}^{RHS} (in Figs. 3(a) and 4(a) with $f_{max}^{RHS} = 1$), then FTL strategy ($f = f_{FTL}$) provides the optimal operation. For instance, for load #3 and load #11, the PGU optimum operating points are f_{FTL}^{3} and f_{FTL}^{11}, respectively. Moreover, if the PGU operating range is on the right side of both f_{opt-o}^{below} and f_{max}^{RHS}, then $f = f_{FEL}$ is the optimum PGU partial load.

For a load above the CCHP operating curve and scenario #3, if the PGU operating range is on the left side of the f_{opt-o}^{above} and on the right side of f_{max}^{LHS}, then $f = f'$ (the MP strategy is applied, see Appendix G) (e.g. load #4 and load #14). When the PGU operating range is on the left side of the both f_{opt-o}^{above} and f_{max}^{LHS}, then FEL strategy is the best to manage the operation of the PGU (e.g. load #12 in Fig. 4(b)). On the other hand, if the PGU operating range is on the right-hand side of f_{opt-o}^{above} then FEL is followed to manage the operation of the CCHP system (e.g. load #6 in Fig. 3(b) and load #16 in Fig. 4(b)).

For load #8, the PGU operating range includes f_{max}^{LHS}; ψ is calculated at two partial loads, f_{FTL}^{8} and f_{FEL}^{8}. The optimum partial load is that one of these two points (f_{FTL}^{8} and f_{FEL}^{8}) which yields the minimum of ψ. The same procedure is utilized for loads where PGU operating ranges include f_{max}^{RHS}. The optimum loads of PGU for different loads below and above the CCHP operating curve (scenario #3) are presented in Table 3. Schematic illustration of the NPC methodology is shown in Appendix D.

For NPC curves in both Fig. 3 and Fig. 4, ψ_{max}^{RHS} occurs when $f = 1$. The same procedure is applied to optimize CCHP performance when $\psi_{max}^{RHS} \neq \psi(1)$.

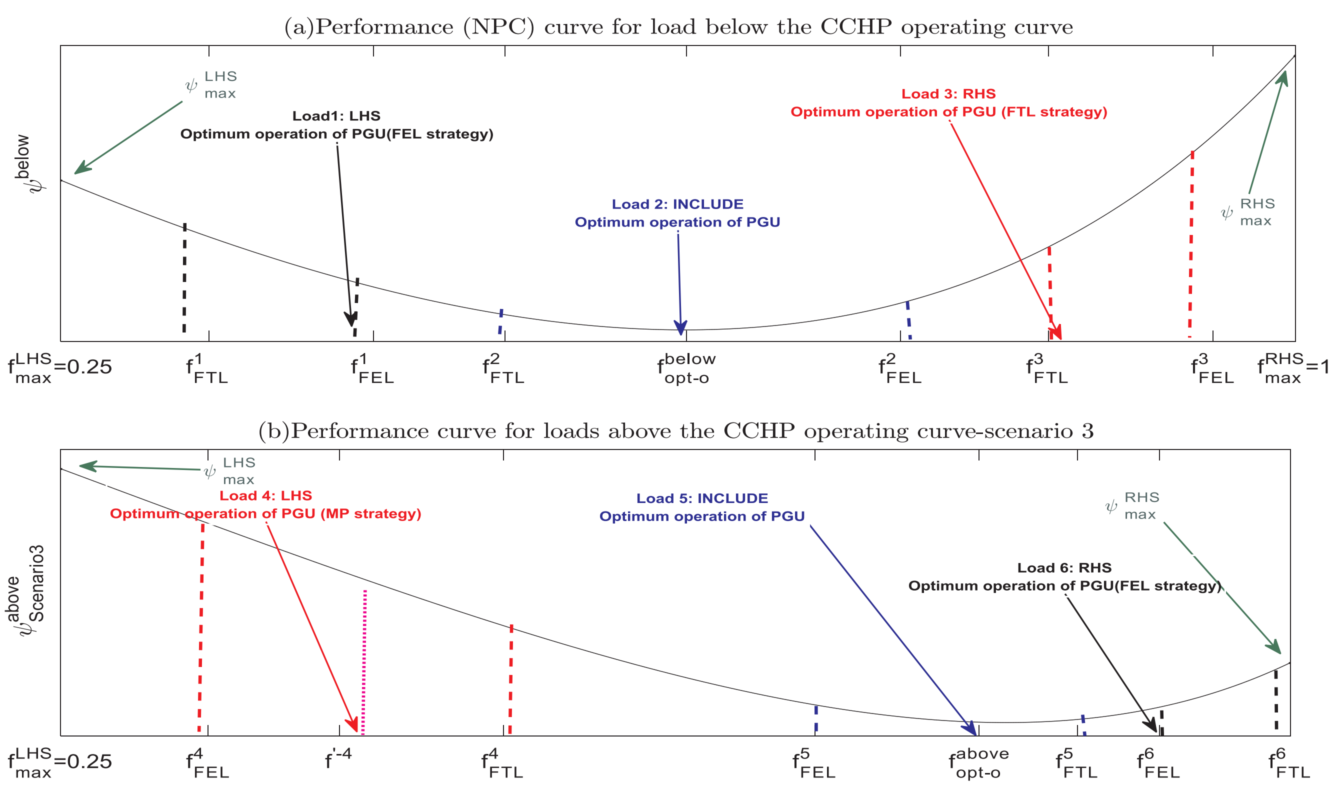

Fig. 3. NPC Curves of loads below and above the operating curve and NPC strategy application.

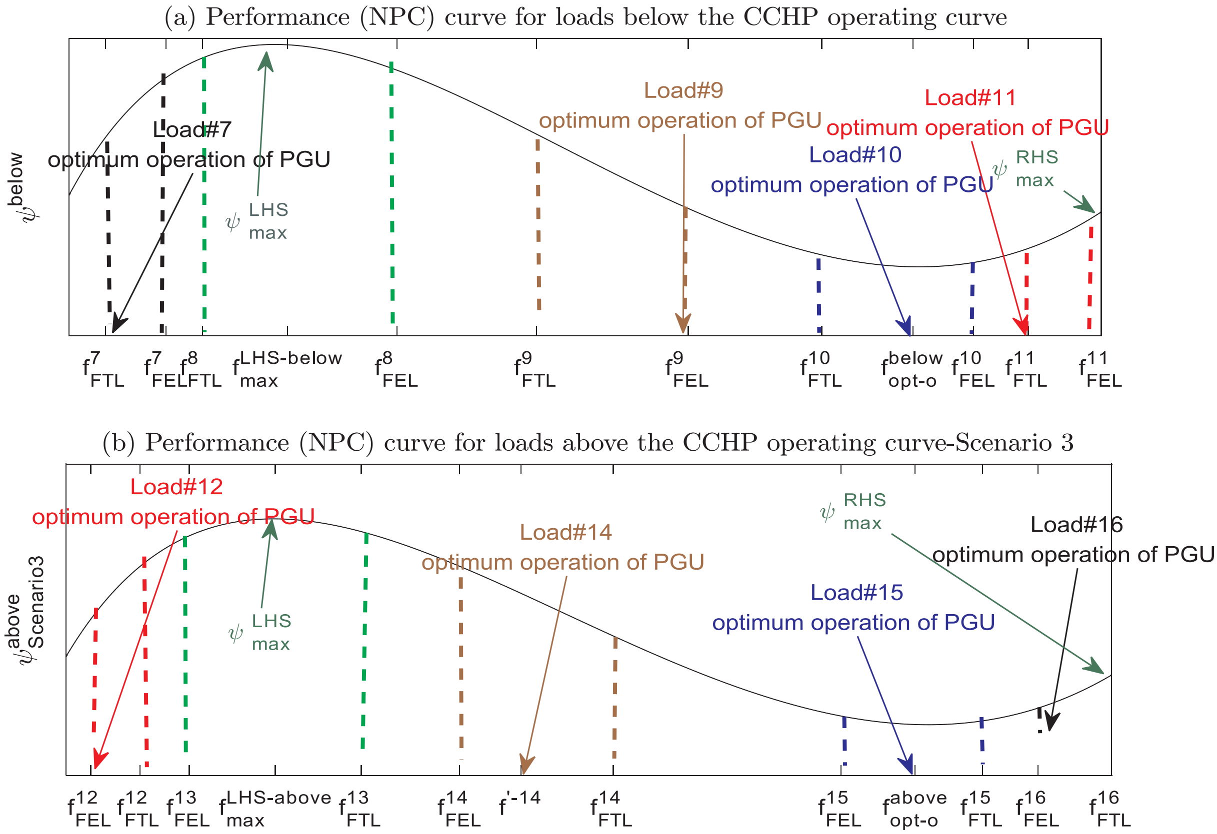

Fig. 4. NPC curves for loads below and above the CCHP operating curve.

Table 3
Optimum partial loads of PGU for different operating ranges.

Load #	Below the operating curve	Location of the operating range with respect to the			Optimum operation of PGU	Strategy
		f_{opt-o}	f_{max}^{LHS}	f_{max}^{RHS}		
1, 9	Yes	LHS	RHS	LHS	f_{FEL}^{1}, f_{FEL}^{9}	FEL
7	Yes	LHS	LHS	LHS	f_{FTL}^{7}	FTL
2, 10	Yes	Include	–	–	f_{opt-o}^{below}	–
3, 11	Yes	RHS	RHS	LHS	f_{FTL}^{3}, f_{FTL}^{11}	FTL
4, 14	No	LHS	RHS	LHS	$f'^{,4}$, $f'^{,14}$	MP
12	No	LHS	LHS	LHS	f_{FEL}^{12}	FEL
5, 15	No	Include	–	–	f_{opt-o}^{above}	–
6, 16	No	RHS	RHS	LHS	f_{FEL}^{6}, f_{FEL}^{16}	FEL
8	Yes	LHS	Include	LHS	*	–
13	No	LHS	Include	LHS	*	–

* The optimum point is determined by finding the minimum of ψ at two points, f_{FEL} and f_{FTL}.

It should be noted that for loads above the CCHP operating curve and scenario #2 (loads in winter), the optimal PGU load is f_{FEL} (PGU operates on FEL strategy). This is because Eq. (14) is an increasing function of f. Hence the lower bound of the operating range yields the minimum of ψ.

6. Case studies

The proposed strategy has been applied to two CCHP systems at two hotel buildings in San Francisco and Miami and for a CCHP system applied in the residential buildings in Dalian, China. These cities have different climate conditions, energy prices, CDE factors and PEC factors. The energy demand profiles of buildings, energy tariffs, CDE factors and PEC factors of these cities (shown in Figs. 5 and 6 and Table 4) are from [32,27]. Cooling, heating and electrical demands of the eight residential buildings are shown in Fig. 6. The demands are presented in the representative days for three different seasons; winter, transition season and summer. Dalian is the city with typical maritime climate; in residential buildings, the peak loads are high while average loads are low [27].

Two 100 kW internal combustion engines are utilized as PGU systems in CCHP systems in Miami and San Francisco. An internal combustion engine of 1000 kW is used for the residential buildings in Dalian [27]. Two different equations are presented in [26,20] to describe the performances of two different internal combustion engines; we name these engines as PGU1 and PGU2, respectively. The analysis has been carried out for both PGU systems (Engine systems). The results obtained by employing PGU1 are presented in the main body of the paper. The results obtained by using PGU2 are presented in Appendix E.

6.1. Results and discussion

Novel performance (NPC) curves related to the optimum operation of a hotel CCHP system in San Francisco are shown in Figs. 7 and 8. As presented in Fig. 7, the variation of the energy prices during a day (on-peak, off-peak and mid-peak) yields different values of the f_{opt-o} and subsequently yields different NPC curves. Also, CCHP performance optimization based on different criteria results in different NPC curves, Fig. 8. Overall optimum partial loads of the PGU for the hotels in San Francisco and Miami are presented in Table 5. Objective functions are expressed in Appendix C. As displayed in Figs. 7 and 8, if the operating range [L, U] includes overall optimal partial load PGU, f_{opt-o}, then the optimal partial load of PGU is f_{opt-o}. For an operating range doesn't include f_{opt-o}, [L*, U*], the PGU load is determined by NPC strategy.

Hourly PGU optimal loads of the CCHP systems utilized in San

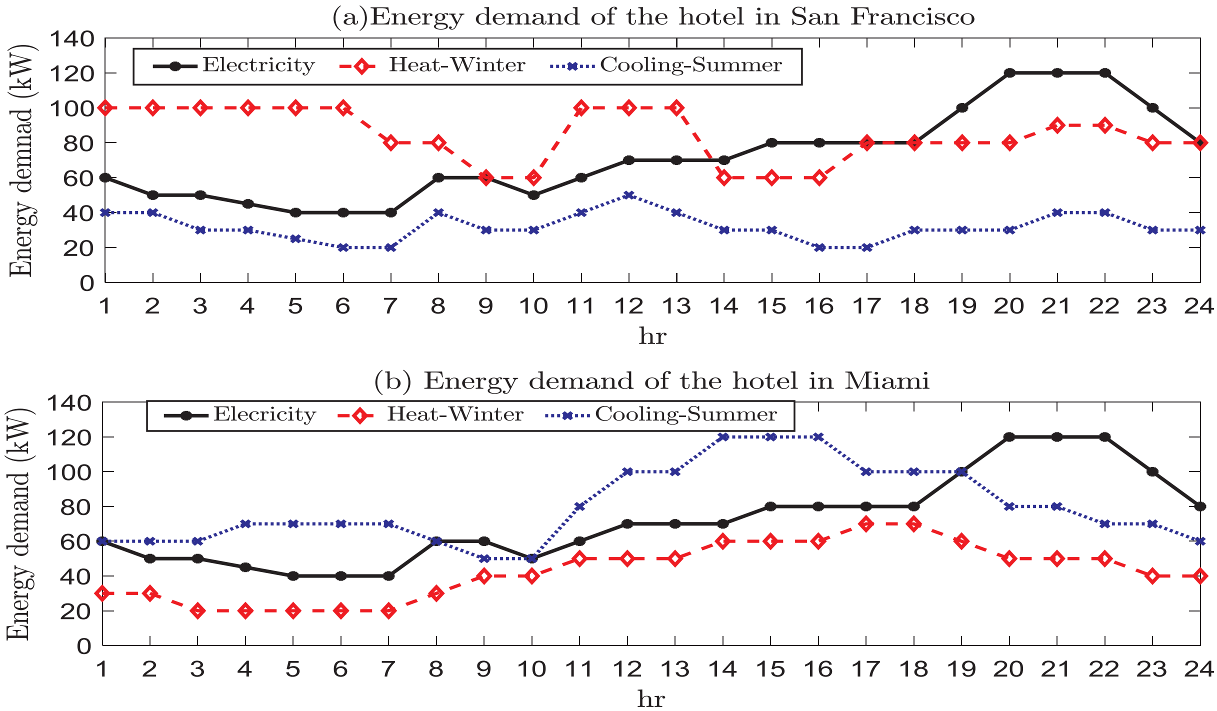

Fig. 5. Energy demand profiles of hotels in San Francisco and Miami for respective days in summer and winter.

Francisco, Miami and residential buildings are shown in Figs. 9, 12 and 15, respectively. It can be seen that by applying NPC strategy, the optimum load of PGU changes if different optimizing criteria is employed. The detailed application of NPC methodology for managing the operation of CCHP system in San Francisco is explained when PGU1 is utilized. Only selected results for Miami and for Dalian will be presented here. Detailed application of NPC methodology for CCHP system in Miami with PGU2 is explained in Appendix E. Application of NPC methodology would be the same for other CCHP systems.

Table 6 classifies the loads of the hotels in San Francisco and Miami into different regions with respect to the CCHP system operating curve. PGU operating ranges for these loads are presented in Appendix F.

For all NPC curves, $f_{max}^{LHS} = 0.25$ and $f_{max}^{LHS} = 1$ except NPC curve of the CCHP system in Miami when the operation is optimized based on the operating cost and $R = 2.9$. In this curve, $f_{max}^{LHS} = 0.3$ and $f_{max}^{LHS} = 1$. For loads which are in Regions **(6)** or **(7)**, in order to verify whether the application of the PGU is effective than separate production system or not, Eq. (20) must be checked.

6.1.1. Optimum operation of PGU of the CCHP system in the hotel in San Francisco

Winter hours 2–6: Loads are above the operating curve (region **(1)**) and belong to scenario #2. Also, $f_{opt-o} = 0.25$ for all the optimization criteria. Therefore for each load, the optimal load of PGU is set at $f = f_{FEL}$ (FEL strategy). The remaining loads in winter and summer are below the CCHP operating curve.

6.1.2. Optimization based on the operating cost

Winter hours 6–18: The PGU operating ranges are on the left-hand side of their f_{opt-o}^{below}. Consequently, as shown in Fig. 7(a) and (c), FEL is applied to manage the PGU operation.

Winter hours 19–22 and summer hours 19–22: The PGU operating ranges include $f_{opt-o}^{below-mid} = 0.84$. Therefore, as depicted in Fig. 7(c), for each load, the PGU optimum load is 0.84. It should be noted that Eq. (20) is satisfied for loads which are in regions **(6)** and **(7)** in summer.

Winter hours 23–24 and summer hour 23–24: In winter, the operating ranges include $f_{opt-o}^{below-off}$, then PGU loads are fixed at 0.63, as demonstrated in Fig. 7(a). In summer, although the operating range includes $f_{opt-o}^{below-off}$, loads are in region **(6)** and Eq. (20) is not met. Hence the PGU is off.

Summer hours 3–5: Eq. (20) is not satisfied. As a result, it is more profitable to turn off the PGU, and the grid provides the electric and cooling demands.

Summer hours 6–19: The PGU operating ranges are on the left-hand side f_{opt-o}^{below}. For these loads, Eq. (20) is satisfied. Therefore, the FEL is selected as an optimum strategy ($f = f_{FEL}$).

6.1.3. Optimization based on the PEC

As shown in Fig. 8(a), for hours 15–24 in both winter and summer seasons, operating ranges of PGU include $f_{opt-o}^{below-PEC} = 0.72$. As a result, the optimum load of PGU is 0.72. Moreover, PGU follows FEL strategy ($f = f_{FEL}$) for rest of demands because PGU operating ranges are on the left-hand side of the $f_{opt-o}^{below-PEC}$. Eq. (20) is also satisfied by loads having thermal demands less than minimum thermal output of PGU (regions **(6)** and **(7)**).

6.1.4. Optimization based on the CDE

As displayed in Fig. 8(c), the overall optimal partial load of PGU is 0.35 for loads below the CCHP operating curve. In winter, for hours 7–8, 16–20 and 23–24, the PGU operating ranges contain $f_{opt-o}^{below-CDE} = 0.35$. Therefore the optimum partial load of PGU is 0.35. Also, for hours 11–13 and 21–22, the PGU operating ranges are on the right-hand side of the $f_{opt-o}^{below-CDE}$. As a result, FTL strategy is used to satisfy the demand ($f = f_{FTL}$). PGU is also off during summer. Since loads are in regions **(6)** and **(7)**, Eq. (20) is not satisfied by them.

6.1.5. Optimization based on the combination of criteria (combination-1)

For winter loads of hours 1 and 6–11, the PGU operating ranges are on the left-hand side of f_{opt-o}^{below}. Consequently, FEL is used to manage the PGU operation. Moreover, as shown in Fig. 9, PGU operating ranges of winter loads during hours of 12–13, 13–22 and 23–24 include corresponding overall optimum loads which are $f_{opt-o}^{on-peak} = 0.69$, $f_{opt-o}^{mid-peak} = 0.64$ and $f_{opt-o}^{off-peak} = 0.57$, respectively. For loads in summer, demands are in region **(6)** and **(7)**, and also Eq. (20) is not satisfied. Consequently, PGU is off.

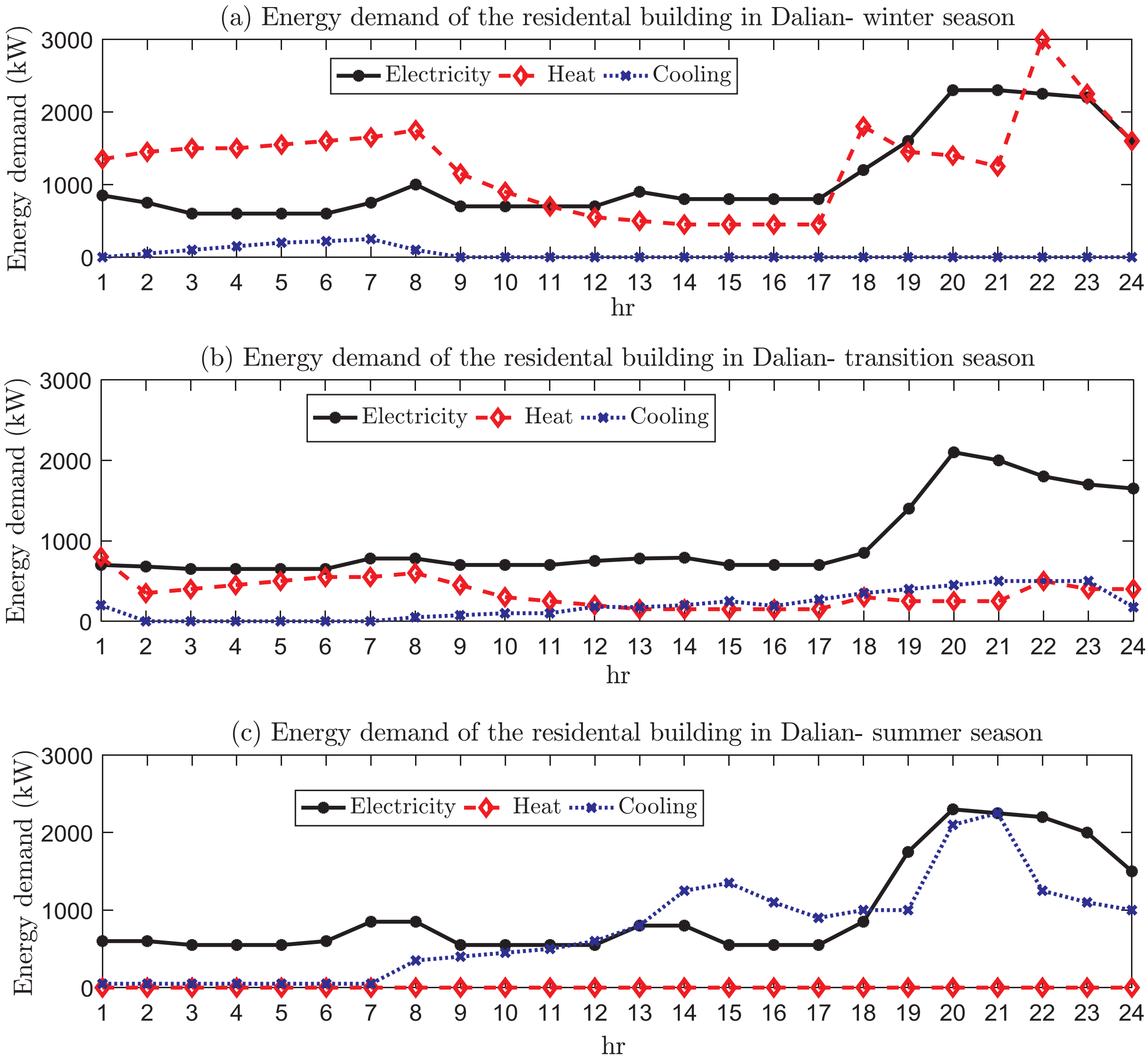

Fig. 6. Energy demand profiles of residential buildings in Dalian for respective days in summer, winter and transition season.

Table 4
Price ratio, CDE factor ratio and PEC ratio of the selected cities.

	$S\left(\frac{CDE_e}{CDE_f}\right)$	$G\left(\frac{PEC_e}{PEC_f}\right)$	*R (off-peak)*	*R (mid-peak)*	*R (on-peak)*
San Francisco	1.72	3.19	2.67	4	5
Miami	3.03	3.19	1.84	2.90	3.68
Dalian	4.4	3.18	2.045	4.09	6.14

6.1.6. Trade-offs between different optimization criteria for the hotel in San Francisco

In the city of San Francisco, electricity price is higher than the fuel price and CCHP usage leads to the operational cost reduction. This can be inferred from the high values of the PGU overall optimum partial loads (f_{opt-o}) for cases of below and of above the CCHP operating curve. Also, application of the CCHP system decreases PEC for all cases. As shown in Fig. 10, the highest percentage of PEC reduction (16.2%) is obtained by optimizing the CCHP performance based on PEC. Furthermore, in cost optimization case and combination-1 optimization case, PEC reductions are still high (15.3% and 16.1%, respectively). Application of CCHP system yields to the increase in the CDE relative to the separate production system except when the CCHP operation is optimized based on the CDE. This is due to the fact that the amount of coal in the fuel mix is low (13%) and the CDE factor of the electricity is low. In CDE optimization case, although the CDE emission decreases by 5.3%, the PEC and operational cost reductions are at their minimum values (11.4% and 12.3%, respectively, respectively).

The highest value of operational cost reduction is 26.8%. Therefore, application of CCHP system for the hotel in San Francisco is more profitable when the CCHP system operation aims to minimize the PEC and the operating cost, or optimizes the combination of criteria (either combination 1 or combination 2). To achieve higher reductions in all three criteria (operating cost, PEC and CDE), it is better to optimize the performance of the CCHP system based on the combination of criteria by using equal weighting factors.

The analysis of different optimization cases when PGU1 is replaced by PGU2 is explained in the Appendix E.

For the city of San Francisco and PGU1, Fig. 11 shows the variations of the operation cost and PEC reduction versus the different amounts of CDE reduction; the higher is the reduction in CDE, the smaller is the reduction of operating cost and PEC. This is explained in Table 5; f_{opt-o}^{CDE} for loads below the CCHP system lower PGU operating bound (0.25) is lower than f_{opt-o}^{PEC} and f_{opt}^{cost}. For high reduction in CDE, the overall optimal partial load has to be low which is not favorable for both operating cost and PEC minimization. Also, as shown in Fig. 11, the operating cost changes faster than PEC as CDE increases.

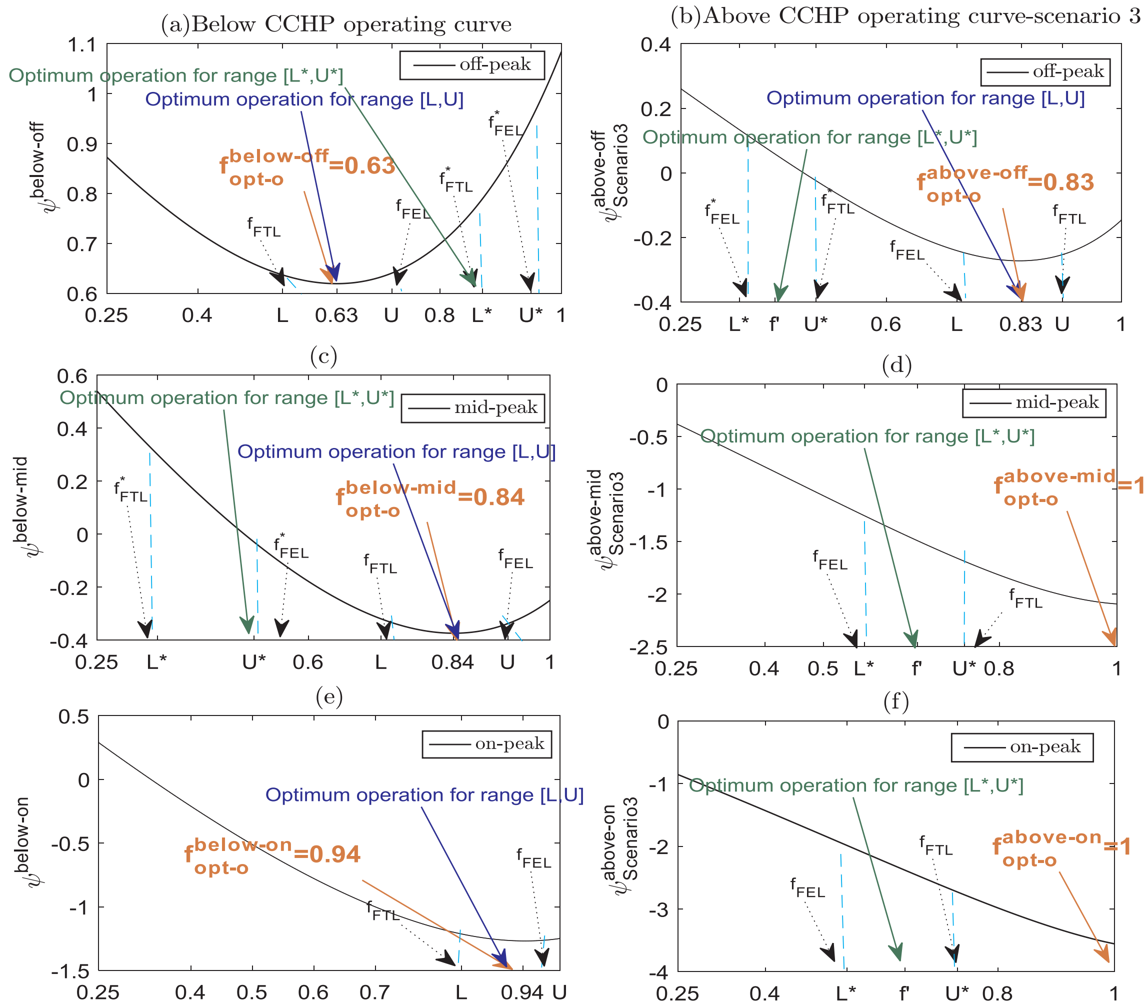

Fig. 7. NPC curves of the San Francisco for loads below and above the CCHP operating curve scenario #3 based on the operating cost optimization.

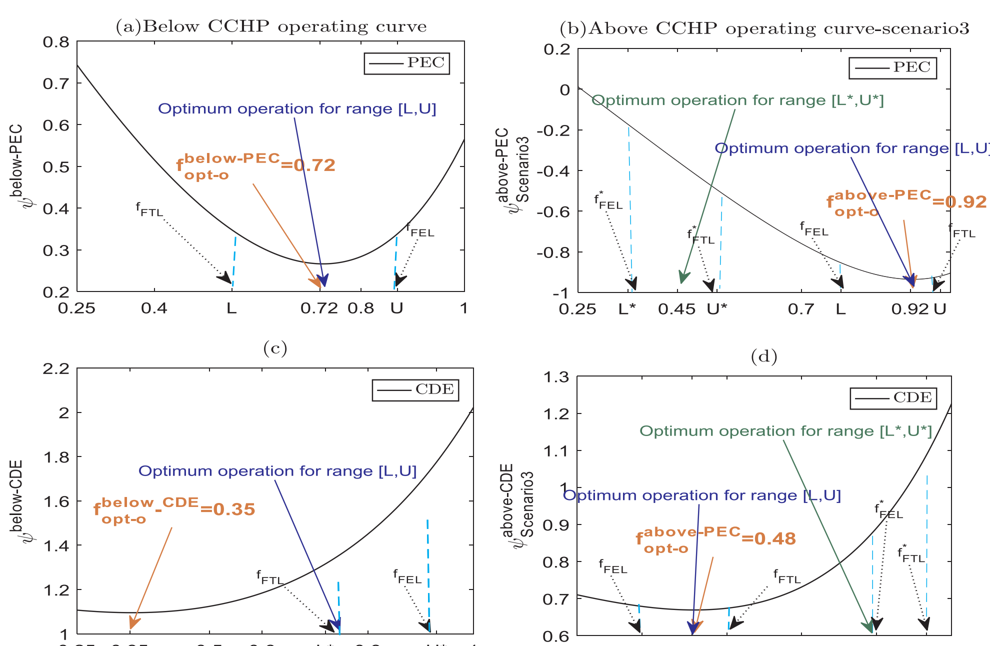

Fig. 8. NPC curves of San Francisco for loads below and above the CCHP system operating curve #3 based on the CDE and PEC optimization.

Table 5
Overall optimum partial loads of PGU (f_{opt-o}) for different optimization criteria.

City	San Francisco				Miami				Dalian			
Criterion	Below the operating curve		Above the operating curve scenario#3		Below the operating curve		Above the operating curve scenario#3		Below the operating curve		Above the operating curve scenario#3	
PGU#	1	2	1	2	1	2	1	2	1	2	1	2
PEC	0.72	0.96	0.92	1	0.72	0.96	1	1	0.72	0.97	0.92	1
CDE	0.35	0.25	0.48	0.25	0.74	0.92	1	1	0.88	1	1	1
Operating cost												
Off-peak	0.63	0.8	0.83	1	0.4	0.25	0.53	0.25	0.47	0.25	0.634	0.80
Mid-peak	0.84	1	1	1	0.67	0.88	0.95	1	0.85	1	1	1
On-peak	0.94	1	1	1	0.8	1	1	1	1	1	1	1
Combination of the criteria $\left[\omega_i = \frac{1}{3}\right]$ *(combination-1)*												
Off-peak	0.57	0.25	0.8	1	0.63	0.79	0.88	1	0.73	0.97	1	1
Mid-peak	0.64	0.9	0.89	1	0.71	0.925	1	1	0.81	1	1	1
On-peak	0.69	1	0.94	1	0.74	1	1	1	0.88	1	1	1
Combination of the criteria $\left[\omega_{cost} = \frac{2}{3}, \omega_{CDE} = \frac{1}{6}, \omega_{PEC} = \frac{1}{6}\right]$ *(combination-2)*												
Off-peak	0.61	0.74	0.85	1	0.53	0.25	0.72	0.96	0.77	0.77	1	0.86
Mid-peak	0.77	1	1	1	0.69	0.9	0.93	1	1	1	1	1
On-peak	0.85	1	1	1	0.77	1	1	1	1	1	1	1

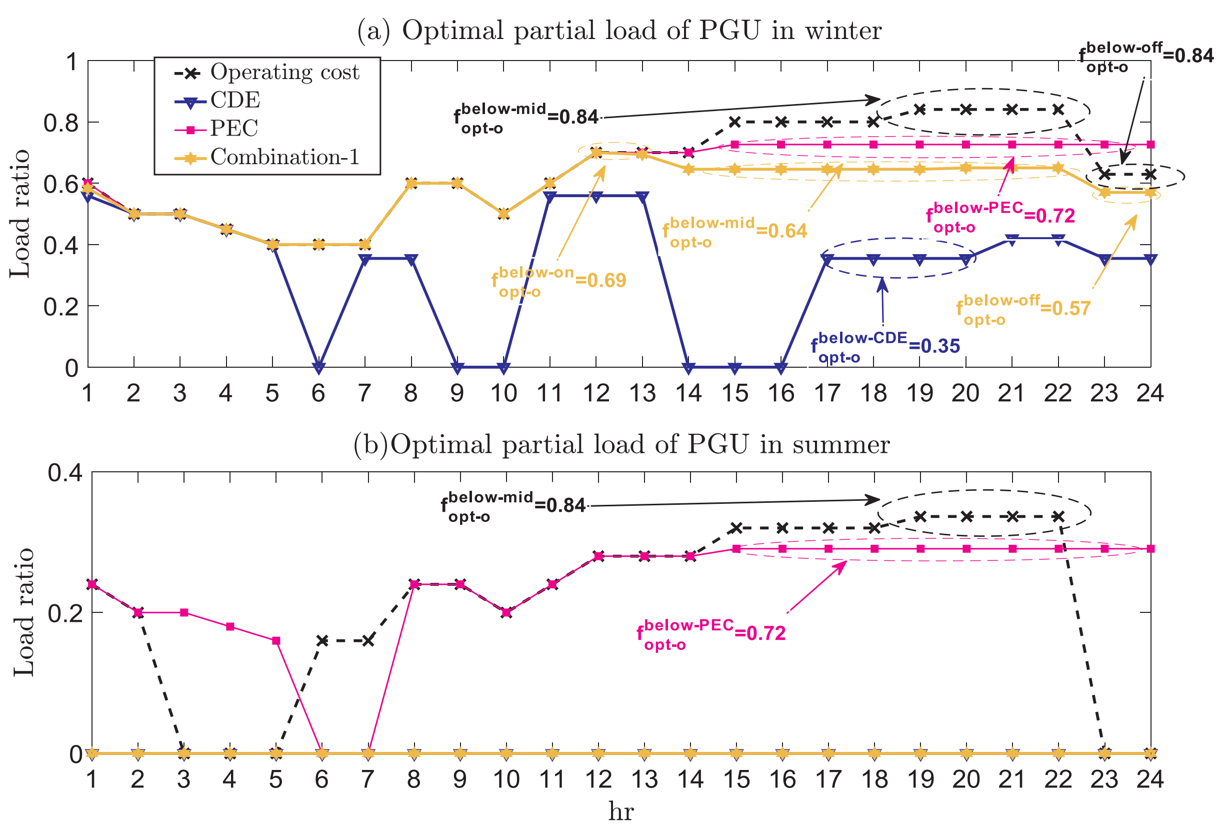

Fig. 9. Optimal partial loads of PGU in a CCHP system with PGU1 for the hotel in San Francisco by considering different optimization criteria.

Table 6
Classification of the hotel loads with respect to the CCHP system operating curve.

Hour	1	2	3	4	5	6	7	8	9	10	11	12	13	14	15	16	17	18	19	20	21	22	23	24
I	**10**	**1**					**6**				**10**			**6**						**7**	**8**		**6**	
II	**6**																			**7**			**6**	
III	**6**																		**8**					**6**
IV	**6**			**10**				**6**			**10**	**1**					**10**		**8**					**6**

I: San Francisco-Winter, II: San Francisco-Summer, III: Miami-Winter, IV: Miami-Summer.

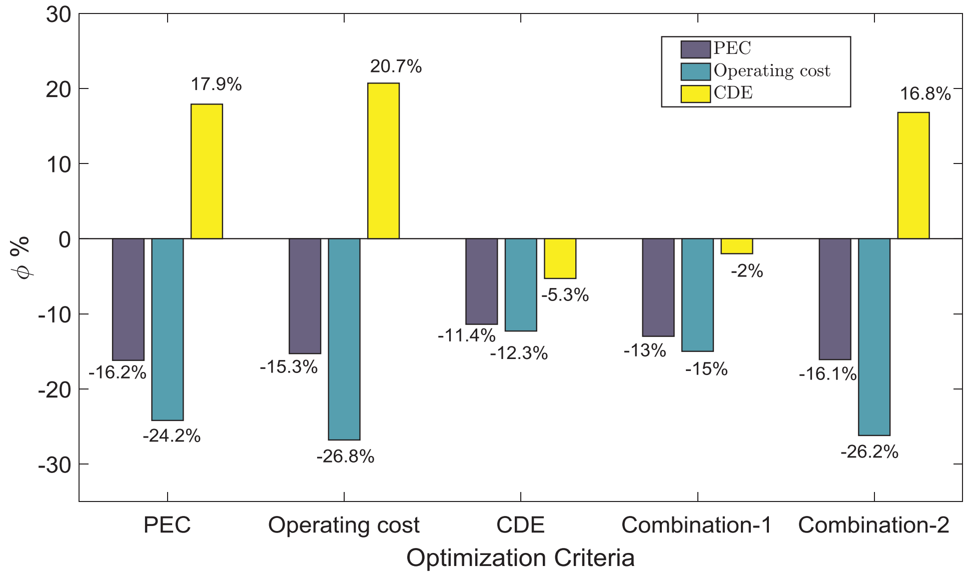

Fig. 10. Change in operating cost, PEC and CDE for the hotel in San Francisco and PGU1 relative to the separate heating, cooling, and electricity production system.

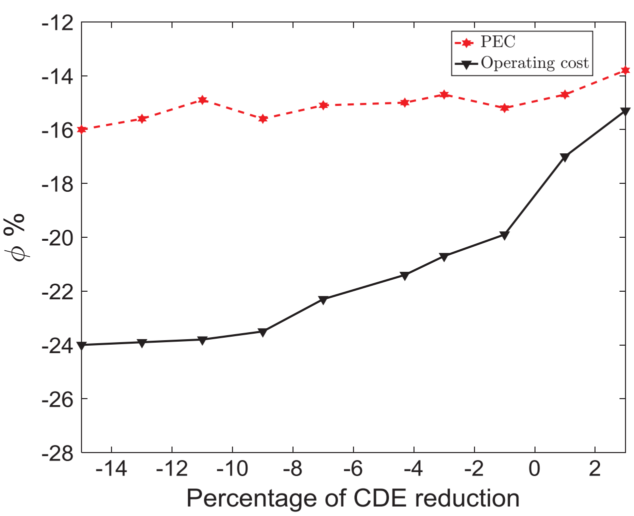

Fig. 11. Reduction of PEC and operating cost versus different percentages of CDE reduction.

6.2. Trade-offs between different optimization criteria for the hotel in Miami

The PGU partial loads calculated based on the NPC methodology for different optimization criteria are shown in Fig. 12. In Miami, as shown in Fig. 13, for all optimization criteria, operating the CCHP system based on NPC methodology results in the reduction of all criteria relative the separate production systems. As presented in Table 5, in Miami, the CDE ratio and PEC ratio are higher than the price ratios of off-peak and mid-peak periods. As a result, the values of f_{opt-o} for PEC and CDE optimization cases are higher than those for operating cost optimization case. Therefore, to achieve higher reductions in PEC and CDE, PGU must operate at upper bounds of PGU operating range for most of the loads. On the other hand, to minimize the operating cost, PGU should operate at the lower bound of the PGU operating range. As a result, higher reductions of PEC and CDE are achieved by optimizing the CCHP system based on either PEC or CDE, which will lead to small reduction in the operating cost. The highest percentage value of PEC saving (14.6%) is obtained when the optimization is done based on PEC. For this optimization case, the operating cost and CDE decrease by 5.2% and 11.4% relative to operating cost and CDE of the separate production system, respectively.

Operation which reduces CDE the most (11.5%) still has a high PEC reduction (14.5%) but the operating cost reduction is low (5.9%). If the objective is to attain the highest reduction in the operation cost (11.2%), then the CDE and PEC reduction values are not favorable; they are at their minimum values (10.5% and 8%, respectively).

As presented in Table 5, PGU overall optimal partial loads, f_{opt-o}, for combination-1 and combination-2 of the optimization criteria are high except for off-peak period. Therefore optimal operations of PGU in these cases are similar to the PGU operation in either CDE or PEC optimization cases. Moreover, in the off-peak period, although the PGU overall optimal loads are not high (the values of $f_{opt-o}^{off-peak}$ are 0.57, 0.61 for combination-1 and combination-2 optimization cases, respectively), the PGU operating limits are on the left side of the $f_{opt-o}^{off-peak}$ and therefore FEL is applied as the strategy. By increasing the weighting factor of operating cost in the objective function, the reduction of operating cost is more but there are less reductions in both PEC and CDE.

In summary, application of the CCHP system in the hotel in Miami is beneficial for all examined optimization criteria. If considerable improvement for all of the criteria is required, then the weighting factor of operating cost has to be higher than the CDE and PEC weighting factors in the optimization problem.

In the city of Miami and when PGU2 is utilized, as shown in Fig. 14, because in cost optimization case, the values of f_{opt-o} for above and below the CCHP operating curve are less than those of CDE and PEC optimization cases, any increase in the operating cost saving (more reduction in the operating cost) leads to the less reduction of the both PEC and CDE. The changes of the CDE and PEC reductions are approximately the same via a change in operating cost reduction; because by changing the cost reduction, the variations of f_{opt-o} of both PEC and CDE are almost the same.

6.3. Optimum operation of PGU of the CCHP systems in the residential buildings in Dalian

The optimum partial load operation for PGU1 is shown in Fig. 15. In transition season, all of the loads are below the CCHP operating curve. In CDE optimization case, for transition season, the operating ranges of loads for hours 19–24 include $f_{opt-o}^{below-CDE} = 0.885$, therefore the PGU operates at this partial load. For the rest of loads, the PGU works at the upper bound of each PGU operating range (FEL strategy). It should be mentioned that Eq. (20) is also satisfied for loads below the CCHP operating curve.

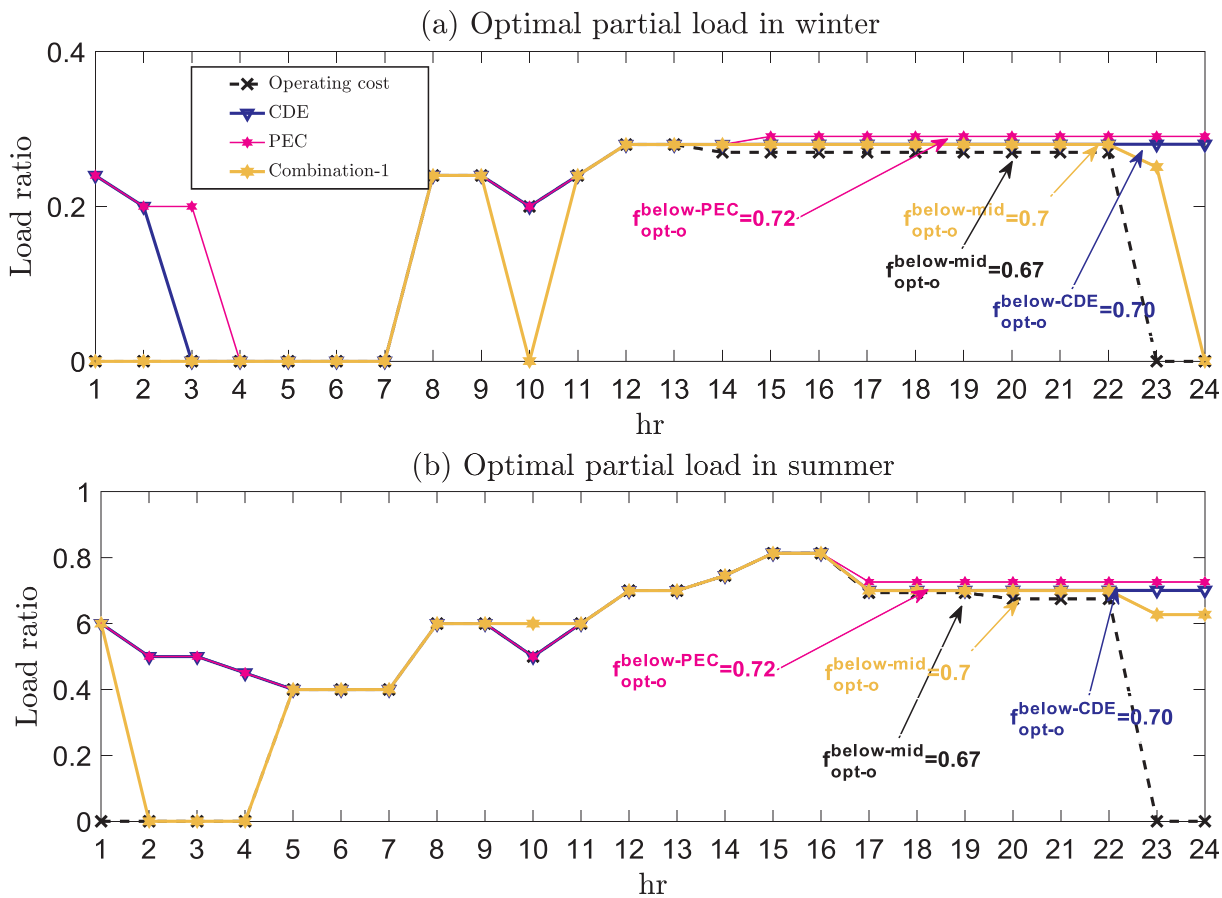

Fig. 12. Optimal partial loads of PGU in a CCHP system with PGU1 applied for the hotel in Miami by considering different optimization criteria.

In transition season, and for PEC optimization case, the PGU partial load is $f_{opt-o}^{PEC} = 0.72$ for any operating range. FEL is followed by PGU for rest of loads. Eq. (20) is also satisfied for loads below the CCHP operating curve.

If optimization of the operation of CCHP system in the transitions season is based on operating cost, then Eq. (20) is not satisfied by loads in region **(6)** for off-peak periods except the loads for hours 1 and 6; hence, for these loads PGU is turned off. For the load in hour 6, the PGU operating range includes $f_{opt-o}^{below-off} = 0.47$, therefore PGU load is set at this value. For the remaining loads, if the operating range includes overall optimal partial load, the PGU works at this load, otherwise FEL strategy is applied.

In the combination-1 case, for transition season, PGU is utilized to satisfy all the loads. PGU operates at the overall optimal load if the PGU operating limits contain this load, otherwise FEL is followed by PGU to satisfy that load. Eq. (20) is also satisfied by the loads in region **(6)**.

As shown in Fig. 16, all optimization criteria, the reductions of operating cost, CDE and PEC based on all optimization cases are near to

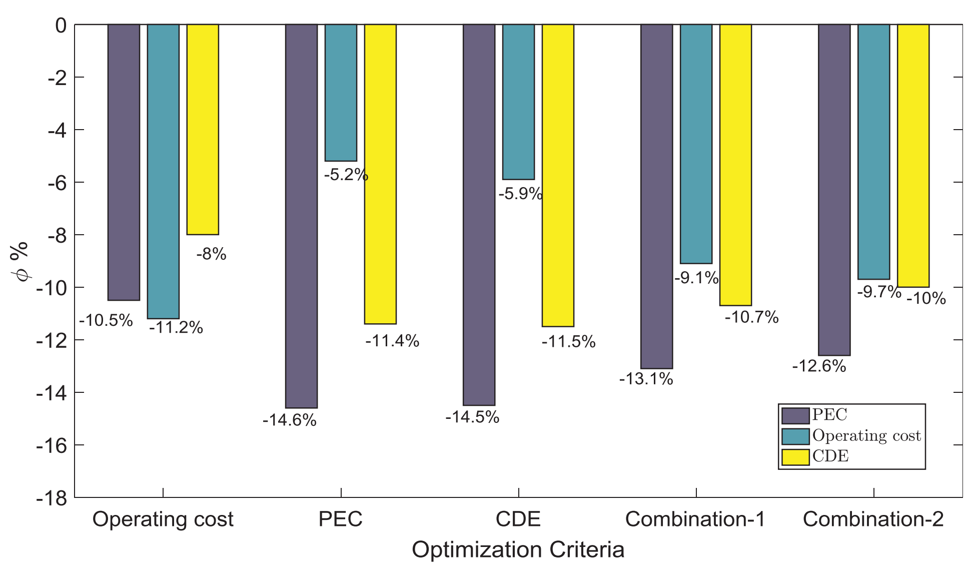

Fig. 13. Change in operating cost, PEC and CDE for the hotel in Miami and PGU1 relative to the separate production system.

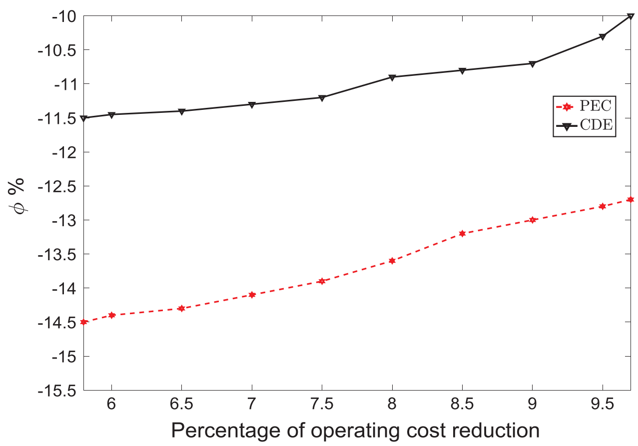

Fig. 14. Percentage variation of PEC and CDE versus different percentages of operating cost reduction.

their maximum values. Percentages of the operating cost reductions are 30.5%, 29.6%, 27.8%, 29.5%, 29.8%, for optimization cases using operating cost, PEC, CDE, combination-1 and combination-2 as objective function, respectively. Percentages of PEC reduction are 15.1%, 17.6%, 16.6%, 17.3% and 16.8% for optimization based on operating cost, PEC, CDE, combination-1 and combination-2 optimization cases, respectively.

6.4. Comparison the CCHP performances when applying novel performance curve, FEL, FTL, MP and FHL strategies

Based on the definition of the overall optimum partial load of PGU and the concept of the NPC curve, other strategies are defined by using hypothetical f_{opt-o} of PGU as presented in Table 7.

As shown in Table 7, other strategies (FEL, FTL, FHL, and MP) hold constant overall optimum partial loads for all of the optimization criteria. In addition, these overall partial loads are different than the overall optimum partial loads obtained from NPC strategy. Let's examine this in more detail on the example of the buildings in San Francisco, in Miami and finally in Dalian.

In San Francisco, as shown in Fig. 17, application of NPC methodology leads to the highest reductions in all of the optimization criteria. In the cost optimization case, the list of strategies in the order of decreasing operating cost is FTL, FHL, MP, FEL, and NPC, where the reductions are 8.1%, 9.6%, 13.24%, 24.09 and 26.8%, respectively. For the CDE optimization cases, the order from highest to the lowest CDE is FEL, FHL, FTL, MP, and NPC. Since the PGU overall optimal partial loads for CDE optimization cases are smaller than those for other optimization criteria, it is more efficient to run PGU at the lower bounds of the PGU operating ranges for most of the hours. Therefore, higher reduction in CDE can be obtained by utilizing the FHL, MP, and FTL strategies instead of FEL. For other optimization cases, the sequence of strategies in order of decreasing the criteria are the same as the sequence of strategies in the cost optimization case.

As shown in Fig. 18, for the hotel in Miami, application of NPC methodology leads to the best savings in all criteria among all operating

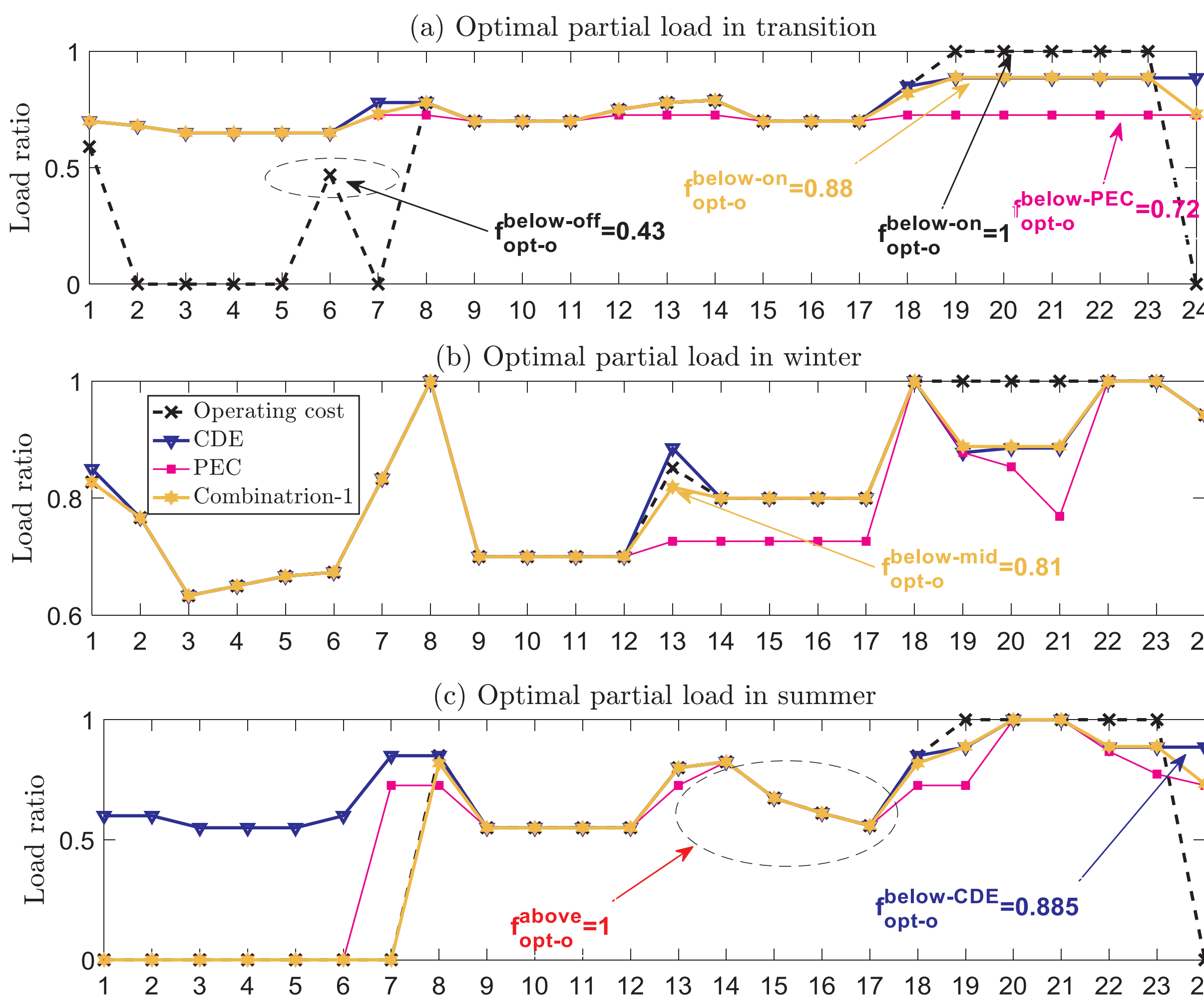

Fig. 15. Optimal partial load of PGU in a CCHP system with PGU1 applied for the residential building in Dalian by considering different optimization criteria.

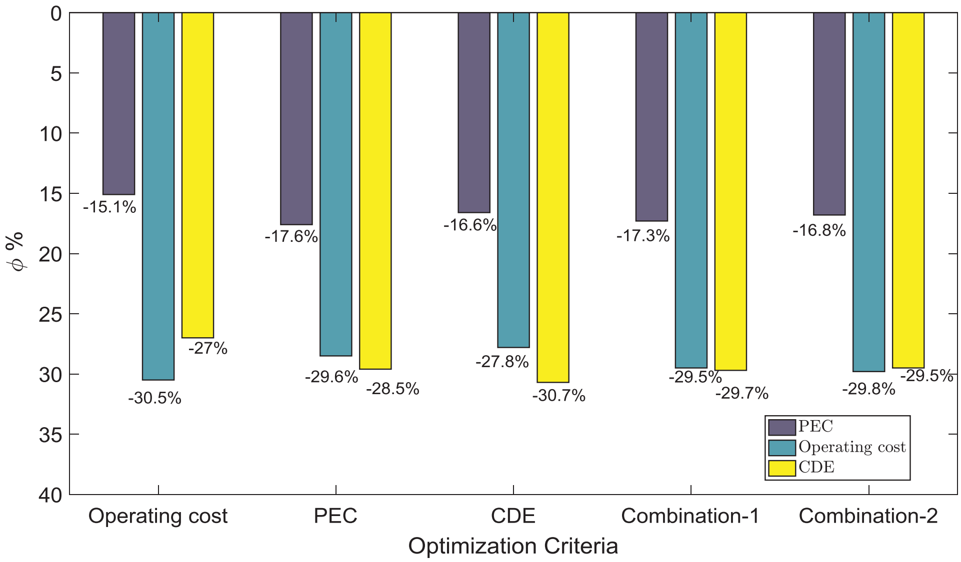

Fig. 16. Change in operating cost, PEC and CDE for residential building in Dalian and PGU1 relative to separate production system.

Table 7
Definition of different strategies by using hypothetical overall optimum partial load of PGU.

	Below the CCHP operating curve	Above the CCHP operating curve scenario#1	Above the CCHP operating curve scenario#2	Above the CCHP operating curve scenario#3
MP	0.25	1	0.25	1
FHL	0.25	0.25	0.25	0.25
FEL	1	0.25	0.25	0.25
FTL	0.25	1	1	1

strategies. In operating cost optimization case, NPC, FTL and MP strategies outperform the FEL and FHL strategies. Decreases in operating costs due to the use of CCHP instead of standalone systems are 11.2%, 6.5%, −2.4%, 0.2% and 4.9% when NPC, MP, FHL, FEL, and FTL strategies are applied, respectively. For CDE optimization case of the CCHP system with PGU1, the CDE reductions are 11.5%, 5.4%, 1.3%, 8.2% and 4.1% when NPC, MP, FHL, FEL and FTL strategies are applied, respectively. This is because the values of f_{opt-o} for the operating cost optimization case are lower than f_{opt-o} of other optimization cases. Therefore, to achieve a higher reduction in operating cost, PGU should operate mostly at the lower bounds of PGU operating limits (the PGU should follow FTL for loads below the CCHP operating curve and should follow FEL for loads above the CCHP operating curve). As a result, although the performances of FTL, FEL, FHL and MP strategies might change by choosing different optimization criteria, application of NPC methodology leads to the highest reduction in all criteria and for all optimization cases.

For residential buildings in Dalian, as shown in Fig. 19, the NPC strategy leads to the best operating cost saving, CDE saving and PEC saving among all optimization strategies. For all optimization criteria, the sequence of the operation strategies in the order of decreasing the optimization criteria is FTL, FHL, MP, FEL, and NPC.

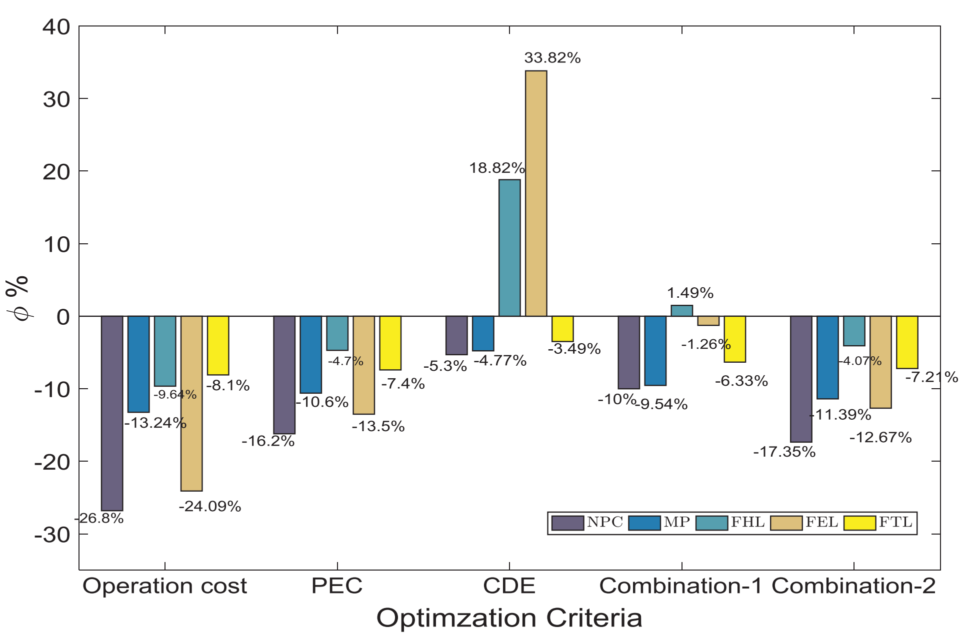

Fig. 17. Comparison of the percentages of the optimization criteria reduction via using different operating strategies-CCHP system with PGU1 in San Francisco.

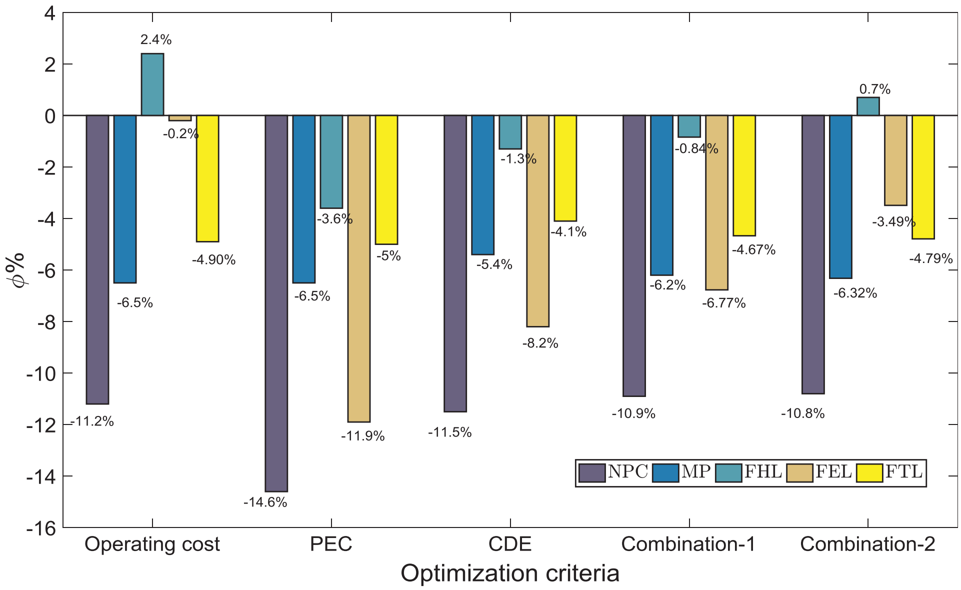

Fig. 18. Comparison of the percentages of the optimization criteria reduction for different operating strategies, CCHP system in Miami PGU1.

7. Conclusions

This work introduces novel CCHP performance curves (NPC) and employs their corresponding overall optimum partial loads as basis for determining optimal operating for a CCHP system. Analytical expressions for computing NPC curves have been presented for cases when the demand loads are above or below the CCHP operating curve. The methodology is flexible since it accounts for energy prices, carbon dioxide emissions (CDE), and primary energy consumption (PEC) factors and weather conditions. This is because the overall optimal partial load and NPC curve change depending on the optimization criteria and the magnitude of the loads.

For all optimization criteria (operating cost or PEC or CDE), NPC strategy determines better operations than any of the previously published strategies for three examined locations.

If operating cost is being minimized, for the hotel in Miami, the improvement due to NPC over the next best strategy for that location (MP) is 4.7%, for the hotel in San Francisco the improvement over the next best strategy for that location (FEL) is 2.7%, while for residential buildings in Dalian the improvement over the next best strategy for that location (FEL) is 2.8%.

When CDE is being minimized, for the hotel in Miami, the improvement due to NPC over the next best strategy for that location (FEL) is 3.3% for the hotel in San Francisco the improvement over the next best strategy for that location (MP) is 0.53%, while for residential buildings in Dalian the improvement over the next best strategy for that location (FEL) is 0.2%.

When PEC is being minimized, for the hotel in Miami, the improvement due to NPC over the next best strategy for that location (FEL) is 2.7%, for a hotel in San Francisco the improvement over the next best strategy for that location (FEL) is 2.7%, while for residential buildings in Dalian the improvement over the next best strategy for that location (FEL) is 1.9%.

Based on these case studies, the following conclusions have been reached:

(1) NPC strategy leads to the best operating cost saving, CDE saving and PEC saving for all of the buildings when compared to other strategies.
(2) NPC strategy can be utilized for different locations with different

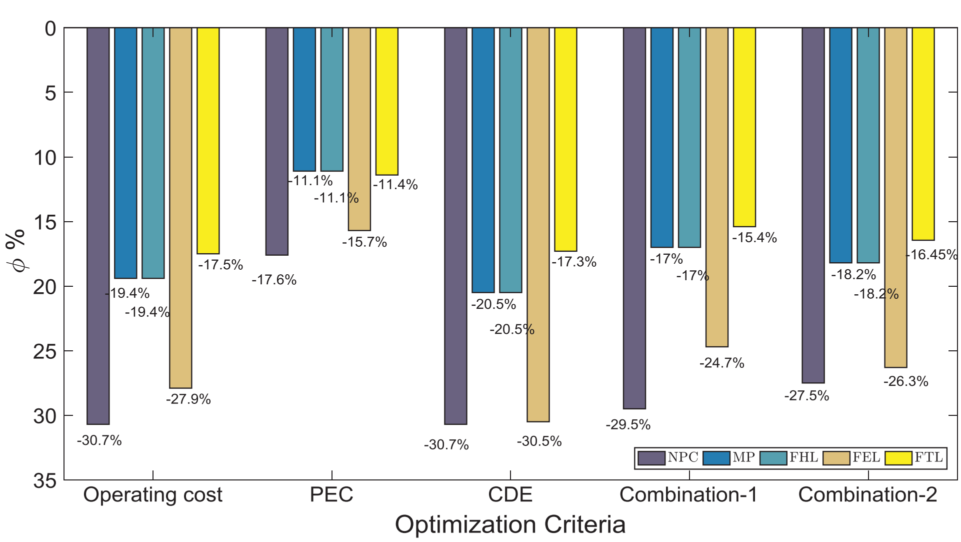

Fig. 19. Comparison of the percentages of the optimization criteria reduction via using different operating strategies-CCHP system with PGU1 in Dalian residential buildings.

energy prices, CDE and PEC factors.
(3) FEL, FTL, FHL and MP strategies can be defined as special (not always optimal) cases of the NPC strategy.
(4) NPC strategy enables optimal operation of CCHP system as the load changes during a day, e.g. from hour to hour.
(5) The relative simplicity of computing the NPC curves makes it possible to identify optimal operating strategies for CCHP systems without having to resort to elaborate model building and complex optimization procedures.
(6) In addition to simplifying the computation of optimal operating conditions, the NPC curves enable rapid evaluation of the impact of changes in energy pricing. Our future work will consider the use of NPC curves for evaluations of changes to the CCHP system structure.

Appendix A

A.1. Derivation of the NPC curve for scenario #1 for loads above the CCHP operating curve

In this scenario, when the PGU operates at a load higher than the lower bound of the operating range; the excess generated electricity is sent to the electric chiller to provide cooling. Because all of the electrical demand can be met by the PGU when it operates at LB load of the operating range, any increase in the PGU partial load leads to the production of electricity which can power the electric chiller. Furthermore, there is more recovered thermal energy which can be utilized in the heating coil to satisfy the heating demand.

It is assumed that the aim is to find an optimum operation of CCHP system corresponding to the minimum operating cost. The net increase in the operating cost due to operating the PGU at a load higher than the base load f_b of the PGU is presented by Eq. (A.1). Please note that if the operating range contains only one scenario, then the base load corresponds to the lower bound of operating range. The second possible scenario has the base load of either E_1 or E_2:

$$\Delta_{cost} = (F-F_b)C_g-(F\eta_{pgu}-F_b\eta_{pgu_b})C_E-\left[\frac{F(1-\eta_{pgu})\eta_{rec}}{\eta_{boiler}}-\frac{F_b(1-\eta_{pgu_b})\eta_{rec}}{\eta_{boiler}}\right]C_g \tag{A.1}$$

The first term in Eq. (A.1), $[(F-F_b)C_g]$ represents the additional natural gas cost when the partial load of the PGU increases from f_b to f. The second term, $[(F\eta_{pgu}-F_b\eta_{pgu_b})C_E]$, is the profit related to the part of cooling demand supplied by the surplus electricity produced in the PGU instead of the electricity purchased from the grid. The last term, $\left\{\left[\frac{F(1-\eta_{pgu})\eta_{rec}}{\eta_{boiler}}-\frac{F_b(1-\eta_{pgu_b})\eta_{rec}}{\eta_{boiler}}\right]C_g\right\}$, is the profit due to the fact that some part of heating demand is satisfied by the recovered heat instead of the boiler.

To convert Δ_{cost} to a dimensionless variable, it is divided by the increase of operating cost when PGU works at upper bound of the operating range, which is defined as:

$$cost_{dif} = (F_{UB}-F_{LB})C_g \tag{A.2}$$

where F_{UB} and F_{LB} are fuels consumed in PGU operating at UB and LB of the operating range, respectively. Finally, the dimensionless cost increase is defined as follows:

$$\delta_{cost} = \frac{\Delta_{cost}}{cost_{dif}} \tag{A.3}$$

To optimize the operating cost of CCHP system, δ_{cost} should be minimized. By replacing F and F_b in Eq. (A.1) by their corresponding partial loads in the PGU and by using Eqs. (2) and (3) in the main body of the paper, δ_{cost} can be rewritten as in Eq. (A.4).

$$\delta_{cost} = E_{nom}\frac{C_g[\psi(f)-\psi(f_b)]}{cost_{dif}} \tag{A.4}$$

where:

$$\psi(f) = \psi^{above}_{Scenario\#1}(f) = f\left[\frac{1}{\eta_{pgu}}\left(1-\frac{\eta_{rec}}{\eta_{boiler}}\right)+\left(\frac{\eta_{rec}}{\eta_{boiler}}-R\right)\right] \tag{A.5}$$

When the partial load f of the PGU changes, only $\psi(f)$ in Eq. (A.4) changes. Consequently, Eq. (A.5) can be utilized to find the minimum of δ_{cost} which correspond to the optimal load of PGU across the operating range.

A.2. Derivation of the NPC curve for scenario #2

In this case, increase in the partial load of the PGU leads to the production of excess electricity which is wasted. At the same time, the boiler duty decreases because of an increase in the recovered heat. To obtain the NPC curve formula, the same procedure as Scenario #1 is carried out.

Any additional cost with respect to base load operation is as follows:

$$\Delta_{cost} = (F-F_b)C_g-\left[\frac{F(1-\eta_{pgu})\eta_{rec}}{\eta_{boiler}}-\frac{F_b(1-\eta_{pgu_b})\eta_{rec}}{\eta_{boiler}}\right]C_g \tag{A.6}$$

The first item, $[(F-F_b)C_g]$ is an excess cost due to the increasing of natural gas consumption, while the second part, $\left\{\left[\frac{F(1-\eta_{pgu})\eta_{rec}}{\eta_{boiler}}-\frac{F_b(1-\eta_{pgu_b})\eta_{rec}}{\eta_{boiler}}\right]c_g\right\}$ is the natural gas cost saving because of the decreasing the boiler duty.

The NPC curve formula of Scenario #2 is as follows:

$$\psi^{above}_{Scenario\#2}(f) = f\left[\frac{1}{\eta_{pgu}}\left(1-\frac{\eta_{rec}}{\eta_{boiler}}\right)+\frac{\eta_{rec}}{\eta_{boiler}}\right] \tag{A.7}$$

A.3. Derivation of the NPC curve for loads blow the CCHP operating curve

By increasing the partial load of PGU from the lower bound (LB), the imported electricity from the grid decreases but some of the recovered heat is wasted. The net cost is expressed as follows:

$$\Delta_{cost} = (F - F_b)C_g - [F\eta_{pgu} - F_b\eta_{pgu_b}]C_E \tag{A.8}$$

Following the same procedure as in Scenario #1, the NPC curve formula is derived to be:

$$\psi^{below}(f) = \frac{f}{\eta_{pgu}} - fR \tag{A.9}$$

If S and G are substituted instead of R in Eq. (A.9), then we arrive at the NPC curve formulas for optimizing CDE and PEC, respectively.

Appendix B

B.1. Derivation of Eqs. (16)–(18)

If separate systems for heating, cooling and electricity production (SP system) are used energy to meet demands (E_d, Q_{cd}, Q_{hd}), then the total operating cost is as follows:

$$cost_{SP} = E_d C_E + \frac{Q_{cd}}{COP_{ec}} C_E + \frac{Q_{hd}}{\eta_{boiler}\eta_{hc}} C_g \tag{B.1}$$

In order to investigate whether a CCHP system is more beneficial than an SP system, the operating cost of SP system is compared to the operating cost of meeting the demand by a PGU running at the minimum partial load. If the operating cost of the PGU is less than the operating cost of the SP system, then the CCHP system is better in the given situation. This is due to the fact that the operating cost per unit of CCHP output decreases when the PGU operates at the load higher than the minimum partial load because of the efficiency of the PGU increases with the increase in the partial load.

The PGU operating cost depends on the amounts of heating and cooling demands. If the heating demand is more than the minimum recovered heat, $\frac{Q_{hd}}{\eta_{hc}} \geqslant Q_{min}$ and the electricity needed to provide electric and cooling demands is more than the minimum electric output of CCHP system, $E_d + \frac{Q_{cd}}{COP_{ec}} > F_{min}\eta_{pgu_{min}}$, then the operating cost is as follows:

$$cost_{CCHP} = F_{min}C_g + \left(\frac{Q_{cd}}{COP_{ec}} + E_d - E_{min}\right)C_E + \frac{1}{\eta_{boiler}}\left[\frac{Q_{hd}}{\eta_{hc}} - F_{min}(1-\eta_{pgu_{min}})\eta_{rec}\right]C_g \tag{B.2}$$

If the heating demand is more than minimum recovered heat, $\frac{Q_{hd}}{\eta_{hc}} \geqslant Q_{min}$, and minimum electric output of CCHP is more than the electricity needed to supply both electric and cooling demand, $E_d + \frac{Q_{cd}}{COP_{ec}} \leqslant E_{min}$, then the operating cost is:

$$cost_{CCHP} = F_{min}C_g + \frac{1}{\eta_{boiler}}\left[\frac{Q_{hd}}{\eta_{hc}} - F_{min}(1-\eta_{pgu_{min}})\eta_{rec}\right]C_g \tag{B.3}$$

If the heating demand is satisfied by some portion of the recovered heat, $\frac{Q_{hd}}{\eta_{hc}} < Q_{min}$ and the remaining amount of the recovered heat and excess electricity produced are not sufficient to provide the cooling demand, $Q_{cd} \geqslant COP_{ac}[F_{min}(1-\eta_{pgu_{min}})\eta_{rec} - \frac{Q_{hd}}{\eta_{hc}}] + COP_{ec}(E_{min} - E_d)$, then the operating cost is expressed as follows:

$$cost_{CCHP} = F_{min}C_g + \frac{1}{COP_{ec}}\left\{Q_{cd} - [F_{min}(1-\eta_{pgu_{min}})\eta_{rec} - \frac{Q_{hd}}{\eta_{hc}}]COP_{ac} - (E_{min} - E_d)COP_{ec}\right\}C_E \tag{B.4}$$

If $\frac{Q_{hd}}{\eta_{hc}} < F_{min}(1-\eta_{pgu_{min}})\eta_{rec}$ B and $Q_{cd} < COP_{ec}\left\{[F_{min}(1-\eta_{pgu_{min}})\eta_{rec} - \frac{Q_{hd}}{\eta_{hc}}] + (E_{min} - E_d)\right\}$, then the operating cost is as follows:

$$cost_{CCHP} = F_{min}C_g \tag{B.5}$$

The use of a CCHP system is more beneficial than an SP system when:

$$cost_{SP} > cost_{CCHP} \tag{B.6}$$

By substituting Eqs. (B.1) and (B.2) into Eq. (B.6) and putting $R = \frac{C_E}{C_g}$, Eq. (16) in the main body of the paper can be derived.

By substituting Eqs. (B.3) and (B.1) into Eq. (B.6) and using R, the Eq. (17) in the main body of the paper is obtained.

Eqs. (B.1) and (B.4) are substituted into Eq. (B.6) to derive Eq. (18) in the main body of the paper.

B.2. Derivation of Eq. (20)

If the demands are satisfied by the SP system, Eq. (B.1) is used to determine the cost. The operating cost when the CCHP operates at the minimum capacity is determined as follows:

$$cost_{CCHP} = F_{min}C_g + (E_d - E_{min})C_E \tag{B.7}$$

By using Eq. (B.6), the inequality of Eq. (20) can be derived.

Appendix C

C.1. Objective functions definition

The following objective function is used to optimize the operating cost of CCHP system:

$$\Phi = \frac{\sum_t \left(E_{grid}R + F + \frac{Q_{boiler}}{\eta_{boiler}}\right)}{\sum_t \left(E_d R + \frac{Q_{hd}}{\eta_{boiler}\eta_{hc}} + \frac{Q_{cd}}{COP_{ec}}R\right)} - 1 \tag{C.1}$$

The evaluation of the operation of CCHP system may be carried out also by employing a linear combination of all the criteria as an objective function, which is defined by Eq. (C.2):

$$\varphi = \sum_i \omega_i \left[\frac{\sum_t \left(E_{grid}Cr_i + F + \frac{Q_{boiler}}{\eta_{boiler}}\right)}{\sum_t \left(E_d Cr_i + \frac{Q_{hd}}{\eta_{boiler}\eta_{hc}} + \frac{Q_{cd}}{COP_{ec}}Cr_i\right)} - 1\right] \tag{C.2}$$

where ω_i is the importance of each criteria and $\sum_i \omega_i = 1$.

Appendix D

Flowcharts of the computation based on the NPC is shown in Fig. D1. The algorithm is applied when $[\psi_{max}^{L.H.S.} = \psi(0.25)]$ and $[\psi_{max}^{R.H.S.} = \psi(1)]$.

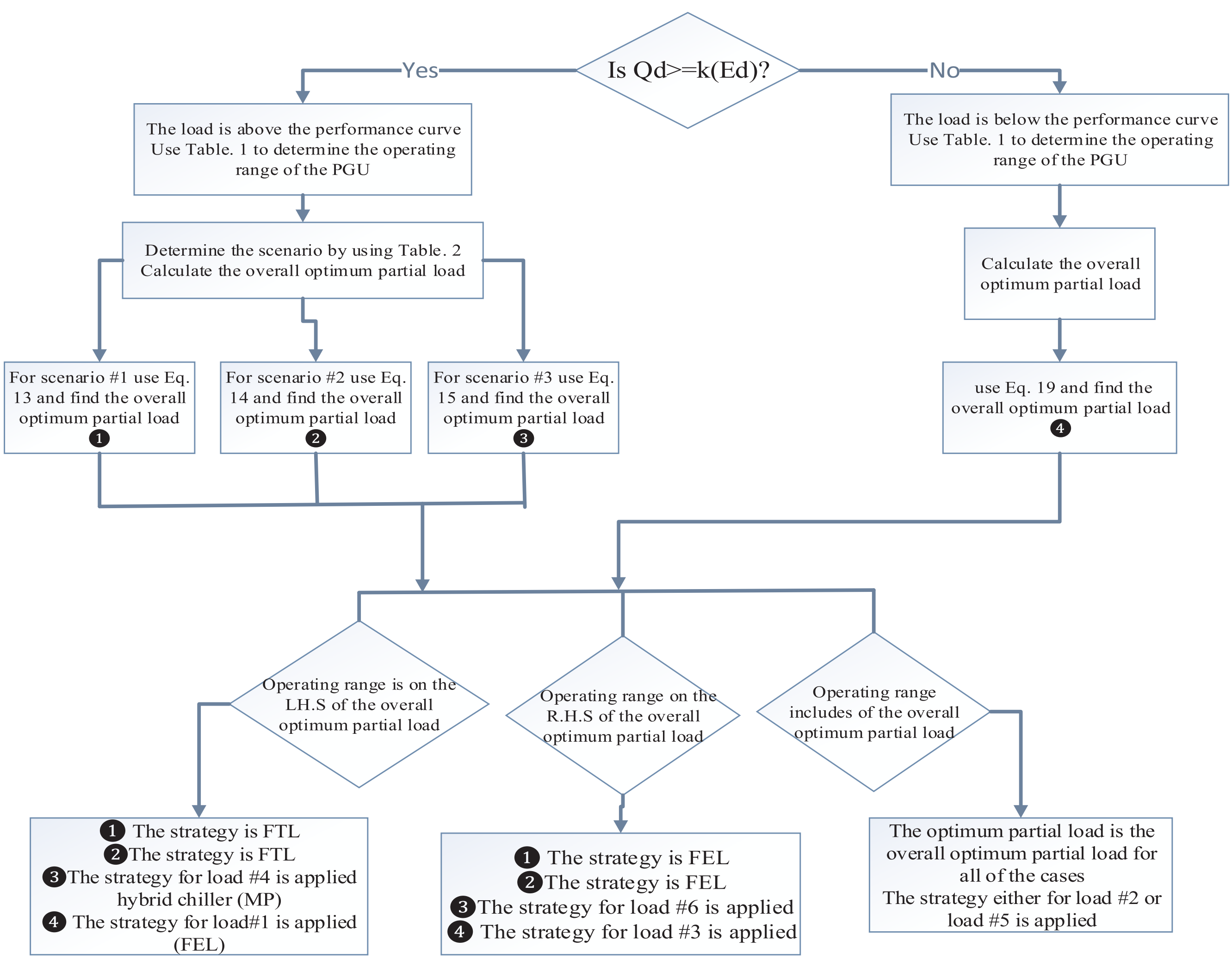

Fig. D1. Determining optimal operating strategy based on NPC.

Appendix E

E.1. Impact of PGU efficiency

Based on different characteristics of the PGU (e.g., partial load efficiency of PGU) and the ratios of optimization parameters (R, parameter of the electricity/ parameter of natural gas), the values of the overall optimum partial loads (f_{opt-o}) might change. As shown in Fig. E1, for both PGU units and for above and below the CCHP operating curve, any increase in the ratio of the optimization criteria leads to an increase in f_{opt-o}. For instance, when price ratio (electricity price/natural gas price) increases, it is more efficient to run the PGU at a higher load and provide higher portion of the electrical demand by CCHP system, although excess thermal energy might be produced. For PGU1 and for below the CCHP operating curve, f_{opt-o} increases gradually with an increase in the R ratio and it reaches 1 when R = 5.8. For loads above the CCHP operating curve, a similar behavior can be seen for f_{opt-o} of PGU1. For PGU2 and for loads below the CCHP operating curve, f_{opt-o} is constant at 0.25 for lower values of optimization criterion R. At R = 2.5, f_{opt-o} increases rapidly to 1. A similar behavior is seen for PGU2 for loads above the CCHP operating curve for f_{opt-o}.

E.2. Optimum operation of PGU of the CCHP system at the hotel in Miami

As presented in Table 6 in the main body of the paper, all of the loads in the winter season are located below the CCHP operating curve. Also, in summer, loads of all hours except loads for hours 12–16 are below the CCHP operating curve. For all optimization criteria, $f_{opt-o}^{above} = 1$; hence for loads during hours 12–16 in summer, MP strategy is followed to manage CCHP operation. The detailed explanation of the NPC methodology application to derive the optimal partial loads of PGU2 is presented here.

E.2.1. Optimization based on the operating cost

Winter off-peak hours 1–4 and 23–24: The overall optimum PGU partial load is $f_{opt-o}^{below-off} = 0.25$. However, even though all the PGU operating ranges include the partial load $f_{opt-o}^{below-off}$ because the loads are in region **(6)**, the Eq. (20) is not satisfied. Hence, SP usage is more beneficial than CCHP system utilization to provide demands for these hours.

Winter hours 5–7: PGU operating ranges are on the left of $f_{opt-o}^{below-mid}$ and as presented in Table 6, the loads are in region **(6)**. Eq. (20) is not satisfied for these loads and therefore the PGU is off.

Winter hours 19–22 and summer hours 19–22: The PGU load ratio is set at $f_{opt-o}^{below-mid} = 0.88$.

Summer off-peak hours: For loads of these hours, $f_{opt-o}^{below-off} = 0.25$. Also, Eq. (20) is not satisfied with any of the loads in region **(6)**. Therefore PGU is off. For loads in region **(10)** (hour 23), $f = f_{FTL}$.

Summer hours 9–10: The operating ranges are on the left of the $f_{opt-o}^{below-mid}$ and also include $f_{max}^{LHS} = 0.3$. Lower bounds of the PGU operating ranges are $f_{min} = 0.25$. Besides, Eq. (20) is not met and therefore PGU is off.

For the rest of the hours in winter and summer, FEL is employed because the PGU operating ranges are located on the left of $f_{opt-o}^{below-mid}$ and Eq. (20) is also satisfied for loads having thermal demands lower than the minimum PGU thermal output.

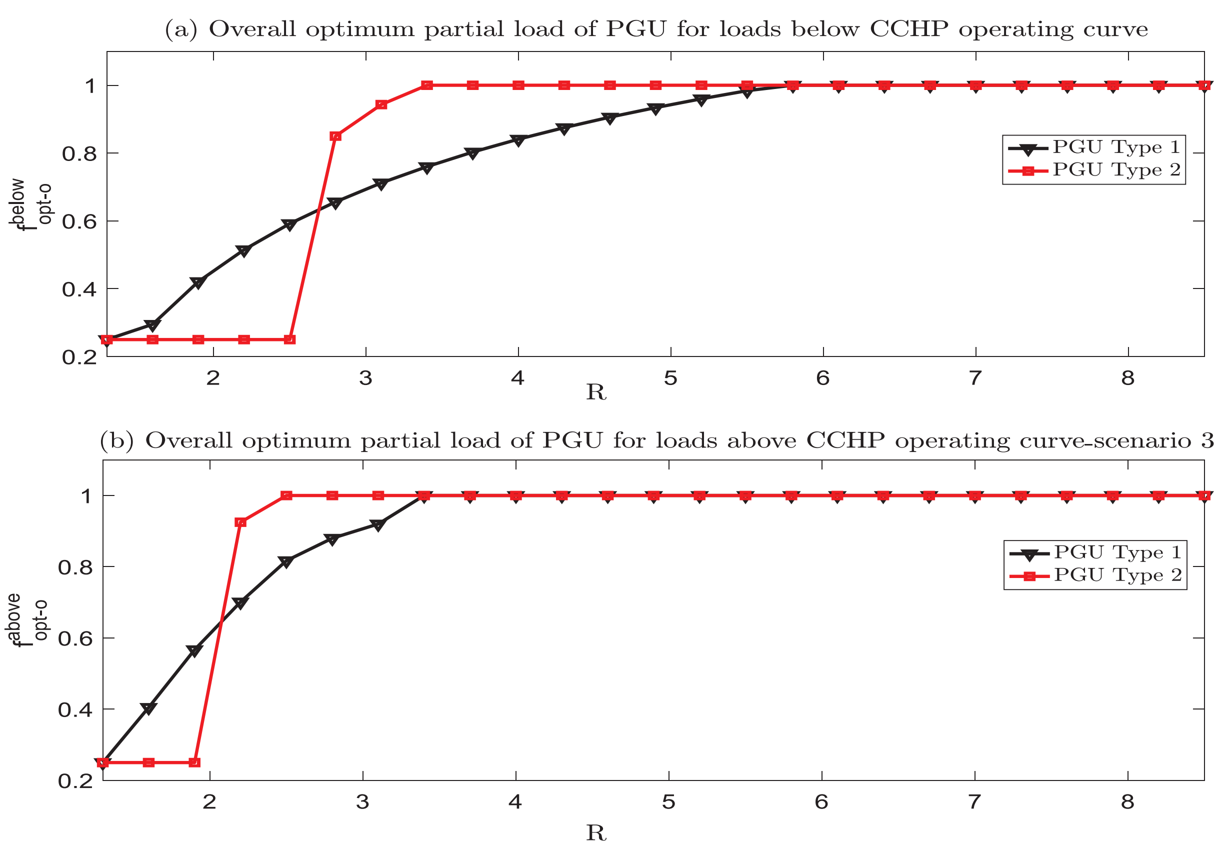

Fig. E1. PGU Overall optimal partial load versus optimization criterion ratio.

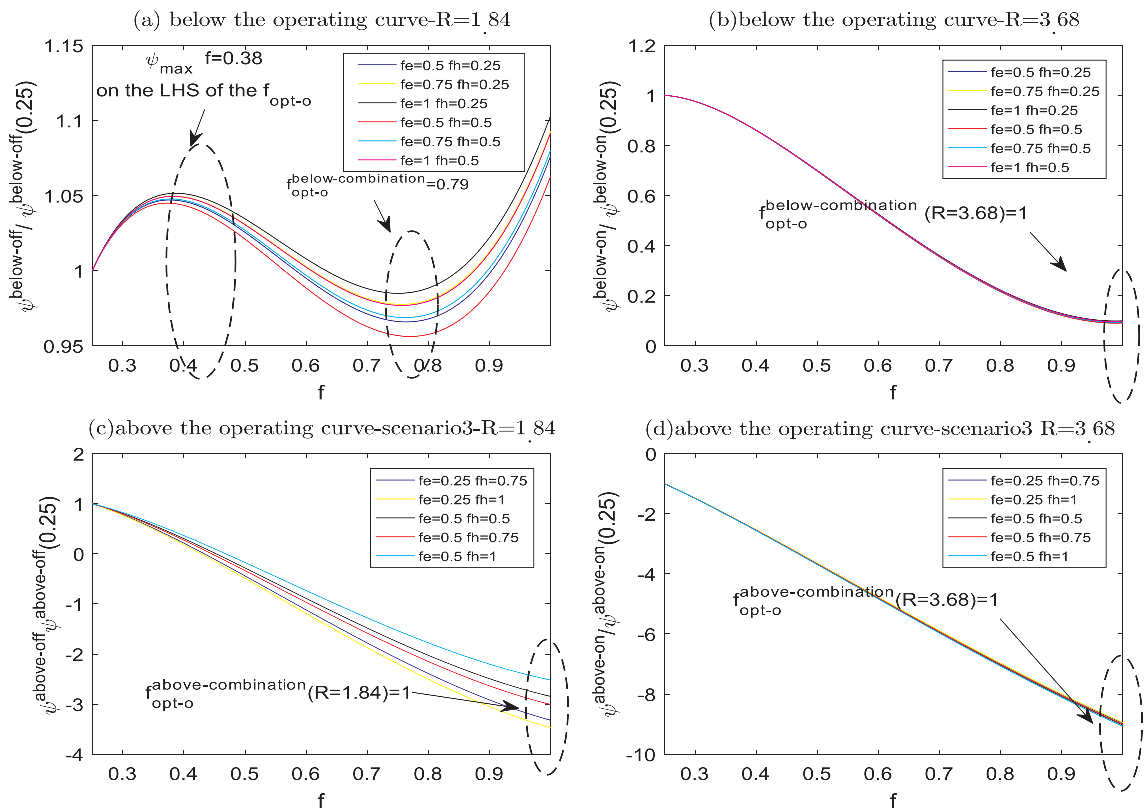

Fig. E2. NPC curves for the upper and the lower regions of CCHP operating curve based on all criteria; hotel in Miami.

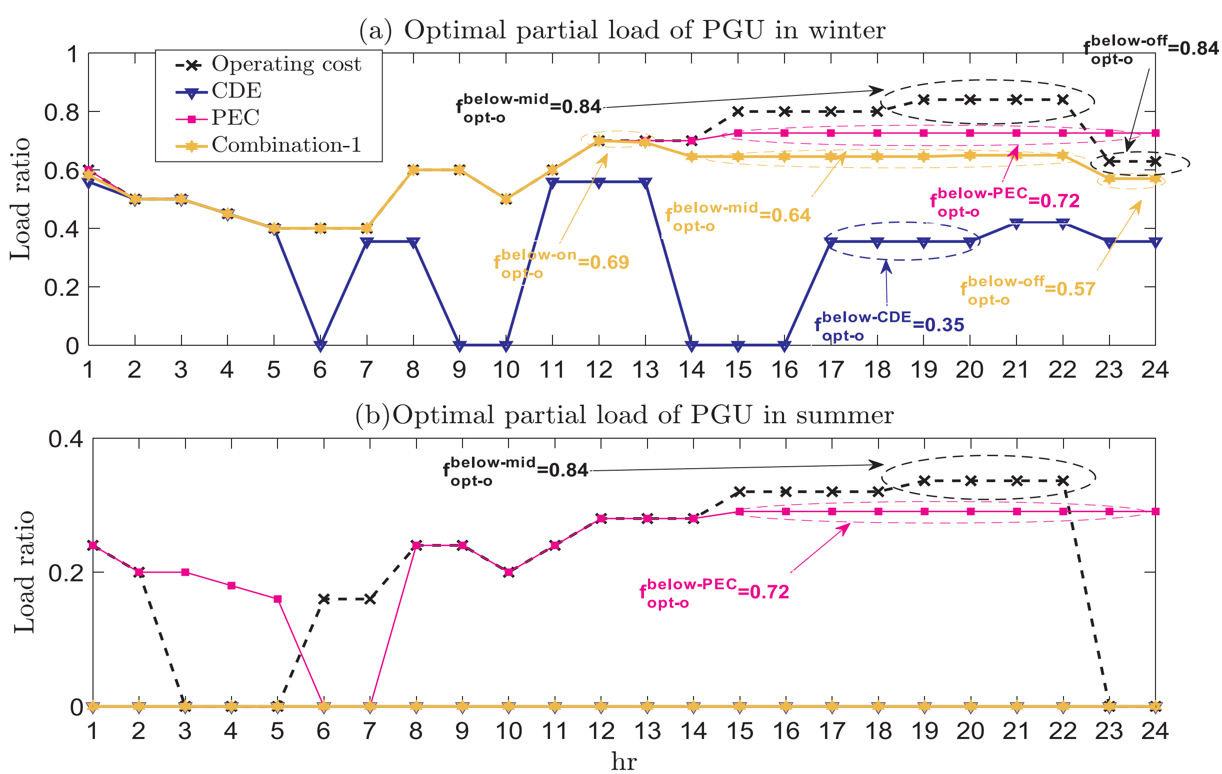

Fig. E3. Optimal partial loads of PGU in a CCHP system with PGU2 applied for the hotel in San Francisco by considering different optimization criteria.

E.2.2. Optimization based on PEC

Winter: The PGU operating ranges for all loads except loads during hours 19–23 are on the left of the $f_{opt-o}^{below-PEC}$ = 0.96. In addition, Eq. (20) is satisfied by them. As a result, PGU power output is adjusted to be $f = f_{FEL}$ for each hour. For loads during hours 19–23, optimal PGU load is 0.96, since their corresponding operating ranges include this load.

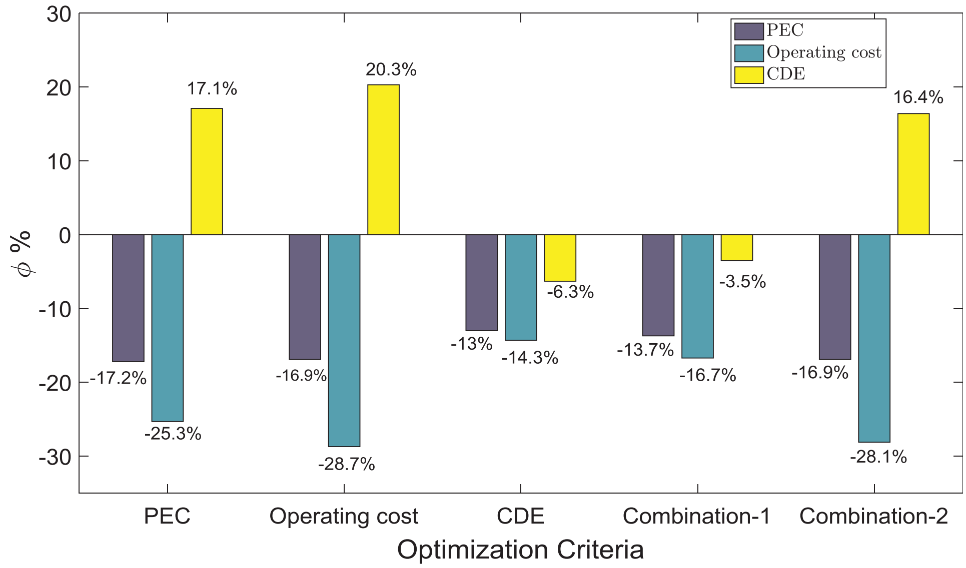

Fig. E4. Change in the operating cost, PEC and CDE for the hotel in San Francisco with PGU2 relative to the separate production system.

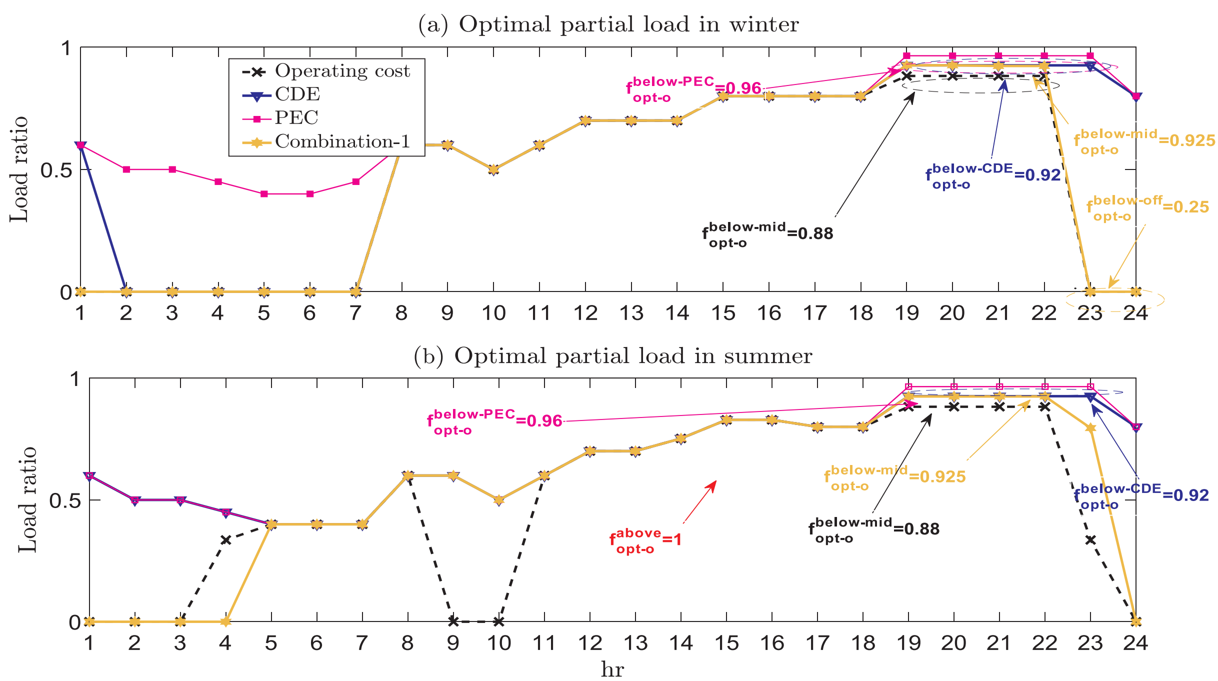

Fig. E5. Optimal partial loads of PGU in a CCHP system with PGU2 applied for the hotel in Miami by considering different optimization criteria.

Summer: PGU runs at the same PGU partial load as in winter, except during hours 12–16, since during these hours the loads are above the CCHP operating curve [Region **(1)**]; MP strategy must be followed by the CCHP system ($f = f'$). Eq. (20) is also satisfied for these loads which are in region **(6)**.

E.2.3. Optimization based on CDE

The overall optimum partial load of PGU for all demands below the CCHP operating curve is 0.92. As a result, except for loads during the hours 19–23 in both seasons, the optimal PGU loads are the same as the PGU loads when the optimization is based on the PEC. For loads during the hours 19–23 in winter and summer, $f_{opt-o}^{below-CDE} = 0.92$ and PGU operates at this load. In winter, Eq. (20) is not satisfied by the load for hour 2 because CDE ratio is lower than PEC ratio; during that hour PGU is off.

E.2.4. Optimization based on a combination of criteria (Combination-1)

NPC curves for the CCHP system at the hotel in Miami are shown in Fig. E2 when optimization is done based on the combination of equally weighted criteria, $\left[\omega_i = \frac{1}{3}\right]$. For loads below the CCHP system operating curve and during the off-peak period *(R = 1.84)*, $f_{max}^{LHS} = 0.38$. The PGU partial loads are the same as the optimal loads obtained by optimizing the operating cost, except for hours 19–22 in winter and summer and for hours 9–10 in summer. For hours 19–22 in both seasons, $f_{opt-o}^{below-mid} = 0.925$. Therefore PGU partial load is fixed at this load. For hours 9–10 in summer, the thermal demand is less than Q_{min}, Eq. (20) is satisfied and therefore $f = f_{FEL}$ is the best mode of PGU operation.

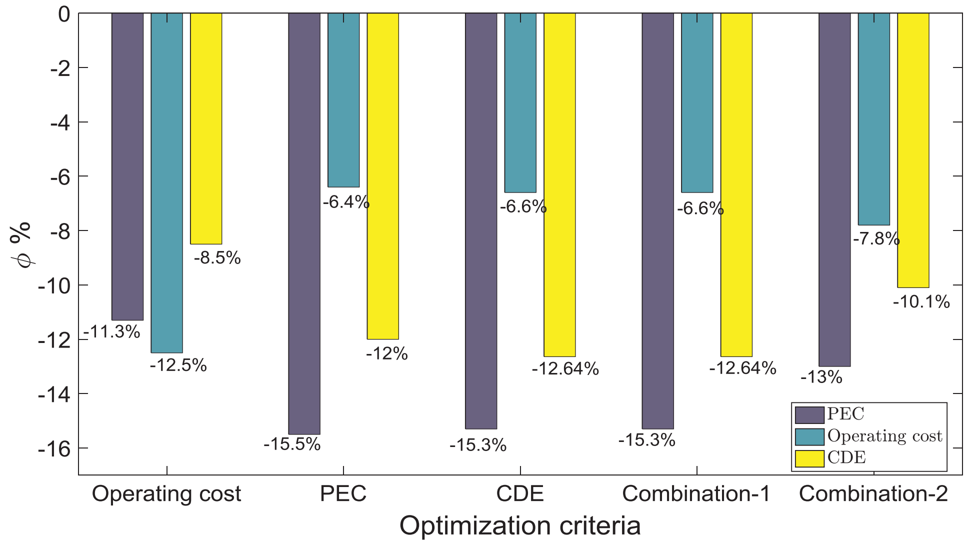

Fig. E6. Change in operating cost, PEC and CDE for the hotel in Miami and PGU2 relative to the separate production system.

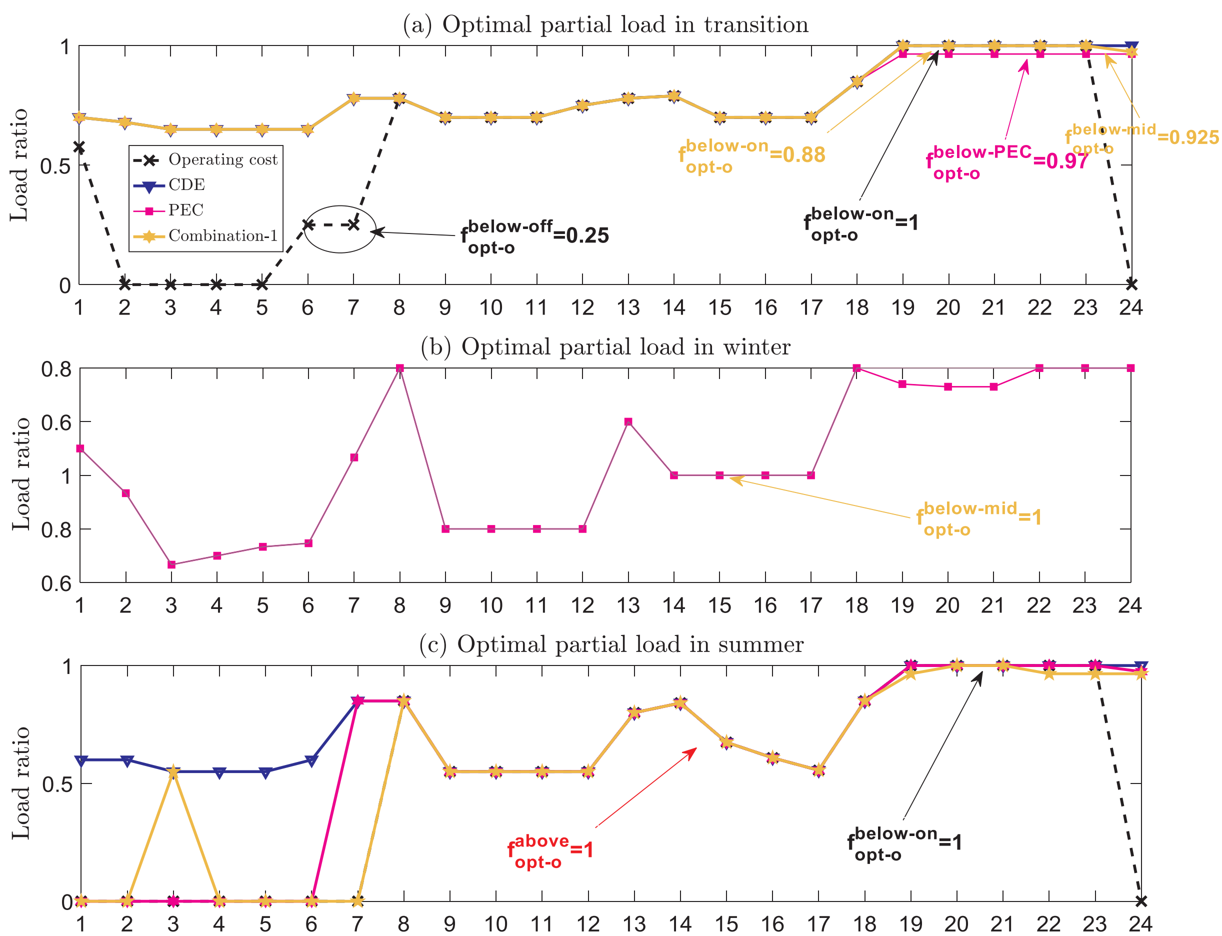

Fig. E7. Optimal partial load of PGU in a CCHP system with PGU2 applied for the residential building in Dalian by considering different optimization criteria.

E.3. Application of novel performance curve methodology for CCHP systems in different cities

The PGU2 optimal loads by using NPC methodology for San Francisco shown in Fig. E3.

If PGU2 is used in San Francisco, similar results can be obtained as the results for PGU1. Using PGU2 improves all the criteria and higher saving can be achieved compared to the savings attained by PGU1. As presented in Fig. E4, the maximum percentage of PEC reduction is 17.2% which is

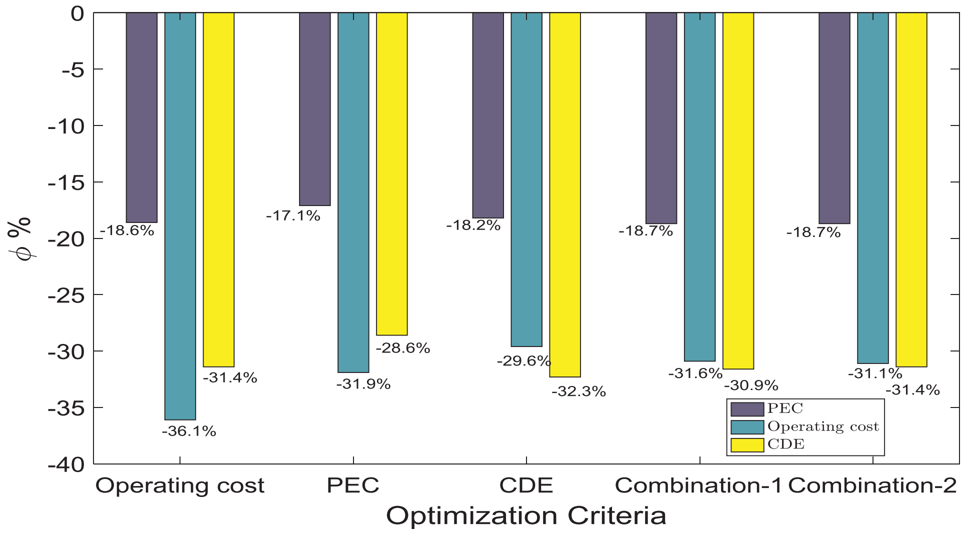

Fig. E8. Change in operating cost, PEC and CDE for residential building in China and PGU2 relative to separate production system.

more than 16.2% achieved with PGU1. In CDE optimization case, although the CDE emission decreases by 6.3%, the PEC and operational cost reductions are at their lowest values (13% and 14.3%, respectively). The highest value of operational cost reduction is 28.7% compared to the cost reduction 26.8% via PGU1 utilization.

PGU optimal loads for the CCHP system in Miami are shown in Fig. E5. Use of PGU2 improves the CCHP performances for all optimization criteria, (Fig. E6). Moreover, for all cases, operating the CCHP system based on the NPC methodology results in the reduction of all criteria. Finally, for all the cases, there are similar trends between variations of criteria by using this CCHP system and variations of criteria by employing CCHP with PGU1.

For the residential building in Dalian, the optimal PGU loads for different optimization criteria calculated by the NPC methodology are shown in Fig. E7.

As shown in Fig. E8, using PGU2 improves all of the optimization results from CCHP PGU1. This is due to the fact that for all partial loads, electrical efficiency of PGU2 is more than the efficiency of PGU1 and because f_{opt-o} of PGU2 is more than f_{opt-o} of PGU 1in most of the optimization cases.

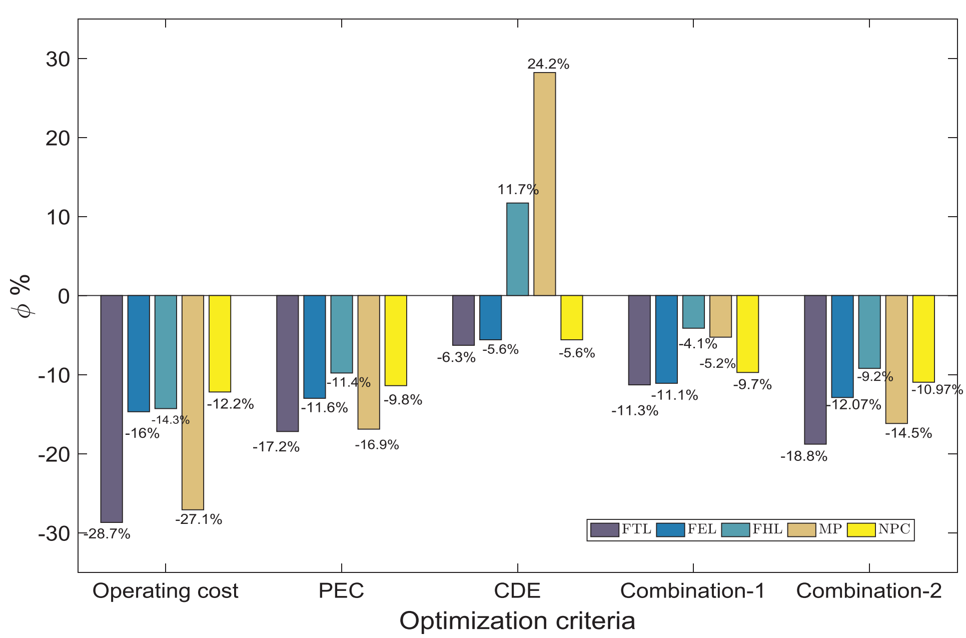

Fig. E9. Comparison of the optimization criteria reduction via using different operating strategies; CCHP system in San Francisco PGU2.

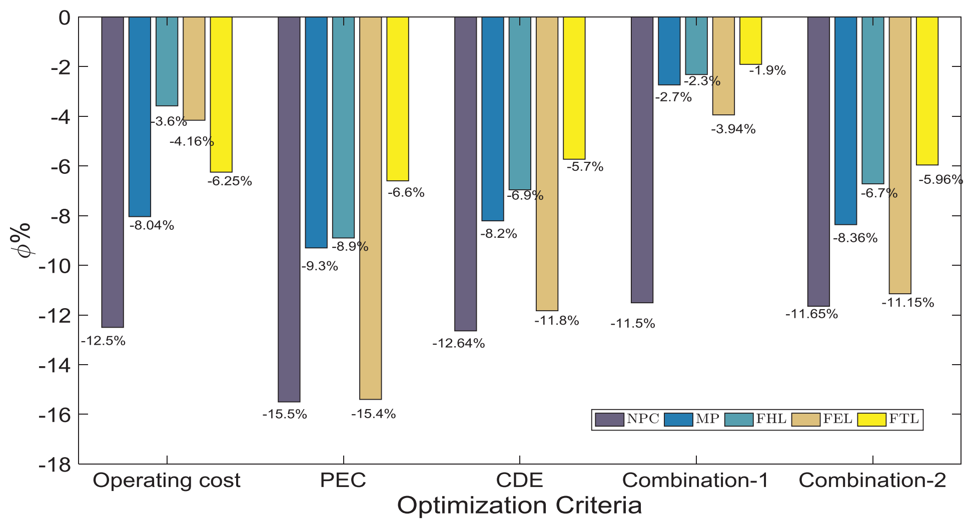

Fig. E10. Optimization criteria reduction via using different operating strategies; CCHP system in Miami PGU2.

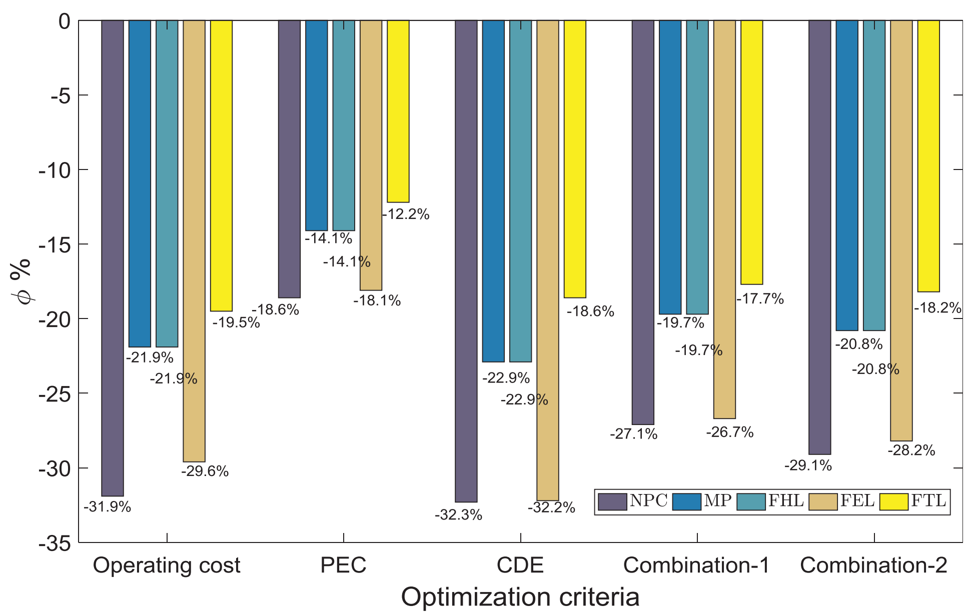

Fig. E11. Optimization criteria reduction via using different operating strategies-CCHP PGU2 system in Dalian residential buildings.

E.4. Comparison of the CCHP performances achieved by applying different operating strategies

Using PGU2 in San Francisco improves performance of the CCHP system for all cases and also for all operating strategies. NPC still is the best among all strategies in terms of reducing the operating cost, PEC, CDE and any combination of them. For instance, NPC, FEL, MP, FHL, and FTL strategies lead to 28.7%, 16%, 14.2%, 27.1% and 12.2% reductions in the operating cost for San Francisco, see Fig. E9, respectively. However when PGU1 is utilized these reductions are 26.8%, 24.09%, 13.24%, 9.6% and 8.1%, respectively.

For residential buildings in Dalian and hotel in Miami all of the criteria are improved for all the strategies by using PGU2. As shown in Figs. E10 and E11, the NPC outperforms all other strategies in all cases. For Dalian, for all optimization criteria, the sequence of the increasing the reductions via various operation strategies is FTL, FHL, MP, FEL, and NPC.

Appendix F

Table F1.

Table F1
PGU operating ranges for different loads of the hotels in San Francisco and Miami.

	Miami (PGU2)				San Francisco (PGU1)			
	Winter		Summer		Winter		Summer	
Hour	LB	UB	LB	UB	LB	UB	LB	UB
1	0.25	0.6	0.25	0.6	0.56	0.6	0.25	0.6
2	0.25	0.5	0.25	0.5	0.5	0.56	0.25	0.5
3	0.25	0.5	0.25	0.5	0.5	0.56	0.25	0.5
4	0.25	0.45	33.58	0.45	0.45	0.56	0.25	0.45
5	0.25	0.4	33.58	0.4	0.4	0.56	0.25	0.4
6	0.25	0.4	33.58	0.4	0.4	0.56	0.25	0.4
7	0.25	0.4	33.58	0.4	0.25	0.4	0.25	0.4
8	0.25	0.6	0.25	0.6	0.25	0.6	0.25	0.6
9	0.25	0.6	0.25	0.6	0.25	0.6	0.25	0.6
10	0.25	0.5	0.25	0.5	0.25	0.5	0.25	0.5
11	0.25	0.6	44.97	0.6	0.56	0.6	0.25	0.6
12	0.25	0.7	0.7	70.23	0.56	0.7	0.25	0.7
13	0.25	0.7	0.7	70.23	0.56	0.7	0.25	0.7
14	0.25	0.7	0.7	91.15	0.25	0.7	0.25	0.7
15	0.25	0.8	0.8	91.15	0.25	0.8	0.25	0.8
16	0.25	0.8	0.8	91.15	0.25	0.8	0.25	0.8
17	25.47	0.8	70.23	0.8	0.25	0.8	0.25	0.8
18	25.47	0.8	70.23	0.8	0.25	0.8	0.25	0.8
19	0.25	1	70.23	1	0.25	1	0.25	1
20	0.25	1	44.97	1	0.25	1	0.25	1
21	0.25	1	44.97	1	0.42	1	0.25	1
22	0.25	1	33.58	1	0.42	1	0.25	1
23	0.25	1	33.58	1	0.25	1	0.25	1
24	0.25	0.8	0.25	0.8	0.25	0.8	0.25	0.8

Appendix G

To find f (the optimal PGU operating load for scenario #3 and for MP strategy) the following three equations should be solved: The electric demand and some part of the cooling demand, $\frac{\alpha Q_{cd}}{Cop_{ec}}$, is provided by the PGU.

$$E'_{pgu} = E_d + \frac{\alpha Q_{cd}}{Cop_{ec}} \tag{G.1}$$

Heating energy balance is expressed as follows:

$$\frac{Q_{hd}}{\eta_{hc}} = \beta E'_{pgu}\left(\frac{1}{\eta_{pgu}} - 1\right)\eta_{rec} \tag{G.2}$$

where β is a part of the recovered heat used to supply the heating demand.

The cooling demand energy balance is expressed as follows:

$$\frac{(1-\alpha)Q_{cd}}{Cop_{ac}} = (1-\beta)E'_{pgu}\left(\frac{1}{\eta_{pgu}} - 1\right)\eta_{rec} \tag{G.3}$$

Solution of these three equations gives α, β and E'_{pgu}, which is required to determine the optimal partial load f' is found.

References

[1] Sa A, Herna J. Trigeneration: an alternative for energy savings. Appl Energy 2003;76:219–27. http://dx.doi.org/10.1016/S0306-2619(03)00061-8.
[2] Mago PJ, Hueffed AK. Evaluation of a turbine driven CCHP system for large office buildings under different operating strategies. Energy Build 2010;42:1628–36. http://dx.doi.org/10.1016/j.enbuild.2010.04.005.
[3] Smith AD, Mago PJ. Effects of load-following operational methods on combined heat and power system efficiency. Appl Energy 2014;115:337–51. http://dx.doi.org/10.1016/j.apenergy.2013.10.063.
[4] Li L, Mu H, Gao W, Li M. Optimization and analysis of CCHP system based on energy loads coupling of residential and office buildings. Appl Energy 2014;136:206–16. http://dx.doi.org/10.1016/j.apenergy.2014.09.020.
[5] Jing Y, Bai H, Wang J, Liu L. Life cycle assessment of a solar combined cooling heating and power system in different operation strategies. Appl Energy 2012;92:843–53. http://dx.doi.org/10.1016/j.apenergy.2011.08.046.
[6] Zheng CY, Wu JY, Zhai XQ, Wang RZ. Impacts of feed-in tariff policies on design and performance of CCHP system in different climate zones. Appl Energy 2016;175:168–79.
[7] Zheng CY, Wu JY, Zhai XQ, Wang RZ. A novel thermal storage strategy for CCHP system based on energy demands and state of storage tank. Electr Power Energy Syst 2017;85:117–29. http://dx.doi.org/10.1016/j.ijepes.2016.08.008.
[8] Mago PJ, Luck R, Knizley A. Combined heat and power systems with dual power generation units and thermal storage. Int J Energy Res 2014;38:896–907. http://dx.doi.org/10.1002/er.
[9] Song X, Liu L, Zhu T, Zhang T, Wu Z. Comparative analysis on operation strategies of CCHP system with cool thermal storage for a data center. Appl Therm Eng

2016;108:680–8. http://dx.doi.org/10.1016/j.applthermaleng.2016.07.142.
[10] Wang J, Sui J, Jin H. An improved operation strategy of combined cooling heating and power system following electrical load. Energy 2015;85:654–66. http://dx.doi.org/10.1016/j.energy.2015.04.003.
[11] Fang F, Wei L, Liu J, Zhang J, Hou G. Complementary configuration and operation of a CCHP-ORC system. Energy 2012;46:211–20. http://dx.doi.org/10.1016/j.energy.2012.08.030.
[12] Knizley A, Mago PJ, Tobermann J, Warren HR. Performance characterization of a power generation unit – organic Rankine cycle system based on the efficiencies of the system components. Energy Convers Manage 2015;105:480–7. http://dx.doi.org/10.1016/j.enconman.2015.08.010.
[13] Holjevac N, Capuder T, Zhang N, Kuzle I, Kang C. Corrective receding horizon scheduling of flexible distributed multi- energy microgrids. Appl Energy 2017. http://dx.doi.org/10.1016/j.apenergy.2017.06.045.
[14] Liu W, Chen G, Yan B, Zhou Z, Du H, Zuo J. Hourly operation strategy of a CCHP system with GSHP and thermal energy storage (TES) under variable loads: a case study. Energy Build 2015;93:143–53. http://dx.doi.org/10.1016/j.enbuild.2015.02.030.
[15] Tan ZF, Zhang HJ, Shi QS, Song YH, Ju LW. Multi-objective operation optimization and evaluation of large-scale NG distributed energy system driven by gas-steam combined cycle in China. Energy Build 2014;76:572–87. http://dx.doi.org/10.1016/j.enbuild.2014.03.029.
[16] Ju L, Tan Z, Li H, Tan Q, Yu X, Song X. Multi-objective operation optimization and evaluation model for CCHP and renewable energy based hybrid energy system driven by distributed energy resources in China. Energy 2016;111:322–40. http://dx.doi.org/10.1016/j.energy.2016.05.085.
[17] Fu L, Zhao X, Zhang S, Li Y, Jiang Y, Li H, et al. Performance study of an innovative natural gas CHP system. Energy Convers Manage 2011;52:321–8. http://dx.doi.org/10.1016/j.enconman.2010.07.003.
[18] Zhao XL, Fu L, Zhang SG, Jiang Y, Li H. Performance improvement of a 70 kWe natural gas combined heat and power (CHP) system. Energy 2010;35:1848–53. http://dx.doi.org/10.1016/j.energy.2010.01.005.
[19] Mago PJ, Chamra LM. Analysis and optimization of CCHP systems based on energy, economical, and environmental considerations. Energy Build 2009;41:1099–106. http://dx.doi.org/10.1016/j.enbuild.2009.05.014.
[20] Liu M, Shi Y, Fang F. A new operation strategy for CCHP systems with hybrid chillers. Appl Energy 2012;95:164–73. http://dx.doi.org/10.1016/j.apenergy.2012.02.035.
[21] Afzali SF, Mahalec V. Optimal design, operation and analytical criteria for determining optimal operating modes of a CCHP with fired HRSG, boiler, electric chiller and absorption chiller. Energy 2017;139:1052–65. http://dx.doi.org/10.1016/j.energy.2017.08.029.
[22] Wang J, Jing Y, Zhang C. Optimization of capacity and operation for CCHP system by genetic algorithm. Appl Energy 2010;87:1325–35. http://dx.doi.org/10.1016/j.apenergy.2009.08.005.
[23] Wang J, Zhang C, Jing Y. Multi-criteria analysis of combined cooling, heating and power systems in different climate zones in China. Appl Energy 2010;87:1247–59. http://dx.doi.org/10.1016/j.apenergy.2009.06.027.
[24] Li L, Mu H, Li N, Li M. Analysis of the integrated performance and redundant energy of CCHP systems under different operation strategies. Energy Build 2015;99:231–42. http://dx.doi.org/10.1016/j.enbuild.2015.04.030.
[25] Kang L, Yang J, An Q, Deng S, Zhao J, Wang H, et al. Effects of load following operational strategy on CCHP system with an auxiliary ground source heat pump considering carbon tax and electricity feed in tariff. Appl Energy 2017;194:454–66. http://dx.doi.org/10.1016/j.apenergy.2016.07.017.
[26] Zheng CY, Wu JY, Zhai XQ. A novel operation strategy for CCHP systems based on minimum distance. Appl Energy 2014;128:325–35. http://dx.doi.org/10.1016/j.apenergy.2014.04.084.
[27] Li M, Mu H, Li N, Ma B. Optimal design and operation strategy for integrated evaluation of CCHP (combined cooling heating and power) system. Energy 2016;99:202–20. http://dx.doi.org/10.1016/j.energy.2016.01.060.
[28] Fang F, Wang QH, Shi Y. A novel optimal operational strategy for the CCHP system based on two operating modes. IEEE Trans Power Syst 2012;27:1032–41. http://dx.doi.org/10.1109/TPWRS.2011.2175490.
[29] Urbanucci L, Testi D. Optimal integrated sizing and operation of a CHP system with Monte Carlo risk analysis for long-term uncertainty in energy demands. Energy Convers Manage 2018;157:307–16. http://dx.doi.org/10.1016/j.enconman.2017.12.008.
[30] Fumo N, Mago PJ, Chamra LM. Emission operational strategy for combined cooling, heating, and power systems. Appl Energy 2009;86:2344–50. http://dx.doi.org/10.1016/j.apenergy.2009.03.007.
[31] Yun K, Luck R, Mago PJ, Smith A. Analytic solutions for optimal power generation unit operation in combined heating and power systems. J Energy Resour Technol 2012;134:1–8.
[32] Sheikhi A, Ranjbar AM, Safe F. Optimal dispatch of a multiple energy carrier system equipped with a CCHP. Int Conf Renew Energy Power Qual 2011;1:1–6.

Chapter 4

Urban community energy systems design under uncertainty for specified levels of carbon dioxide emissions

The contents of this chapter have been published in the following peer reviewed journal:

Afzali SF, Cotton JS, Mahalec V. Urban community energy systems design under uncertainty for specified levels of carbon dioxide emissions. Appl Energy 2019. doi:10.1016/j.apenergy.2019.114084.

Applied Energy 259 (2020) 114084

Contents lists available at ScienceDirect

Applied Energy

journal homepage: www.elsevier.com/locate/apenergy

Urban community energy systems design under uncertainty for specified levels of carbon dioxide emissions

Sayyed Faridoddin Afzali[a], James S. Cotton[b], Vladimir Mahalec[a,*]

[a] *Department of Chemical Engineering, McMaster University, 1280 Main St. West, Hamilton, ON L8S 4L8, Canada*
[b] *Department of Mechanical Engineering, McMaster University, 1280 Main St. West, Hamilton, ON L8S 4L8, Canada*

HIGHLIGHTS

- An optimization framework for optimal ES design under uncertainty is presented.
- The ES design is performed by minimizing the ATC and limiting the risk of CDE.
- Change in the size of system components is presented as a function of CDE.
- Random vector sampling significantly speeds up convergence.
- Significant technological changes are required to attain 90% reduction in CDE.

ARTICLE INFO

Keywords:
Two-stage stochastic programming
Energy system design
CO_2 emission strategies
Uncertainty
Random vector sampling
Combined cooling
Heat
Power system

ABSTRACT

This study examines how the optimal system design of an urban community energy system changes under the presence of uncertainties in energy prices and demands for a specified level of carbon dioxide emissions (CDE), which is measured as a percentage of CDE associated with the operation of standalone systems. In order to account for uncertainties and to reduce the computational times and retain accuracy, moment matching is used to discretize uncertain distributions. Diverse scenarios are constructed by random sampling of the vectors which contain discrete distributions of uncertain parameters. System design is carried out to minimize the annual total cost and to limit the average of the worst-case emissions with the 5% probability which corresponds to the conditional value at risk (CVaR) of emissions for the confidence level of 95%. The effects of the different values of CVaR on the design of the system are examined. It is shown how the system size changes due to uncertainty and as a function of the CDE target value. Design of an energy system for office buildings in Dalian, China, is presented. Since there is no significant amount of flat surfaces available in a dense urban core, photovoltaics and thermal solar are not considered as candidates for system components. It is shown that with the present-day technology, the lowest amount of CDE is 37% of emissions from standalone systems which use coal-based grid electricity. This indicates the necessity of a significant technological change to reduce CDE to be 10% of standalone systems.

1. Introduction

Application of on-site generation combined cooling, heat, and power (CCHP) systems and distributed energy systems (DES) is increasing [1] since they can reduce the total cost and CO_2 emissions [2] relative to the use of the standalone systems. A typical energy system consists of multiple technologies for generating energies, converting energies, storing them, and finally distributing them among buildings. The energy system can be applied to different kinds of building such as residential buildings, office buildings, hotel buildings, commercial buildings and industrial plants. The economic, environmental and energy performances of the energy system depend on the configuration of the system, the size of each component and the system operating strategy [3]. By choosing the proper size and operation of the system, the operational cost and greenhouse gas (GHG) emissions might decrease drastically.

The simple CCHP system comprises of a power generation unit (PGU), a heat recovery system, a heating coil or a heat exchanger, an absorption chiller, and a backup boiler [4]. Some energy systems (ESs) include hybrid chillers to enhance cooling efficiency [1–3,5–7]. Liu

* Corresponding author.
E-mail address: mahalec@mcmaster.ca (V. Mahalec).

https://doi.org/10.1016/j.apenergy.2019.114084
Received 19 July 2019; Received in revised form 23 September 2019; Accepted 5 November 2019
Available online 07 December 2019

Nomenclature

Acronyms

ATC	Annual total cost
CCHP	Combined cooling, heating and power
CDE	CO_2 emission
CHP	Combined heating and power
COP	Coefficient of performance
CVaR	Conditional value at risk
DES	Distributed energy system
ES	Energy System
GSHP	Ground source heat pump
MCS	Monte Carlo Sampling
MILP	Mixed integer linear programming
MINLP	Mixed integer non-linear programming
kW	kilowatt
ORC	Organic Rankine cycle
PGU	Power generation unit
PV	Photovoltaic
RVS	Random Vector Sampling
SAA	Sample average approximation
a, b, c	Dimensionless coefficients
C	Cost [$/kW]
Ca	Size of each component
CO2R	Carbon dioxide emission ratio
d	Design variable
E	Electric energy [kW]
F	Fuel energy [kW]
f	Partial load
HnC	Heating network cost
InC	Investment cost
ir	Interest rate
K	Number of sets of three scenarios
l	Limit of the CVaR of CDE
LC	Life cycle
P	Number of uncertain parameters
Pen	Penalty variable
Q	Heating energy [kW]
R	Recovery factor
S	Number of scenarios
U	Charging/discharging status
VC	The variable cost of each component
x	First-stage binary variable
battery	Battery/electrical storage
boiler	Boiler
cd	Cooling demand
CDE	Carbon dioxide emission
cost	Cost
d	Demand
EL	Electricity from the grid
f	Partial load
gshp	Ground source heat pump
gshp-h	GSHP for heating
gshp-c	GSHP for cooling
tst	Thermal energy storage
s	scenario
SP	Separate production
t	time
E	Electricity
ec	Electric chiller
fl	Partial load at f
NG	Natural gas
grid	Grid
hc	Heating coil
hd	Heating demand
i	component
in	Input energy
nom	Nominal
y	Second-stage variable

Greek

η	Efficiency
μ	Emission conversion factor
δ	Auxiliary binary variable
π	Probability of each scenario
ζ	Auxiliary binary variable
γ	Auxiliary binary variable
θ	Uncertain parameter
β	On/off coefficient
ν	Auxiliary binary variable
λ	Auxiliary binary variable

Subscripts

ab	Absorption chiller
rec	Recovery

Superscripts

charge	Charging status
disch	Discharging status
min	minimum
max	maximum
E	Energy
Nr	Normalized
op	Operating

et al. [5] proposed an operating strategy for a CCHP system, including hybrid chillers such that the ratio of cooling energy provided by the electric chiller to the cooling load varies at each hour. Zheng et al. [6] employed hybrid chillers and investigated the economic performance of the CCHP system following a feed-in tariff policy. Zheng at al. [1] studied the operation of CCHP system and hybrid chillers by proposing a novel operating strategy based on the minimum distance between loads and the CCHP operating curve. Novel performance curves were derived by Afzali and Mahalec [7] to improve the operation of the CCHP system. It was shown that the proposed strategy is the best amongst all other strategies such as following electrical load, following thermal load and following hybrid load. Short-term thermal energy storage might be employed to obtain a wide range of the ratio of electric output to thermal output, [8]. Mago et al. [9] studied the operation of a combined heat and power (CHP) system comprising dual power generation units and short-term thermal energy storage. Wang et al. [10] modelled the operation of a community energy system. In this study, a day-ahead scheduling strategy was proposed. In addition, the effect of multiple energy storage devices on the system flexibility was examined. Addition of a battery to manage the electric output of the system has been studied by [11]. The ground source heat pump (GSHP) has been added to an energy system (ES) [12-14] to attain flexibility in heating, and cooling outputs, Liu et al. [15] analyzed the performance of a CCHP system which included a GSHP and thermal energy storage. The application of a CCHP system driven by a gas-steam combined cycle at an educational center in China was investigated in [16]. Distributed energy resources (e.g., solar energy and wind energy) have been integrated with a CCHP system to enhance the economic and environmental performances of the system [17]. Fu et al. [18,19] analyzed the performance of a CCHP system comprised of an internal combustion engine, a flue gas heat exchanger, a jacket water heat exchanger, and an absorption heat pump.

Most of the previously published papers have designed the energy systems for deterministic case studies, considering deterministic profiles of energy demands and deterministic values for the natural gas and electricity price. However, building energy demands and market energy prices cannot be predicted precisely at the time of the design. If these uncertainties are not incorporated into the model, the design and operation of the system might differ from the calculated deterministic optimum and emissions, and the system cost might be underestimated.

Two often used approaches to study the effect of the uncertainty on the design and operation of the system are: (i) stochastic model which is created by adopting different realizations of the uncertain parameters, and (ii) sensitivity analysis which determines how the output uncertainty is apportioned to the different sources of uncertainty in inputs [20].

If uncertain parameters are known to lie within specific intervals without information on probabilities of their occurrence, then the robust optimization method can be employed. If additional information such as probability distributions is provided for the uncertain parameters, then the stochastic programming models (which are similar in style to robust optimization) are employed. Stochastic programming aims to find the optimal solution which is feasible for all uncertain data and then optimizes the expected value of the objective function.

Several researchers have used a robust optimization approach to design energy systems. Akbari et al. [21] considered the uncertainty in energy demands, energy prices, carbon emission cost, and primary energy consumption. Rezan et al. [22] assumed the uncertainty in demand and determined the size of the DES. Yokoyama et al.[23] proposed a three-level mixed-integer linear programming algorithm to solve a robust optimization model to determine the optimal design of DES under demand uncertainty. Yokoyama and Kiochi [24] proposed a multi-level nonlinear programming model to determine the optimal sizes of the components in the energy system while minimizing the maximum regret rate in the annual total cost. The robust optimization design model was proposed by Niu et al. [25] to design the cooling system under cooling load uncertainty. The proposed robust model was applied to a hospital in China to minimize the cost of the cooling system design.

Two-stage stochastic programming approach for determining the optimal design of energy systems has recently attracted more attention. Zhou et al. [26] used a two-stage stochastic model of a DES which they optimized by using genetic algorithm and Monte Carlo simulation. They concluded that the proposed system possesses the inherent robustness under uncertainty because of the connection to the grid and the storage facility. Fuentes-Cortes et al.[27] presented a two-stage stochastic optimization model to design a cogeneration system for a housing complex in Mexico. The aim was to minimize the expected annual total cost (ATC), expected operational CO_2 emissions (CDE), and minimize the worst-case scenarios of the ATC and CO_2 emissions. Yang et al. [28] applied two-stage stochastic programming [29] for sizing a DES under uncertainty of energy demands, energy prices, and renewable energies. They considered the discrete size of equipment capacities. Rezan et al. [30] modeled the uncertain energy demands using a probabilistic approach and investigated the design of a DES for both stochastic and deterministic cases. The sample average approximation method was employed to build the objective function (expected annual total cost), and the optimal design for multiple cases was performed considering various percentages of change in uncertain parameters.

The uncertain programming framework was proposed by Li et al. [31] to investigate the design of a CCHP system under energy demand uncertainty. The authors built a probabilistic model based on the integration of the mixed integer nonlinear programming (MINLP) model and Monte Carlo simulation. They concluded that capacities of assistant facilities (e.g., gas boiler, electric chiller, etc.) are more sensitive to the uncertainty of energy demands than the capacities of core facilities (Gas turbine, heat exchanger and absorption chiller). Mavromatidis et al. [32] proposed a sensitivity analysis framework to determine the essential uncertain parameters which affect the economics of DES more than the others. A two-stage stochastic model was developed by Mavromatidis et al. [33] to design a DES considering multiple uncertainties of energy demands and energy prices. The optimal design of DES was estimated based on the minimization of the system expected cost while the expected value of CO_2 emissions was kept below a defined threshold. Urbanucci and Testi [34] applied a two-stage stochastic programming model to design a CHP system for a hospital in Italy under long-term demand uncertainty. The paper provided a framework for decision-makers who are looking for determining the optimal CHP size while following a specific operating strategy. Mavromatidis et al. [35] investigated the design of a DES under different optimization criteria; optimistic, pessimistic, risk-neutral, and risk-averse criteria. They presented a two-stage stochastic programming model for the energy system employed in a Swiss neighborhood. A multi-objective optimization model was proposed by Hu and Cho [36] to minimize the cost, CDE and primary energy consumption of a CCHP system. The uncertainty was included by the use of probability constraint method. The impact of uncertainty on the energy and economic performances of a hybrid CCHP and PV system was investigated in [37]. It was shown that the uncertainty influences the operational cost of the system more than the performance with respect to energy utilization. A unified scheduling strategy was proposed by Lv et al. [38] to improve the operation of a community energy system. The proposed model adopted the uncertainty related to the environment and building loads. Jing et al. [39] performed Multi-objective optimization of an urban energy network. Novel benefit allocation constraints inspired by the game theory were added to the system model to ensure the individual benefit of each building in the energy network.

Some of the researchers investigated the effect of different uncertain parameters on the operation of the energy system. Carpaneto et al. [40] investigated cogeneration operation planning regarding while considering uncertain parameters in energy demands and energy prices. A fuzzy programming model was proposed by Mavrotas et al. [41] for multi-objective planning optimization of large service sectors under load uncertainty to maximize the demand satisfaction and minimize the system cost. Mavrotas et al. [42] presented energy planning for a CCHP system using a mathematical programming framework (MILP model) and Monte Carlo simulations. In their paper, they considered the uncertainty in all economic parameters, including energy prices and economic interest rate. Recently, Ersoz and Colak [43] applied four different simulation methods (Monte Carlo method, scenario-based method, historical trend method, and parametric method) to investigate the profitability of a CCHP system for long-term operation under uncertain parameters. Marino et al. [44] investigated the operation of a CCHP microgrid using a two-stage stochastic model. Hybrid sample average approximation (SAA) with the Bender decomposition algorithm was developed to examine the performance of this system under a different level of uncertainties. Microgrid energy operation management under multiple uncertainties has also been examined by [36,45-48]. Mohammadi et al. [47] proposed a scenario-based stochastic framework for the microgrid system. They investigate the role of energy storages to reduce the operational cost of the system under multiple uncertainties of renewable energy resources, energy prices, and energy demands.

Design of the system considering both system cost and CO_2 emissions has been attracting a lot of attention. Mavromatidies et al. [33] have examined two approaches to consider the effect of CO_2 emissions on the energy system design. In the first approach, CO_2 emissions of all scenarios are constrained to be less than a fixed value. This approach constrains the design of the system since unlikely scenarios are also satisfied by design. The second approach constrains the expected value of emissions of all possible scenarios to be less than a threshold value. Although this is a conservative approach to the design of an energy system, some worst-case scenarios with large amounts of the emissions might happen since there is no control for the scenarios on the tail of the CO_2 emissions distribution. The authors mentioned that as possible future work decision criteria which introduce the risk have to be considered in the problem.

Optimal design and operation of an energy system considering both economic and environmental criteria is a complex task. Realistic equipment models introduce nonlinear terms, which makes the model more difficult to solve. The commonly used approach is to use only some of the available equipment as possible candidates for ES design and to replace some or all of the nonlinear models with linear approximations. In addition, two-stage stochastic programming increases very significantly the computational burden.

In order to design an optimal ES and operate it under uncertainties in energy prices and uncertainties in demand, this work removes previous simplifying assumptions and models the uncertainties in a manner which enables efficient computation of the optimal designs. Specifically:

- The paper proposes a framework for the optimal use of energy resources and optimization of the energy system operation. The objective of this paper is to mitigate the environmental impact of the energy system and to minimize the annual total cost of the energy system. We propose a methodology that addresses the problems related to the optimal design and optimal operation of the energy system under multiple uncertainties, including also a novel method to generate system scenarios thereby simplifying the system modelling and reducing the computational times.
- Portfolio of DES components included in the model includes all practically available technologies (primary electricity generator, boiler, heat recovery system, electric chiller, GSHP, absorption chiller, heating coil, battery, and thermal storage). Since our case study site is in the city, we assume that there is not enough space to install solar thermal, PV, and wind turbines.
- A detailed MILP model capturing equipment performance characteristics is presented to model the ES operation. Nonlinear performance characteristics of the equipment have been approximated by piecewise linearization. Even though such formulation introduces binary variables, the solution times are acceptable since the problem is a linear one and the uncertainties are constructed by a new strategy.
- The risk of occasionally high CDE is added to the model. To limit CDE and consider the high emission risk in the problem, conditional value at risk is applied to the CO_2 emissions. This enables a design which is not constrained by an unlikely scenario of high CDE.
- A new strategy is developed to provide scenarios for the stochastic problem which we call RVS (random vector sampling) method. The strategy uses selected discrete points from distribution of any uncertain parameters. Candidate vectors for different sets of three scenarios are built, and their probabilities are normalized. Finally, the scenarios are provided by randomly sampling of the candidate vectors. Discrete distributions of the uncertain parameters are obtained by the moment matching technique with three points.

2. The two-stage stochastic programming approach

The two-stage stochastic program partitions variables in two sets: the first-stage variables which have their values decided upon before the realization of the uncertainty and the second stage variables that are calculated after observation of uncertainties. The first-stage variables designate "here-and-now" decisions, and the second-stage variables are called recourse or "wait-and-see" decisions. As Zhou et al. [26]presented, the general form of two-stage stochastic programming for the system design is as follows:

$$
\begin{aligned}
&(Master-problem)\min_{x,\,d} f_d(x,\,d) + E_{\theta\in\Theta}[f_s(x,\,d,\,\theta)]\\
&s.\ t.\ h^d(x,\,d) = 0\\
&g^d(x,\,d) \le 0\\
&d \in \Re^l,\ x \in \{0,\,1\}\\
&(sub-problem) f_s(x,\,d,\,\theta) = \min f_s(x,\,d,\,y,\,\theta)\\
&s.\ t.\ g^{op}(x,\,d,\,y,\,\theta) \le 0\\
&h^{op}(x,\,d,\,y,\,\theta) = 0\\
&y \in \Re^n
\end{aligned}
\tag{1}
$$

where x and d are the continuous and binary variables, respectively, for the first-stage decision, $y$is the second stage variable and θ represents any uncertain parameter in the problem. h^d and g^d are equality and inequality design constraints, $h^{op}$and $g^{op}$are operational constraints.

When applied to an energy system design, the decision variables of the first-stage are design variables. The types of these variables are both binary and continuous; binary variables determine which of the available technologies should be installed in the system while continuous variables determine the sizes of these devices. The second stage variables are the operational variables of all energy generation components, converter and storage systems. First-stage variables are decided before uncertainty occurs, but the second stage variables are determined after the realization of the uncertainty.

This paper investigates the design of the system under the existence of uncertainty in a group of parameters over an extended time horizon. We use a series of scenarios with values of the parameters based on the attributes of their uncertainty over a long period. Description (distribution) of the uncertainty is derived from parameter variations over long time periods. This is different from the uncertainty considered in the optimization problem of short-term system operation. For example, when optimizing real-time operation of an energy system, scenarios are used to predict the demands and energy prices with a high probability of occurrence for a short time in the future.

3. Energy demand uncertainty

Energy demands are described by their average values, associated uncertainties, and their historical peak values. The average values are provided as the energy profiles of some representative days. Various probability distribution functions have been used to describe the fluctuation of energy demands at each daily sampling time. In this study, similar to most of the studies such as [26,28,32,33] a normal distribution is assumed to describe the uncertainty of energy demands at each sampling time.

It is assumed that the probability distribution of energy demand at each sampling time follows a normal distribution in which 95% of the real energy demand is within the range of ± 20% of their average values [20]. The uncertainty related to the natural gas price and the electricity price is assumed to be uniform distribution as provided in [28].

In general, two approximation methods are applied to approximate a continuous probability distribution by some discrete points: the discretization method and the Monte Carlo method. Most of the related studies have employed the Monte Carlo method to approximate the continuous distributions by some randomly generated discrete points. All scenarios have the same probability of occurrence (N discrete points of N scenarios, the probability of each scenario is 1/N). This approach is called the sample average approximation (SAA) method. The main drawback of this approach is that a large number of samples are needed to reach the state of convergence in the expected value of the objective function. For this reason, we use the discretization method as explained below.

3.1. Scenario generation by discretization

Discretization of continuous uncertain parameters into a set of representative points that these points are selected from intervals of the same lengths is a common way of generating scenarios. Vahidinasab [49] and Li et al. [20] discretized the normal distribution into seven and nine points, respectively. The drawback of this approach is that the generated points may not match the statistical moments (mean, variance, skewness, and kurtosis) of the normal distribution. In order to mitigate this issue, it is common to use a large number of discrete points thereby ensuring that the characteristics of the uncertainty are adequately preserved in the problem; however, this leads to an increase in the computational times.

To obtain maximum accuracy in discretization, one can apply moment matching to each input distribution. The most accurate moment matching methods are Gaussian Quadrature Formulas [50]. When the probability distribution function is either normal or uniform or exponential distribution, Gaussian Quadrature formulas exactly match *2N-1* underlying moments of that probability distribution. Therefore, they can be employed to provide N discrete points for each probability distribution. Similarly to a recent study [33], we adopted a discretization method provided by Miller and Rice[51]. Each normal distribution function can be discretized by N points that match the *2N-1* statistical moments (excluding zeroth moment) of that distribution.

In this paper, we choose the value of $N = 3$. The uncertainty of each parameter is characterized by three discrete points corresponding to their probability of occurrence instead of a continuous distribution. The three discrete points for a normal distribution N (μ, σ^2) and a uniform distribution U (a, b) are represented in Fig. 1.

3.2. Scenario construction by random vector sampling (RVS) method

In each scenario, uncertain parameters take on the value of one of their corresponding discrete points that are shown in Fig. 1. To create a scenario, one might randomly select a point from the set of discrete points for each uncertain parameter. This would still lead to a large number of scenarios to ensure the objective function reaches the state of convergence and the objective function does not change by adding the number of scenarios. The reason is that some of the discrete points might not be assigned to uncertain parameters via the random assignment of a point. Therefore, a strategy for generating scenarios should be such that the uncertain parameter can take on the values of all discrete points. One possible approach is that an uncertain parameter takes on values of a set of three discrete points in three consecutive scenarios. At each time, three scenarios are built, and at each scenario, one point from three discrete points is assigned to an uncertain parameter. For example, to assign a value to an uncertain parameter, in the first scenario of a set of three scenarios, one point is randomly selected among three discrete points, in the second scenario, one point among the remaining two points is randomly chosen and finally, in the last scenario, the last point is used. To explain this as a mathematical point of view, consider a set of three discrete points (dp_1, dp_2, dp_3) which will be assigned to an uncertain parameter in three consecutive scenarios (s, $s+1$, $s+2$). The number of all possible orderings (permutations) for assigning these three points to the three scenarios is six:

$$D = \{(dp_1, dp_2, dp_3), (dp_1, dp_3, dp_2), (dp_2, dp_1, dp_3), (dp_2, dp_3, dp_1), (dp_3, dp_1, dp_2), (dp_3, dp_2, dp_1)\}.$$

Consider the desired number of scenarios is S, which should be the multiple of three; S = 3 K. At each time, one of the six vectors (permutations) in D is selected randomly for each parameter p and a set of three scenarios (k = 1). The same procedure is performed for the subsequent sets of three scenarios (k = 2, 3 …, K) and all the uncertain parameters (p = 1, 2, … P). We call this strategy as a Random Vector Sampling (RVS) method.

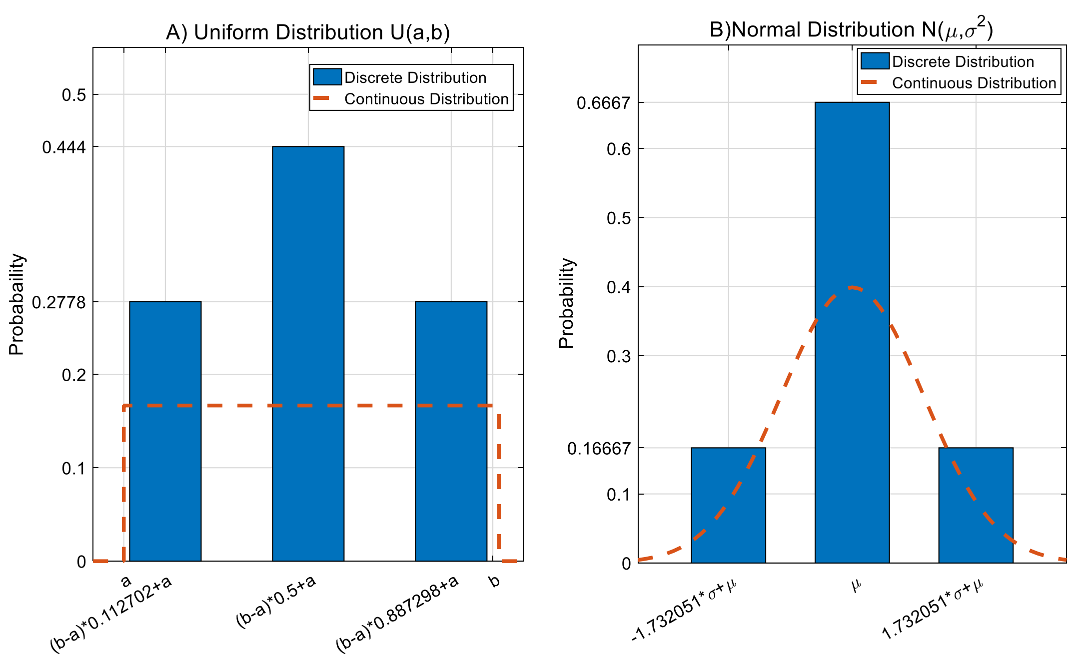

Fig. 1. Discrete approximation of a Uniform distribution (A) and a Normal distribution (B).

In summary, the following method is used to construct scenarios by the RVS method:

Start
1- Set the number of desired scenarios; $S = 3K$ and Number of uncertain parameters P, set $k = 1$, set $p = 1$.
2- For the uncertain parameter p and for the kth set of three scenarios:
3- Select one of the six-vectors of set D randomly,
4- Assign the values of the selected vector to the uncertain parameter p for a set of three-scenarios k.
5- $p = p + 1$.
6- Is $p < P$? **Yes**: go back to step 2, **No**: go to the next step.
7- $k = k + 1$.
8- Is $k > K$? **Yes**: end, **No**: set $p = 1$ and refer to step2.
end

4. Probability Normalization

In this paper, uncertain parameters are electrical demand at each hour, heating demand at each hour, cooling demand at each hour, electricity price and natural gas price. After assigning discrete points to all uncertain parameters by the RVS method, there are three different profiles of electrical, heating, and cooling demands in each set of three scenarios.

Once the scenarios are generated by using the RVS method, the normalized probabilities are assigned to all scenarios. Because different sets of three scenarios are built independently, it is assumed that the probability of occurrence of all sets of three scenarios is equal to each other and is 1/K.

Normalization of the probability of occurrence takes place in two steps. In the first step, in each set of three scenarios k, the probability of each profile is calculated (multiplication of probabilities of all hours) and then normalized by considering the probabilities of the other two profiles in that set. For example, the probability of an energy demand profile is calculated for three scenarios and then normalized such that the summation of the probabilities of occurrence of three energy demand profiles in the set equals one. Eq. (2) is applied to normalized the probability of each energy demand profile for each set of three scenarios k.

$$\pi_s^{E,k,Nr} = \frac{\pi_s^{E,k}}{\sum_{s\in k}\pi_s^{E,k}} \qquad \forall\, k \in K, \quad s \in S \tag{2}$$

where $\pi_s^{E,k,Nr}$ is the normalized probability of an energy demand profile E in scenario s of a kth set of three scenarios, $\pi_s^{E,k}$, is the probability of the energy demand profile in scenario s in the kth set.

In the second step, to calculate the probability of each scenario, first, the product of the normalized probability of occurrence of all profiles is calculated.

$$\pi_s^k = \prod_P \pi_s^{P,k,Nr} \qquad \forall\, k \in K, \quad s \in S,\, p \in P \tag{3}$$

Then the obtained probability value of each scenario in the kth set of three scenarios are normalized by using Eq. (4)

$$\pi_s^{k,Nr} = \frac{\pi_s^k}{\sum_{s\in k}\pi_s^k} \qquad \forall\, k \in K, \quad s \in S \tag{4}$$

and finally, the result is multiplied by the 3/S to obtain the normalized probability of each scenario.

$$\pi_s^{Nr} = \frac{3}{S}\pi_s^{k,Nr} \qquad \forall\, k \in K, \quad s \in S \tag{5}$$

Therefore, in each set of three scenarios, the summation of the probabilities of all three scenarios is 3/S.

5. Description of the energy system

The energy system in this work (Fig. 2) consists of several technological components: an engine or power generation unit (PGU), heat recovery system, absorption chiller, electric chiller, backup boiler, GSHP, heating coil, battery, and short-term thermal energy storage. Power generation unit provides the electricity; then the waste heat is recovered through the heat recovery system. The recovered heat is sent to the heating coil to produce heat or is given to the absorption chiller to supply the cooling. Electric chiller might be used to provide cooling via the electricity from either PGU or from the grid. The backup boiler is employed to provide additional steam when the recovered heat is not sufficient to provide the heating or cooling. Utilizing the waste heat through a heat recovery system increases the energy efficiency of the CCHP system to more than 80% [52]. The ground source heat pump (GSHP) is another option to provide heat during winter and cooling during summer. Integrating the CCHP system with renewable energy resources increases the overall efficiency of the system compared to the CCHP system alone [53]. Battery and thermal storage also are applied to store excess electricity and excess thermal energy, respectively, and discharge them during the peak period. Finally, the connection to the electrical grid is also provided that the system can import electricity from the grid, but there is no option to sell the power to the network. In this work, the solar heat collector and photovoltaic are not employed,

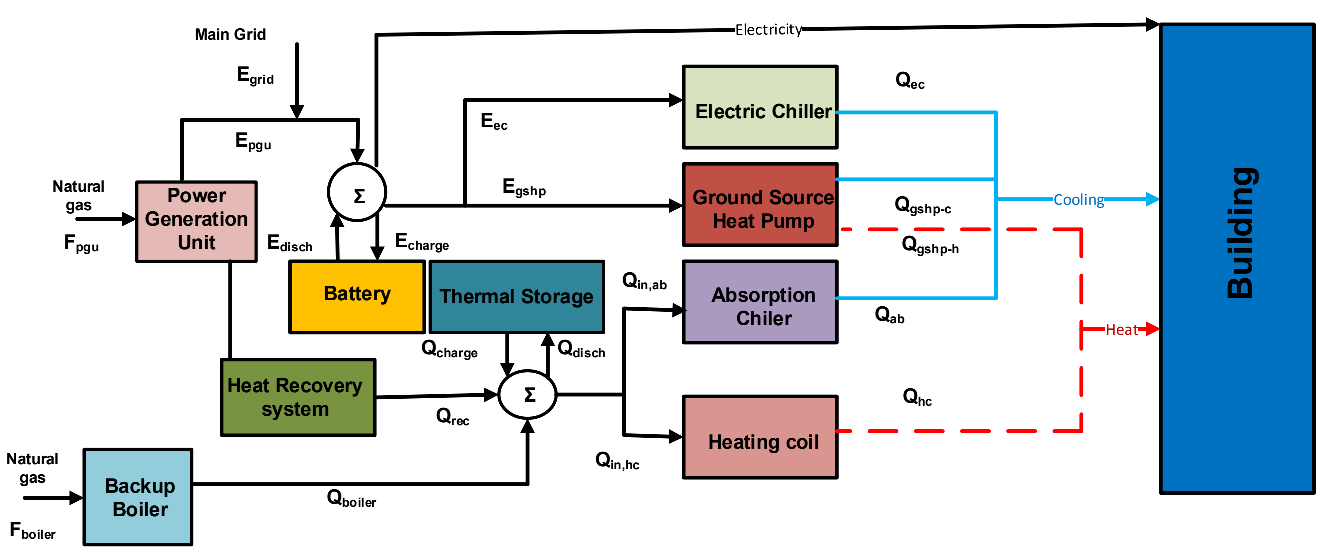

Fig. 2. Schematic illustration of the energy system.

since the case study assumes that the buildings are in an urban core and that there is no significant surface area available to install either the thermal solar or PV cells.

5.1. Model of the System

Energy balance for each of the equipment is used to describe the performance of the system. The electrical output of the engine or power generation unit (PGU) is described by the following equation:

$$E_{pgu,t,s} = F_{t,s}\eta_{pgu,t,s} \tag{6}$$

where $\eta_{pgu,t,s}$ is PGU efficiency and $F_{t,s}$ is the energy produced by combustion of fuel at each time t and for any scenario s.

The efficiency of the engine is a function of its operational loads [54] which is described by, the following equation:

$$\eta_{pgu,t,s} = \eta_{nom}(c_{pgu} + b_{pgu}f_{pgu,t,s} + a_{pgu}f^2_{pgu,t,s}) \tag{7}$$

η_{nom}, it the nominal efficiency of the engine depends on the size of the engine, a_{pgu}, b_{pgu} and $c_{pgu}$are dimensionless parameters and $f_{pgu,t,s}$ is the partial load of the engine at each time t and for any scenario s which is defined by Eq. (8).

$$f_{pgu,t,s} = \frac{E_{pgu},\ t,\ s}{E_{nom}},\quad f_{min} = 0.25\quad and\quad f_{max} = 1 \tag{8}$$

E_{nom} is the nominal power of the engine, f_{min} the minimum partial load (on/off coefficient) for the engine which is fixed at 0.25. The engine efficiency is low when the partial load of the engine is under 0.25. In this case, the engine must be turned off to prevent energy loss and damage to the engine.

The heat recovered from the engine at any time t and in each scenario s is calculated by the following equation:

$$Q_{rec,t,s} = F_{t,s}(1 - \eta_{pgu,t,s})\eta_{rec} \tag{9}$$

where η_{rec} is the heat recovery system efficiency.

Recovered heat can be used both in the heat exchanger and in the absorption chiller to provide heating and cooling, respectively. A part of the recovered heat is sent to the absorption cooling system to provide cooling energy. The energy balance of the absorption cooling system is shown in Eq. (10).

$$Q_{ab,t,s} = COP_{ab,t,s}Q_{in,ab,t,s} \tag{10}$$

where $Q_{in,ab,t,s}$ is the thermal input energy to the system, $Q_{ab,t,s}$ is the cooling output from the absorption chiller, and $COP_{ab,t,s}$ is the coefficient of the performance of the absorption chiller. $COP_{ab,t,s}$ is also a function of the operating load of the absorption chiller. Similar to the Eq. (7) expression for the engine efficiency, Zheng et al.[1] and Tian et al. [55] presented the following relation to express the absorption chiller's COP as a function of its partial load.

$$COP_{ab,t,s} = a_{ab}f^2_{ab,t,s} + b_{ab}f_{ab,t,s} + c_{ab} \tag{11}$$

where a_{ab}, b_{ab}, c_{ab} are nondimensional parameters and $f_{ab,t,s}$ is the absorption chiller partial load. The minimum value of $f_{ab,t,s}$ is assumed to be 0.2.

GSHP also provides heating and cooling in winter and summer, respectively. The energy balance is as follows:

$$Q_{gshp,t,s} = COP_{gshp,t,s}E_{gshp,t,s} \tag{12}$$

$Q_{gshp,t,s}$ is the energy output of the GSHP, $E_{gshp,t,s}$ is the energy input to the GSHP, and $COP_{gshp,t,s}$ is the coefficient of performance of the GSHP. COP of GSHP is also provided by kang et al. [13,14] by different coeffieicnts which are used for summer and winter.

$$COP_{gshp,t,s} = a_{gshp}f^2_{gshp,t,s} + b_{gshp}f_{gshp,t,s} + c_{gshp} \tag{13}$$

The minimum partial load operation of GSHP is assumed to be 0.3.

Another candidate device for cooling energy production is the electric chiller. Electricity generated by the engine or taken from the grid can be sent to the electric chiller. The following equation calculates the amount of energy consumed by this device:

$$Q_{ec,t,s} = COP_{ec,t,s}E_{ec,t,s} \tag{14}$$

The $COP_{ec,t,s}$ is described by Eq. (15):

$$COP_{ec,t,s} = a_{ec}f^2_{ec,t,s} + b_{ec}f_{ec,t,s} + c_{ec} \tag{15}$$

Heating coil or a heat exchanger are utilized to produce the thermal energy needed for the building.

$$Q_{hc,t,s} = \eta_{hc}Q_{in,hc,t,s} \tag{16}$$

η_{hc} is the heating coil efficiency and $Q_{in,hc,t,s}$ is the input energy provided for the heating coil.

When the energy provided by the thermal storage and heat recovery system is not enough, this shortfall is satsified by the boiler:

$$Q_{boiler,t,s} = \eta_{boiler}\ \ F_{boiler,t,s} \tag{17}$$

$F_{boielr,t,s}$ is the amount of natural gas burned inside the boiler to provide thermal energy.

The heat recovery system, the boiler, and the thermal storage provide the thermal energy for both absorption chiller and heating coil (heat exchanger).

$$Q_{rec,t,s} + Q_{disch,t,s} + Q_{boiler,t,s} \geq Q_{in,ab,t,s} + Q_{charge,t,s} + Q_{in,hc,t,s} \tag{18}$$

Since the engine is the only component for generating the electricity, the size of the engine might not change considerably (e.g., more than 1 MW) because of either the existence of the uncertainty or the implementation of CDE limits. In addition, the nominal efficiency of the engine changed slightly via change of the engine size. For instance, by changing the size of the engine from 2800 to 3400 kW, the nominal efficiency increases slightly[56]. As a result, the nominal efficiency of the engine is considered to be constant in the range of [2800, 3400] in this paper, independent of the engine size and similar to previous studies [1,5,6,8,14,26].

The stochastic model includes a set of constraints which describe the energy demands of the building and are supplied by the energy system for any time step *t* and each scenario *s*. Engine, battery, and the grid provide the electricity needed by the building as well as the electricity required by the GSHP and the electric chiller. Also, a portion of the electricity produced by the engine can be stored in the battery. The electrical energy balance for the whole system is expressed as follows:

$$E_{grid,t,s} + E_{pgu,t,s} + E_{disch,t,s} = E_{gshp,t,s} + E_{ec,t,s} + E_{d,t,s} + E_{charge,t,s} \tag{19}$$

$E_{pgu,t,s}$ is the electricity provided by the engine at each time step *t* and for scenario *s*, $E_{ec,t,s}$ and $E_{gshp,t,s}$ are the electrical energy required by the electric chiller and the GSHP, respectively, $E_{disch,t,s}$ and $E_{charge,t,s}$ are battery discharged and charged energies, $E_{d,t,s}$ is the energy demand of the building, and $E_{grid,t,s}$ is the electricity taken from the power grid.

Additional constraints are needed to describe the operation of both electrical storage and thermal storage at each time step *t* and scenario *s*. A group of binary variables is applied to limit the charging/discharging rate of the storage systems and keep the storage models linear.

$$\begin{cases} U^{charge}_{battery,t,s}E^{min}_{charge} \leq E_{charge,t,s} \leq U^{charge}_{battery,t,s}E^{max}_{charge} \\ U^{disch}_{battery,t,s}E^{min}_{disch} \leq E_{discht,s,} \leq U^{disch}_{battery,t,s}E^{max}_{disch} \\ U^{charge}_{battery,t,s} + U^{disch}_{battery,t,s} \leq 1 \\ W_{battery,t,s} = W_{battery,t-1,s}\delta_{battery} + E_{charge,t,s}\eta^{charge}_{battery} - E_{disch,t,s}\eta^{disch}_{battery} \\ W^{min}_{battery} \leq W_{battery,t,s} \leq W^{max}_{battery} \end{cases} \tag{20}$$

$U^{charge}_{battery,t,s}$ and $U^{disch}_{battery,t,s}$ are both binary variables that show the status of the battery at each time *t* and scenario *s*, for instance, if the battery is charged, then $U^{charge}_{battery,t,s} = 1$, and $U^{disch}_{battery,t,s} = 0$,

E^{min}_{charge} and E^{max}_{charge} are minimum and maximum charging rates of the battery, respectively, E^{min}_{disch} and E^{max}_{disch}, are minimum and maximum discharging rates of the battery, respectively, $W_{battery,t,s}$ is the energy content of the battery, $W_{battery}^{min}$ and $W_{battery}^{max}$ are maximum and minimum values of the battery energy content at each time step t and scenarios s, $\eta_{battery}^{charge}$, $\eta_{battery}^{disch}$ are charging and discharging efficiencies of the battery and $\delta_{battery}$ is the energy loss rate.

Similar constraints are applied for the thermal energy storage as follows:

$$\begin{cases} U_{tst,t,s}^{charge} Q_{tst}^{min} \leq Q_{charge,t,s} \leq U_{tst,t,s}^{charge} Q_{charge}^{max} \\ U_{tst,t,s}^{disch} Q_{disch}^{min} \leq Q_{disch,t,s} \leq U_{tst,t,s}^{disch} Q_{disch}^{max} \\ U_{tst,t,s}^{charge} + U_{tst,t,s}^{disch} \leq 1 \\ W_{tst,t,s} = W_{tst,t-1,s}\delta_{tst} + Q_{charge,t,s}\eta_{tst}^{charge} - Q_{disch,t,s}\eta_{tst}^{disch} \\ W_{tst}^{min} \leq W_{tst,t,s} \leq W_{tst}^{max} \end{cases} \tag{21}$$

$U_{tst,t,s}^{charge}$ and $U_{tst,t,s}^{disch}$ are both binary variables that show the status of the thermal storage at each time t and scenario s, for instance, if the thermal storage is charged, then $U_{tst,t,s}^{charge} = 1$, and $U_{tst,t,s}^{disch} = 0$, Q_{charge}^{min} and Q_{charge}^{max} are minimum and maximum charging rates of the thermal storage, respectively, Q_{disch}^{min} and Q_{disch}^{max}, are minimum and maximum discharging rates of the thermal storage, respectively, $W_{tst,t,s}$ is the energy content of the thermal storage, W_{tst}^{min} and W_{tst}^{max} are maximum and minimum values of the thermal storage energy content at each time step t and scenarios s, $\eta_{battery}^{charge}$, $\eta_{battery}^{disch}$ are charging and discharging efficiencies of the thermal storage and δ_{tst} is the energy loss rate.

Typically, the maximum charging and discharging rates of both battery and the thermal storage depend on their energy contents. Similar to the previous works [12,57–59], in this paper, we assume the maximum allowable charging/discharging rates of both storage systems are constant and are independent of the storage level. Both thermal energy storage and electrical storage are short-term energy storage systems. Another model assumption is that the operation of both storage systems is considered as a daily operation, which means they are applied to cover the daily energy fluctuations. Therefore, additional constraints are added to the model to describe that the energy stored at the beginning of a day equals the energy stored at the end of the day.

$$W_{tst,1,s} = W_{tst,24,s}\delta_{tst} + Q_{charge,1,s}\eta_{tst}^{charge} - Q_{disch,1,s}\eta_{tst}^{disch} \tag{22}$$

Analogously, for the battery:

$$W_{battery,1,s} = W_{battery,24,s}\delta_{battery} + E_{charge,1,s}\eta_{battery}^{charge} - E_{disch,1,s}\eta_{battery}^{disch} \tag{23}$$

Cooling energy balance equation is added to the model to balance the cooling energy at any time *t* and for each scenario *s*; the total output cooling energy of absorption chiller, GSHP, and electric chiller will provide the cooling energy needed for the building.

$$Q_{gshp-c,t,s} + Q_{ab,t,s} + Q_{ec,t,s} = Q_{cd,t,s} \tag{24}$$

A similar energy balance relation holds for the heating mode. The total heating output of the GSHP and the heat exchanger meets the heating demand at each time and scenario.

$$Q_{gshp-h,t,s} + Q_{hc,t,s} = Q_{hd,t,s} \tag{25}$$

Additional equations are included that limit the energy output of each component to be less than or equal to the capacity of that component.

$$\begin{gathered} E_{pgu,t,s} \leq Ca_{pgu} \\ Q_{i,t,s} \leq Ca_i \quad \forall\ i = \{GSHP, ab, ec, boiler\} \end{gathered} \tag{26}$$

The maximum stored energy within a storage system is limited to the storage capacity.

$$W_{i,t,s} \leq Ca_i \quad \forall\ i = \{tst, battery\} \tag{27}$$

5.2. Objective function

As mentioned, the first-stage decision variables are binary and continuous design variables which select the optimal components and determine their associated sizes. Therefore, the investment cost consists of two terms: (i) fixed cost related to the installation cost of each component, and (ii) variable cost determined based on the size of each element. Moreover, the expenses associated with the heating, and electrical networks must be added to the first stage cost of the system. Therefore, the first stage cost is expressed as follows:

$$COST_{1st} = R[\sum_i x_i InC_i + Ca_i VC_i + HnC] \tag{28}$$

where x_i, is the binary variable which determines whether the technology is selected or not for the energy system, InC_i, is the installation cost of technology i, Ca_i is the continuous variable describing the size of the technology i, VC_i is the cost per unit energy output for the technology ($/ kW for generators and converters, $/kWh for the storages), *HnC* is the cost of distribution heating network, and R is the capital recovery factor which is calculated by the following equation:

$$R = \frac{ir(1+ir)^{LC}}{(1+ir)^{LC} - 1} \tag{29}$$

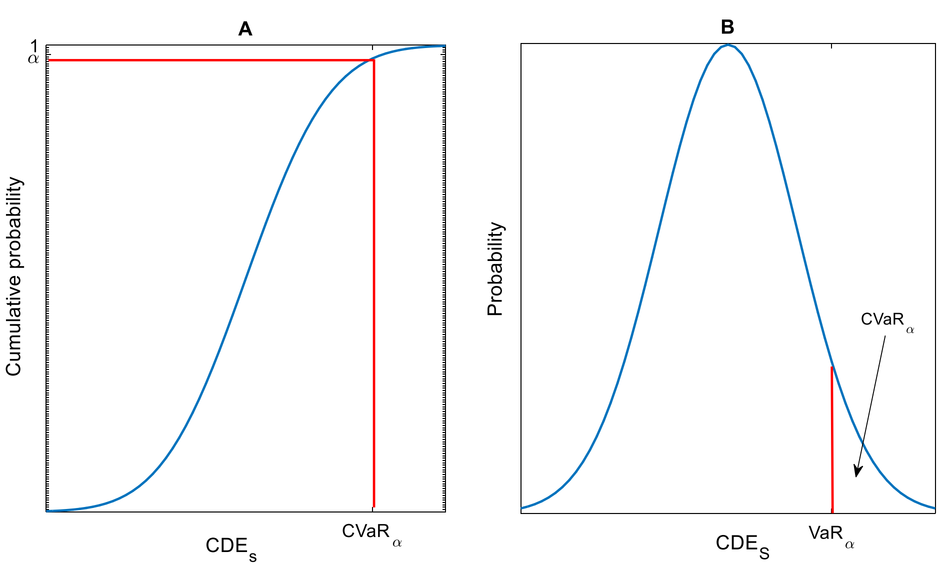

Fig. 3. $CVaR_\alpha$ definition of the CDE distribution.

where *ir* is the interest rate, and *LC* is the service life of the equipment. It is assumed that all equipment items have the same service life.

Second-stage cost for each scenario is the annual operational cost associated with that scenario and includes the total cost of the natural gas consumed in the engine and the boiler, as well as the cost of the electricity imported from the network grid. Compared to the deterministic case, the operational cost is calculated for all scenarios, and hence second stage cost is different for all scenarios. The total cost of each scenario s is determined by following the equation:

$$Cost_{total,s} = Cost_{1st} + \sum_{t} C_{EL,s} E_{grid,t,s} + C_{NG,s}(F_{boiler,t,s} + F_{pgu,t,s}) \tag{30}$$

$C_{EL,s}$ and $C_{NG,s}$ are electricity and natural gas prices of each scenario s, respectively.

Given the first-stage system cost and second-stage cost for all the scenarios, the objective function which is the expected annual total cost is defined as follows:

$$Cost_{total} = \sum_{s\in S} \pi_s^{Nr} Cost_{total,s} \tag{31}$$

Optimal design of the energy system regarding the technology selection and system sizing is carried out for both deterministic and stochastic cases. For each case, the optimal configuration is sought for different specified levels of CDE reduction.

The annual operational CO_2 emissions (CDE) for each scenario is calculated as follows:

$$CDE_s = \mu_{CO2,EL} E_{grid,t,s} + \mu_{CO2,NG}(F_{boiler,t,s} + F_{pgu,t,s}) \tag{32}$$

where $\mu_{CO2,EL}$ and $\mu_{CO2,NG}$ are emissions conversion factors of electricity and natural gas, respectively.

Adding uncertainty to the model and limiting the total expected CDE is a way that can reduce the risk of CO_2 emissions; such an approach in the optimization problem is called a risk-neutral strategy. Although the risk-neutral approach might keep the expected value of the CDE scenarios below a certain level, it might provide poor outcomes for some extreme scenarios since it ignores the management of risk that such scenarios may take place. To overcome these challenges a suitable risk measure which is the conditional value at risk, $CVaR_\alpha$, is added as a constraint to the problem

We have assumed that the average of CO_2 emissions of (1-α) 0.100% worst-case scenarios is limited. The average value of the CO_2 operational emissions is called $CVaR_\alpha$ (See Fig. 3). Eq. (33) is applied to limit the $CVaR_\alpha$ of the CO_2 operational emissions [35].

$$\begin{aligned} CVaR_\alpha &= \zeta + \tfrac{1}{1-\alpha} \textstyle\sum_{s\in S} \pi_s^{Nr} \gamma_s \le l \\ CDE_s &\le \zeta + \gamma_s \\ \gamma_s &\ge 0 \end{aligned} \tag{33}$$

whereζ and γ_s are auxiliary variables and π_s^{Nr} is the probability of occurrence of scenario s; l is the threshold value.

The expected value of the CDE of the system is calculated as follows:

$$CDE = \sum_{s\in S} \pi_s^{Nr} CDE_s \tag{34}$$

To see how much the CDE can be reduced by the use of the energy system compared to the CDE amount generated by the standalone system, the following ratio is defined.

$$CO_2R = \frac{CDE}{CDE_{SP}} \tag{35}$$

CDE_{SP} is the carbon dioxide emissions from the standalone system which is defined as follows:

$$CDE_{sp} = \sum_{s\in S} \pi_s^{Nr} \sum_{t} (E_{d,t,s} + \frac{Q_{cd,t,s}}{COP_{ec,sp}})\mu_{CO2,EL} + \frac{Q_{hd,t,s}}{\mu_{boiler}\mu_{hc}}\mu_{CO2,NG} \tag{36}$$

$COP_{ec,sp}$ is the COP of the electric chiller of the separate production system is utilized to limit the CDE for the deterministic case.

$$CO_2R = \frac{CDE_{det}}{CDE_{sp-det}} \le z \tag{37}$$

CDE_{det} and CDE_{sp-det} are CDE calculated for the deterministic case for ES and Standalone system, respectively. For each deterministic case, z is defined in Table 1 as a CO_2R obtained from the corresponding stochastic case.

6. Case study

Data from the four-building office complex located in Dalian, China [54] are used to evaluate the applicability of the design framework

Table 1
Different cases of the design optimization problem.

	Objective function	Constraints
Case-1S (Stochastic)	The expected value of the annual total cost is minimized by using Eq. (31)	There is no limit on the CVaR of CO_2 and the value of Co_2R, C_1,is calculated by using Eq. (35)
Case-2S (Stochastic)	The expected value of the annual total cost is minimized by using Eq. (31)	A constraint is built by using Eq. (33) and setting l=1.030 $CVaR_\alpha^{min}$ and the value of Co_2R, C_2, is calculated by using Eq. (35)
Case-3S (Stochastic)	The expected value of the annual total cost is minimized by using Eq. (31)	A constraint is built by using Eq. (33) and setting l=1.022 $CVaR_\alpha^{min}$ and the value of Co_2R, C_3, is calculated by using Eq. (35)
Case-4S (Stochastic)	The expected value of the annual total cost is minimized by using Eq. (31)	A constraint is built by using Eq. (33) and setting l=1.018 $CVaR_\alpha^{min}$ and the value of Co_2R, C_4, is calculated by using Eq. (35)
Case-5S (Stochastic)	The expected value of the annual total cost is minimized by using Eq. (31)	A constraint is built by using Eq. (33) and setting l=1.010 $CVaR_\alpha^{min}$, the value of Co_2R, C_5, is calculated by using Eq. (35)
Case-6S (Stochastic)	The CVaR of CO_2 is minimized by using Eq. (33) and setting$\alpha = 0.95$	There is no limit on CVaR of CO_2, the objective function ($CVaR_\alpha^{min}$)is determined and the value of Co_2R, C_6, is calculated by using Eq. (35)
Case-1D (Deterministic)	The annual total cost is minimized by using Eq. (31) considering one deterministic scenario.	A constraint is built by using Eq. (37) and by setting the value of z as C_1(this value is calculated from Case-1S)
Case-2D (Deterministic)	The annual total cost is minimized by using Eq. (31) considering one deterministic scenario.	A constraint is built by using Eq. (37) and by setting the value of z as C_2(this value is calculated from Case-2S)
Case-3D (Deterministic)	The annual total cost is minimized by using Eq. (31) considering one deterministic scenario.	A constraint is built by using Eq. (37) and by setting the value of z as C_3(this value is calculated from Case-3S)
Case-4D (Deterministic)	The annual total cost is minimized by using Eq. (31) considering one deterministic scenario.	A constraint is built by using Eq. (37) and by setting the value of z as C_4(this value is calculated from Case-4S)
Case-5D (Deterministic)	The annual total cost is minimized by using Eq. (31) considering one deterministic scenario.	A constraint is built by using Eq. (37) and by setting the value of z as C_5(this value is calculated from Case-5S)
Case-6D(Deterministic)	The annual total cost is minimized by using Eq. (31) considering one deterministic scenario.	A constraint is built by using Eq. (37) and by setting the value of z as C_6(this value is calculated from Case-6S)

presented in this paper. In [54], optimal design and operation of the CCHP system were investigated for three different buildings (hotel buildings, office buildings, and residential buildings) located in Dalian, China. Applications of the various system configurations and operating strategies have been studied. The authors studied the deterministic design and operation of the CCHP system from the economic operation, energetic analysis, and environmental effect viewpoints. This example has been chosen so that the solution derived by the proposed strategy can be compared with designs derived by other approaches. Note that in Dalian, electricity from the grid is generated mostly by burning coal. We selected office complex comprised of four buildings for the case study in this paper. The energy system applied in this case study is shown in Fig. 2. The characteristics of the energy system, including the partial load efficiency of the components, the unit price of each component and on/off coefficients are presented in [14,55,59]. Design of the system is investigated for six different cases in both stochastic optimization problem and deterministic optimization problem. The deterministic model is a particular scenario of the stochastic problem. This model is optimized by adopting a deterministic value for each uncertain parameter. The mean of the probability distribution of each uncertain parameter is selected as the deterministic value for that parameter. The remaining five cases are determined by limiting the amount of carbon dioxide emissions (CDE) generated by the operation of the system. All stochastic and deterministic problems are constructed according to Table 1. In the first stochastic optimization case (Case-1S), optimizing the system design is performed without any restriction on CO_2 emissions. In the last stochastic case, (Case-6S), the two-stage stochastic model limits the $CVaR_{0.95}$ of the operating CO_2 emissions to its minimum value. $CVaR_{0.95}^{min}$ is the minimum of 5% of worst-case scenarios of CO_2 emissions which is obtained by using Eq. (33) as the objective function. The next four stochastic cases are built by using Table 1.For the deterministic problem, the CO_2R obtained from the stochastic case is applied to set the constraint for CDE ratio by using Eq. (37). For example, if Co_2R for the stochastic problem Case-1S is C_1, this value is substituted instead of z in Eq. (37) to build the corresponding deterministic problem.

7. Results and discussion

7.1. Linearization of the MINLP model

A MILP model of the system has been developed by approximating each nonlinear function of the component performance curve by an appropriate piece-wise linear function. A formulation presented in the Appendix is utilized to approximate the nonlinear function and convert a mixed integer nonlinear model into a MILP model. Five different MILP models have been built by using a different number of linear segments. Deterministic Case-1D with no limits on the CDE emissions has been solved with five versions of MILP models in order to determine the error introduced by linearization (see Table 2). Based on these results, the model which employs piecewise-linear functions with two segments for engine and GSHP and one-piece linear functions for the absorption chiller and the electric chiller is selected as the system model.

All optimization cases have been solved by GAMS version 25.0.3 and CPLEX version 12.8.0.0 for the MILP problem and ANTIGONE solver for the MINLP. The problem size and computational times of the proposed MILP model and the MINLP model are presented in Table 3. As demonstrated in Table 3, although the problem size increases considerably by employing the MILP model, the computational times decrease drastically compared to the MINLP model

Table 3
Computational time for MILP and MINLP models.

# of scenarios	15		30		45	
Models	MILP	MINLP	MILP	MINLP	MILP	MINLP
# of equations	78,909	5229	157,809	112,449	236,709	168,669
# of single variables	64,875	46,515	129,735	93,015	195,595	139,515
# of the discrete variables	18,360	9720	36,720	19,440	55,080	2619
Optimality gap	0.002	0.002	0.002	0.002	0.002	0.002
Computational time (s)	3253	8125	8512	18,140	15,122	*1

* 1: Results cannot be computed in a reasonable amount of time.

7.2. Convergence behaviour

Typically, solving a stochastic problem needs an appropriate number of scenarios to guarantee that the results (optimal system size and the objective function value) are reliable and that the results are optimal. If the number of scenarios is too small, then the solution might not be feasible and may not be optimal for some further scenarios. On the other hand, if the number of scenarios is large, then the computational time increases, and there is no guarantee that the optimal solution will be computed in a reasonable time.

In order to determine the number of scenarios needed to solve the optimization problem, two methods have been used to generate scenarios; Random Vector Sampling (RVS) as presented above and Monte Carlo sampling (MCS) method. The stochastic problem of Case-1S has been solved repeatedly by increasing the number of scenarios from 1 to 81. For the RVS method, the number of scenarios in each stochastic problem is multiple of three. The first problem is solved by three scenarios; the second problem is solved by six scenarios and so on. Therefore, to complete 81 scenarios, seventeen problems are solved.

Fig. 4 displays the changes in the expected annual total cost (ATC) under changes in the number of scenarios. For both approaches, the objective function initially fluctuates considerably when the number of scenarios is less than 60. When the number of scenarios exceeds 60, for RVS, the changes in the objective function are negligible, and the objective function tends to be stable and converges the optimal value. On the other hand, for MCS the number of scenarios increases from 60 to 81, the fluctuation in the objective function is still significant between 60 and 81 scenarios. This illustrates that RVS requires a significantly smaller number of scenarios to converge to a stable value of the objective function.

7.3. Variation of individual scenario ATCs

In the stochastic optimization problem, the ATC varies from one scenario to another and depends on the values assigned to the uncertain

Table 2
Accuracy of different MILP models vs. MINLP model for Case-1D.

	Number of linear segments for each piece-wise linear function					MINLP
Engine	1	2	2	2	2	–
GSHP	1	1	2	2	2	–
Absorption Chiller	1	1	1	2	2	–
Electric chiller	1	1	1	1	2	–
Annual total cost ($)	1604503.25	1649244.88	1672995.56	1672593.02	1672501.14	1,672,473
Error %	−4%	−1.4%	0.03%	0.007%	0.001%	–

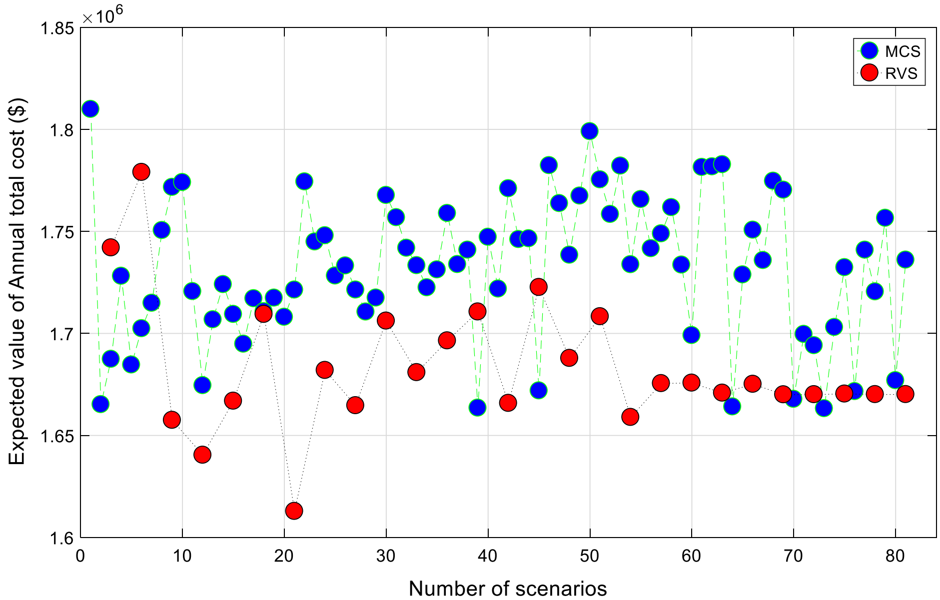

Fig. 4. Expected value of annual total cost (ATC) versus the number of scenarios for RVS and MCS methods for Case-1S.

parameters. In order to obtain a reliable design, the problem should be solved by considering all possible changes in uncertain parameters that lead to all possible variations of ATC. Therefore, solving a problem by adopting an appropriate set of scenarios can result in the total possible variations in ATC. The economic performance of the energy system has been investigated for a different number of scenarios for the stochastic problem of Case-S1. Two approaches provide scenarios; the Monte Carlo sampling (MCS) method and the paper's approach, RSV method.

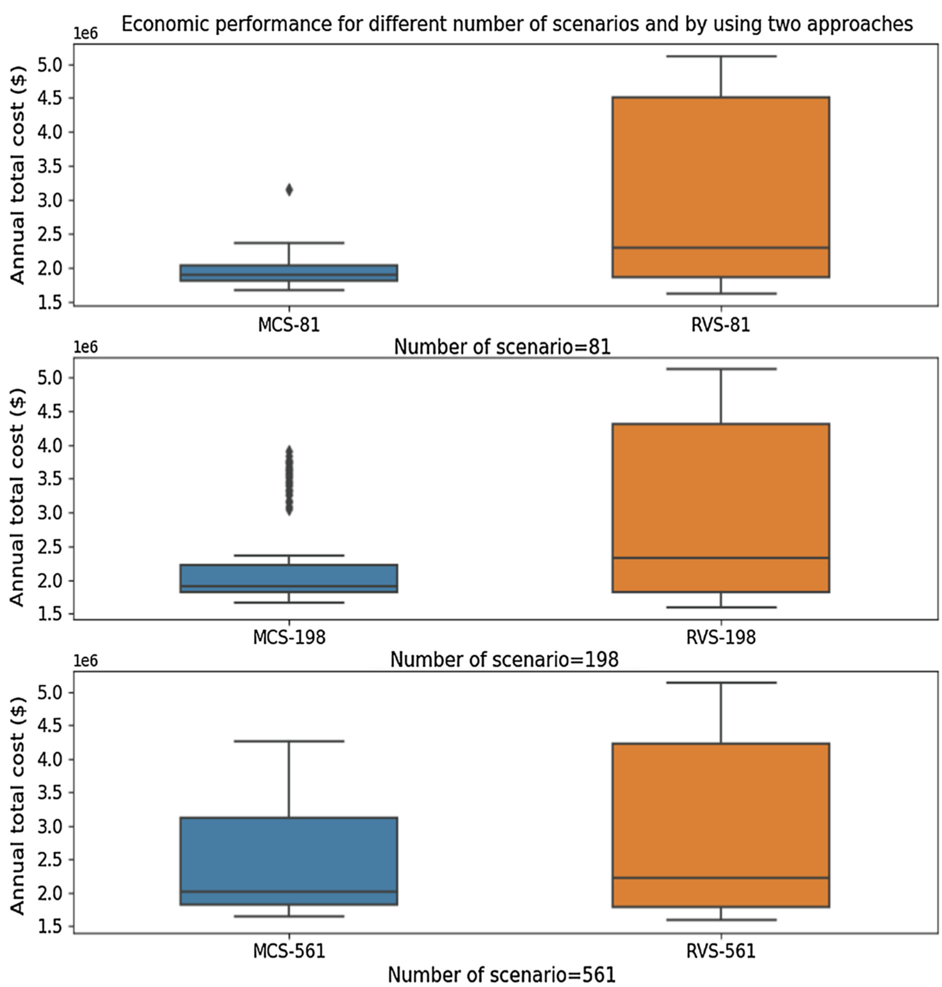

Fig. 5. Variation of individual scenario ATCs of Case-1S for two approaches.

The variation of the annual total cost (ATC) is presented in Fig. 5 for a different number of scenarios. As shown, by the use of the MCS method, as the number of scenarios increases the ATC variation increases. Using the MCS approach, when the numbers of scenarios are 81, 198, and 561, the third quartile values of ATC are 2.04E + 06, 2.22E + 06, and 3.12E + 06 $, respectively. Hence, by employing the Monte Carlo sampling approach, the full range of ATC scenarios cannot be obtained even with 561 scenarios. Consequently, a considerable number of scenarios is needed to see all possible variation in the annual total cost. On the other hand, by using the RVS approach, most of the possible variations of the uncertain parameters are considered in the optimization problem; even with only 81 scenarios, there is a high variety of ATC. Therefore, a relatively small number of the scenario is needed to solve a design problem via the RVS method; feasibility and optimality of the design values can be guaranteed for any possible real case scenario.

7.3.1. Optimal system design

In this section, the results of the optimization of both two-stage stochastic and deterministic models are presented and are compared to each other in order to evaluate how the uncertainties in energy demands and energy prices affect the size of each component.

When Eq. (33) is applied as the optimization criterion (to minimize $CVaR_{0.95}$ of CDE), the expected value of CDE scenarios is 6.72E + 03-ton CO_2/year. In this case, (Case-6S) the ratio of the carbon dioxide emissions of the system to the carbon dioxide emissions of the standalone system, CO_2R (is determined as C_6 in Table 1), is 0.37. This means the application of the energy system decreases the expected CDE by 63%. When the optimization criterion is Eq. (31) (Case-1S, without any CO_2 limitation), the expected value of CDE is 9E + 03-ton CO_2/year and CO_2R is 0.55. Other stochastic cases are built by setting a limit to $CVaR_{0.95}$ for each case, as explained in Table 1. By solving these stochastic problems, the CO_2R values of Case-5S, Case 4S, Case 3S, and Case-2S (are determined as C_5, C_4, C_3, C_2 and C_1 in Table 1) are 0.40, 0.43, 0.45 and 0.47, respectively. All the corresponding deterministic problems are solved by limiting CO_2R by these values calculated in the stochastic cases.

As shown in Fig. 6, the value of the expected cost in all stochastic cases is higher than the annual total cost in the deterministic cases. The cost increases due to the presence of the uncertain parameters for all optimization cases. The expected cost also increases due to the decrease in the limit of $CVaR_{0.95}$and CO_2R for stochastic and deterministic cases, respectively. From an environmental point of view, at the given ATC, the expected CDEs of the stochastic cases are all higher than the CDE of the deterministic cases. One can conclude that although the sizes of the engine and thermal storage in the stochastic cases are higher than their corresponding dimensions in the deterministic cases, the emissions in the stochastic cases are dominated by the uncertainties in energy demands. Therefore, CDEs cannot be lower than those of the deterministic cases, even if one chooses a larger engine and thermal storage. At the same time, it should be noted that the increase in ATC due to the inclusion of uncertainties is less than 1%.

7.3.2. Optimal system Design: Effect of CDE constraints

The variations of component sizes for both stochastic and deterministic cases are shown in Figs. 7 and 8, respectively. For the stochastic problem, by changing the maximum limit of $CVaR_{0.95}$ of CO_2, the size of the component might change. By limiting the CDE, the size of the engine, absorption chiller, battery and, GSHP increases for both stochastic and deterministic cases. This is due to the electricity from the grid being generated mostly from coal; hence, the carbon dioxide conversion factor of electricity is much higher than that of the natural gas. Therefore, to reduce the CDE ratio and $CVaR_{0.95}$ (for the stochastic case), a larger size of the engine and battery has to be selected to decrease the electricity imported from the grid. Also, since the GSHP has a higher efficiency than the electric chiller, an increase in the size of GSHP lower the electricity consumption required to provide a specific amount of cooling. For the stochastic case, the significant increase in the system size is seen in the battery; the size of the battery in Case-6S is 37% higher than that in the Case-1S. This size of the battery for the deterministic case, (Case-6D) is also considerable and is 27% higher than that in Case-1D. In the stochastic case, as shown in Fig. 7, the lowest capacity increase is observed in the engine; the engine size

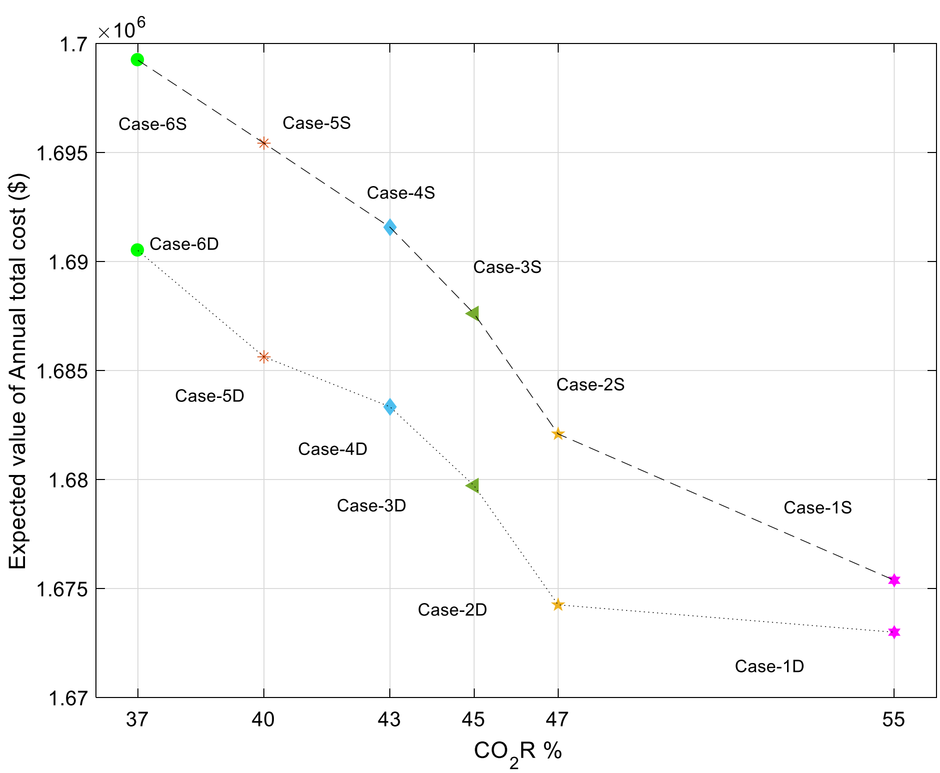

Fig. 6. ATC versus CDE ratio for all stochastic and deterministic cases.

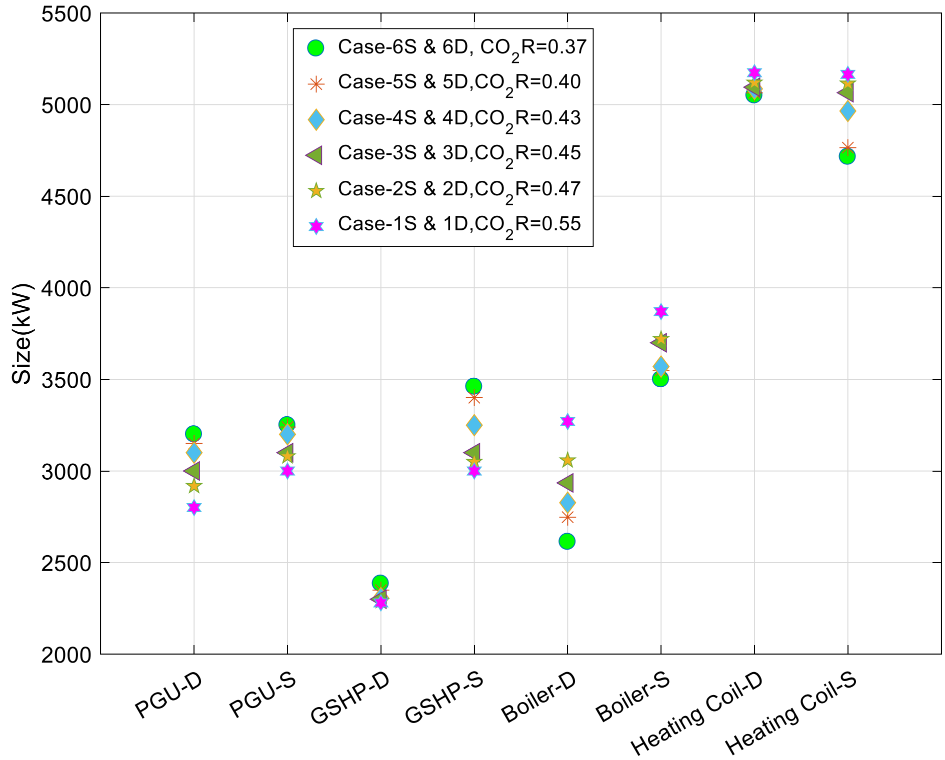

Fig. 7. Variation of the optimal size of each component due to the change in CDE ratio for the stochastic and deterministic cases for PGU, GSHP, Boiler, and Heating Coil.

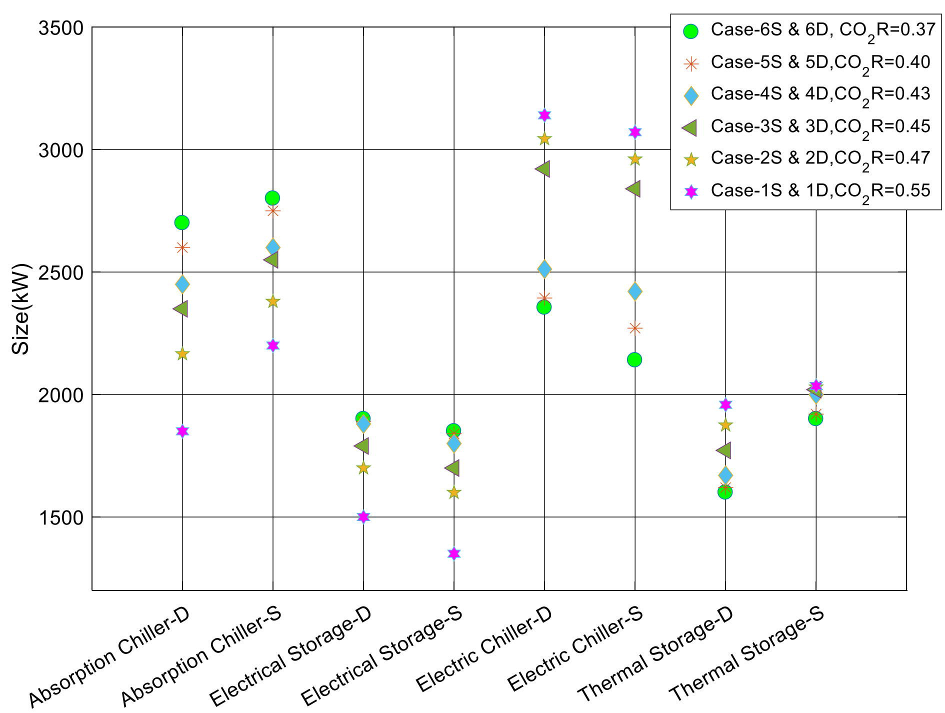

Fig. 8. Variation of the optimal size of each component due to the change in CDE ratio for the stochastic and deterministic cases for Absorption Chiller, Electrical Storage (Battery), Electric Chiller, and Thermal Storage.

required in Case-6S is only 8% higher than that in Case-1S. However, for the deterministic case, the increase in the engine size for Case-6D is 14% compared to the Case-1D, and the lowest increase in the size is only 5% for GSHP. The increase in the size of GSHP in the stochastic Case-6S compared to the stochastic Case-1S is 15%. This significant increase in the size of GSHP for the stochastic case is due to the presence of the uncertainty. For both stochastic and deterministic cases, the maximum increase values in the size of the absorption chiller are 27% and 45%, in Case-6S and Case-6D, respectively, compared to the corresponding sizes in Case-1S and Case-1D.

By decreasing the threshold values of CDE and $CVaR_{0.95}$ for Case-1 to Case-6 of both stochastic and deterministic cases, the size of the electric chiller, boiler, thermal storage, and heating coil decreases. From Fig. 8, in the stochastic case, the most significant decrease in the size is observed for the electric chiller which is 30% in Case-6S. Similar reduction (25%) is also seen for the deterministic Case-6D. The reason is that the sizes of both GSHP and absorption chiller increase as the CDE threshold value is decreased, which reduces the size of the electric chiller. The size of the thermal storage is almost constant for all cases in the stochastic case; the maximum size reduction is only 6% in Case-6S relative to storage size in Case-1S. However, for the deterministic problem, the capacity reduction of the thermal storage is much higher (about 18% in Case-6D compared to the size in Case-1D). That is because the inclusion of uncertainty in the optimization problem leads to a larger thermal storage; consequently, the reduction in the size of the thermal storage in the stochastic case is small compared to the deterministic case. Similar pattern is observed for the boiler. The maximum reductions in the size of the boiler are 10% and 20%, respectively, and can be seen in Case-6S and Case-6D. The maximum reductions of the heating coil capacity are 8% and 5% for the stochastic problem and deterministic problem, respectively.

By expanding the restriction level on CDE, the size of the thermal storage decreases for both stochastic and deterministic case. The greater size reduction is observed in the deterministic case compared to the size reduction in the stochastic case because the thermal storage is still desirable in the presence of uncertainty.

It should be mentioned that for the standalone system and in the deterministic case, the sizes of the electric chiller, boiler, and the heating coil are 7050, 8750 and 7000 kW, respectively. These sizes are 8271, 10265, and 8212 kW, respectively, for the stochastic case.

7.3.3. Optimal system design: Effect of the uncertainty

Compared to the deterministic case, the existence of the uncertainty in energy demands and energy prices results in a larger engine (Fig. 9). Fig. 9 represents the change in the size of each component because of the uncertainty as a function of the CDE ratio. In addition, the absorption chiller has a higher capacity in all stochastic cases. Since the absorption chiller is mostly heated by the heat recovered from the engine, a larger engine makes it profitable to use a larger absorption chiller to provide the cooling energy.

For the engine, the uncertainty has the greatest impact on its size for Case-1S (when there is no constraint on CDE) and has the least effect for Case-6S where the CDE constraint is the tightest. This is because the optimal size of the engine in the deterministic case and specifically for Case-6D is large enough that it can handle the uncertainties in an almost optimal manner. The same trend is also observed for the absorption chiller.

As shown in both Figs. 7 and 9, compared to the deterministic case, the capacity of GSHP is larger for all stochastic cases. Although the unit price of GSHP is higher than the unit price of the electric chiller, the GSHP provides both heating and cooling energy during winters and summers, respectively. Moreover, the COP of GSHP is higher than that of the electric chiller. Therefore, for a given amount of cooling energy, the electricity required for the electric chiller is higher than the electricity required for GSHP. Consequently, a larger GSHP is employed to boost the economic and environmental performances of the system in the stochastic cases. In addition, due to the increase in the size of the absorption chiller and GSHP, the system designed under uncertainties requires a smaller size electric chiller compared to the deterministic case.

The most significant change in the size of the equipment compared to its corresponding deterministic size is observed for the GSHP. When uncertain parameters are included, the increase in the GSHP size ranges from the smallest increase of 31% for Case-1S to the maximum increase of 45% for Case-6S, which is in the direction opposite of the changes in the size of the engine. The reason is that providing cooling via GSHP is more efficient than using either an absorption chiller or an electric chiller. Therefore, by imposing a tighter constraint on the CDE emissions and introducing the uncertainty into the problem, the optimal solution contains a larger GSHP when compared to the deterministic case, as well as a smaller absorption chiller and electric chiller.

For all stochastic cases, the required size of the heating coil is the same or a bit lower than its corresponding size in the deterministic case (maximum 5% decrease in Case-6S compared to its corresponding Case-1D). The reason is that the optimal size of the GSHP is so large that the energy system requires a smaller heating coil even for very high heating demands. It should be mentioned that the size of the engine in the stochastic case is higher than its size in the deterministic case and there

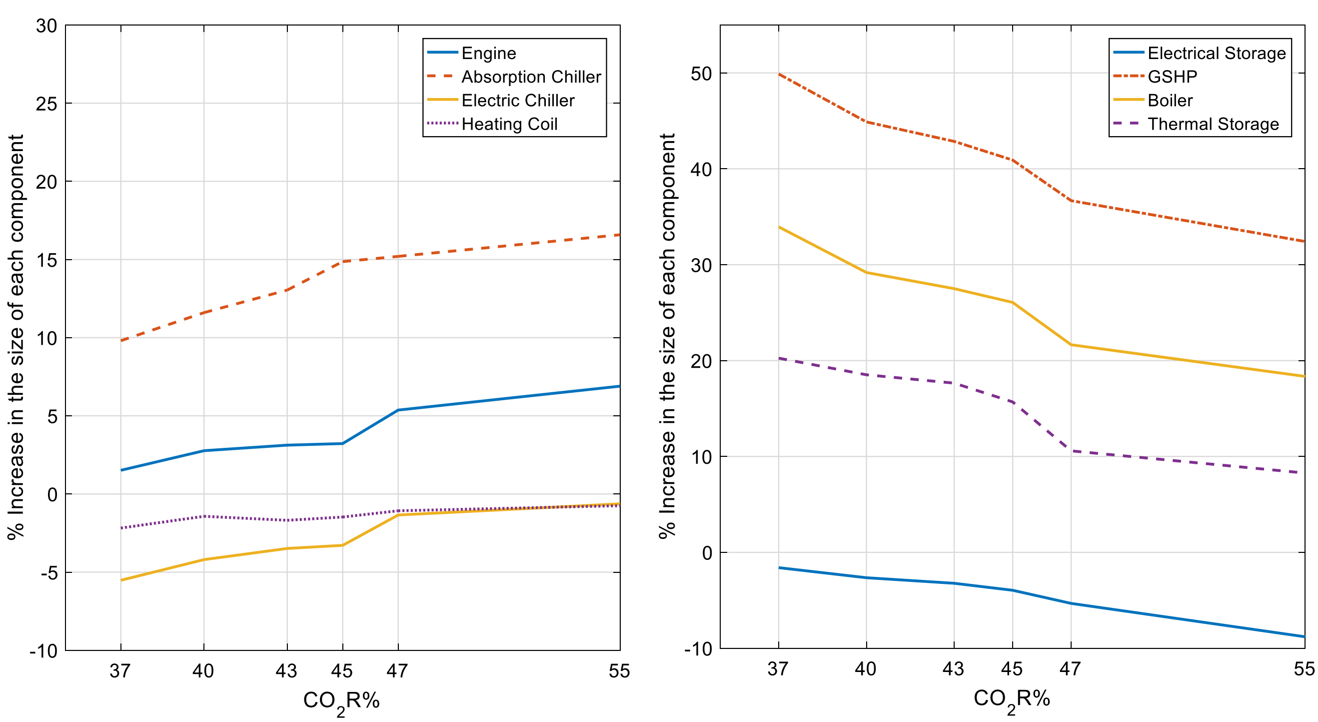

Fig. 9. Stochastic case: Change in the size of system components vs. CO_2 emissions ratio relative to the deterministic case.

is a potential to recover more heat from the engine over the winter period. However, the engine doesn't operate at a full load during winters and it runs at a lower load compared to those loads in the deterministic formulation. Therefore, the recovered heat may not be enough to meet the heating demand. This leads to providing the energy to the heating coil by a combination of a larger size boiler and provides the incremental thermal energy from the thermal storage.

On the other hand, the required size of the electrical storage (battery) for the stochastic case doesn't change compared to the deterministic case, or it may even be somewhat lower than the deterministic one (maximum 10% smaller battery in Case-1S than its corresponding size in the deterministic Case-1D). This is due to the high cost of the electric battery and due to the possibility to supply some of the electricity by running the engine at a higher load. Therefore, it is economical to use the same battery or even a battery with a lower capacity. Consequently, from the economic point of view, for the stochastic case, somewhat larger engine and somewhat smaller battery are needed when compared to their required sizes for the deterministic case.

7.4. Economic and environmental performances of the system in stochastic cases

More detailed investigation of the economic and environmental performance of the optimal size of the energy system is investigated more in this section. For each distinct value of the CDE constraint in stochastic problems (6 cases) 300 scenarios are generated randomly, and the two-stage stochastic modeling is solved with the size of each component being equal to the optimal size. The variation of the annual total cost and operational CDE for all of these scenarios and all the stochastic cases are shown in Fig. 10 as violin plots. As mentioned, threshold value changes in different cases of stochastic optimization; the $CVaR_{0.95}$ threshold value decreases (moving from Case-6S to Case-2S), the 95th percentile of the CDE data decreases. For instance, the CDE value of 95th percentile for Case-6S is 1.6E + 04 ton CO_2/year and, that value for Case-5S is 1.66E + 04 ton CO_2/year. Therefore, for Case-6S to Case-2S, the problem is solved in such a way that the CDE values of 95% of the scenarios are below the CDE value at risk of that

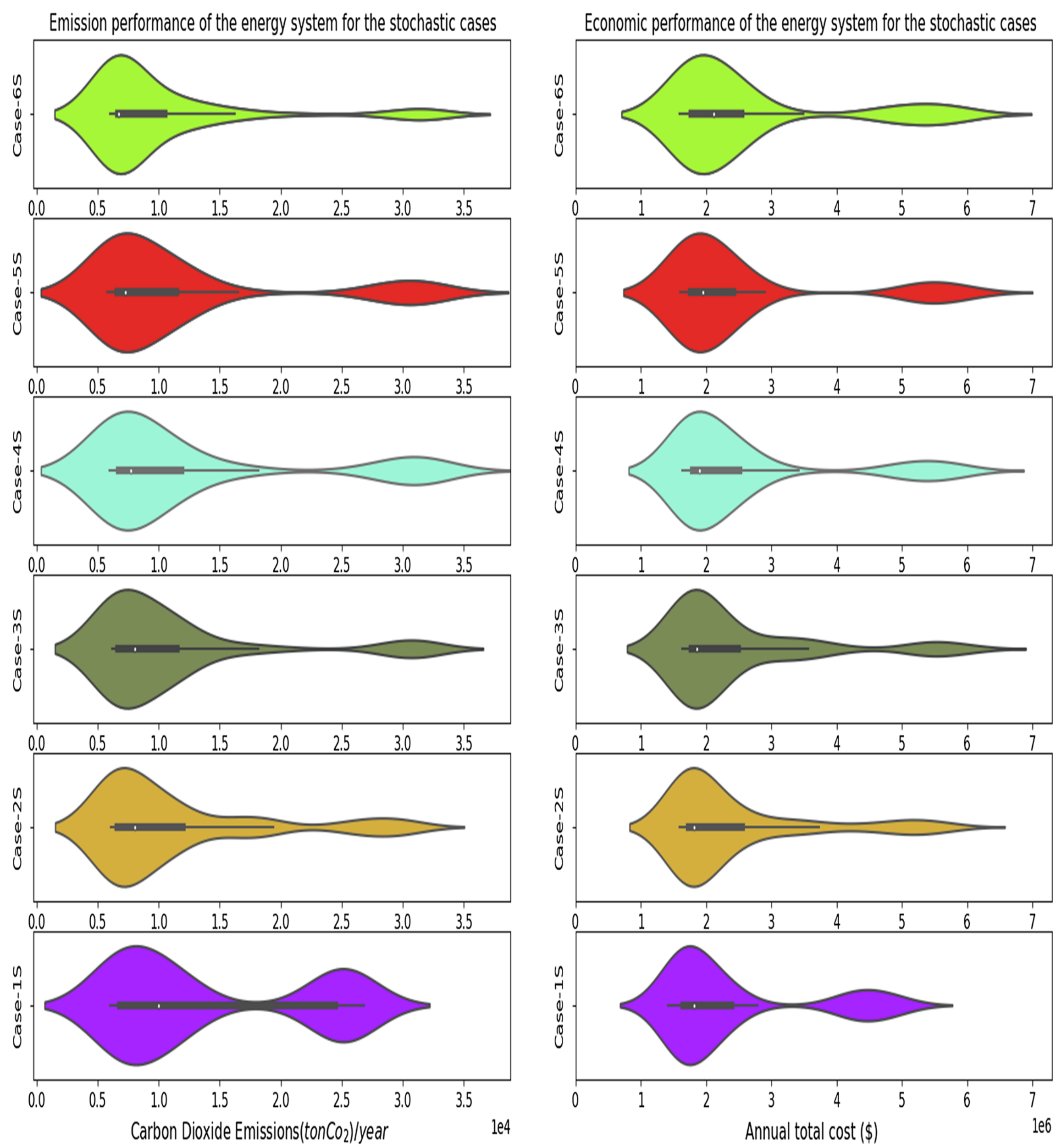

Fig. 10. Economic and Environmental performances of the energy system.

case. Thus, by applying tighter restriction on CDE via different threshold values, the 95th percentile of the data decreases and can guarantee that the CDE of 95% of the scenarios is below that value. For the first case (Case-1S), although the expected value of CDE is 9E + 03 ton CO_2/year, the 95th percentile is 26.7 E + 3 ton of CO_2/year and, there might be many scenarios with high values of CDE. So, Case-1S can be called as a risk-neutral problem and, other cases are risk-averse cases regarding to the CO_2 emissions.

As shown in Fig. 10 the annual total cost of all of the scenarios have the same shape as the CDE violin plot. Also, as shown in this figure, the 95 percentiles of the total yearly cost doesn't follow any trend because the objective function is the expected annual total cost and from the economic point of view, the objective function is risk neutral.

To investigate the effect of constraints presented by Eq. (33) on the CDE performance of the system, two more stochastic optimization problems are solved by using the constraint on the expected value of CDE scenarios in Eq. (35) without constraint given by Eq. (33). Then the results are compared to those of Case-6S and Case-5S. We call these two more optimization cases as Case-6(E) and Case-5(E). For the problem of Case-6(E), the maximum limit of CO_2R is set to 0.37, which is the CDE ratio obtained in Case-6S. For Case-5 (E) the maximum limit CO_2R is set to 0.4. Fig. 11 compares the environmental performance of the system with two different types of CO_2 constraints. The annual total cost of Case-6(E) and Case-5(E) are 1.6942E + 6 and 1.690426E + 6 $, respectively, which are lower than 1.6992E + 6 and 1.6954E + 6 $ of Case-6S and Case-5S, respectively. But the variation of 95% of CDE values of Case-6(E) and Case-5(E) is larger than those of Case-6S and Case-5S, respectively. The 95th percentile of CDE data for Case-6(E) is 3.46E + 04-ton CO_2/year which is almost more than two times of that of Case-6S. There is also the same situation for Case-5(E). The 95th percentile of CDE data for this case is 3.26E + 04-ton CO_2/year which is two times of that of Case-5S. Therefore, by applying Eq. (33), it is ensured with the probability of 95%, that the CDE value is lower than the specified limit. But by imposing a constraint on CED as given by Eq. (35), there is no control on the CDE value, and it is likely that some worst-case scenarios can take place.

8. Conclusions

This paper proposes a framework for the design of the energy system under multiple uncertainties. The two-stage stochastic programming model is proposed to determine the optimal size of each component by minimizing the expected annual total cost. Underlying MILP model is created by piecewise linearization of nonlinear equipment characteristics, thereby enabling rapid optimization of design and operation of the energy system consisting of power generation unit (engine), heat recovery system, absorption chiller, electric chiller, ground source heat pump, backup boiler, heating coil, short-term thermal storage and the electrical storage (battery). Proposed new strategy to develop the scenarios for the stochastic problem by random sampling of vectors which represent discrete distributions of the uncertain parameters (RVS method) is very efficient and provides a substantially better computational performance than Monte Carlo sampling. The proposed computational procedure has been applied to an office complex in Dalian, China. The stochastic optimization problem has been solved in six different cases. The cases are built based on different levels of carbon dioxide emissions (CDE) reductions and different levels of the conditional value at risk of CDE. At each case, the expected cost is minimized, and a value restricts the average of the high emissions risk with a probability of 0.05. By using different limitation values, different stochastic optimization cases are built. Each of the cases is also solved for the deterministic case. In each deterministic case, the annual total cost is minimized, and the ratio of CDE of the system to CDE of the standalone system is constrained by the value obtained from its corresponding stochastic case. The following main results are obtained:

- The optimal size of the energy system can lead to a decrease in both the annual total cost and also CDE. We have determined what is the lowest CDE which can be attained based on present-day technology.
- Variation of the optimal size of each component due to the change in CDE ratio for both stochastic and deterministic cases are presented.
- By using RVS method, after 60 scenarios, the objective function converges to the optimum value, however, by using the Monte Carlo Sampling method the objective function has a fluctuation even for more than 81 scenarios. Therefore, the proposed methodology for scenario construction greatly simplifies the optimization of the system design, while yielding better results than Monte Carlo Sampling. It is our hope that it will find wide use in practice.
- The design performance curves presented in this work can be applied to a real application to see the change of the size of each component from the deterministic case to the cases with

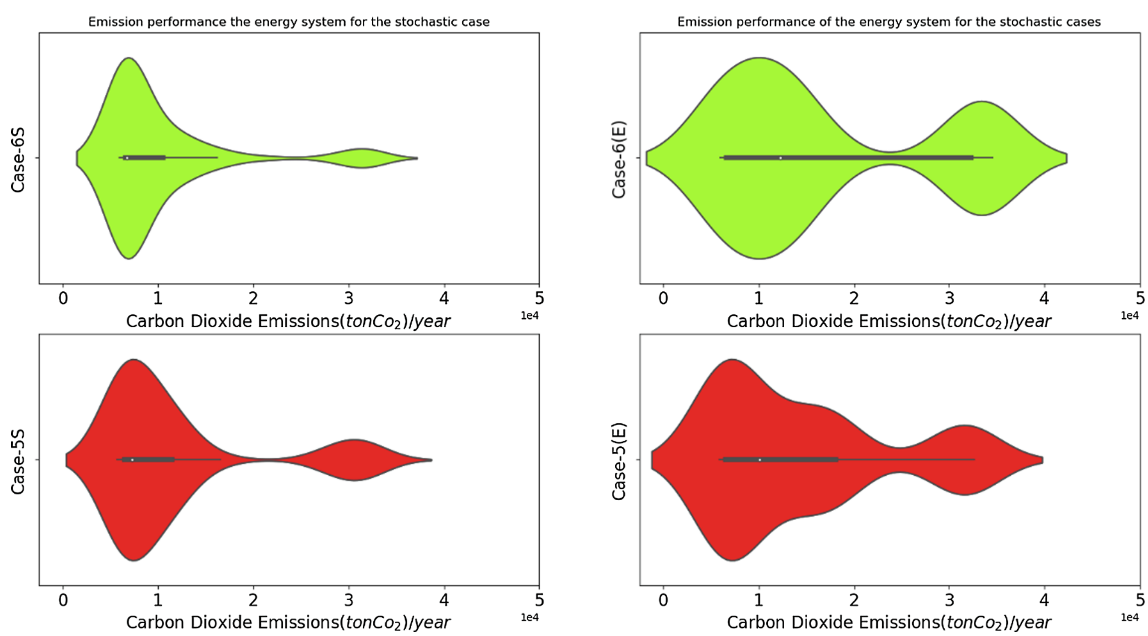

Fig. 11. Comparisons of the environmental performance of the energy system using two types of constraints.

uncertainty.

- The variation of the annual total cost and CDE has been shown through violin plots. It can be seen that by the proposed method, it can be guaranteed with 95% probability to avoid high CDE occurrences.
- By limiting the CDE, the size of the engine, absorption chiller, battery, and GSHP increases for both stochastic and deterministic cases.
- By decreasing the specified level of CDE, for the stochastic case, the significant increase in the size is seen in the battery such that the size of the battery of Case-6S is 37% higher than that of the Case-1S. This value for the deterministic case is also considerable and is 27% compared to Case-1D.
- The required size of the electric chiller, boiler, thermal storage, and heating coil decreases for both stochastic and deterministic case by increasing the limitation of the CDE. The most significant decrease in the size is observed for the electric chiller, which is 30% for Case-6S of the stochastic problem compared to its size in Case-1S. This reduction amount is also seen for the deterministic case, which is almost 25%.
- In stochastic problem, the size of the engine, GSHP, absorption chiller, thermal storage for all cases of CDE strategies is higher than those of deterministic case. For all stochastic cases, the required sizes of the heating coil and battery are the same or a somewhat lower than their corresponding sizes in the deterministic case.
- The required size of the electric chiller decreases a lot for the stochastic cases compared to the size needed for deterministic cases.
- The percentage of the increase in the size of the GSHP, thermal storage, and boiler increases by decreasing the specified level of the CDE.
- The percentage of the increase in the size of the engine, absorption chiller, and electric chiller decreases by increasing the CDE limitation.

Even though the electricity from the grid is assumed to be generated from coal, the lowest ratio of the CDE emissions from the integrated community energy system to the CDE emissions from the stand-alone systems has been found to be in the high 30 s% (37%). This is far away from the target 10% CDE emissions, which is a widely accepted target if we are to avoid runaway global warming. Our results show that a very significant technological changes are required to the energy systems for the dense urban core if we are to attain 90% reduction in CDE.

In this paper, the application of PV cells, thermal solar cells and seasonal thermal energy storage has not been investigated as potential candidates of the energy system components, since we assume that the buildings are in the urban core where space is very limited. We will include these components in our subsequent work which will add life cycle GHG emissions as one of the optimization criteria.

Declaration of Competing Interest

The authors declare that they have no known competing financial interests or personal relationships that could have appeared to influence the work reported in this paper.

Acknowledgement

The authors gratefully acknowledge the financial support from ORF, OCE, and NSERC.

Appendix A

As presented in Eq. (7), the efficiency of the equipment might be described by a nonlinear equation $g(f)$, where f is the partial load operation of that component. For the problem presented in this paper, the polynomial function of order two is applied for the components. If Eqs. (6),(7),(8) are combined to each other, therefore we have:

$$\frac{Q_{in}}{Ca} = \frac{f}{g(f)} \tag{A1}$$

where Q_{in} is the input energy to the component and Ca is the capacity of that equipment. For instance, for the engine, $Q_{in} = F$ and $Ca = E_{nom}$. The term $\frac{f}{g(f)}$ can be linearized by N pieces of linear equations. Therefore, the term could be represented by a piecewise linear function as bellow:

$$\frac{f}{g(f)} = \begin{cases} A_1^{'}f + B_1^{'}\beta \leq f \leq \nu_1 \\ A_2^{'}f + B_2^{'}\nu_1 < f \leq \nu_2 \\ \cdots \\ A_N^{'}f + B_N^{'}\nu_{N-1} < f \leq \nu_N = 1 \end{cases} \tag{A2}$$

$A_i^{'}$ and $B_i^{'}$ are the coefficients of each piece of the linear equation, β is the on/off coefficient of the equipment and ν_is are utilized to divide the partial load axis into N segments.

By combining Eqs. (A1) and (A2), we have:

$$Q_{in} = \begin{cases} A_1^{'}Q_{out} + B_1^{'}Ca\beta Ca \leq Q_{out} \leq \nu_1 Ca \\ A_2^{'}Q_{out} + B_2^{'}Ca\nu_1 Ca < Q_{out} \leq \nu_2 Ca \\ \cdots \\ A_N^{'}Q_{out} + B_N^{'}Ca\nu_{N-1}Ca < Q_{out} \leq \nu_N Ca \end{cases} \tag{A3}$$

where Q_{out} is the output power of the system, for example, for the engine$Q_{out} = E_{pgu}$.

To write the MILP model for the component for a continuous design model, the bunch of the following equations is applied:

$$\begin{cases} Q_{in}^{n} = A_{n}^{'}Q_{out}^{n} + B_{n}^{'}Ca^{n} n = \{1, 2, \cdots, N\} \\ Q_{in} = \sum_{i=1}^{N} Q_{in}^{n} \\ Ca = \sum_{i=1}^{N} Ca^{n} + Pen^{1} \\ Q_{in}^{n} \leq \lambda^{n} * M \\ Pen^{1} \leq \lambda^{'} * M \\ \sum_{i=1}^{N} \lambda^{n} + \lambda^{'} \leq 1 \\ Q_{out} = \sum_{i=1}^{N} Q_{out}^{n} \\ Q_{out}^{n} \geq \gamma_{n-1}Ca - Pen^{n} n = \{1, 2, \cdots, N\} \\ Q_{out}^{n} < \nu_{n}Ca \\ Pen^{n} \leq \delta^{n} * M' \\ \lambda^{n} + \delta^{n} \leq 1 \end{cases} \tag{A4}$$

In the above equations, it is assumed piecewise function Eq. (A3) is employed to build the model of each component. At each time, t, the energy input, Q_{in}, of the component is determined by one of N pieces linear functions. Also, when the component is off, all the values Q_{in}^{n} are zeros. λ^{n}s and $\lambda^{'}$ are binary variables, if $\lambda^{1} = 1$ the partial load operation of the component is in the first range and energy input is calculated by the first piece linear function, if λ^{2} is one, the system partial load, f, is in the second range and so on, also if $\lambda^{'} = 1$ the component is off. Ms are big values. Pen^{n}s and $Pen^{'}$ are penalty values and they can take the value of more than zero when a component is off or their corresponding operating range is not selected. But if the corresponding operating range is selected their values should be zero and it means the binary variable δ^{n} is zero.

Appendix B

(Description of the Case study)

In this paper, the buildings are in Dalian, China. Dalian has a maritime climate. The average annual temperature is 10 °C. The warmest and the coldest months are August and January, respectively, with an average temperature of 24 and −6°C, respectively.

In [54], the application of the energy system was studied for three different buildings; hotels, offices, and residential buildings. The office buildings include four single 24 floors office building; each has the area of 49392 m^{2}. For the office buildings, the highest percentage of CDE saving relative to the CDE of the stand-alone system was reported to be about 53.2% which is achieved by the use of the energy system including the internal combustion engine, heat recovery system, boiler, hybrid chiller, thermal storage, and heating coil. In this paper, the energy system design was performed for the deterministic case, and the effect of the uncertainty which exists in demands and energy prices was not examined. The COP of the absorption chiller and electric chiller were held fixed, and on/off coefficients of these components were assumed to be zero. Furthermore, the application of the GSHP and battery also was not investigated in this work.

The required electricity, heat, and cooling demands of the office buildings are shown in Fig. B1. The peak values of electrical demand, cooling demand, and heating demand are 3198, 7056, and 7050 kW, respectively.

Qadratic fitting coefficients [14,55] of part load performance of each component are presented in Table B1. The average efficiencies of the heat recovery system and boiler are assumed 0.8 and 0.85, respectively. The operating temperatures of the components are presented in [60].

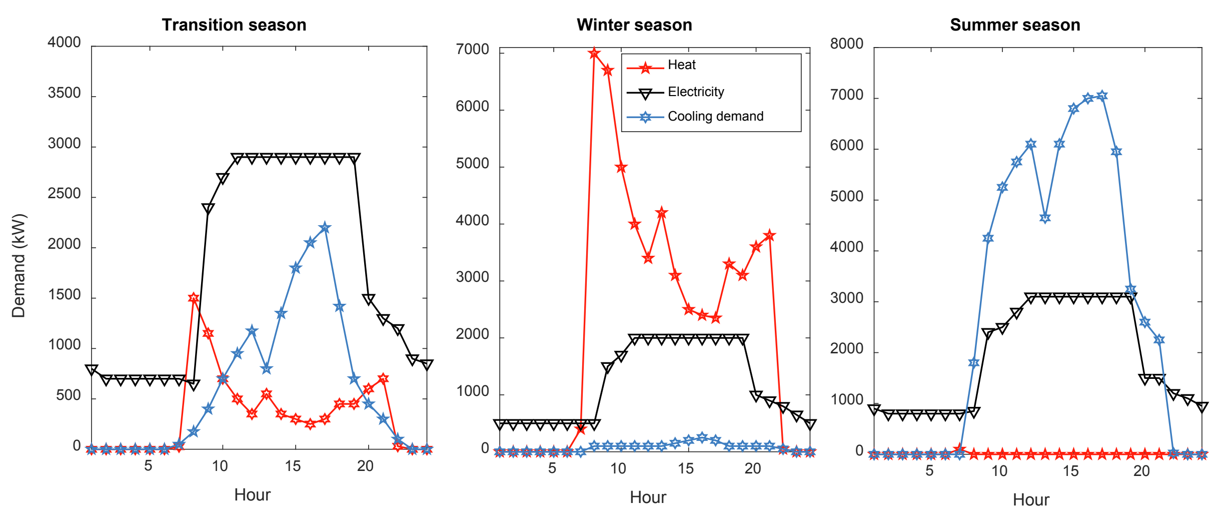

Fig. B1. the energy demand of the office buildings in repective days.

Table B1
Quadratic fitting coefficients for the partial load performance of each component.

	PGU	Electric Chiller	Absorption Chiller	GSHP/COP_{rate}
a	−0.721	−5.714	−1.388	0.635
b	1.124	8.010	1.972	0.299
c	0.022	3.010	0.546	0.052

References

[1] Zheng CY, Wu JY, Zhai XQ. A novel operation strategy for CCHP systems based on minimum distance. Appl Energy 2014;128:325–35. https://doi.org/10.1016/j.apenergy.2014.04.084.
[2] Wang J, Zhang C, Jing Y. Multi-criteria analysis of combined cooling, heating and power systems in different climate zones in China. Appl Energy 2010;87:1247–59. https://doi.org/10.1016/j.apenergy.2009.06.027.
[3] Wang J, Jing Y, Zhang C. Optimization of capacity and operation for CCHP system by genetic algorithm. Appl Energy 2010;87:1325–35. https://doi.org/10.1016/j.apenergy.2009.08.005.
[4] Jing Y, Bai H, Wang J, Liu L. Life cycle assessment of a solar combined cooling heating and power system in different operation strategies. Appl Energy 2012;92:843–53. https://doi.org/10.1016/j.apenergy.2011.08.046.
[5] Liu M, Shi Y, Fang F. A new operation strategy for CCHP systems with hybrid chillers. Appl Energy 2012;95:164–73. https://doi.org/10.1016/j.apenergy.2012.02.035.
[6] Zheng CY, Wu JY, Zhai XQ, Wang RZ. Impacts of feed-in tariff policies on design and performance of CCHP system in different climate zones. Appl Energy 2016;175:168–79.
[7] Afzali SF, Mahalec V. Novel performance curves to determine optimal operation of CCHP systems. Appl Energy 2018;226:1009–36. https://doi.org/10.1016/j.apenergy.2018.06.024.
[8] Zheng CY, Wu JY, Zhai XQ, Wang RZ. A novel thermal storage strategy for CCHP system based on energy demands and state of storage tank. Electr Power Energy Syst 2017;85:117–29.
[9] Mago PJ, Luck R, Knizley A. Combined heat and power systems with dual power generation units and thermal storage. Int J Energy Res 2014;38:896–907. https://doi.org/10.1002/er.
[10] Wang C, Lv C, Li P, Song G, Li S, Xu X. Modeling and optimal operation of community integrated energy systems: A case study from China. Appl Energy 2018;230:1242–54.
[11] Wang J, Sui J, Jin H. An improved operation strategy of combined cooling heating and power system following electrical load. Energy 2015;85:654–66. https://doi.org/10.1016/j.energy.2015.04.003.
[12] Holjevac N, Capuder T, Zhang N, Kuzle I, Kang C. Corrective receding horizon scheduling of flexible distributed multi- energy microgrids. Appl Energy 2017. https://doi.org/10.1016/j.apenergy.2017.06.045.
[13] Kang L, Yang J, An Q, Deng S, Zhao J, Li Z, et al. Complementary configuration and performance comparison of CCHP-ORC system with a ground source heat pump under three energy management modes. Energy Convers Manag 2017;135:244–55. https://doi.org/10.1016/j.enconman.2016.12.055.
[14] Kang L, Yang J, An Q, Deng S, Zhao J, Wang H, et al. Effects of load following operational strategy on CCHP system with an auxiliary ground source heat pump considering carbon tax and electricity feed in tariff. Appl Energy 2017;194:454–66. https://doi.org/10.1016/j.apenergy.2016.07.017.
[15] Liu W, Chen G, Yan B, Zhou Z, Du H, Zuo J. Hourly operation strategy of a CCHP system with GSHP and thermal energy storage (TES) under variable loads: A case study. Energy Build 2015;93:143–53. https://doi.org/10.1016/j.enbuild.2015.02.030.
[16] Tan ZF, Zhang HJ, Shi QS, Song YH, Ju LW. Multi-objective operation optimization and evaluation of large-scale NG distributed energy system driven by gas-steam combined cycle in China. Energy Build 2014;76:572–87. https://doi.org/10.1016/j.enbuild.2014.03.029.
[17] Ju L, Tan Z, Li H, Tan Q, Yu X, Song X. Multi-objective operation optimization and evaluation model for CCHP and renewable energy based hybrid energy system driven by distributed energy resources in China. Energy 2016;111:322–40. https://doi.org/10.1016/j.energy.2016.05.085.
[18] Fu L, Zhao X, Zhang S, Li Y, Jiang Y, Li H, et al. Performance study of an innovative natural gas CHP system. Energy Convers Manag 2011;52:321–8. https://doi.org/10.1016/j.enconman.2010.07.003.
[19] Zhao XL, Fu L, Zhang SG, Jiang Y, Li H. Performance improvement of a 70 kWe natural gas combined heat and power (CHP) system. Energy 2010;35:1848–53. https://doi.org/10.1016/j.energy.2010.01.005.
[20] Li CZ, Shi YM, Huang XH. Sensitivity analysis of energy demands on performance of CCHP system. Energy Convers Manag 2008;49:3491–7. https://doi.org/10.1016/j.enconman.2008.08.006.
[21] Akbari K, Nasiri MM, Jolai F, Ghaderi SF. Optimal investment and unit sizing of distributed energy systems under uncertainty: A robust optimization approach. Energy Build 2014;85:275–86. https://doi.org/10.1016/j.enbuild.2014.09.009.
[22] Rezvan AT, Gharneh NS, Gharehpetian GB. Robust optimization of distributed generation investment in buildings. Energy 2012;48:455–63. https://doi.org/10.1016/j.energy.2012.10.011.
[23] Yokoyama R, Tokunaga A, Wakui T. Robust optimal design of energy supply systems under uncertain energy demands based on a mixed-integer linear model. Energy 2018;153:159–69. https://doi.org/10.1016/j.energy.2018.03.124.
[24] Yokoyama R, Ito K. Optimal design of energy supply systems based on relative robustness criterion. Energy Convers Manag 2002;43:499–514. https://doi.org/10.1016/S0196-8904(01)00027-9.
[25] Niu J, Tian Z, Lu Y, Zhao H, Lan B. A robust optimization model for designing the building cooling source under cooling load uncertainty. Aplied Energy 2019;241:390–403.
[26] Zhou Z, Zhang J, Liu P, Li Z, Georgiadis MC, Pistikopoulos EN. A two-stage stochastic programming model for the optimal design of distributed energy systems. Appl Energy 2013;103:135–44. https://doi.org/10.1016/j.apenergy.2012.09.019.
[27] Henrich L, McClure J, Crozier M. Optimal design of residential cogeneration systems under uncertainty. Comput Chem Eng 2016;88:36–44. https://doi.org/10.1016/j.actamat.2015.02.029.
[28] Yang Y, Zhang S, Xiao Y. Optimal design of distributed energy resource systems based on two-stage stochastic programming. Appl Therm Eng 2017;110:1358–70. https://doi.org/10.1016/j.applthermaleng.2016.09.049.
[29] Yang Y, Zhang S, Xiao Y. An MILP (mixed integer linear programming) model for optimal design of district-scale distributed energy resource systems. Energy 2015;90:1901–15. https://doi.org/10.1016/j.energy.2015.07.013.
[30] Rezvan AT, Gharneh NS, Gharehpetian GB. Optimization of distributed generation capacities in buildings under uncertainty in load demand. Energy Build 2013;57:58–64. https://doi.org/10.1016/j.enbuild.2012.10.031.
[31] Li CZ, Shi YM, Liu S, Zheng ZL, Liu YC. Uncertain programming of building cooling heating and power (BCHP) system based on Monte-Carlo method. Energy Build 2010;42:1369–75. https://doi.org/10.1016/j.enbuild.2010.03.005.
[32] Mavromatidis G, Orehounig K, Carmeliet J. Uncertainty and Sensitivity Analysis for the Optimal Design of Distributed Urban Energy Systems. In: Syst Think Built Environ Sustain Built Environ Reg Conf Zurich, June 15th – 17th 2016;214:234–9. http://doi.org/10.3218/3774-6.
[33] Mavromatidis G, Orehounig K, Carmeliet J. Design of distributed energy systems under uncertainty: a two-stage stochastic programming approach. Appl Energy 2018;222:932–50. https://doi.org/10.1016/j.apenergy.2018.04.019.
[34] Urbanucci L, Testi D. Optimal integrated sizing and operation of a CHP system with Monte Carlo risk analysis for long-term uncertainty in energy demands. Energy Convers Manag 2018;157:307–16. https://doi.org/10.1016/j.enconman.2017.12.008.
[35] Mavromatidis G, Orehounig K, Carmeliet J. Comparison of alternative decision-making criteria in a two-stage stochastic program for the design of distributed energy systems under uncertainty. Energy 2018;156:709–24. https://doi.org/10.1016/j.energy.2018.05.081.
[36] Hu M, Cho H. A probability constrained multi-objective optimization model for CCHP system operation decision support. Appl Energy 2014;116:230–42. https://doi.org/10.1016/j.apenergy.2013.11.065.
[37] Ahn H, Rim D, Pavlak GS, Freihaut JD. Uncertainty analysis of energy and economic performances of hybrid solar photovoltaic and combined cooling, heating, and power (CCHP + PV) systems using a Monte-Carlo method. Appl Energy 2019;255.
[38] Lv C, Yu H, Li P, Wang C, Xu X, Li S, et al. Model predictive control based robust scheduling of community integrated energy system with operational flexibility. Appl Energy 2019;243:250–65.
[39] Jing R, Wang M, Liang H, Wang X, Li N, Shah N, et al. Multi-objective optimization of a neighborhood-level urban energy network: considering Game-theory inspired multi-bene fi t allocation constraints. Appl Energy 2018;231:534–48.
[40] Carpaneto E, Chicco G, Mancarella P, Russo A. Cogeneration planning under uncertainty. Part I: Multiple time frame approach. Appl Energy 2011;88:1059–67. https://doi.org/10.1016/j.apenergy.2010.10.014.
[41] Mavrotas G, Diakoulaki D, Florios K, Georgiou P. A mathematical programming framework for energy planning in services' sector buildings under uncertainty in load demand: The case of a hospital in Athens. Energy Policy 2008;36:2415–29. https://doi.org/10.1016/j.enpol.2008.01.011.
[42] Mavrotas G, Florios K, Vlachou D. Energy planning of a hospital using Mathematical Programming and Monte Carlo simulation for dealing with uncertainty in the economic parameters. Energy Convers Manag 2010;51:722–31. https://doi.org/10.1016/j.enconman.2009.10.029.
[43] Ersoz I, Colak U. A stochastic evaluation of investments in combined cooling, heat, and power systems. Appl Therm Eng 2019;146:376–85. https://doi.org/10.1016/j.applthermaleng.2018.09.130.
[44] Marino C, Marufuzzaman M, Hu M, Sarder MD. Developing a CCHP-microgrid operation decision model under uncertainty. Comput Ind Eng 2018;115:354–67. https://doi.org/10.1016/j.cie.2017.11.021.
[45] Alavi SA, Ahmadian A, Aliakbar-Golkar M. Optimal probabilistic energy management in a typical micro-grid based-on robust optimization and point estimate method. Energy Convers Manag 2015;95:314–25. https://doi.org/10.1016/j.enconman.2015.02.042.
[46] Niknam T, Golestaneh F, Malekpour A. Probabilistic energy and operation management of a microgrid containing wind/photovoltaic/fuel cell generation and energy storage devices based on point estimate method and self-adaptive gravitational search algorithm. Energy 2012;43:427–37. https://doi.org/10.1016/j.energy.2012.03.064.
[47] Mohammadi S, Soleymani S, Mozafari B. Scenario-based stochastic operation management of microgrid including wind, photovoltaic, micro-turbine, fuel cell and energy storage devices. Int J Electr Power Energy Syst 2014;54:525–35. https://doi.org/10.1016/j.ijepes.2013.08.004.
[48] Ersoz I, Colak U. Combined cooling, heat and power planning under uncertainty. Energy 2016;109:1016–25. https://doi.org/10.1016/j.energy.2016.04.071.
[49] Vahidinasab V. Optimal distributed energy resources planning in a competitive electricity market: Multiobjective optimization and probabilistic design. Renew Energy 2014;66:354–63. https://doi.org/10.1016/j.renene.2013.12.042.
[50] Bickel JE, Lake LW, Lehman J. Discretization, simulation, and swanson's (Inaccurate) mean. SPE Econ Manag 2011;3. https://doi.org/10.2118/148542-PA.
[51] Miller AC, Rice TR. Discrete approximations of probability distributions. Manage Sci 1983;29:352–62. https://doi.org/10.1287/mnsc.29.3.352.
[52] Shah KK, Mundada AS, Pearce JM. Performance of U. S. hybrid distributed energy systems: solar photovoltaic, battery and combined heat and power. Energy Convers Manag 2015;105:71–80.

[53] Basrawi F, Yamada T. Economic and environmental based operation strategies of a hybrid photovoltaic – microgas turbine trigeneration system. Appl Energy 2014;121:174–83.
[54] Li M, Mu H, Li N, Ma B. Optimal design and operation strategy for integrated evaluation of CCHP (combined cooling heating and power) system. Energy 2016;99:202–20.
[55] Tian Z, Niu J, Lu Y, He S, Tian X. The improvement of a simulation model for a distributed CCHP system and its influence on optimal operation cost and strategy. Appl Energy 2016;165:430–44. https://doi.org/10.1016/j.apenergy.2015.11.086.
[56] Hajabdollahi H. Evaluation of cooling and thermal energy storage tanks in optimization of multi-generation system. J Energy Storage 2015;4:1–13. https://doi.org/10.1016/j.est.2015.08.004.
[57] Luo Z, Wu Z, Li Z, Cai H, Li B, Gu W. A two-stage optimization and control for CCHP microgrid energy management. Appl Therm Eng 2017;125:513–22. https://doi.org/10.1016/j.applthermaleng.2017.05.188.
[58] Luo Z, Gu W, Wu Z, Wang Z, Tang Y. A robust optimization method for energy management of CCHP microgrid. J Mod Power Syst Clean Energy 2017. https://doi.org/10.1007/s40565-017-0290-3.
[59] Zhou Z, Liu P, Li Z, Ni W. An engineering approach to the optimal design of distributed energy systems in China. Appl Therm Eng 2013;53:387–96. https://doi.org/10.1016/j.applthermaleng.2012.01.067.
[60] Afzali SF, Mahalec V. Optimal design, operation and analytical criteria for determining optimal operating modes of a CCHP with fired HRSG, boiler, electric chiller and absorption chiller. Energy 2017;139:1052–65. https://doi.org/10.1016/j.energy.2017.08.029.

Chapter 5

A New Flexible Borehole Thermal Energy Storage Model

A New Flexible Borehole Thermal Energy Storage Model

1. Introduction

In order to store and extract heat seasonally and to reduce the investment cost, it is beneficial to determine the optimum size and optimum operation of seasonal thermal energy storage. In the design phase, the space between boreholes, length of boreholes, the type of the grout material, location of U-tube in the borehole, and the number of boreholes have to be determined. The optimal design is performed to obtain the highest system efficiency and also the minimum annual total cost.

For a large-scale seasonal thermal energy storage takes typically between two to five years to reach the saturation design condition and to become stable in terms of operating conditions. Hence, a comprehensive design study requires a long-term evaluation of the borehole storage system. This long-term required analysis makes the design problem of the underground storage systems complex. Moreover, the performance of this system has to be investigated during interaction with other energy system components. This further increases the complexity of the optimization problem in terms of computational time and system modelling. As a result, deriving an accurate and straightforward model for the seasonal thermal energy is the most critical step in the design optimization problem.

This work presents an overview of various models for representing the heat transfer process of borehole heat exchangers. Also, this work proposes a new flexible semi-analytical methodology to model the heat transfer process of the borehole thermal energy storage. Some of the results and concepts introduced by Hellstrom are utilized to create a new model.

1.1. Literature reviews

Buildings use a large portion of worldwide energy sources [1]. To solve this issue, most of the countries have followed some policies [2] for constructing buildings in a way to be more energy-efficient. Heating demand in residential sectors for supplying domestic hot water (DHW) and space heating is engaged for almost 80% in the north of Europe [3] and Canada [4]. Due to the increase in electricity price and shortage of fossil fuel resources, renewable energies and energy storage technologies could be great alternative solutions to energy-related problems as energy sources and technologies, respectively.

As the energy demand of the buildings rises, it is becoming more crucial to discover effective ways to employ the energy and to reduce the use of fossil fuels. It is highlighted that the consumption of natural gas and oil would increase drastically by 92% and 48%, respectively, from 2003 to 2030 [5]. The reason is that it is predicted that the consumption of the world's total energy will rise by 71% from 2003 to 2030 [5] [6].

This causes severe environmental challenges, as the concentration of greenhouse gas emissions in the atmosphere has been significantly increased. Thus, if some preventive or corrective actions are not employed to reduce the level of greenhouse gas emissions, the influences of climate change will be further worsened. By the use of either small scale engine or large scale engine for producing electricity in residential sectors or power plants, respectively, there is a considerable amount of waste heat generated. Using this waste heat throughout the utilization of the community energy systems can significantly increase the efficiency of a system when compared to a separate production energy system. The efficiency of a power-producing system would be improved from 35-55% to more than 90% by harvesting the waste heat for heating and cooling demands usage.

The application of renewable energies and onsite community energy systems is a promising way to decrease the primary energy consumption and environmental effects of greenhouse gas emissions. There are various types of renewable technologies that can be applied for community energy systems such as biofuels, wind turbines, photovoltaic (PV), solar thermal collectors, and photovoltaic/ thermal (PV/T).

Community energy systems provide electricity and thermal energy simultaneously by recovering heat from the exhaust gas of the power generation unit [7]. This thermal energy can be sent to either heating coil or absorption chiller for providing heat and cooling energy to buildings close to the community energy systems, respectively. Although the coupling of power generation units and other energy system technologies enhances the overall system efficiency, compared to the separate production system, there are still economic and environmental shortcomings. Because there are operational constraints of community energy systems and the seasonal variations in building demands and fossil fuel availability.

The thermal load limits electricity production, and peak periods in demand for energy often do not align with supply [8]. These limitations lead to increased energy rates and short supplies in the periods of highest demand. One of the effective methods to alleviate the discrepancy between the supply and demand for energy and to increase the electrical generation capacity of the energy system is the application of thermal energy storage (TES).

Moreover, there might be an imbalance of the cooling and heating demands for some locations. Significant fluctuations in outdoor temperatures during summer and winter cause substantial heat load and cooling load variations across the year. However, the heat load and cooling load are frequently not well-matched with thermal energy provided by community energy systems or separate production systems [9]. Taking industrial waste heat as an example of the available thermal energy; the amount of recovered heat depends on the working load of an industrial process or the industrial electricity demand, and it is probably constant all year. In this case, a considerable portion of heat will be unused during the summer when there is a small heating demand and cooling demand. Therefore, the operational limitations and seasonal demand mismatch signify an opportunity for the application of the seasonal thermal energy storage (STES) systems. Seasonal storage systems are integrated with either large-scale solar thermal collectors or community energy systems or industrial waste heat to compensate for the operational limitations and demand mismatch. STES systems can be charged during the summer by thermal energy provided either through solar thermal collectors or combined heat and power (CHP) system and then preserve the energy for later use during the wintertime.

Among different storage technologies, thermal energy storage and battery have been mostly applied to increase the efficiency of the energy system. Short-term thermal energy storage has approximately 100% round trip efficiency, and the efficiency of the battery is roughly 80% [10]. Applying thermal storage and integrating with solar thermal collectors to utilize solar energy and then meet building heat demands becomes the subject of the most recent studies [11]. Excess thermal energy from different generation technologies can be stored during either short or seasonal periods in short-term thermal storage or seasonal storage or both of them, respectively [12]. Since charging and discharging rates in seasonal storage is pretty slow, seasonal storage coupling with diurnal storage might compensate these slow rates. The application of the thermal storage tank as a buffer tank in conjunction with solar collectors has been investigated in different studies [12][13].

Daily thermal energy storage can be in the form of either a hot water storage tank or ice storage and has a high heat transfer rate [12][13]. Seasonal thermal storage can store the thermal energy when there is an excessive amount of energy sources or when the available thermal energy is low-priced. The system can help to provide enough energy during a shortage of energy due to the limited sun exposure and also can avoid the demand for thermal energy with high energy costs.

Seasonal thermal energy storage (STES) is not a stand-alone component since it cannot produce energy by itself. Accordingly, the performance of STES mostly depends on its own operating situation and the way it communicates with other components. The flow rate and temperature of the fluid heat carriers during charging and discharging periods influence the storage performance and determine storage overall efficiency. Moreover, storage energy performance is affected by weather conditions and soil properties such as soil thermal conductivity, underground water, flow velocity, ground surface temperature, and the ambient temperature so on. The relation between the fluid temperatures in U-tube and the ground temperatures is entirely dependent on ground thermal conductivity. The ground properties and its specific heat capacity are essential factors in determining ground temperature distribution and the temperature at the borehole wall. The borehole resistance is another crucial parameter and depends on the dimension of the borehole exchanger, the thermal conductivity of the U-tube and the thermal properties of the grout material. These parameters control the specific heat rate of the borehole heat exchangers. According to information obtained from different cases of seasonal thermal energy storage schemes around the world, the specific heat rate might vary from 10 W/m to 120 W/m [14].

1.2. Review of the available models for ground heat exchanger (GHEs) and ground heat storage (GHS)

Investigation of the heat transfer process in borehole GHEs or GHS is still a significant challenge because of difficulty with the transient heat process analysis inside and outside of the borehole. A large number of studies have been done to resolve this complicated task through analytical and numerical studies.

A borehole field consists of vertical boreholes usually connected in either series or parallel or a combination of series and parallel and supplied with a fluid carrying heat at a temperature (T_f). The heat pump system can be integrated into the borehole field to increase the temperature level of the water comes out from the field in the wintertime. The design and operational optimization of the seasonal storage (borehole heat exchangers) relies on the precise modelling of the heat transfer in the bore fields during the system performance [15]. GHEs can also be used as seasonal thermal energy storage or borehole thermal energy storage (BTES). The application of the seasonal thermal energy storage is to store heat during summertime and then to extract the stored heat during the wintertime to supply heat demand of the buildings. When BHEs are applied to provide energy for the GSHP, the energy extraction and injection to the ground has to be maximized. By contrast, when GHEs are used as seasonal thermal energy storage, the heat exchange between heat exchanger and ground has to be minimized to decrease the heat loss. Therefore, in seasonal thermal energy storage, the distances between the borehole heat exchangers are much less than their distance in the ground-coupled heat pump system.

It has to be mentioned first that most of the proposed solutions do not consider the operating strategy of the system. Some proposed numerical and analytical models are based on the assumption that all of the boreholes have the same heat rate. This assumption was taken to determine the analytical g-function factor. It is a dimensionless unsteady thermal resistance, which is the temperature response due to the unit step change in the heat flux.

The complete heat transfer model of this system comprises a heat transfer model inside the boreholes (using borehole resistance concept) and a heat transfer in the ground outside the borehole. Developing thermal response factors and integrating them with a thermal superposition scheme is a common approach to prepare the heat transfer model of the outside of the borehole.

Kelvin's theory [16] of heat sources and the Laplace transform method are analytical tools that have been utilized extensively for obtaining analytical solutions of the heat transfer process in the ground around the boreholes. Different solutions such as line source, volume source and cylindrical source can be derived by the use of the Kelvin's point-source solution and the proper space integrating over that solution. The line source theory developed by Kelvin, supposed BHE as an infinite line in an infinite medium that was subjected to the constant heat rate per length of the line.

The Laplace transform method has two stages [16]. At first, the Laplace transform is applied to the original problem to provide the problem in the Laplace domain. Usually, solving a problem in the Laplace domain is more straightforward than solving the original problem. After converting the original problem into that in the Laplace domain, the inversion theorem would be used to determine the solution of the original problem. The Laplace theorem has been used extensively to determine the short-term response of the heat transfer process in GHEs.

Duhamel's theorem is another useful theorem that has been employed frequently for developing models of the heat transfer process in the bore field. In the real application, heat transfer in the boreholes varies due to the different heating and cooling demands. In this case, using the principle of the superposition, which is known as Duhamel's theorem, can provide a solution to a problem with a unit-step load.

Eskilson [17] developed thermal response factors numerically, assuming uniform and equal temperature along borehole walls. This assumption is taken based on the parallel connection of the boreholes and the equal temperature of the input fluids to all the borehole heat exchangers. Thermal response factors developed by Eskilson, which are known as g-functions, are often considered as a reference for comparison with other thermal response factors, which can be developed by the use of the analytical models.

Various analytical solutions (e.g., finite line source model, infinite line source model) are applied to generate thermal response factors for the heat transfer model of the outside of the boreholes. Moreover, different boundary condition assumptions have been taken into account such as (i) Uniform and equal heat extraction rate along the length of all boreholes (ii)Uniform heat extraction rate and equal average temperature along the length of the boreholes (iii)Uniform and equal borehole wall temperature along the length of the boreholes. Eskilson first developed the concept of the g-function. As mentioned earlier, this kind of equation is applied to determine the change in the borehole wall temperature due to a constant heat extraction/injection rate in the borehole field. It is assumed that the wall temperature is constant for all borehole heat exchangers.

1.3. Heat transfer models of the surrounding ground around Borehole heat exchanger

Cimmino et al. [15] expressed that different g-functions can be utilized to model the heat transfer process within the ground encompassing the BHEs at different time scales. Cimmino et al. [15] expressed that the heat transfer process in GHEs can be described in different regions (periods). For the first region (at the beginning of the heat injection/heat extraction), the borehole wall temperature is not affected by ground surface temperature and interaction between boreholes. Accordingly, an infinite line source model can be applied to describe the heat transfer in the ground closed to the borehole. In the second region (second period), an appropriate model (g-function) has to reflect the influence of the borehole interactions to explain the heat transfer process. Hence, on the contrary to the first region, different borehole configurations have different g-function curves in this region. The starting time of this region for each borehole heat exchanger depends on the borehole dimensions. Additionally, for all BHEs, the g-function value increases with time and approaches to their value of the last region. In the last region, the g-function curves of different borehole fields would be different, and g-functions represent the steady-state heat transfer process. It implies that the borehole wall temperature is constant and is not affected by heat injection/extraction.

Analytical solutions are usually favoured over numerical solutions since it is simpler to obtain thermal response factors by analytical solutions rather than numerical solutions. Ingersoll and Plass [18] employed an infinite line source (ILS) model to determine the thermal response of buried pipes of infinite length. They developed temperature distribution in the ground encompassing a line source during the heat extraction process at a constant rate. They implemented temporal superposition and spatial superposition to estimate the temperature response for a field of multiple pipes or boreholes [19]. Carslaw and Jaeger [20] applied a cylindrical heat source (CHS) model to determine the temperature distribution around a source of heat of a cylindrical shape and infinite length. The CHS model was initially challenging to be solved numerically and was employed through some provided solutions presented in tables. To solve this issue, Beaudoin [21] applied Gaver–Stehfest algorithm to express the CHS solution in terms of some series of the Bessel functions. Next, Ingersoll [19] applied the temporal superposition and spatial superposition to the CHS model to calculate the temperature response of a bore field having multiple boreholes.

The finite line source (FLS) solution was employed by Eskilson [17] to derive the g-function of a borehole heat exchanger. The solution gives the temperature distribution in the ground around a line source of length H, which has a uniform heat extraction q.

Zeng et al. [22] utilized the FLS solution to attain the average of borehole wall temperature. They assumed a uniform heat extraction rate along each borehole and equal heat extraction rate for all boreholes. The authors showed that there is a little difference between FLS solution evaluated at H/2 and integral mean temperature along the borehole length. They expressed the integral mean temperature at the borehole wall by a relation which involves a double integral.

Lamarche and Beauchamp [23] utilized the FLS solution and derived a relation for calculating the integral mean temperature at the borehole wall. The expression was more straightforward than that proposed by Zheng et al. [22] since it involves only a single integral. The proposed relation has a weakness and is used for a case when the distance between the ground surface and head of the borehole is zero. Though, the proposed relation performed better than the FLS evaluated at the mid-length for approximating Eskilson's g-function.

Claesson and Javed [24] solved the deficiency of the relation in and suggested a relation for the integral mean temperature at the borehole wall for the case when the distance between the ground surface and the borehole head is more than zero.

Fossa [25] analyzed thermal response factors obtained from the FLS assuming uniform heat rate extraction for each borehole and equal heat rate extraction for all boreholes. He compared the factors to those of Eskilson's g-functions for two different bore fields having 3*3 and 8*2 borehole configurations. The author remarked that the obtained factors are higher than Eskilson's g-functions for large values of the time and for bore fields having a small distance between boreholes.

Fossa et al. [26] examined the thermal response factor of an 8*4 borehole field, assuming a uniform heat extraction rate for each borehole and equal average temperature for all the boreholes. Heat extraction rates of single boreholes were set until the wall temperature of all boreholes reaches a constant value. The thermal response factor was observed to be comparable to that obtained from FLS and boundary conditions used by Eskilson (uniform heat extraction rate for each borehole and the unequal average temperature at all borehole walls).

A new method based on the analytical FLS model is introduced by Cimmino et al. [27] to approximate thermal response factors (g-functions). The method takes into account the variety of heat extraction rates between boreholes and considers the buried depth, which was not incorporated into Eskilson's work. The heat extraction rates obtained with the proposed method confirmed that there is an excellent match between the new model and Eskilson's numerical model.

Cimmino and Bernier [28] presented a simplified version of the method proposed by Cimmino et al. in [27] for calculating the thermal response factors (g-functions). They presented a methodology for an estimate of thermal response factors of vertical borehole fields, accounting for the change in heat extraction rates of individual boreholes with time, variable borehole lengths and variable buried depths.

1.4. Heat Transfer model inside the borehole heat exchanger (short-term response factors)

Yavuzturk [29] proposed a short-term response of GHEs for the first time by taking benefit from the non-dimensional temperature response functions given by Eskilson. He employed a two-dimensional implicit finite volume numerical approach to derive appropriate short-term g-functions. The g-function accounted for the heat capacities of pipe and grout and convective resistance of the fluid. The provided g-functions are applicable to model the heat transfer process for the time scale of 2.5 min to 200 hours. However, the issue regarding the application of the proposed model is the computational time. The computational time is as much as the time needed for the application of the g-function proposed by Eskilson.

Young [30] utilized the buried electrical cable (BEC) method developed by Carslaw and Jaeger and modified it to obtain a short-term response of the GHEs. Young expressed that there is an analogy between a buried electric cable and a vertical borehole. He mentioned that the core, the insulation and the sheath of the cable in the BEC method could be replaced by the equivalent diameter fluid pipe, the resistance and the grout of the GHE, respectively, to derive the short-term response g-function. He also added the grout allocation factor, which allocates a share of the grout heat capacity in the model to improve the performance of his model.

Xu and Spitler [31] developed a new short time-step model for vertical ground loop heat exchanger. The proposed model is an extension to the original long-term response developed by Eskilson. However, whereas Eskilson's model used a g-function to account for short time-step effects, Xu and Spitler proposed a one-dimensional numerical model for this aim. The numerical model considers the thermal mass of the fluid and the convective resistance as a function of flow rate, fluid mixture, and fluid temperature.

A classical analytical solution by Bandyopadhyay et al. [32], which accounts for the thermal capacity of the fluid, has been used to model the temperature response of the fluid inside the U-tubes. The results of the proposed analytical solution were validated through Finite Element Modeling (FEM) and agreed firmly with the results of FEM.

Analytical solutions in the Laplace domain were applied by Bandyopadhyay et al. [33] to obtain the short-time transient temperature response of ground heat exchangers. The solution accounted for the thermal capacities of fluid and grout material. The average temperature of the fluid and the temperature of the borehole wall were evaluated utilizing Gaver–Stehfest numerical inversion algorithm from the proposed analytical solutions.

Javed and Claesson [34] presented the development and the validation of new analytical and numerical solutions in the Laplace domain for the modelling of the short-term response of borehole heat exchangers. A set of equations represented by a thermal network was obtained for the Laplace transforms for the boundary temperatures and heat fluxes. The proposed analytical solution took into account the thermal capacities, thermal properties and the thermal resistances of all elements of the borehole.

Minaei and Maerefat [35] developed an accurate and straightforward analytical solution to the short-term heat transfer process in the borehole exchanger. They presented the thermal resistance and capacity circuit of two borehole configurations having a single U-shaped pipe and a double U-shaped pipe. The radial heat transfer model was presented considering the thermal capacities of fluid, grout and pipe. Laplace theorem was applied to solve the model and provide an analytical relation for short-term response inside the borehole. The outputs of the proposed analytical solution were in good agreement with numerical results. Moreover, authors claimed that by the use of their approach the computational time would reduce drastically.

Li and Lai [36] offered a composite-medium line-source model to derive short-term responses of ground heat exchangers. Short-term responses of the GHEs include transient heat process within the borehole, which traditional models did not take into account its effect on the GHEs model. It was expressed that short-term responses of GHEs have a significant influence on the design, operation and control of ground coupled heat pump (GCHP) system. It was declared that the fluid temperature prediction error between the proposed model and experimental data is less than 1 % for time step less than 1 hour. However, that error by the use of the traditional model would be less than 6%. Therefore, it can be inferred that the traditional model still has acceptable accuracy for being used seasonal storage modelling for this time range.

1.5. Thermal borehole resistance

As mentioned, analyzing the heat transfer process inside the borehole exchanger is a crucial step toward an appropriate design and optimal operation of GHEs. Performing an accurate heat transfer analysis requires taking into account the effect of all components inside the borehole [35]. A borehole heat exchanger includes the backfilling (grout), the U-tubes and the circulating fluid inside the pipes. The outputs of heat transfer analysis inside a borehole are inlet and outlet temperatures of the circulating fluid in the exchanger by considering borehole wall temperature and heat transfer rate. The dimension and thermal mass inside the borehole are less than those of the ground outside of the borehole. Moreover, there is a small temperature variation inside the borehole during the heat transfer process. Therefore, it is a frequently used assumption that the heat transfer process inside the borehole is supposed as a steady-state process. It has been demonstrated that this simplification is an appropriate and acceptable hypothesis for most engineering purposes except for dealing with responses within a few hours since the error of the fluid temperature calculation raises.

In summary, the heat transfer from the fluid to the ground is affected by the borehole thermal resistance, which holds the convection resistance between the fluid and borehole pipes, resistance between the two (or four) pipes, the resistance between U-tube and borehole perimeter and conduction heat resistance in the U-tube. Different studies have proposed empirical and theoretical relations to estimate these resistances. Also, they have been provided with some methodologies to evaluate these resistances experimentally [37].

$$R_p = \frac{1}{2\pi k_p} \ln \frac{r_o}{r_i} + \frac{1}{2\pi r_i h} \qquad \text{Eq. 1}$$

k_p is the thermal conductivity of the U-shaped pipe ($\mathrm{Wm^{-1}K^{-1}}$) , r_o and r_i are outer and inner radius of the legs of the U-shaped pipe, respectively and h is the convective heat transfer coefficient ($\mathrm{Wm^{-2}K^{-1}}$). Many formulas have been provided to calculate the convective heat transfer coefficient and are presented in [38]. A simple relation to calculate this coefficient is as follows:

$$Nu = \frac{2hr_i}{k_f} = 0.023 Re^{0.8} Pr^{n} \qquad \text{Eq. 2}$$

k_f is the thermal conductivity of the fluid, Re is the Reynold's number, Pr is Prandtl's number, calculated at the mean temperature of the fluid, n equals to 0.4, when the fluid is being heated (winter time) and is 0.3 when the fluid is being cooled (summer time). As expressed in [39] , eq.() is a good approximation of the convective heat transfer coefficient when $0.7 \leq Pr \leq 120$ and $2500 \leq Re \leq 124000$, and the ratio of the length to diameter of the borehole is greater than 60. The influence of the convective heat transfer on the borehole thermal resistance is negligible since the convective resistance term only accounts for 2-3% of total borehole thermal resistance for most of the cases and for turbulent flow inside the U-shaped pipe.

The third term in the borehole thermal resistance is two-dimensional resistance of the backfilling material.

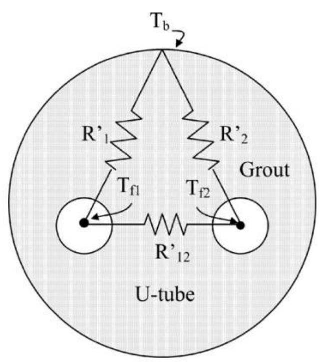

Fig. 1: Thermal resistance diagram inside the borehole [38][37]

One of the most common relations for determining the borehole resistance per unit length was proposed by Paul [40] based on experiments on three different configurations:

$$R_b = \frac{1}{\beta_0 \left(\frac{r_b}{r_p}\right)^{\beta_1} k_g} \qquad \text{Eq. 3}$$

Where β_0 and β_1 are parameters and depend on system configuration and are calculated based on the fitting experiment.

Another relation was proposed by Hellstrom [38], known as line-source formula, which is used in DST model. The thermal resistance diagram inside the borehole is shown in Fig. 1. Following equation was developed by Hellstrom [38],

$$R_b = \frac{1}{4\pi k_g}\{\ln\left(\frac{r_b}{r_p}\right) + \ln\left(\frac{r_b}{2x_c}\right) + \sigma \ln\left(\frac{m}{m-1}\right)\} \quad \text{Eq. 4}$$

x_c is the half of the distance between the centers of the two legs of U-shaped pipe, m is defined as follows:

$$m = (\frac{r_b}{x_c})^4 \quad \text{Eq. 5}$$

Also σ is as follows:

$$\sigma = (k_g - k_s)/(k_g + k_s) \quad \text{Eq. 6}$$

k_g is the thermal conductivity of the grout and k_s is the thermal conductivity of the soil (ground).

Discretized three-dimensional models usually describe very well the heat transfer process inside and outside of the borehole exchanger. However, they are more complicated than analytical solutions, and their application is not efficient in terms of computational time. Also, the application of fully discretized models is not practical in optimization software or during design calculation due to their complexity. On the contrary, analytical solutions are widely utilized for simulating the heat process within borehole exchangers due to their simple structure, which leads to a considerable reduction of computational time.

1.6. Short-term response via thermal network analysis

Borehole heat exchanger modeling via thermal network analysis has been attracted much attention in recent years. As it is simple to apply the concept of the thermal network to derive the heat transfer model and also the outputs of models are in good agreement with experimental results. The application of the thermal network analysis is based on the similarity between thermal and electrical conduction. Different studies have been utilized this methodology to simulate the heat transfer ground inside the borehole and the ground surrounding the borehole.

De Carli et al. [41] proposed CaRM (Capacity Resistance Model) to model the heat transfer of the borehole heat exchanger. The proposed model can consider fluid patterns in different borehole configurations such as single U-tube, a double U-tube or coaxial pipes. The authors validated the model utilizing commercial software based on the finite difference method. Also, they made further comparisons against data derived from the ground thermal response test.

Zarrella et al. [42] modified the CaRM model published by De Carli et al. [41]. Based on that modification, the short-term heat transfer analysis of double U-tube was investigated because the modified model accounts for the heat capacitances of fluid and filling materials. The authors proved that there is good agreement between the results of the model and outputs of the finite element method and measurements of the ground thermal response test.

Similarly, Bauer et al. [43] generated a two-dimensional thermal resistance and capacity model (TRCM) for different types of borehole heat exchangers. The authors expressed that by considering the thermal capacitance of the grout, the model is capable of assessing the short-term thermal process in the borehole. They also mentioned that in addition to considering the thermal capacitances of the grout, the placement of these capacitances in the thermal network has great importance.

2. BTES performance criteria

Assessing the performance of BTES systems can be performed using different criteria. For instance, the COP of the heat pump used in the system is an essential criterion if the purpose of the heat pump application is to improve its performance by increasing the evaporator temperature [44].

A mostly used criterion is the BTES efficiency since the efficiency of the whole system depends on its value [45][46]. BTES efficiency is a ratio of the total heat extracted per total heat injected into the storage, as expressed in below Eq. 7:

$$\eta_{BTES} = \frac{heat\ extracted\ from\ thestorage}{heat\ injected\ into\ the\ storage} \qquad \text{Eq. 7}$$

It can be inferred that by increasing the temperature of the BTES, the efficiency of BTES would decrease since raising the BTES temperature leads to higher heat losses [6]. Also, during the warm-up period (first two-five years) that the BTES is charged to reach the design temperature point, smaller heat might be extracted compared to the time of the normal operation of storage and that might head to low efficiency during the warm-up period [47].

Another important criterion is the solar fraction [48], which is used for the application of solar collectors coupled with seasonal storage. A solar fraction is the total of the heat demand provided by solar energy.

Sweet and McLeskey [49] proposed another metric. They defined internal system efficiency, which is the heat provided to the home divided by the total solar energy collected. Therefore, the proposed criterion includes the heat loss terms.

Another performance criterion which is mostly used during system design of small-scale storage systems is cost savings, generally represented as a payback period or annual total cost [50].

3. System model

The conventional models proposed by Hellström [38] are applied widely to model the heat transfer inside and outside the boreholes. The proposed conventional model did not take into account the short-term responses of the GHEs. The purpose of the proposed models was to design seasonal thermal energy storage and optimal operation of the system. The application of that model might cause some errors when it is used to model the short-term thermal response of GCHP.

Two models are available in the thermal storage library of TRNSYS to model the seasonal thermal energy storage; 557a and 557b [51]. Both of these models are formed based on the work of Hellström. In 557a, the borehole thermal resistance within each borehole is calculated by the software by giving the input parameters of boreholes. However, 557b is applicable when the borehole thermal resistance is considered as an input parameter, which might be calculated from an experiment. As mentioned, for both of these models, the boreholes layout is hexagonally, and boreholes are uniformly distributed in a cylindrical volume.

In this study, it is assumed that the storage consists of a bunch of boreholes that are uniformly located in cylindrical region and in hexagonal patterns. It is assumed that each borehole has a single U-tube pipe (Fig. 2). As shown in Fig. 3, a certain ground region is assigned to each borehole heat exchanger. The average temperature for each ground region is designated by T_m and is known as local average temperature of that region. As presented in [38], the difference between fluid temperature and average temperature of a ground region is an interesting factor which shows the thermal capacity of that storage.

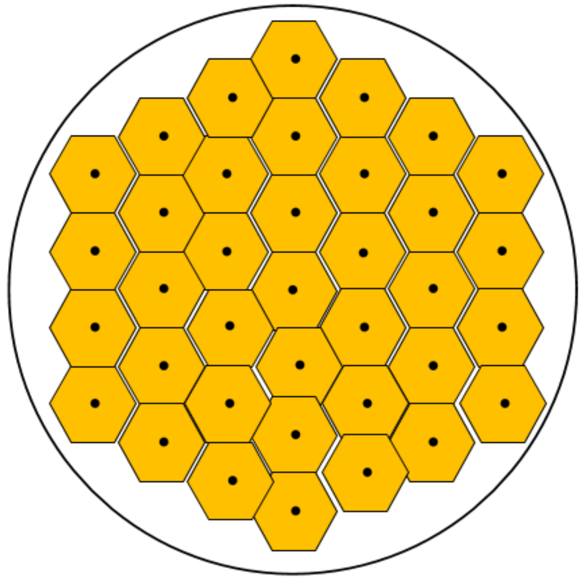

Fig. 2: Borehole thermal energy storage in a cylindrical region and hexagonal pattern

As shown in Fig. 4, the total storage is divided into a certain number of annular sections (zones) on the ground plane to provide the model of the seasonal thermal energy storage and provide an operating strategy. Two concentric circles bound each annular section (annulus). The first region is a circle or annulus with zero radii for the smaller (inner) circle. Moreover, each region consists of a different number of boreholes. For each section, it is assumed there are a water distributor and a water collector. For the series connection of the boreholes, each section is in connection with the adjacent section via water pipes. In a parallel connection, the flow rate of the fluid in each borehole might vary for different sections and is identical with boreholes of the same section. The flow rate inside each borehole and the operation of boreholes in each annular section is determined by solving the optimization problem.

As mentioned in previous sections, during the first period, there is no interaction between two adjacent borehole heat exchangers. After a specific time, the interaction between boreholes would be completed. If the heat flux through the boundary of the region ground encompassed a borehole is zero, it could be assumed that the heat transfer process is a steady-flux process. By considering the steady-flux process, the average temperature of the ground region increases linearly with time. As expressed in [38], for the steady flux process, there is no heat flow across the boundary of the ground region. In this regime, the shape of the temperature distribution in the ground region does not change with time. The heat flux is constant at all points in the ground region, and the increase in the temperature is the same for all points. Also, the difference between the average of the fluid temperature and the local average temperature is constant. As a result:

$$T_{ave} - T_m = R_{sf} q \qquad \text{Eq. 8}$$

T_{ave} is the average fluid temperature, T_m is the ground region (local) average temperature, and R_{sf} is the steady-flux thermal resistance.

As presented in [38], the required time to reach the steady-flux situation in the hexagonal duct pattern is given by:

$$\frac{\alpha t_{sf}}{A_p} = 0.065 \qquad \text{Eq. 9}$$

As presented in [38], for hexagonal duct pattern a superposition of two rectangular duct patterns with spacing $B$and B_1 is calculated as follows:

$$R_{sf} = \frac{1}{2\pi k}\{\ln\left(\frac{B}{2\pi r_b}\right) + \frac{\pi B_1}{6B} - \frac{1}{2}\ln\{2[\cosh(\pi\sqrt{3}) + 1]\} + \frac{5\pi\sqrt{3}}{12}\} + R_b \qquad \text{Eq. 10}$$

The above equation is calculated for a single pipe in the hexagonal duct pattern. The constant flux thermal resistance of the U-shaped pipe in hexagonal duct pattern can be derived by superposing two patterns with single pipe in two rectangular regions (totally four patterns) and heat injection rate for each of two pipes is q/2.

Four points are as follows:

$$(0,0), (D,0), (\tfrac{1}{2}B + D, \tfrac{\sqrt{3}B}{2}),\ (\tfrac{1}{2}B, \tfrac{\sqrt{3}B}{2})$$

The steady-flux thermal resistance for a single U-shape pipe would be as follows:

$$\begin{aligned} \mathrm{R_{sf}}(\text{single U} - \text{pipe}) \\ &= \frac{1}{4\pi k_s}\left\{\ln\left(\frac{B}{\pi d_b}\right) + 7\sqrt{3}\frac{\pi}{12} - \frac{1}{2}\ln 2[\cosh(\sqrt{3}\pi) + 1]\right. \\ &\left. + \ln 2\left[\cosh(\sqrt{3}\pi) + \cos\left(\frac{2\pi D}{B}\right)\right] + \ln 2\left[1 - \cos\left(\frac{2\pi D}{B}\right)\right]\right\} + R_b \end{aligned} \qquad \text{Eq. 11}$$

The local average temperature for all boreholes of the same annular region is equal to each other. The reason is that all boreholes are uniformly placed in each annular region, and they follow the same operating strategy during charging and discharging. In other words, the fluid inlet temperature, the flow rate of the circulating fluid, and communication to the adjacent boreholes are the same for all borehole heat exchangers in the same annular region.

Heat transfer analysis inside the encompassing ground region of each borehole is performed for two periods. After a step-pulse change in heat injection q to a borehole, for the first period, when there is not any interaction between boreholes, an infinite line source model is applied to determine the local average temperature of the surrounding ground region. After a specific time, the interaction of the boreholes would be fully developed. For this period, thermal energy balance is developed for a ground region, as shown in Fig. 3.

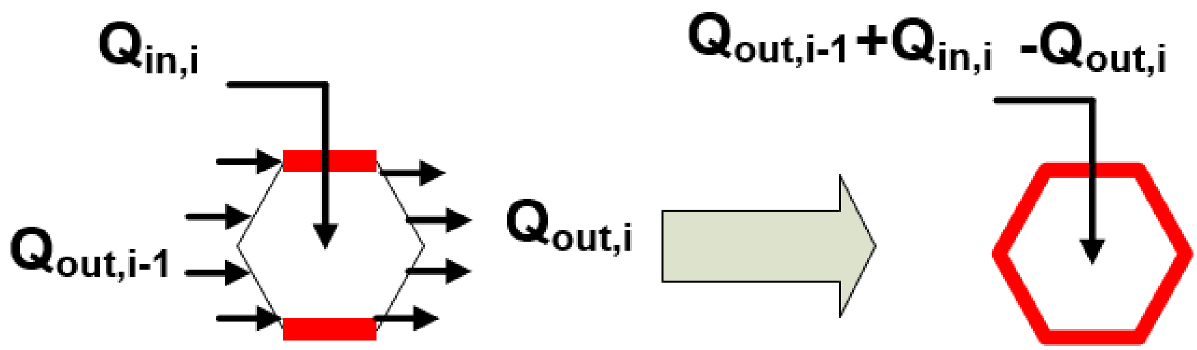

Fig. 3: Thermal energy balance for each ground region of a borehole

For each borehole, there is a heat flux from the previous region via heat conduction, the heat sent to the next region via conduction and there is an inlet heat from the fluid to the borehole heat exchanger. It has to be mentioned that there is no heat flux through the bottom and top boundaries of the control volume. The reason is that each borehole itself and boreholes above and below it all belong to the same annular region and they have the same local average temperature. Therefore there would be no heat flux between them. Moreover, it is assumed that the temperature for all points in the surrounding ground region of each borehole is the same and is the average local temperature. As a result, the ground region is supposed to be a lumped mass. Therefore, both the thermal control volume shown in Fig are identical. So, it can be seen that for each borehole, the boundary conditions of the steady-flux heat process can be established (since the heat flux across the boundaries of that control volume is zero).

Since all the boreholes have the same heat process experience, instead of proposing the model for individual borehole, the model is applied to each section as shown in Fig. 5.

In summary, following steps for discretization are performed for both storage and ground around it:

- The storage is divided into P sections. Each section contains $N_i \; i = 1,\ 2,\ 3, \ldots,\ P$ boreholes.
- The soil outside of the storage is divided into M sections. Each has L meter far from each other.
- The value of L should be selected such that it can be ensured the soil temperature after the Mth section is always 10 ℃ during the entire operation of the storage.

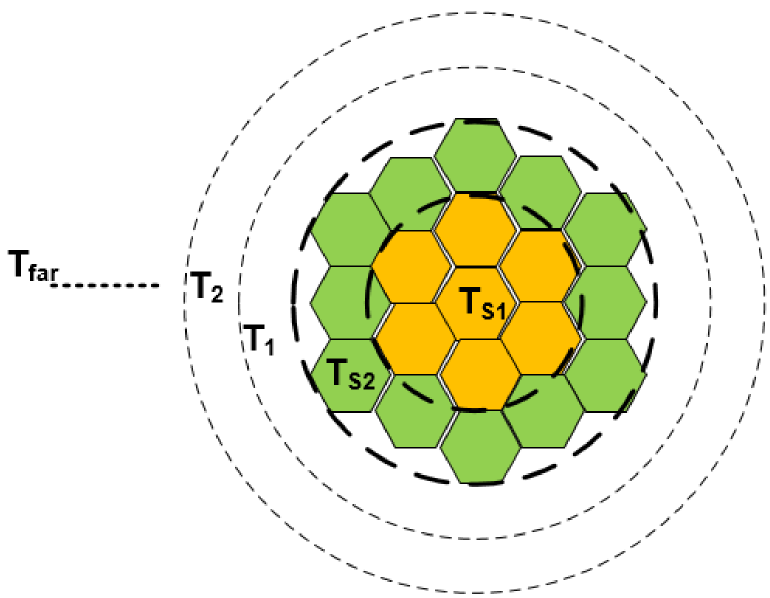

Fig. 4: Different storage sections (zones) and ground sections around it

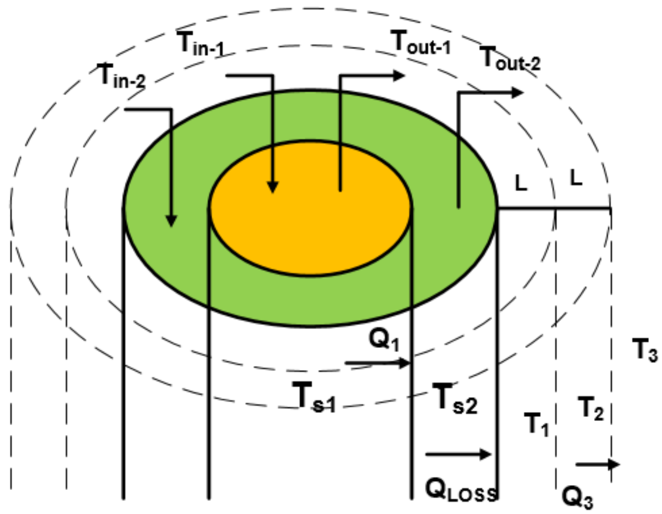

Fig. 5: Schematic diagram of different operating strategies in different storage regions

The ground temperature for the i^th section is calculated as follows:

$$T_{s,i}(t) = T_{S,i}(t-1) + \frac{[Q_{in,i}(t) + Q_{out,,i-1}(\mathrm{t}) - Q_{out,i}(\mathrm{t})] \times 3600}{\rho C_s V_{section,i}} \quad \text{Eq. 12}$$

$T_{s,i}$ is the average temperature of section i, $Q_{in,i}$ is the input energy to the region i by circulating the fluid, $Q_{out,i}$ is the heat conduction to the next region by section I, $Q_{out,i-1}$ is the input conduction heat from the previous section i $-$ 1, $V_{earth,i}$ is the section volume, ρ is the density of the soil, and C_s is the heat capacity of the soil.

The heat input (injection during charging) to the system is calculated as follows:

$$Q_{in,i}(t) = \dot{m}_\iota C\big(T_{in,i}(t) - T_{out,i}(t)\big) \quad \text{Eq. 13}$$

$\dot{m}_\iota$ is the total fluid flow rate to the section i, C is the heat capacity of the circulating fluid, $T_{in,i}$ is the inlet fluid temperature to section I, and $T_{out,i}$ is the outlet fluid temperature of section i.

The heat flux due to the conduction between two regions are as follows:

$$Q_{out,i-1} = -kA_{i-1}[T_{s,i}(t) - T_{s,i-1}(t)]/L_i \quad \text{Eq. 14}$$

A_{i-1} is the side area of section $\mathrm{i}-1$,and L_i is the distance between two annular region.

The combination of the infinite line source model and constant heat-flux model can be applied to each annular region [38]:

$$\left(T_{ave,i}(t) - T_{s,i}(t)\right) N_i H = \sum_{j=1}^{n} (Q_{in,i}(t_n) - Q_{in,i}(t_{n-1})) R((t) - (t_n)) \qquad \text{Eq. 15}$$

N_i is the total number of borehole in section i , H is the length of the borehole and R is the total thermal resistance.

Thermal resistance is calculated as follows:

$$R(t) = R_{sf} \qquad t - t_n > t_{sf} \qquad \text{Eq. 16}$$
$$R(t) = R'(t) \qquad t - t_n < t_{sf}$$

As expressed by Hellstrom [38] the borehole thermal resistance for short-term period is calculated as follows:

$$R'(t) = \frac{1}{2}\left\{\frac{1}{4\pi k_s} E_1\left(\frac{r_b^2}{4\alpha t}\right) + R_b + \frac{1}{4\pi k_s} E_1\left(\frac{D^2}{4\alpha t}\right)\right\} \qquad \text{Eq. 17}$$

By assuming fluid temperature as an average temperature of the inlet and outlet flows the analysis of the temperature variation along the flow channels becomes simple. Therefore, the fluid temperature is calculated as follows similar to:

$$\boldsymbol{T_{ave,i}(t)} = \frac{\left(\boldsymbol{T_{in,i}(t)} + \boldsymbol{T_{out,i}(t)}\right)}{2} \qquad \text{Eq. 18}$$

The energy balance equation for each annular region around the storage is as follows:

$$-kA_{j-1}[T_j(t) - T_{j-1}(t)]/L * 3600 = -kA_j[T_{j+1}(t) - T_j(t)]/L * 3600 + \rho C_s V_j [T_j(t) - T_j(t-1)] \qquad \text{Eq. 19}$$

V_j is the volume of the ground region j, and A_j is the side area of ground region j.

4. Case study

It is assumed that the recovered heat from the industrial waste heat is applied to charge the storage. The design fluid flow rate inside each U-tube during charging and discharging is assumed to be 0.4 kg/s. In the non-heating season, water is heated up to 65 degrees through the heat recovery system installed in the industrial plant. The hot water is then sent to the seasonal thermal energy storage. The water transfers sufficient heat to the storage and then comes back to the heat recovery system of the industrial plant to be warmed up again.

5. Results and discussions

Two different case studies are solved to study the performance of the seasonal thermal energy storage (STES) using the proposed model. It is assumed that the recovered heat from the waste heat of the industrial plant can be stored in the STES. The fluid inlet temperature during the charging period is less than 65℃. The reason for setting this maximum value is the threshold limit temperature of the U-shape pipe in the borehole. We also set a fluid inlet temperature as an optimization variable to show there is further control on the heat exchanger side close to the industrial plant. It means if the minimum flow rate is fixed as a constraint in the optimization problem, the fluid inlet temperature has to be calculated by an optimization problem. The reason is that it is not allowed to charge the storage by our desired value, and every time the charging rate is limited by considering the temperature of the ground (available driving force for heat transfer) and ground geotechnical properties.

The performance of the storage is investigated for one year. The charging takes place for the first four months, then there would be no charging and discharging for the next four months, and the discharging happens for the last four months.

Case1: there is no limitation on the charging rate, and we can charge the storage as much as we can.

Case 2: The available heat for charging the storage is limited to 50% of the maximum value.

The reason for setting constraints of Case #2 is that the heating demand of the building in the early time of the charging period might be considerable. As a result, the optimizer might decide to send the recovered heat to the building directly for the early days of the charging period. Therefore, we are only allowed to charge the storage for the second period of the charging time, and as a result, there would be a constraint on the maximum available heat for charging.

The borehole thermal energy storage in the case study consists of 200 boreholes in total. Each borehole includes a single-U tube heat exchanger with 30 meters length. The distance between each pair of boreholes is 1.5 m, which is a distance between the centers to center of the boreholes. The total borehole field surface area is 389.657 m^2 and the volume is 11689.7 m^3. As mentioned in order to minimize the heat loss, the arrangement of borehole heat exchangers is in hexagonal pattern, and they are placed uniformly in a cylindrical region. The storage is divided into five sections for purposes of monitoring and controlling the operational strategy. In this case study, it is assumed that all boreholes are connected in parallel. The ground outside of the storage is divided into ten sections or annular regions. The distance between each pair of the sections outside of the storage is 5 meter.

Number of boreholes and dimension of each annular region or section are presented is in Table 1.

Table 1: Borehole configuration and dimension of each section

section	1	2	3	4	5
# of Boreholes	1	18	42	78	61
Volume m^3	60.288	1047.965	2443.0487	4561.050	3556.850
Side Area m^2	150.72	646.212	1156.776	1748.352	2096.892

5.1. Results of the Case#1:

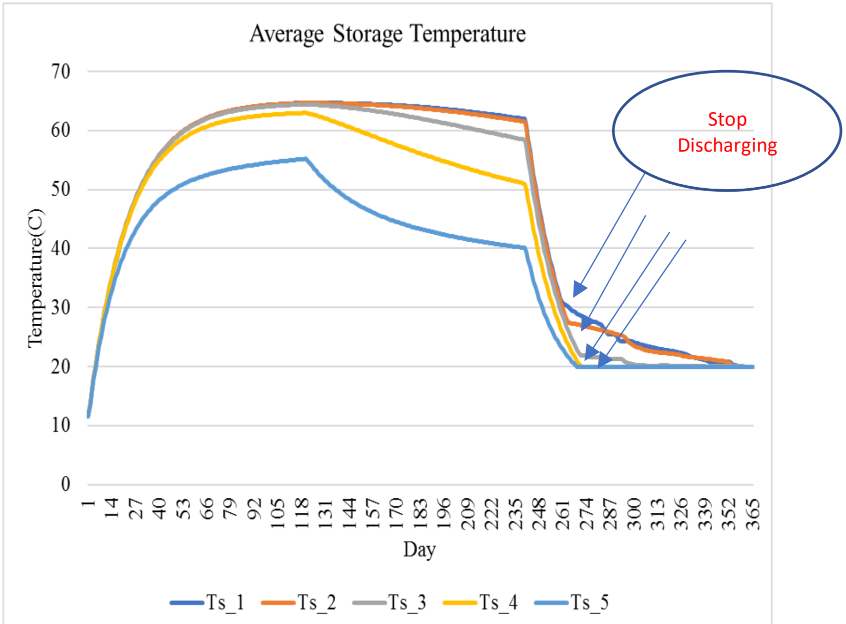

Fig. 6: Daily average storage temperature in different storage sections (zones) for case study #1

In this case, as shown in Fig. 6 and Fig. 7, all storage sections are charged with available heat on the first day of the charging period. It indicates that the charging strategy for all of the storage zones is identical. The daily average temperature of the different sections is shown in Fig. 6. The storage section #1 located at the center of the storage (first section with only one borehole heat exchanger) always has a higher temperature than other sections. The reason is that the heat loss is least from this section because the closest zone to it is also charging, and therefore the temperature difference between two these storage sections is small. The outermost zone (section #5 with 61 boreholes) has the lowest temperature amongst storage regions. On the contrary to section #1, the heat loss of section #5 is highest since this section is the outermost section of the storage and there is no charging for the section next to it (since it is the ground region).

During the intermediate period, when there is no charging and discharging, the temperature of all storage sections (annular regions) drops. Section #5 has the largest temperature reduction in this period due to the maximum heat loss, which happens because of the maximum temperature difference between storage and surrounding ground. Discharging takes place for all sections from the first day of the discharging period. After a certain time, the discharging would end for section

#1 first. However, discharging continues for other sections. The days in which discharging stops are 24, 58,125 for section #2, section 3, section #4, and section #5, respectively.

Fig. 7 and Fig. 8 show the rates of heat charging and heat discharging in different sections for one year period.

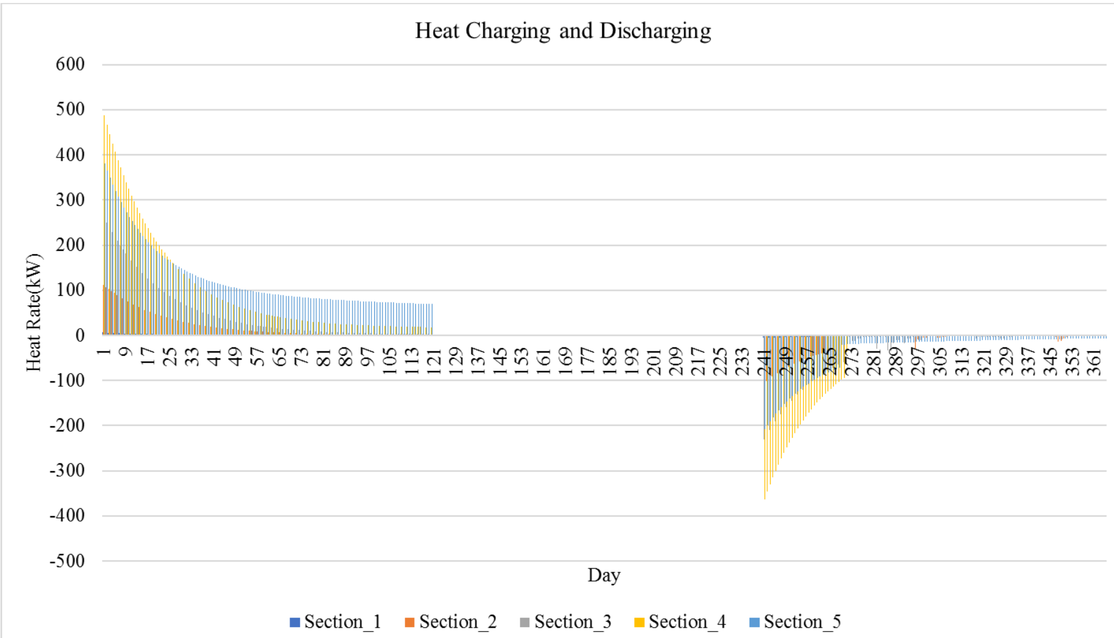

Fig. 7: Daily average charging and discharging heat rates for different storage sections (zones) of case study #1

The magnitude of charging and discharging depends on the number of boreholes. As it is clear, section #4 has the maximum boreholes (78), therefore for both charging and discharging periods, it has maximum heat transfer rate. Throughout the charging period, the charging rate of all boreholes (sections of the storage) reduces with time. The reason is that the average storage temperature rises, and as a result, the temperature difference between fluid and storage drops (driving force decreases). Therefore heat charging decreases. The opposite scenario might happen during the discharging period. Fig. 9 displays total heat charging (input) and discharging (output) for the first year operation of the storage system. As presented in that figure, the borehole thermal energy efficiency of the borehole is 47%.

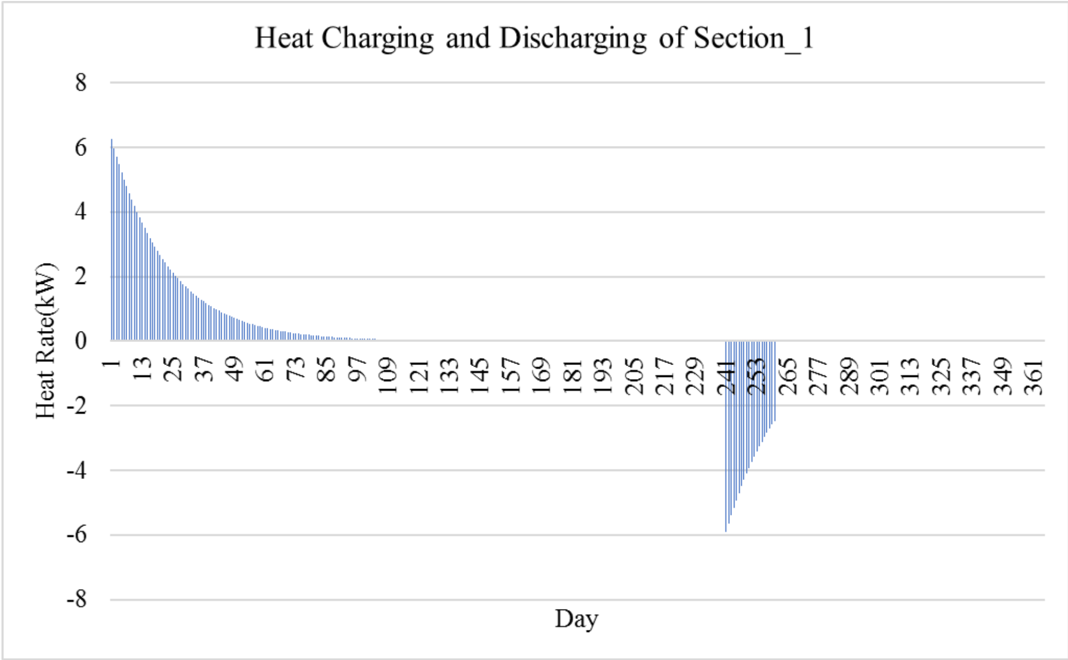

Fig. 8: Daily average charging and discharging heat rates for section #1 (zone #1) of case study #1

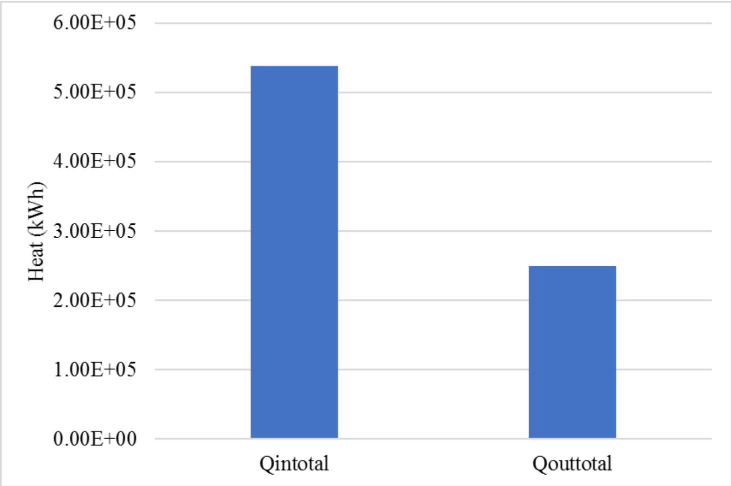

Fig. 9: Heat charging and discharging when there is no limit on the available heat

5.2. Results of Case #2:

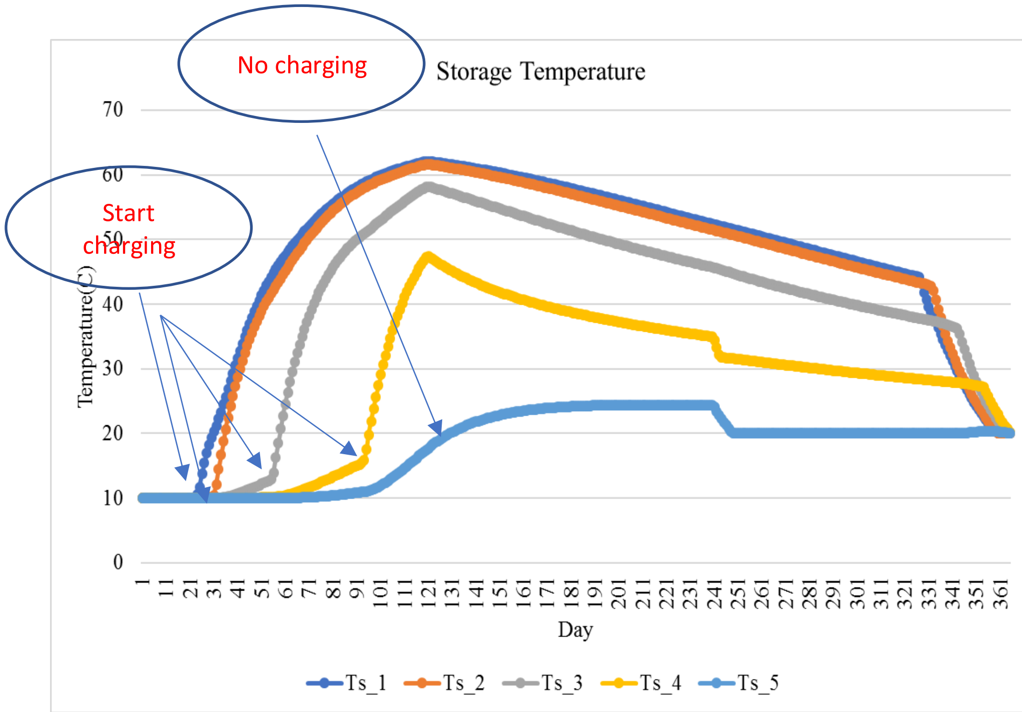

Fig. 10: Daily average charging and discharging heat rates for section #1 (zone #1) of case study #1

Because of the limitation on the available heat, charging does not take place from the first day of the charging period. Charging starts for the first section after 40 days. After 47 days, the charging starts for boreholes located in section #2. For section # 3 and section #4, charging begins after 73 and 117 days, respectively. For section 5, which is the outermost storage section, there would be no charging, and it is only heated up by the conduction with inner sections.

On the contrary to the first case study, the temperature drop during the intermediate period for section #5 is not significant (Fig. 10). The reason is that the temperature of section #5 and temperature of the ground section surrounding it increase simultaneously and with the same order during the charging period via heat conduction. Therefore, the temperature difference between section #5 and the ground section close to it is not considerable. Accordingly, the temperature reduction during the intermediate period is negligible, which can lead to minimizing heat loss.

For discharging, it is more efficient to commence discharging from the outer sections. The reason is that a part of extracted heat would be from the soil. In another way, the ground itself serves as a source of energy. The discharging pauses for a while and begins again from the core (section #1).

After certain times, discharging starts for other inner sections. There would be no discharging for the outermost section of boreholes. It can be concluded that by extracting heat from the outer sections of storage first, a hypothetical insulation layer can be built around the inner sections of storage that leads to the minimum heat loss.

Fig. 11 and Fig. 12show the rates of heat charging and heat discharging in different sections for one year period.

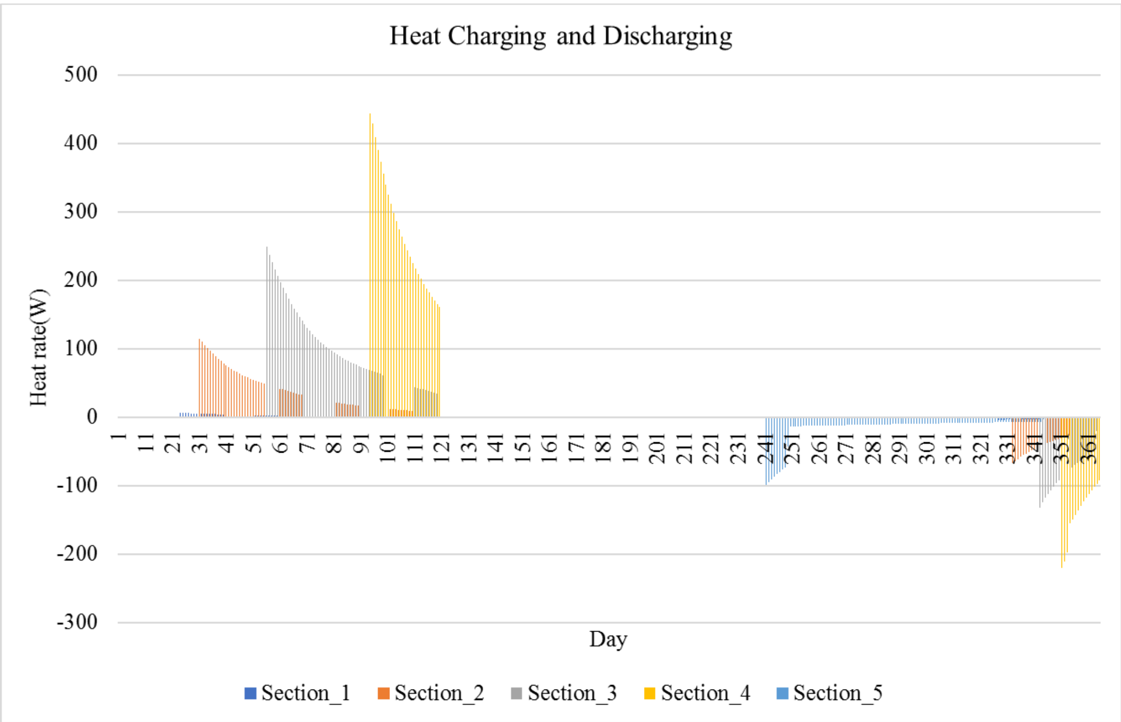

Fig. 11: Daily average charging and discharging heat rates for different storage sections (zones) of case study #1

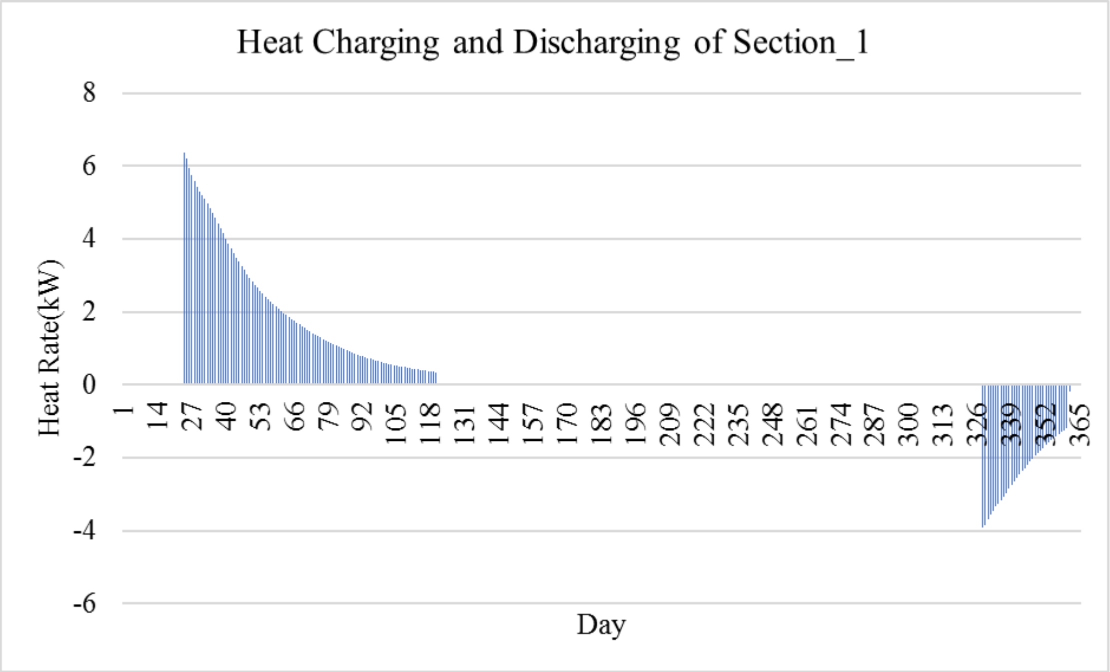

Fig. 12: Daily average charging and discharging heat rates for section #1 (zone #1) of case study #1

6. Performance comparison of the proposed model and the black-box model

In this section, the performance of the system using the proposed model is compared to the system performance using the simpler model, known as the black-box model. For this aim, it is assumed that charging is performed for three months, and the discharging happens for the next three months. It is assumed that there is no transition period between the charging and discharging periods. The objective function is the seasonal thermal energy storage.

In the black-box model, the storage is considered as a large heat exchanger considering constant effectiveness during the whole operation of that system. The following equation is applied instead of to establish a relation between fluid inlet and outlet temperatures and the average storage temperature.

$$\left(T_{out}(t) - T_{in}(t)\right) = -\varepsilon(T_{in}(t) - T_s(t)) \qquad \text{Eq. 20}$$

ε is the effectiveness of the storage and it depends on the number of the boreholes.

The following equation is utilized as an energy balance relation for the whole storage.

$$T_{s,i}(t) = T_{S,i}(t-1) + \frac{[Q_{in,i}(t) + Q_{loss}(\mathrm{t})] \times 3600}{\rho C_s V_{storage}} \quad \text{Eq. 21}$$

where Q_{loss} is the heat loss of the storage and is calculated as follows:

$$Q_{loss}(t) = \frac{[T_s(t) - T_{far}(\mathrm{t})]}{R_{loss}} \quad \text{Eq. 22}$$

T_{far} is the far field temperature and is assumed to be 10 degrees.

The results of the proposed model are expressed considering different configurations. The number of boreholes in different sections varies for different configurations and is shown in Table 2.

Table 2: Number of boreholes for different configurations

section	1	2	3	4	5
Configuration #1	1	18	42	78	61
Configuration #2	20	30	40	50	60
Configuration #3	19	42	78	61	-

Fig. 13 shows the daily average temperature of the storage considering different configurations by using the proposed model and the daily average storage temperature by using the black-box model.

From this figure, the daily average temperatures of the storage using the proposed model are entirely identical for all storage configuration. This can be inferred considering a different number of the boreholes in different sections has a small effect on the analysis since the model is able to adjust the performance of the storage by choosing appropriate sections of the system operation. Also, by comparing the daily average temperature using the proposed model with that of the black-box model, it can be concluded that the proposed model is accurate in analyzing the performance of the system. The reason is that there is a small difference between the results of these two models.

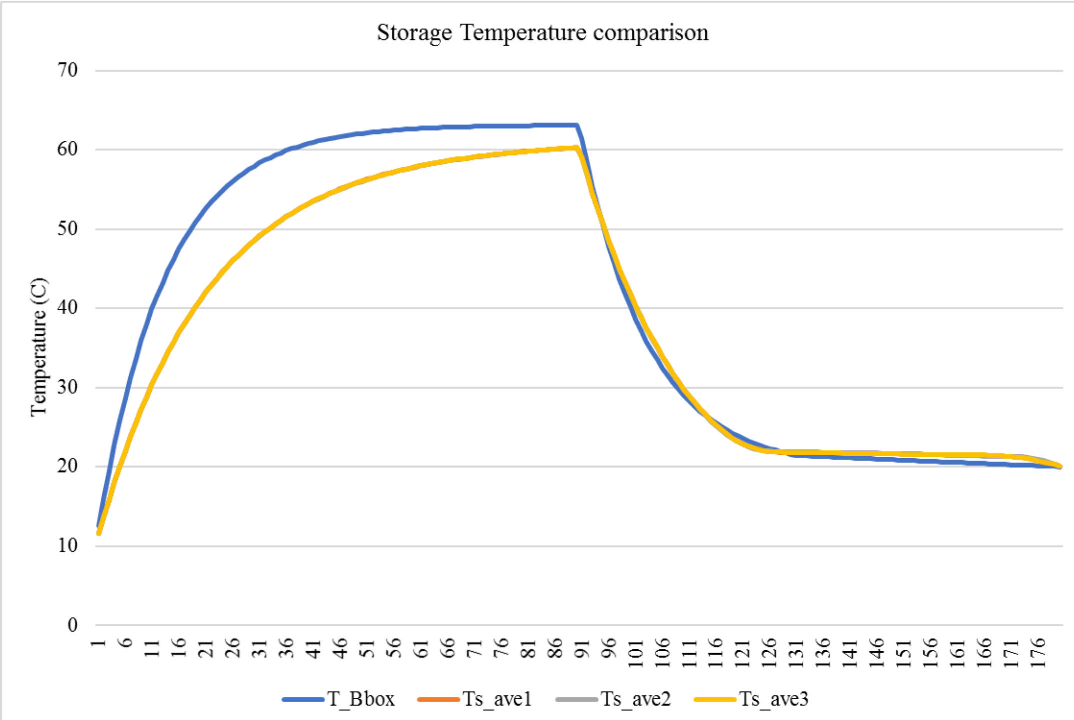

Fig. 13: Comparison of the storage temperature for three different configurations of the proposed model and black box model

7. Conclusions

This work presents an overview of various methodologies and thermal response factors (g-functions) for modelling the heat transfer process of borehole heat exchangers. The extensive literature review includes various numerical approaches and analytical solutions to determine the temperature at the borehole wall over the short-term and long-term. It is pretty complex to use the previously published models in optimization software for the purpose of storage design and optimal storage operation. It is a significant workload to model a large scale BTES using already developed g-functions. Besides, the high computational time is required to get an optimum size and operation of BTES from optimization software. To solve these challenges, in the second part of this work, the work proposes a new flexible semi-analytical, semi-numerical methodology to model the heat transfer process of the borehole thermal energy storage. Some of the results and concepts proposed by Hellstrom (as DST model) are utilized to form the new model. In the new model, both storage and its surrounding ground are divided into a finite number of annular regions (zones or sections). Each storage section contains several boreholes having an equal fluid flow rate at each time step. Thermal energy balance is developed for each storage section and ground section. The infinite line source model and the concept of a steady-flux heat process are applied to develop the model. The heat extracted/ injected from/into the storage can be controlled by either changing the water flow rate inside each borehole or adjusting the inlet water temperature. However, by proposing the new model, the flexibility of the storage operation increases since one can control the heat input or heat output by choosing an appropriate storage section. In other words, one more degree of freedom in terms of controllability is added to the model for controlling the operation of the storage.

- The proposed model can be adopted by any optimization software to determine the optimal size and operation of the system. The reason is that the model is linear and does not have the improper integral or function. Furthermore, the optimization problem is not complicated, and the computational time of the optimization problem is reasonable (for a one-year hourly analysis, the computational time is around 15 minutes).
- The model is able to determine the size of the storage, including borehole distance, length of the borehole, number of boreholes, etc.
- The model is able to control the operation of the storage by deciding the appropriate storage zone for charging and discharging. Furthermore, the storage operating strategy might vary amongst storage zones. It implies that each storage zone might adopt different fluid flow rates and fluid inlet temperature through their boreholes. This increases the flexibility of the storage operation since the extracting or injecting a load can be adjusted by changing the water flow rate, selecting the appropriate section of storage for storing and extracting heat, and adjusting the fluid inlet temperature.
- The proposed model in this work is applied to storage, including several numbers of boreholes in hexagonal duct pattern and are located uniformly in a cylindrical region.
- The concept of the proposed model can be applied to develop a model for different storage configurations (line, L-shaped, square, rectangular).

8. References

[1] Beerepoot M, Ada M. Policies for renewable heat. International Energy Agency; 2012.

[2] Helm D. The European framework for energy and climate policies. Energy Policy 2014;64:29–35. doi:10.1016/j.enpol.2013.05.063.

[3] Economidou M, Atanasiu B, Despret C, Maio J, Nolte I, Rapf O. Europe's buildings under the microscope. A country-by-country review of the energy performance of buildings. 2011.

[4] Energy use data handbook tables (Canada)—Residential Sector. Http://DataGc.ca/Data/En/Dataset/ 27155507-0644-4077-9a97-7b268dfd8e58 n.d.

[5] Som SK, Datta A. Thermodynamic irreversibilities and exergy balancein combustion processes. Prog Energy Combust Sci 2008;34:351–76.

[6] McDaniel B, Kosanovic D. Modeling of combined heat and power plant performance with seasonal thermal energy storage. J Energy Storage 2016;7:13–23. doi:10.1016/j.est.2016.04.006.

[7] Afzali SF, Mahalec V. Novel performance curves to determine optimal operation of CCHP systems. Appl Energy 2018;226:1009–36. doi:10.1016/j.apenergy.2018.06.024.

[8] McDaniel B. Thermodynamic Analysis of the Application of Thermal Energy Storage to a Combined Heat and Power Plant, Master's Thesis. University of Massachusetts Amherst, 2015.

[9] Xu L, Torrens JI, Guo F, Yang X, Hensen JLM. Application of large underground seasonal thermal energy storage in district heating system: A model-based energy performance assessment of a pilot system in Chifeng, China. Appl Therm Eng 2018;137:319–28. doi:10.1016/j.applthermaleng.2018.03.047.

[10] Evans A, Strezov V, Evans TJ. Assessment of utility energy storage options for increased renewable energy penetration. Renew Sustain Energy Rev 2012;16:4141–7. doi:10.1016/j.rser.2012.03.048.

[11] Rad FM, Fung AS. Solar community heating and cooling system with borehole thermal energy storage - Review of systems. Renew Sustain Energy Rev 2016;60:1550–61. doi:10.1016/j.rser.2016.03.025.

[12] Dincer I, Rosen MA. Thermal Energy Storage: Systems and Applications. 2nd ed. John Wiley & Sons: Hoboken; 2010.

[13] Bauer D, Marx R, Nußbicker-Lux J, Ochs F, Heidemann W, Müller-Steinhagen H. German central solar heating plants with seasonal heat storage. Sol Energy 2010;84:612–23. doi:10.1016/j.solener.2009.05.013.

[14] Philippe M, Marchio D, Hagspiel S, Riederer P, V. Partenay. Analysis of 30 underground thermal energy storage systems for building heating and cooling and district heating. Conf. proceedings, Effstock. Stock., 2009.

[15] Cimmino M, Bernier M. A semi-analytical method to generate g-functions for geothermal bore fields. Int J Heat Mass Transf 2014;70:641–50. doi:10.1016/j.ijheatmasstransfer.2013.11.037.

[16] Carslaw HS, Jaeger. JC. Conduction of heat in solids. 2nd ed. Oxford: Clarendon Press; 1959.

[17] Eskilson P. Thermal Analysis of Heat Extraction Boreholes. 1987.

[18] Ingersoll LR PH. Theory of the ground pipe source for the heat pump. ASHRAE Trans., vol. 54, 1948, p. 339–48.

[19] LR I. Theory of earth heat exchangers for the heat pump. Am Soc Heat Vent Eng J Sect Heating, Piping, Air Cond 1950:113–22.

[20] Carslaw HS JJ. Chapter 13: The Laplace transformation: Problems on the cylinder and sphere. Conduct. Heat Solids, 1959, p. 327–52.

[21] Baudoin A. Stockage intersaisonnier de chaleur dans le sol par batterie d’échangeurs baïonnette verticaux: modèle de prédimensionnement. Université de Reims Champagne-Ardenne, France, 1988.

[22] Zeng HY, Diao NR, Fang ZH. A finite line-source model for boreholes in geothermal heat

exchangers. Heat Transf - Asian Res 2002;31:558–67. doi:10.1002/htj.10057.

[23] Lamarche L, Beauchamp B. A new contribution to the finite line-source modelfor geothermal boreholes.pdf. Energy Build 2007:188–98.

[24] Claesson J, Javed S. An analytical method to calculate borehole fluid temperatures for time-scales from minutes to decades. ASHRAE Trans 2011;117:279–88.

[25] Fossa M. The temperature penalty approach to the design of borehole heat exchangers for heat pump applications. Energy Build 2011;43:1473–9. doi:10.1016/j.enbuild.2011.02.020.

[26] Fossa M, Cauret O, Bernier M. Comparing the thermal performance of ground heat exchangers of various lengths. Proc from 11th Int Conf Energy Storage 2009.

[27] Cimmino M, Bernier M, Adams F. A contribution towards the determination of g-functions using the finite line source. Appl Therm Eng 2013;51:401–12. doi:10.1016/j.applthermaleng.2012.07.044.

[28] Cimmino M, Bernier M. Preprocessor for the generation of g-functions used in the simulation of geothermal systems. Proc BS 2013 13th Conf Int Build Perform Simul Assoc 2013:2675–82.

[29] YAVUZTURK C. MODELING OF VERTICAL GROUND LOOP HEAT EXCHANGERS FOR GROUND SOURCE HEAT PUMP SYSTEMS. Oklahoma State University, 1999.

[30] Young TR. Development, verification, and design analysis of the borehole fluid thermal mass model for approximating short term borehole thermal response. Oklahoma State University, 2001. doi:10.1017/CBO9781107415324.004.

[31] Xu X, Spitler. Modeling of Vertical Ground Loop Heat Exchangers with Variable Convective Resistance and Thermal Mass of the Fluid. Proc. Ecostock, 10th Int. Conf. Therm. Energy Storage,New Jersey, 2006, p. 8.

[32] Bandyopadhyay, Gopal, Manohar Kulkarni and MM. A New Approach to Modeling Ground Heat Exchangers in the Initial Phase of Heat-Flux Build Up. ASHRAE Trans

2008;2.

[33] Bandyopadhyay G, Gosnold W, Mann M. Analytical and semi-analytical solutions for short-time transient response of ground heat exchangers. Energy Build 2008;40:1816–24. doi:10.1016/j.enbuild.2008.04.005.

[34] Javed S, Claesson J. New analytical and numerical solutions for the short-term analysis of vertical ground heat exchangers. ASHRAE Trans 2011;117:3–12.

[35] Zeng H, Diao N, Fang Z. Heat transfer analysis of boreholes in vertical groundheat exchangers.pdf. Int J Heat Mass Transf 2003:4467–81.

[36] Li M, Lai ACK. Analytical model for short-time responses of ground heat exchangers with U-shaped tubes: Model development and validation. Appl Energy 2013;104:510–6. doi:10.1016/j.apenergy.2012.10.057.

[37] Lamarche L, Kajl S, Beauchamp B. A review of methods to evaluate borehole thermal resistances in geothermal heat-pump systems. Geothermics 2010;39:187–200. doi:10.1016/j.geothermics.2010.03.003.

[38] Hellström G. Ground heat storage: Thermal analyses of duct storage systems. 1991.

[39] Li M, Lai ACK. Review of analytical models for heat transfer by vertical ground heat exchangers (GHEs): A perspective of time and space scales. Appl Energy 2015;151:178–91. doi:10.1016/j.apenergy.2015.04.070.

[40] Paul ND. The effect of grout thermal conductivity on vertical geothermal heat exchanger design and performance. South Dakota State University, 1996.

[41] De Carli M, Tonon M, Zarrella A, Zecchin R. A computational capacity resistance model (CaRM) for vertical ground-coupled heat exchangers. Renew Energy 2010;35:1537–50. doi:10.1016/j.renene.2009.11.034.

[42] Zarrella A, Scarpa M, De Carli M. Short time step analysis of vertical ground-coupled heat exchangers: The approach of CaRM. Renew Energy 2011;36:2357–67. doi:10.1016/j.renene.2011.01.032.

[43] Bauer D, Heidemann W, Muller-Steinhagen H, Diersch H-JG. Thermal resistance and

capacity models for borehole heat exchangers. Int J Energy Res 2011;35:312–20. doi:10.1002/er.

[44] Lanahan M, Tabares-Velasco PC. Seasonal thermal-energy storage: A critical review on BTES systems, modeling, and system design for higher system efficiency. Energies 2017;10. doi:10.3390/en10060743.

[45] Wang H, Qi C. Performance study of underground thermal storage in a solar-ground coupled heat pump system for residential buildings. Energy Build 2008;40:1278–86. doi:10.1016/j.enbuild.2007.11.009.

[46] Sibbitt B, McClenahan D, Djebbar R, Thornton J, Wong B, Carriere J, et al. The performance of a high solar fraction seasonal storage district heating system - Five years of operation. Energy Procedia 2012;30:856–65. doi:10.1016/j.egypro.2012.11.097.

[47] McClenahan D, Gusdorf J, Kokko J, Thornton J, Wong B. Okotoks: Seasonal storage of solar energy for space heat in a new community. In Preceeding of ACEEE, 2006.

[48] Xi C, Hongxing Y, Lin L, Jinggang W, Wei L. Experimental studies on a ground coupled heat pump with solar thermal collectors for space heating. Energy 2011;36:5292–300. doi:10.1016/j.energy.2011.06.037.

[49] Sweet ML, McLeskey JT. Numerical simulation of underground Seasonal Solar Thermal Energy Storage (SSTES) for a single family dwelling using TRNSYS. Sol Energy 2012;86:289–300. doi:10.1016/j.solener.2011.10.002.

[50] Zhang L, Xu P, Mao J, Tang X, Li Z, Shi J. A low cost seasonal solar soil heat storage system for greenhouse heating: Design and pilot study. Appl Energy 2015;156:213–22. doi:10.1016/j.apenergy.2015.07.036.

[51] Thorén Å. Practical evaluation of borehole heat exchanger models in TRNSYS An example of a TRNYS model with borehole heat exchangers and dry coolers Practical evaluation of borehole heat exchanger models in TRNSYS. KTH, 2016.

Chapter 6

Conclusions and Recommendations

1. Conclusions

This thesis proposed different frameworks for the design and operation of the energy system for either deterministic case problems or stochastic case problems. In each design framework, a detailed MILP model of the energy system is proposed by converting non-linear terms to the linear ones using a piecewise linearization method. By the use of the proposed design frameworks, the optimal size of the energy system is investigated considering all applicable technologies and different optimization criteria. Furthermore, the change is the size of energy system components due to various levels of greenhouse gas (GHG) emission is investigated. Moreover, some straightforward operating strategies (season-based scenario and NPC methodology) of various energy system configurations have been developed that enables to optimize the operation of the energy system without solving a complex optimization problem. A new model is also proposed for the seasonal thermal energy storage. The model can be efficiently employed in optimization software and is an appropriate model for determining the optimal design and operation of the storage. Several main conclusions are as follows:

- By the use of community energy systems, considerable achievements in terms of the high system efficiency, GHG emissions reduction and annual total cost saving can be attained compared to the stand-alone system application.
- Application of the fired Heat recovery steam generator (HRSG) in the community energy system causes a more reduction in primary energy consumption, annualized total cost, carbon dioxide emission compared to the system of the same structure but without having supplementary firing.
- The use of supplementary firing decreases the optimal size of the gas turbine, boiler and electric chiller, particularly for the climate zones with hot summers.
- The two-stage stochastic programming model is proposed to build a design framework under uncertainties in energy demands and energy prices.
- A new strategy to generate the scenarios for the stochastic problem is proposed by random sampling of vectors (RVS method), which express discrete distributions of the uncertain parameters. The application of the proposed strategy is very efficient and provides a substantially better computational performance than Monte Carlo sampling.

- For the stochastic problem, by using RVS method, after 60 scenarios, the objective function converges to the optimum value. However, by using the Monte Carlo Sampling method, the objective function has a fluctuation even for more than 81 scenarios.
- The design framework under uncertainty adapts a restriction on the risk of high carbon dioxide emissions. In this frame, the expected annual total cost is minimized, and a value restricts the average of the high emissions risk with a probability of 0.05.

Variation of the optimal size of each component due to the change in the carbon dioxide emissions (CDE) ratio for both stochastic and deterministic cases are examined (chapter 4)

- The design performance curves presented as a function of the GHG emission ratio. The curves are developed for the energy system without photovoltaics (PV).The minimum GHG emission ratio that can be obtained for the energy system without PV and solar collectors is 0.37.
- In stochastic problems, the sizes of the engine, GSHP, absorption chiller, thermal storage for all ranges of carbon dioxide emissions strategies are larger than those of deterministic cases.
- For stochastic problems, the required sizes of the heating coil and battery are identical or moderately lower than their corresponding sizes in the deterministic cases.
- The required size of the electric chiller decreases a lot for the stochastic cases compared to the size needed for deterministic cases.

The proper model for the seasonal thermal energy storage modelling is proposed and leads to an increase in the flexibility of the system operation. The model considers the heat transfer process inside and outside of the borehole heat exchangers. The model is able to determine the size of the storage and can control the operation of the storage by deciding the appropriate storage zone for charging and discharging.

The application of the NPC methodology is investigated for different case studies. Based on that:

- Application of the NPC strategy leads to the best-operating cost-saving, carbon dioxide emissions saving, and PEC saving for all case studies when compared to the usage of other strategies.
- All the well-known strategies are defined as specific cases of the NPC strategy.

- The relative simplicity of computing the NPC curves makes it possible to identify optimal operating strategies for CCHP systems without having to resort to elaborate model building and complex optimization procedures.

2. Recommended Future Works

In the thesis, steady-state models are employed for modelling power generation unit (PGU), absorption chiller, GSHP, boiler, electric chiller and storage tank. As future work, it is recommended that dynamic models [1] for CCHP components are adopted in the design framework instead of employing steady-state models. Although implementing dynamic models makes the optimization problem more complicated, the methodology would be more reliable and can be used for any real application case study. Based on the literature review, the main shortcoming of the proposed methodologies is the lower reliability of feasibility analysis. Hence, proposing an approach based on a detailed dynamic system simulation is necessary to assure that the optimal operation of energy systems is feasible and calculated economic and environmental achievements are reliable. In addition, most of the proposed methodologies have not considered the real-control strategies for different components. Proposing an optimum control strategy is crucial to achieving the economic and environmental benefits of energy systems. The real-time control strategy for each component has to be developed, considering the temperature range of each component operation. Also, proposing a dynamic simulation model, which includes the temperature level of each component and each flow, can enhance the reliability of the design frame.

The environmental performance of a community energy system can improve by using seasonal thermal energy storage. The recovered heat from the heat recovery system can be directly sent to the storage to be stored in the ground during summer for use during winter. As a result, the use of seasonal thermal energy storage can reduce the need for a boiler to provide heat demands during peak periods. The optimal design and operation of a community energy system integrated with a seasonal thermal energy system become a complicated task. Since the dynamic model of the storage has to be applied to control the inlet and outlet temperature of the circulating fluid. Also, the operation of the whole system cannot be analyzed by using the demands of representative days for different seasons, and the yearly operation of the system has to be included in the model.

Consequently, the complexity of the design framework increases. The model presented in chapter six of the thesis can be applied as a precise and straightforward model of storage for this aim. Following future works are as follows:

- Compare the performance of the proposed model against most frequently used models.
- Improve the proposed model for modelling storage, including borehole heat exchangers connected in series.

After doing the above projects, some possible future works in terms of the community energy system application can be performed:

- Proposing a detailed model for community energy system integrated with seasonal thermal energy storage.
- Proposing a design framework for the optimal design of a community energy system integrating with seasonal thermal storage.
- Proposing an optimal operation framework for the design and operation of the seasonal storage integrated with solar collectors.
- Design of the community energy system integrated with seasonal storage considering the uncertainty in the ground thermal conductivity.

3. References

[1] Calise F, Dentice d'Accadia M, Libertini L, Quiriti E, Vanoli R, Vicidomini M. Optimal operating strategies of combined cooling, heating and power systems: A case study for an engine manufacturing facility. Energy Convers Manag 2017;149:1066–84. doi:10.1016/j.enconman.2017.06.028.